STUDYING NORMAL MODES IN AMORPHOUS THERMOPLASTICS: POLY(METHYL METHACRYLATE), POLYSTYRENE, AND POLYVINYL CHLORIDE

A Dissertation
Presented to
The Academic Faculty

by

Alfred “Freddy” Nicholas DeAngelis

In Partial Fulfillment
of the Requirements for the Degree
Ph.D. in Mechanical Engineering in the
The George W. Woodruff School of Mechanical Engineering

Georgia Institute of Technology
May 2020

STUDYING NORMAL MODES IN AMORPHOUS THERMOPLASTICS: POLY(METHYL METHACRYLATE), POLYSTYRENE, AND POLYVINYL CHLORIDE

Approved by:

Dr. Asegun Henry, Advisor
School of Mechanical Engineering
Georgia Institute of Technology

Dr. Kyriaki Kalaitzidou
School of Mechanical Engineering
Georgia Institute of Technology

Dr. Shannon Yee
School of Mechanical Engineering
Georgia Institute of Technology

Dr. Martin Maldovan
School of Physics
Georgia Institute of Technology

Dr. Samuel Graham
School of Mechanical Engineering
Georgia Institute of Technology

Date Approved: [December 20, 2019]

ACKNOWLEDGEMENTS

First and foremost, I would like to thank my parents, Fred and Corinne, for their unending encouragement throughout my life, especially of my natural curiosity. My passion for science, learning, and problem solving comes from many places, but none more so than my mother and father. They, along with my brother and sister, have provided me with more love and support than I could ever say, and I am eternally grateful to them.

Second, I would like to thank my advisor, Dr. Asegun Henry. Throughout my time at Georgia Tech, Dr. Henry was a relentlessly optimistic and encouraging figure who, no matter what, was always excited to discuss and ponder incredibly hard but engaging questions. He was a continual source of support and direction, and he has profoundly influenced how I think about and solve problems.

Third, I would like to thank my dissertation committee. Along with Dr. Henry, Drs. Graham, Yee, Kalaitzidou, and Maldovan were all excellent mentors to me and pushed me to think even more deeply about my research and its implications. The detail and thought that has gone into this dissertation have been greatly increased by their continued input.

I would also like to thank the many other educators I have had the privilege of studying under throughout my life, in a variety of subjects technical and otherwise. I have been profoundly lucky to study so many subjects under the tutelage of such engaging teachers throughout my life, and as a result, have become a better, more well-rounded student.

My friends have also been a steadfast source of invaluable support for me. No matter when or how much I've struggled, in graduate school or in life, I have always had friends to turn

to for advice and encouragement. I am fortunate indeed to know I have so many people rooting for me.

Finally, I would like to acknowledge funding that has afforded me the opportunity to research a subject about which I am quite passionate. This material is based upon work supported by the National Science Foundation Graduate Research Fellowship under Grant No. DGE-1148903.

Freddy

TABLE OF CONTENTS

LIST OF TABLES

LIST OF FIGURES

LIST OF SYMBOLS

A	area (m^2)
C	modal heat capacity ($J\ K^{-1}$)
C_q	quantum-corrected modal heat capacity ($J\ K^{-1}$)
D	modal diffusivity ($m^2\ s^{-1}$)
E	total energy (Kcal/mol)
M	number of atoms in a polymer chain
N	atom number
PR	participation ratio
P	normalized probability of placing an atom
$\mathrm{P}_{\mathrm{raw}}$	non-normalized probability of placing an atom
$\mathrm{P}_{\mathrm{raw,old}}$	old non-normalized probability of placing an atom
$\mathrm{P}_{\mathrm{raw,new}}$	new non-normalized probability of placing an atom
$\mathbf{Q}$	heat flux
$\mathbf{S}$	structure factor
T	temperature (K)
X	modal displacement amplitude
$\dot{X}$	modal velocity amplitude (s^{-1})
b	atom index
$\mathbf{e}$	vibrational eigenvector
g	the radial distribution function
$\hbar$	Planck's reduced constant (J s)

i	atom index
j	atom index
k	atom index thermal conductivity (W m^{-1} K^{-1})
$\mathbf{k}$	phonon wavevector thermal conductivity vector (W m^{-1} K^{-1})
l	unit cell index
m	mass (g) mode index
n	mode index
r	atomic separation (Å)
$\mathbf{r}$	atomic separation (Å)
$\mathbf{r}_0$	atomic equilibrium position (Å)
t	time (ps)
u	atomic coordinate (Å)
$\mathbf{u}$	atomic coordinate (Å)
$\dot{\mathbf{u}}$	atomic velocity (Å ps^{-1})
$\ddot{\mathbf{u}}$	atomic acceleration (Å ps^{-2})
$\mathbf{v}_g$	group velocity (Å ps^{-1})
Υ	second order force constant
Φ	potential energy (Kcal/mole)
α	Cartesian directional index
β	Cartesian directional index
γ	Cartesian directional index
λ	wavelength (nm)

ν	dispersion branch index
ρ	density (kg m^3)
τ	phonon relaxation time (ps)
ψ	third order force constant
ω	frequency (THz)

LIST OF ABBREVIATIONS

a-Ge	amorphous germanium
a-PMMA	amorphous poly(methyl methacrylate)
a-PS	amorphous polystyrene
a-PVC	amorphous polyvinyl chloride
a-SiO_2	amorphous silicon dioxide
C	carbon
Cl	chlorine
DFT	density functional theory
DOS	density of states
EIP	empirical interatomic potential
EPP	eigenvector periodicity parameter
GA	genetic algorithm
Ge	germanium
GK	Green-Kubo
GKMA	Green-Kubo Modal Analysis
GULP	General Utility Lattice Program
IF	imaginary frequency
INMA	instantaneous modal analysis
LAMMPS	Large-scale Atomic/Molecular Massively Parallel Simulator
LD	lattice dynamics
MD	molecular dynamics
MFL	mean free path

O	oxygen
PCPR	polymer chain participation ratio
PE	polyethylene potential energy
PES	potential energy surface
PGM	Phonon Gas Model
PMMA	poly(methyl methacrylate)
PR	participation ratio
PS	polystyrene
PVC	polyvinyl chloride
RDF	radial distribution function
RF	real frequency
SCLD	supercell lattice dynamics
SF	structure factor
TBC	Tersoff-Born-Coulomb
TC	thermal conductivity

SUMMARY

This dissertation explores how heat propagates in amorphous materials at the atomic level. Most of the discussion is devoted to how normal modes give rise to thermal transport in amorphous polymers, a subject which has not been studied via large-scale numerical simulations (specifically, molecular dynamics) previously. The work focuses on two particularly interesting aspects of polymers, namely the anomalously high degree of localization observed in the normal vibrational modes in the systems, and the presence of modes with an imaginary frequency.

While the focus of this dissertation is on thermally characterizing polymers, it also includes the development of new descriptors of mode localization in disordered materials. These descriptors quantify localization spatially or based on the number of polymer chains a mode spans. Surprisingly, more highly-localized modes exhibit, on average, a larger magnitude of thermal conductivity than more localized modes. Further some high-frequency modes have been discovered that span multiple polymer chains (rather than being localized to a single chain); these modes have some of the largest thermal conductivities of any modes in the given system being studied.

Furthermore, modes with an imaginary frequency are found to resemble real frequency modes, even though previous findings indicate these modes describe a structural change (e.g. conformation flipping) in a material. The imaginary frequency modes behave quite similarly to real frequency modes, except that imaginary frequency modes exhibit much higher degrees of localization at a lower (magnitude of) frequency. Their contribution to thermal conductivity however is on the same order as that of real frequency modes.

CHAPTER 1. INTRODUCTION

Heat transfer is a rich, diverse subject matter, spanning length scales from the subatomic to the intergalactic and timescales ranging from femtoseconds to the age of the Universe. The basic mechanisms by which heat is transported at the macroscale (i.e., convection, conduction, and radiation) are well-understood and can be accurately described by, for example, Fourier's law or Planck's law. But much remains to be learned about heat transfer at the atomic level. This dissertation is an attempt to advance science's understanding of heat transport in one such situation, namely, thermal conduction at the atomic scale in structurally disordered (i.e. amorphous) solid materials. In particular, the work will focus on the study of thermal transport in a few amorphous thermoplastic polymers: poly(methyl methacrylate), polystyrene, and polyvinyl chloride. Though theoretical descriptions of thermal transport at the atomic scale have existed for nearly a century, a growing body of work has indicated that the most well-established methods fail to describe the thermal conductivity (TC) of materials with a significant degree of disorder [1-13]. Furthermore, to fully understand the thermal properties of a material, it is desirable to understand how the properties are affected by individual modes of vibration within the material. The shortcomings of current theories and the demand for mode-level details of thermal transport have necessitated the development of a new framework to better describe TC more generally in a manner that includes disordered solids, namely Green-Kubo Modal Analysis, which will both be described later in detail and used throughout this work.

To appreciate why a new framework is called for, and to understand the shortcomings of existing theories, it is useful to briefly review those existing theories to understand why they fail.

1.1 The Phonon Gas Model

The Phonon Gas Model (PGM) [14-16] is a 100+ year-old description of thermal transport, developed for simple, crystalline, periodic systems. While a detailed derivation can be found elsewhere [14], this section will cover the important details of the theory and why the theory breaks down upon the introduction of any kind of disorder to the material being modeled.

1.1.1 Details of the Phonon Gas Model

It has been understood since Einstein explained Brownian motion [17] that atoms exist and vibrate quasi-randomly in any material. In a three-dimensional solid comprised of N atoms, each atom will have three degrees of freedom, (i.e., it can move in the *x*-, *y*-, and *z*-directions), and consequently there exist $3N$ normal modes of vibration[1]. These vibrational modes can be obtained as solutions to the equations of motion that govern the motions of atoms in a material. The modes can vary widely in character and appearance, images of a few different modes in different materials can be seen in Fig. 1.

Vibrational modes can be calculated via lattice dynamics (LD, which will be described in detail later) and serve as the primary means by which heat is stored (i.e., via the heat

[1]This includes three translational modes which are present for any molecule. However, these modes do not participate in thermal conduction and can be ignored.

capacity) and transported (i.e., via the TC) in solid materials (along with electrons in electrically conductive materials). In simple, periodic, crystalline structures, these normal modes are plane-waves and are termed *phonons*[2]. Einstein [18] was the first to describe phonons mathematically in a solid material; his model assumes that all phonons oscillate at a single frequency, termed the *Einstein frequency*. Debye [19] modified Einstein's model, assuming 1) a simple dispersion relationship for the distribution of phonon wavelengths and 2) that frequency is inversely proportional to wavelength, and therefore phonons exist on a spectrum, rather than at a single frequency. Images of some vibrational modes can be seen below in Fig. 1.

[2]Throughout this dissertation, the term *phonon* will be restricted to referring to a vibrational mode with a well-defined wave-vector. As will be discussed later, some normal modes in disordered materials do not always fit this criterion, thus they will simply be termed *modes* and not *phonons*.

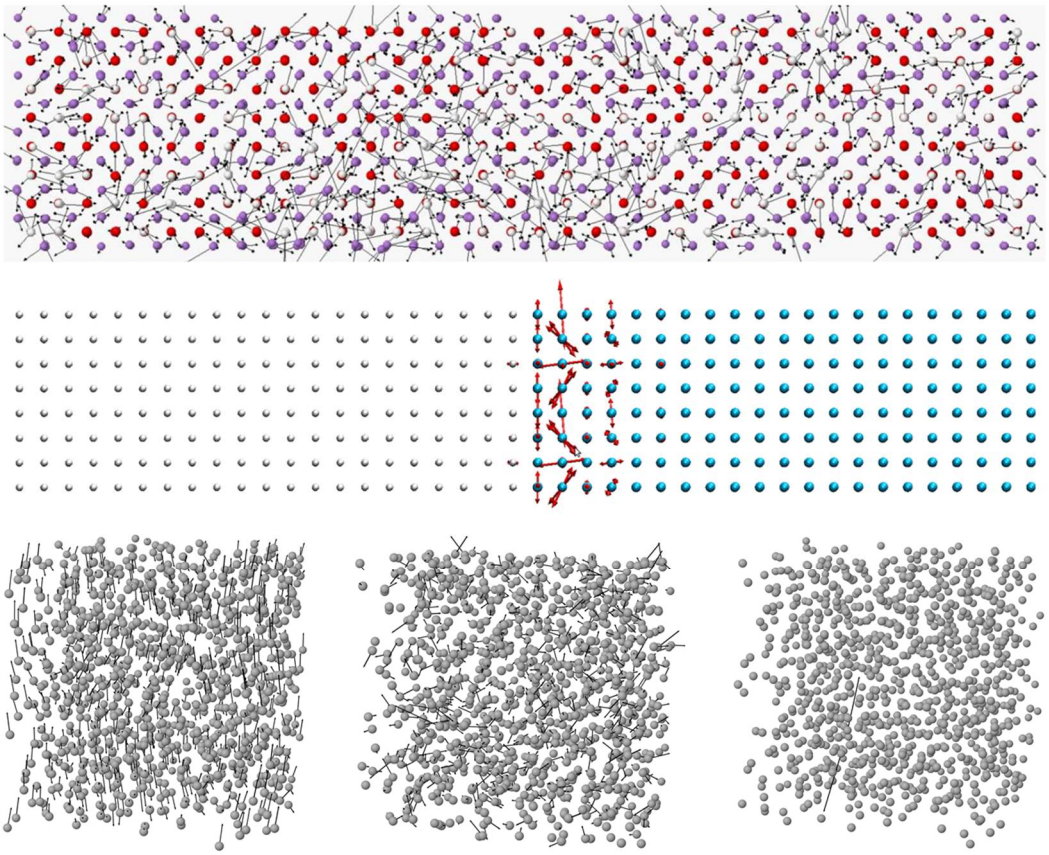

Figure 1. Vibrational modes in a random $In_{0.53}Ga_{0.47}As$ alloy [20] (top), at a Si-Ge interface [21] (center), and in amorphous Ge (bottom). The arrows represent the magnitude and direction that each atom moves as it participates in the particular normal mode of vibration.

Debye's description of phonons in solid materials has been further expanded to describe thermal transport in dielectric crystalline solids via the PGM [14-16]. In the PGM, phonons are treated as quasi-particles. Each phonon mode has a frequency, ω with a corresponding energy, $\hbar\omega$, (where $\hbar$ is the reduced Planck constant), a wavelength, λ, with a wavevector, $\mathbf{k} = 2\pi/\lambda$, and moves along a straight path at its group velocity, $\mathbf{v}_g = d\omega/d\mathbf{k}$. (The group velocity is generally defined for a wave packet of vibrations at similar frequencies, all with the same k-vector. It is the velocity at which the wave-packet propagates.) Each phonon also has a polarization vector field which describes the

magnitude and direction of each atom's vibration in the phonon. Phonons are bosons and consequently are subject to Bose-Einstein statistics [15, 22].

The physical picture described by the PGM is that phonons are particles that scatter as they encounter other phonons, material boundaries, imperfections, or any other feature that breaks the crystal symmetry and deviates from a perfect lattice. This scattering limits the average distance traveled, termed the phonon mean free path (MFP). By solving the Boltzmann transport equation, which can be used to model the transport of a collection of particles (e.g., gas molecules, phonons, electrons etc.), the TC due to the full phonon spectrum can be determined. One can derive (via simple analogy to kinetic theory) the TC of a material as

$$k = \frac{1}{V}\sum_i C_i D_i \tag{1}$$

where k is the TC of the material, V is its volume, C_i is the modal heat capacity of mode i, and D_i is the diffusivity of mode i, which is given in turn by $D_i = \mathbf{v}_i^2 \tau_i$ where τ_i is the relaxation time of the mode. This equation is a powerful means by which the TC of a material can be calculated in a straightforward manner. More advanced techniques exist for determining TC, including obtaining a solution to the full linearized Boltzmann Transport Equation, but these are typically not needed for low TC materials where phonon-phonon scattering is dominated by Umklapp processes [23].

1.1.2 Failures of the Phonon Gas Model

The PGM is widely accepted [24-35] and has provided great insights into thermal transport in crystals [14-16]. However, there is growing evidence to suggest that when one attempts

to apply the PGM to understand behavior in disordered materials[3], the PGM is insufficient, such as in materials with interfaces, random alloys, and amorphous materials [1-13, 15, 24, 34, 36-45]. In such cases, disorder causes a drastic change in the character of vibrational modes in the material. The two most noticeable changes to the mode character are: 1) There exists a pronounced degree of localization among many vibrational modes, particularly those at high frequencies. For these modes, all atoms in a material no longer participate; instead, the mode is often localized to a single small region of space within a larger structure. 2) Spatially delocalized vibrational modes can also change in character such that the displacement field associated with mode (i.e., the magnitude and direction that each atom is moving as it participates in a specific mode – depicted as arrows in Fig. 1 for example) appears random and lacks periodicity.

In such cases, the PGM fails not just quantitatively, but even qualitatively, including in complex crystals [10], simple crystalline lattices at high temperatures [11], amorphous materials [12], and random alloys [46]. These failures cannot be addressed with simple corrective terms or slight modifications to the PGM: they are due to an inherent oversimplification of the model when describing vibrational modes, particularly, the lack of wave-like behavior by most modes in the system; in this case, a group velocity (and consequently, a wave vector) cannot be assigned to the modes. When disorder is introduced to the system, there is a fundamental change in how the modes behave, and entirely new theories are necessary for accurately describing the behavior of the modes. Some of the

[3]Here, the term "disordered material" is used to refer to any solid that has some degree of randomness, within either its structure or composition. That is, it is not a perfect, crystalline solid, where the positions and identities of all atoms can be described by a lattice and a basis. This definition includes disorder in the form of composition, ranging from dilute impurities in crystals (e.g., isotopes, substitutions) up through multi-component alloys. It also includes the structural disorder found in an amorphous material.

means by which modes in disordered materials can be studied will be discussed in the next section, with emphasis on these methods' generality and their advantages over the PGM, while acknowledging some remaining shortcomings with these more recent approaches.

1.2 Existing Descriptions of Thermal Transport in Amorphous Materials

When studying thermal transport in disordered materials, one typically considers a supercell comprised of 10^2-10^3 (or more) atoms with periodic boundary conditions, and the supercell is treated as a single large "unit cell". Ideally, the supercell is so large that its characteristic length is on the order of the largest phonon wavelengths that exist in the material of interest; in practice, it is computationally intractable to study supercells of such size, as they would typically include many millions of atoms. In silicon for example, the MFP of long-wavelength phonons can exceed 100 μm [47-50]; given a crystal lattice constant of 0.453 nm with 2 atoms per unit cell, this means a simulation to treat the full phonon spectrum should include $> 10^{16}$ atoms, which is infeasible. Instead, smaller supercells are usually studied, and some long-wavelength vibrational modes are ignored. Such cases, however, still provide a rich amount of information about the systems being studied and are widely accepted as providing useful insight into the behaviour of the material in question.

The primary means by which modes in disordered materials are understood – and the approach followed in this work – is the propagon, diffuson, locon (PDL) paradigm, developed by Allen & Feldman [51]. Propagons are phonon-like modes with a well-defined wave vector and a clear periodic nature. They tend to be low-frequency modes that are spread throughout the entire system. In general, propagons resemble phonons, and they can

likely be understood using the PGM. Diffusons, while spatially delocalized, exhibit no apparent periodicity in the atomic vibrations; instead, these vibrations appear random. For this reason, it is not possible to define a wave-vector (and consequently, a group velocity), so the modes cannot be treated with the PGM. Finally, locons are localized modes that exist in a small minority of the supercell. These modes have been assumed to be too localized to contribute to TC in materials [2, 3, 12, 52-56], though there has been recent evidence published indicating this may not be the case [6]. Example illustrations of all three mode types in amorphous germanium (a-Ge) are included in Fig. 2 below[4].

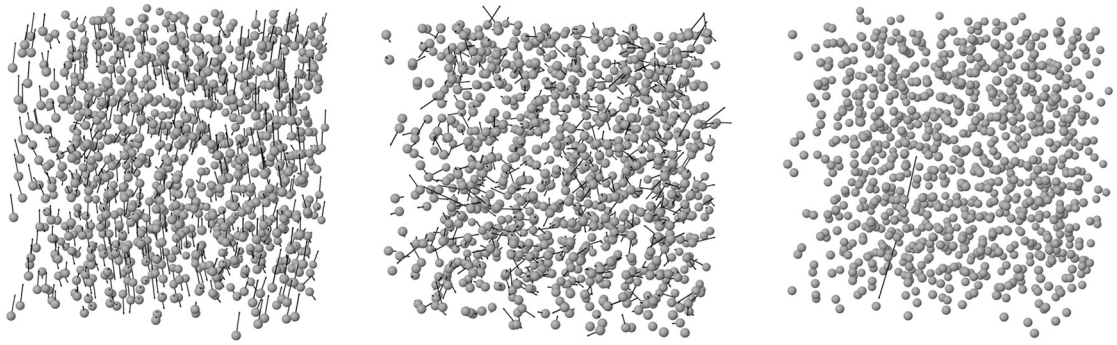

Figure 2. Illustration of a propagon (left), diffuson (center), and locon (right) in a-Ge. Atoms are shown as white spheres, and the corresponding eigenvector – which expresses the direction and magnitude that each atom would displace as it participates in the given mode – is shown by the black arrows. For clarity, the eigenvector magnitude of the locon has been scaled down by 5x compared to the other two examples and to other images in this document (unless explicitly noted).

This framework for classifying modes first gained traction when it was successfully applied to the TC of glasses [55-67], and has since been used to interpret TC behavior in amorphous semiconductors, [34, 68-80] solid solutions, [81, 82] organic compounds, [83-86] composites [87, 88] and phase change materials [89]. In addition to bulk materials, lower

[4]Many modes will be illustrated using arrows to represent the eigenvectors of vibration. The scaling of these eigenvectors is consistent across the dissertation, so that the relative magnitude of vibrations can be understood.

dimensional materials like 1-dimensional nanotubes, nanowires, and thin films [90, 91] were also subjected to such mode characterization.

Notably, there do not appear to be any attempts in the literature to categorize modes in amorphous polymers. The only work on polymers that even discusses modes is that of *Shenogin et al.* [65]. In their study of amorphous polystyrene (a-PS), they found that all modes with frequency > 5 THz are localized and do not contribute to TC. Their treatment of the topic was only brief however, and they did not classify the modes under the PDL paradigm or discuss at length anything about the characteristics of the modes. This dissertation is aimed at addressing this gap in the literature and is a first attempt at trying to understand and classify normal modes in amorphous polymers.

What is notable about the different mode classifications introduced by Allen and Feldman is that the various modes are in fact solutions to the equations of motion. This means that if one were to, for example, simulate the atoms with displacements according to the exact eigenvectors that result from the supercell LD (SCLD) calculation for one mode, the atoms would subsequently and indefinitely (for small displacements), vibrate back and forth at the corresponding frequency associated with the eigenvalue. This simple thought experiment then leads to an important realization. Specifically, when one considers the diffusons and locons, the displacement/velocity vectors may appear to be random, but in fact they are not. On the contrary, these motions are quite specific to the underlying random structure. In this sense, the vectors appear to be random because the underlying structure is in some sense random, but the normal modes are affected by this randomness in a very specific and exact way, as the selection of a random set of displacements would not

correspond to an actual normal mode of the system. Instead, one must perform an SCLD calculation to find the specific vectors/normal modes that correspond to a given system.

The taxonomy introduced by Allen and Feldman has provided insights into thermal transport in amorphous materials. It does not matter whether the disorder is in the structure or the composition (due to either the strength of the interactions or masses of the atoms), as any source of disorder in the LD dynamical matrix will affect the modes. In this way, it is useful to note that the changes in mode character/shape occur because of a break in symmetry.

In an ideal crystal, all atoms are arranged in a periodic fashion and there is perfect periodicity in structure, composition and mass. The material does not have to be monatomic i.e., the same mass and species for every atom, as one can have a unit cell with more than one basis atom and still have entirely propagating modes. In such a situation, the normal modes of vibration for the atoms must be described by periodic functions, since no one unit cell in the material is distinguishable from any other. Thus, they must all exhibit the same vibrations as a natural consequence of the symmetry, since the equations of motion will be the same for every copy of the unit cell. However, whenever there is any break in symmetry, such that the dynamical matrix is no longer periodic, the break in symmetry must be reflected in the final solutions to the equations of motion. Thus, whenever any atom or unit cell becomes distinguishable from all others, either by experiencing a different atomic environment (e.g., it has different neighboring atoms, or they are located at different distances/angles), or the atom is of a different species (e.g., an alloying element or interstitial), or the atom or its neighbors have a different mass (e.g., an isotope), or if there

exist defects, interfaces or other deviations from a perfectly periodic crystal, there will exist a change in mode character/shape [21, 92-95].

The PDL paradigm is built upon Allen & Feldman's previous work, which introduced a means by which one could perform calculations based on SCLD to estimate the TC contribution of vibrational modes in the material [2]. Their approach calculates the diffusivity, D, of a mode as

$$D(\omega_m) = \frac{\pi V^2}{\hbar^2 \omega_m^2} \sum_{n \neq m} \left| \mathbf{S}_{mn} \right|^2 \delta(\omega_m - \omega_n) \tag{2}$$

where ω_m is the frequency of the m^{th} diffuson mode, δ is the Dirac-delta function, and $\mathbf{S}_{mn} = \langle m | \mathbf{S} | n \rangle$ is the inter-mode matrix element of the heat current operator between modes m and n. This calculation determines the coupling of vibrational modes with the same frequency with a strength that is based on the overlap between their mode shapes. It is desirable to use as large a supercell as possible when calculating the mode diffusivities in an amorphous solid, in order to avoid any issues due to periodic effects.

In this work, to distinguish between propagons and diffusons, the methodology suggested by *Seyf et al.* [79] will be used: this methodology defines a propagon as a vibration with an eigenvector periodicity parameter (EPP) of > 0.2. The EPP is a value that compares the periodicity of a given mode to a perfectly periodic sinusoidal mode by comparing the dot product of nearest neighbor; a mode with a large EPP (and therefore one that is periodic) will result in consistently large dot products for a mode, whereas the dot product of vectors in a non-periodic mode will on average result in much smaller values. The EPP, and indeed the distinction between propagons and diffusons, is not the focus of this work; however, it

is important to note that EPP is effectively a measure of how periodic a mode's displacement field is: the value of EPP describes mathematically how closely the motion of atoms for a given vibrational mode resembles a pure plane-wave.

Other means of distinguishing between propagons and diffusons have been proposed, most notably, the use of the Ioffe-Regel cut-off frequency [96-99]. This method entails determining by inspection the frequency crossover point (typically ~1 THz) at which mode character changes. Above this cut-off, the relaxation times deviate from the ω^2 relaxation behavior observed at low frequencies. There is, however, still the potential for ambiguity with this approach, since it relies on defining a transition frequency. It may be possible that this transition frequency, and exactly which modes fall on one side of the cut-off versus the other, may shift slightly with temperature or a specific trajectory. Thus, an individual mode's classification may be difficult to concretely define or might become temperature/trajectory dependent. Nonetheless, the identification of a transition frequency is in practice likely to be a reasonable and useful approach, given that that the structures studied typically include > 10^3 atoms.

Another method proposed to distinguish between propagons and diffusons is the use of a structure factor (SF) [9, 100-109]. This approach performs a space and time Fourier transform of the eigenvectors to determine an effective dispersion curves of disordered and amorphous materials experimentally and numerically. In a perfect crystal, the SF for each mode appears as a delta function. However, several drawbacks exist with the SF, namely that it is not always possible to assign a wave-vector to a mode, even at low frequencies. Also, the SF is not a normalized quantity and therefore values must be considered independently for each material. Thus, similar to the Ioffe-Regel crossover method, the SF

method only identifies a cut-off frequency above which modes are defined as diffusons and below which they are defined as propagons.

Ultimately, the method used to distinguish between propagons and diffusons (or indeed diffusons and locons) should be material-agnostic and should not require comparison or normalization based on other modes in a system. Thus, methods like using the SF are less-desirable, as they require an arbitrary normalization between different materials.

For these reasons, EPP seems to be the best single quantity to define diffusons. In particular, because modes have other characteristics besides their frequency (in contrast to, for example, electromagnetic waves), using a single frequency as a distinguishing criterion can be an oversimplification and incorrectly categorizes many modes.

While EPP has been identified as a useful quantity for distinguishing propagons and diffusons, using a cut-off based on PR is less well established. The means by which one can distinguish between propagons, diffusons and locons are still being developed, and different methods have been proposed. Chief among these methods is that of Bell & Dean [110], who introduced the usage of the participation ratio (PR) as a means of distinguishing localized modes – namely locons – from delocalized modes (i.e., propagons and diffusons). The PR for a mode n is defined as

$$PR_n = \frac{\left(\sum_i^N \mathbf{e}_{i,n}^2\right)^2}{N\sum_i^N \mathbf{e}_{i,n}^4} \tag{3}$$

where $\mathbf{e}_{i,n}$ is the eigenvector of the i^{th} atom for the n^{th} vibrational mode, and N is the number of atoms in the supercell. If only a few atoms have large eigenvectors, the PR is

small, and the mode is a locon. On the other hand, if the majority of the atoms have large eigenvectors, the PR is large, and the mode is delocalized, thus it is either a propagon or diffuson. One way to view the PR is that it represents the fraction of atoms participating in a vibration. Thus, for a mode with PR = 1, 100% of the atoms participate in the vibration, whereas when the PR is $\sim 1/N$, only a single atom would be participating.

There has not been any definitive statement made in the literature regarding exactly where the "cut-off" in the transition between propagons/diffusons vs. locons occurs, although PR values anywhere from 0.1 to 0.4 have been suggested [78, 79, 91, 111]. Regardless, the PR can vary by several orders of magnitude in various structures that have been studied [17, 79, 112], and it seems reasonably acceptable that somewhere in the 10^{-2}–10^{-3} regime, a mode could undeniably be referred to as localized, since it would mean that only 0.1-1% of the atoms in the system are participating in such a mode. While 0.1 is typically the lowest cut-off used in the literature, one could argue that a mode with PR=0.1 is still at least partially delocalized, considering 10% of the atoms still participate in the vibration.

Allen and Feldman [3] have also suggested using a single cut-off frequency where the character changes from diffusons to locons. This frequency is termed the mobility edge", a name borrowed from electron transport theory, where it describes the cut-off between localized and delocalized valence electrons [113, 114]. Subsequent work however has indicated that the use of a cut-off frequency is perhaps not the best means for distinguishing locons from other modes, as locons are not necessarily the highest-frequency modes in the system [6].

This lack of a well-defined and fixed cut-off point between mode classifications is a lingering issue. It is likely that an absolute and strict cut-off criterion may never emerge. In this sense, one can think of the situation as similar to that of the classification of photons, which, while classified based on photon frequency, are generally characterized based on the nature of their interactions with matter. For example, long-wavelength microwaves have a somewhat arbitrary cutoff to distinguish them from short-wavelength radio waves; similarly, it is to be expected that a similar approximate and "gray area" or transition regime will exist for classifications of vibrational modes.

Regardless of the cut-off used, in all materials studied thus far, only a small minority of modes have been reported to be locons. Lv & Henry [6, 12] have reported the highest known fraction of locons in a fully dense material at 18% in amorphous silica (a-SiO_2)[5]; in other amorphous materials and alloys, locons comprise less than 3-5% of vibrational modes [115]. Furthermore, a-SiO_2 is peculiar in that the locons occur in two separate frequency regions, separated by a group of high frequency diffusons [6, 112] . This result negates the idea that there is a single transition frequency between diffusons and locons (i.e., a single "mobility edge" [3]). The large number of locons was therefore also cited as a likely reason their contributions became non-negligible in this system, as opposed to all preceding work [2, 3]. Follow-on studies that investigate other systems with a large fraction of locons are also warranted, to see if the locons are non-negligible in those systems as well.

In theory, one could presumably concoct a fictitious structure with so much chemical inhomogeneity that an even higher percentage of the modes could become localized, as

[5]Shenogin *et al.* provided a plot of PR vs. frequency for modes in a-PS, and while it appears >18% of the modes may have PR < 0.1, individual PR values were not given, the fraction of locons was not reported.

compared to a-SiO_2. For example, Moon and Minnich [78] studied a nanostructured amorphous alloy of amorphous silicon (a-Si) and a-Ge, in which 31% of the modes in the a-$Si_{0.45}Ge_{0.55}$ composition were locons. This finding then leads to the question: "How high the locon fraction can be?" There is not theoretical upper limit on the total possible fraction of locons in a system. In theory, long wave propagons (i.e. acoustic waves) must exist at low frequencies, and it seems unlikely that locons and propagons could exist without any diffusons. Nevertheless, perhaps a significant fraction of the total modes in the system, say 90%, could be locons in a very inhomogeneous material. However, no such material has been shown to exist.

1.3 Thermal Transport in Disordered Materials

Work has been done to quantify the degree to which different classes of modes contribute to TC in disordered materials [2, 3, 9, 12, 13, 116]. Propagons have been estimated to contribute anywhere from 10-90% of total TC, depending on the material [2, 3, 9, 12, 13, 116]. Diffusons have for a long time been assumed to make up the rest of the contribution to TC [2, 3, 12, 52-56], but more recent work by Lv & Henry [6, 12] has shown for the first time that locons can contribute to TC in some materials. Using many of the same simulation methods detailed later in this work, they found that in amorphous silica (a-SiO_2) at elevated temperatures, the contribution to TC by locons is > 10% of the total TC. Thus, while there remains some question as to the extent to which locons can affect TC, it seems that at least in some materials, their effect on TC cannot be neglected.

One particularly interesting finding by Lv & Henry is a general correspondence between the size/extent of delocalization and the contributions of these modes. Larger – i.e. more

delocalized – locons contributed more to TC than the smaller locons, which Lv & Henry inferred to mean locons contribute to heat conduction through their interactions with other modes. This interaction is possible because a larger locon involves more participating atoms that can serve as points of interaction with other modes. Essentially, larger locons overlap spatially with other modes to a greater extent and therefore should theoretically be able to couple with a greater number of other modes.

Based on the expression for diffusivity derived by Allen and Feldman, this spatial delocalization would result in a greater degree of overlap with other modes and consequently a greater diffusivity. Here, it is important to note that a single normal mode in any system is incapable of transferring any heat, since the solutions to the equations of motion (i.e. the vibrational modes) are standing waves, which cannot transport energy on its own. Instead, a mode must couple to another vibrational mode via anharmonic interactions to transfer energy between modes. One can test this assertion by exciting atoms in a supercell exactly according to the eigenvectors of a mode: in the case of small (i.e. harmonic) displacements, the atoms will exhibit simple linear harmonic motions, oscillating back-and-forth around their equilibrium positions at the frequency of the vibrational mode. If, however, one displaces the atoms further from equilibrium such that the potential energy with respect to position of the atoms is no longer described by a simple quadratic equation, the trajectory of the atoms will not persist indefinitely as simple harmonic motion, but instead become ergodic.

Due to the necessity of mode coupling to conduct heat, Lv & Henry argue that locons likely serve as bridges that allow transport between other modes – particularly diffusons – and

may only contribute indirectly to TC through their interactions with other modes that do extend throughout the material.

Lv & Henry's results suggest that locons can contribute to TC in a-SiO_2, and additional studies of more materials are warranted to determine if locons contribute significantly in other materials as well. From a theoretical standpoint, an endeavor to investigate this issue should focus on materials that are likely to have a large percentage of locons, such as the amorphous alloys studied by Moon and Minnich [42].

Revisiting the idea of a locon rich (i.e. >90% of modes) material, considering the TC contribution from an individual locon has been found to be extremely small, it might be possible to design a material system that could exhibit roughly an order of magnitude lower TC than other comparable materials with less atomic/structural inhomogeneity. It is intuitively difficult to imagine a system of continually interacting atoms in which ~90% of the vibrational modes are localized, but there has been no study to date that theoretically demonstrates that this cannot happen.

It is conceivable that such a material could exist. Low thermal conductivities for insulation are usually achieved through porosity, while fully dense materials usually have TC above ~0.1 W m^{-1} K^{-1} [117-120]; the lowest recorded fully dense material TC is 0.03 W m^{-1} K^{-1} [120]. In polymers, the presence of more than one type of atom and a wider variance in interatomic forces are likely to directly lead to an increased number of locons, which could result in a substantially lower TC. Consider for example, the possibility of achieving a fully dense bulk solid material with a room temperature TC on the order of 0.001 W m^{-1} K^{-1};

such a material does not currently exist, but it would have significant technological applications.

1.4 Thermal Transport in Amorphous Polymers

Polymers are a particularly interesting sub-class of disordered materials, because they tend to consist of long chain molecules that are entangled when in their amorphous state. In many commercial/industrial applications, they are often used in their amorphous state, because they can usually be melted, injection molded, or cured at moderate temperatures, making them very inexpensive to form into complicated shapes. One of the unique attributes of polymers is the fact that many of them can take on varying degrees of disorder, and through processes such as mechanical stretching, one can make polymers that traverse the full range of order – from fully disordered to fully ordered/crystalline [85, 88, 89]. In this sense, polymers are special because they are the one class of solids whose degree of order can be tuned on a continuous spectrum; thus, they provide a means for studying how disorder affects phonon transport in a continuous manner. Fundamentally, this characteristic of polymers derives from their chemical bonding nature. Polymers, especially thermoplastics, generally consist of strong/stiff covalently bonded atoms that form a single molecule from a repeating monomer, and the macromolecules tend to interact through much weaker interactions, such as van der Waals forces hydrogen bonding. A rather intrinsic feature of a bulk polymer is this disparity in bond strength. In a bulk amorphous polymer, both of these interactions are present, but it is the weaker interactions that tend to dominate, as amorphous polymers tend to have thermal conductivities on the order of 0.1 W m^{-1} K^{-1} and are regarded as thermal insulators.

In theory, as with all other disordered materials, amorphous polymers should contain propagons, diffusons, and locons, but detailed studies of vibrational modes in polymers are lacking. Of the few that have been carried out, *Shenogin et al.* [36] found that TC in amorphous polymers is due almost entirely to a few low-frequency propagating modes, while most modes were found to be localized and had negligible contribution to TC. Conversely, *Hsieh et al.* [90], found that the vast majority of thermal transport in amorphous polymers is due to diffusons, not propagons. They also point out that such findings are consistent with Allen and Feldman's model for minimum TC [2, 25], which itself is a more rigorous treatment of Einstein's model [91, 92]. More work is necessary to resolve these conflicting results and determine definitively whether propagons or diffusons or possibly even locons are responsible for TC within amorphous polymers. It is expected that one could employ the same techniques such as SCLD, Greek-Kubo analysis, and normal mode dynamics to polymers, just as they have been applied to amorphous semiconductors [4, 6, 12, 13, 69, 74, 75, 93-96]. However, there is a key problem that one is likely to encounter that opens up many interesting scientific questions worth exploring. Specifically, because polymers are usually formed from a chain of monomers, one must address the problem of structural changes in the polymer such as e.g. conformational changes due to the rotation of a monomer on a chain about the chain axis between two or more alternative metastable states.

In considering the SCLD problem, one might expect to find many unstable modes in an amorphous polymer, which would manifest as solutions with negative eigenvalues (i.e., imaginary frequencies). Such solutions are in general a useful and meaningful indication of the behavior of a material, and the corresponding eigenvectors could offer interesting

insights. However, it is not clear how one should interpret the existence and behavior of such modes. It is clear that from a purely mathematical standpoint, one could use Green-Kubo Modal Analysis (GKMA – see Section *3.2.2 Green-Kubo Modal Analysis*) to treat the imaginary frequency (IF) modes in the modal decomposition and complete the calculation, but it is not clear how to physically interpret the TC contribution of these modes. This is then an interesting and open question that should be addressed in future work, as this work only engages the very beginning of studying this question.

Furthermore, it would be useful to understand what role, if any, such modes play in the phonon-phonon interactions. For example, do IF modes preferentially interact with one particular class of modes (i.e., propagons, diffusons, or locons)? Is it possible IF modes actually contribute substantially to the TC, or are their contributions within the GKMA framework near zero, or perhaps even predominantly negative, indicating that they only serve to reduce TC? Prior work by Zhang & Luo [121] has shown that for a single polyethylene chain, as one increases temperature and reaches a regime where conformation changes begin to happen, there is a dramatic reduction of TC. Whether such pronounced effects are observed in an amorphous state is an open question, as the effect may be outweighed by the drastically different mode character that occurs in the amorphous state. Nonetheless, many interesting questions remain when it comes to polymers and many new studies are needed that apply the most advanced and detailed modeling techniques to this class of materials, so that a deeper understanding of the mode level interactions, contributions and behaviors can be developed.

This dissertation will investigate the thermal behavior of three amorphous thermoplastics: amorphous poly(methyl methacrylate) (a-PMMA), a-PS, and amorphous polyvinyl

chloride (a-PVC). All three polymers are comprised of carbon (C) and hydrogen (H), while PMMA contains oxygen (O) atoms, and PVC contains chlorine (Cl). The molecular structure of a monomer of each polymer is shown below in Fig. 3.

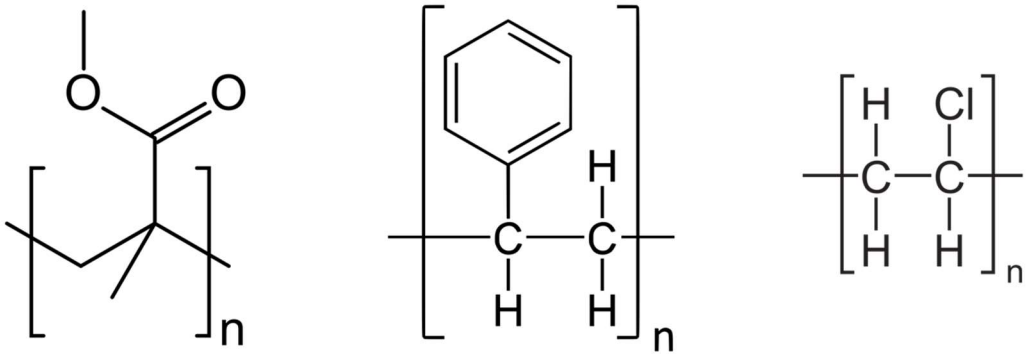

Figure 3. Chemical structure of a monomer of a-PMMA (left), a-PS (center), and a-PVC (right).

This work is restricted to the aforementioned thermoplastics for two primary reasons: 1) Due to the nature of thermoplastics, they can be annealed and/or melted using MD to relax the structure without concern about significant changes to the structural properties of the materials (as opposed to thermosets, which are irreversibly cured). 2) There is a limit to the number of polymers that can be studied, given finite computational resources. By focusing only on these thermoplastics, there will perhaps be some observations that may apply more broadly to thermoplastics in general: due to the significant differences between the three thermoplastics selected, the findings that hold across all three polymers are more likely generalizable to a large number of other thermoplastics than if three very similar thermoplastics were to be studied. Although several results detailed in this work will likely apply to many other thermoplastics, because only three polymers are being studied here, this work will refrain from making broad claims about thermoplastics in general.

1.5 Outline of the Remainder of the Dissertation

Chapter 2. Initial Observations begins with some critical technical details necessary for understanding all proceeding results, particularly molecular dynamics and LD, then shows some results that are highly disparate from findings for other classes of materials. In particular, the PR of the modes in a-PMMA is found to be unusually low, and IF modes are observed, even in a relaxed supercell. These anomalies raise five primary questions and corresponding hypotheses that form the basis of this dissertation and which are listed at the end of the chapter.

Chapter 3. Analysis Techniques and Methods provides some further technical details that, while not necessarily critical for understanding the broad implications of this work, will allow for further insight and understanding of the results. These details include methods for generating 1) a monatomic amorphous supercell and 2) an empirical interatomic potential based on fitting results from Density Functional Theory. The chapter also describes the basics of the Greek-Kubo and GKMA methods.

Chapter 4. Localization and Thermal Conductivity of Normal Modes in Amorphous investigates the relationship between mode localization and TC in amorphous polymers. Two new methods are proposed to describe mode localization, and the relationship between modal TC and mode localization according to both PR and these new descriptors is investigated. The findings of this chapter are rather unexpected based on previous findings in the literature, and some possible explanations are presented.

Chapter 5. Imaginary Frequency Modes in Amorphous Polymers applies many of the same methods used in *Chapter 4* to IF modes. The nature of these modes, their localization, and

their TC is discussed. Here again, the results were not anticipated and result in many open questions.

Finally, *Chapter 6. Conclusions* provides some concluding remarks summarizing the work presented here and offers some further avenues of inquiry, both theoretical and experimental.

CHAPTER 2. INITIAL OBSERVATIONS

This chapter describes the methods and findings that have motivated the work in subsequent chapters. The chapter starts with a discussion of the critical technical details of how results were calculated, then describes some initial results obtained from simulations of a-Ge and a-PMMA. From there, several questions are raised from the initial results, each with an accompanying hypothesis. Answering the questions raised at the end of this chapter comprises the main subject matter of the remaining chapters.

2.1 Methodology

All original results presented in this dissertation are obtained via calculation/simulation, with heavy utilization of molecular dynamics (MD) simulations and LD calculations. While more will be said about these methods and MD in particular in *Chapter 3. Analysis Techniques and Methods*, all the necessary details to understand the major findings of the initial results discussed in this chapter are provided here.

2.1.1 Details of Molecular Dynamics Simulations

All MD simulations described herein were carried out using the open-source Large-scale Atomic/Molecular Massively Parallel Simulator (LAMMPS) MD software [122]. LAMMPS is an open-source software package that can be modified by the user, which will be of great importance in subsequent sections of this work.

MD is a method whereby the trajectory of one or several atoms is propagated forward in time in real-space according to Newton's laws of motion. Atoms are modeled as rigid

point-particles that experience forces based on the location and type of neighboring atoms in the system.

Two primary inputs are required for any MD simulation. First, one must have a means of describing the forces between atoms, typically accomplished by using an interatomic potential, which is a mathematical expression that describes energy/forces between atoms as a function of atomic species and the atoms' relative positions. Second, one must specify the initial conditions of the system by providing a description of where each atom is located in space and its velocity. Although describing the locations of the atoms straightforward in crystal with a simple unit cell, it is not immediately obvious how best to position the atoms in an amorphous material.

2.1.1.1 Interatomic Potentials

To run a "classical" MD simulation requires an empirical interatomic potential (EIP). EIP's are functions that may take many forms, but they are generally fitted to results from either experiments or first-principles calculations. A well-fitted EIP should in theory reproduce physical properties of the material it is modeling. In practice, fitting EIP's is quite challenging, and even highly-sophisticated EIP's are fitted to accurately reproduce only a subset of material properties (e.g. accurately describing elastic properties of Si, but failing to correctly reproduce surface energies [123]). Simulations employing an EIP are readily parallelized and their computational cost scales linearly with the number of atoms in the simulation. MD simulations utilizing EIP's can include the full anharmonicity of the atomic interactions, allowing for an explicit treatment of disorder, but are generally limited by their classical nature, i.e. they cannot reproduce quantum mechanical phenomena, although

other methods have been developed to account for these effects [124]. For the systems studied here, their size and simulation times required for a converged TC prediction precludes the direct use of first-principles, necessitating a reliance on EIP's.

The simulations described herein have used two different sets of potentials. Models of amorphous polymers implemented the DREIDING force field, a sophisticated EIP that can be used "for predicting structures and dynamics of organic, biological, and main-group inorganic molecules" [125]. The DREIDING potential has been tested against real-world systems in numerous cases for organic molecules, including predictions of crystal structure [125], rotational energy barriers [125], conformational energies [125-129], and binding energies [128, 130, 131], with agreement ranging from satisfactory to excellent.

Models of a-Ge used a hybrid potential comprised of a linear sum of the Tersoff [132], Buckingham [133], and damped-shifted force Coulomb [134] (hereafter referred to as TBC) potentials; while the form of each potential was unaltered, the specific parameters of the potential were fit using a genetic algorithm-based method [135]. More details of the fitting procedure can be found in *Chapter 3. Analysis Techniques and Methods*.

2.1.1.2 Generating Amorphous Structures

While an accurate EIP is a key component to an accurate MD simulation, it is not the only necessary factor for accurately reproducing experimental results. Of equal importance is the structure being simulated, and in particular, ensuring it accurately represents the structure of an actual sampled used in an experiment. The reasons are apparent if one considers simulating different allotropes of an otherwise chemically identical compound, or in the extreme case, crystalline vs. amorphous materials. In such cases, the EIP to

describe the materials may be the same, but differences in structure alone will lead to drastically different material properties.

Creating a MD crystalline structure (i.e. creating a list of atomic positions for atoms in a crystal) is straightforward. One need only identify atomic coordinates for a single unit cell, then tesselate the cell to fill the simulation domain. Selecting atomic coordinates for an amorphous structure is considerably more challenging, as by definition, there is no long-range order to amorphous structures.

One successful approach employed to generate such structures is the melt-quench procedure [136], whereby a MD simulation is carried out in a crystalline material, which is then melted and quickly quenched, freezing the atoms in a random, amorphous configuration. While such an approach is certainly useful, the method requires performing a MD simulation, which in turn requires an accurate EIP[6]. However, in the case where an EIP is fitted, as is the case for a-Ge in this work, such structures were not available to use as inputs to density functional theory (DFT) – a first-principles method for obtaining a high-accuracy solution to the Schrödinger equation, yielding the charge distribution of electrons in a material. Instead, for the work described herein, a different method was used to generate small clusters of a-Ge. This newly-developed method uses a probabilistic approach to determine the position of atoms based on an amorphous material's radial distribution function (RDF), which in turn is determined from experiments. The RDF

[6]One way to run MD and ensure an accurate description of interatomic forces is to use DFT-based MD. In such a case, rather than use an EIP to describe interatomic forces, they are calculated at each timestep using density functional theory. Such calculations are quite expensive computationally however and as with other DFT-based methods, scale with N^3. They are therefore infeasible for MD simulations on a reasonably-sized supercell ($\gtrsim 10^3$ atoms), necessitating the use of an EIP instead.

measures the average number of neighboring atoms as a function of distance from a central atom. More about this method and the RDF will be discussed in *Chapter 3. Analysis Techniques and Methods*.

Accurately creating amorphous polymer structures is even more challenging: not only are polymers polyatomic, but they are also comprised of varying individual units that consist of different atom types, functional groups, etc., all of which increases the heterogeneity of the structure substantially. Thus, more sophisticated methods are needed to accurately produce such amorphous structures. Fortunately, prior work has been done to create a tool capable of building such structures, namely the Polymer Modeler [98]. All polymer simulations in this work are carried out on structures created using the Polymer Modeler and were then allowed to relax using LAMMPS. The specifics of how each polymer supercell was created is detailed in *Appendix A. Commands used to Generate Amorphous Polymer Supercells via the Polymer Modeler*. Once a relaxed structure and an accurate EIP to describe it are obtained, one can begin to study the properties of the material using various computational methods.

2.1.1.3 Example Relaxation Procedure for Poly(methyl methacrylate) - PMMA

This section describes the relaxation procedure applied to a-PMMA. As discussed in the previous section, the polymer was relaxed in LAMMPS using the DREIDING potential, with the initial structure being determined from the Polymer Modeler code. The simulation domain was a cube 30.4 Å on each side with periodic boundary conditions. The a-PMMA consisted of 4 isotactic linear chains of 50 monomers each; given that a single monomer is

comprised of 15 atoms, and accounting for the 2 H atoms at the end of each polymer chain, the total number of atoms in the supercell is 3008.

The relaxation process involved several successive minimizations via the LAMMPS *minimize* command. This minimization process involves LAMMPS iteratively computing the local energy gradient (i.e., forces) for every atom and moving the atom some distance down the gradient. The process is repeated until the change in energy is below a specific tolerance value, or the process reaches a maximum number of iterations. For details of the specific LAMMPS commands used, see *Appendix B. Description of Relaxation Process for Amorphous Structures Created in the Large-Scale Atomic/Molecular Massively Parallel Simulator*. (The appendix also contains details of the relaxation applied to a-Ge, which was a very similar process.) After this series of minimizations, the atoms are simulated at a finite temperature using MD with a 1 fs timestep. It should be noted that a timestep of 0.1 fs is necessary to adequately resolve the dynamics of H atoms in the polymer when calculating its TC, however a timestep ~10x that necessary for accurate dynamics is considered sufficiently small for the purposes of structural relaxation, as an accurate atomic trajectory is unimportant [137]. The atoms are simulated using a constant atom number, volume, and temperature (NVT) ensemble. The temperature is controlled by means of a Langevin thermostat.

The atoms were first heated and held at 300 K for 1 ns, after which time they were cooled from 300 K to 0 K linearly over the course of 1 ns, at which point they were held at 0 K for an additional 1 ns. To ensure the structure was relaxed, the Langevin thermostat was removed so the atoms were operating under a constant atom number, volume, and energy (NVE) ensemble. If the atoms were in an unstable configuration, they would develop non-

zero velocities, through the conversion of potential energy (PE) into kinetic energy, and their position would change after some small (~10 fs) amount of time. However, in the simulations described here, after simulating the relaxed structure for an additional 100 ps, the atoms did not change position appreciably (<< 10^{-3} Å), and the temperature remained ~10^{-4} (effectively 0) K.

It is worth discussing this relaxation method further, as it will be important to demonstrate for some future calculations that the structure was indeed relaxed. This relaxation has been checked by several means, all of which lead to the conclusion that the a-PMMA supercell is indeed relaxed. As mentioned, the first test performed was to determine whether, after the polymer had been held for some time at 0 K, the atoms moved in the absence of a thermostat, which they did not. Next, the PE of the system throughout the relaxation process was plotted (see Fig. 4), and the results indicate that he polymer is in fact relaxed. To understand this conclusion, first note that while the PE drops quickly at first, by the time 1 ns has elapsed, the PE has leveled off. Next, as the polymer is cooled over the next ns, the PE follows a linear trend, remaining proportional to temperature. This trend indicates no structural changes are occurring, which is what would be expected if there were instabilities in the structure; in such a case, one would observe step changes in the PE. At 0 K, the PE fluctuates around 0 with a magnitude on the order of 0.01 kcal/mol (compare this with an energy of 3000 kcal/mol at 300 K). These fluctuations exist both while a Langevin thermostat is applied (from 2 to 3 ns in the figure), and after it is turned off (the final 100 ps in the figure, during which the system was operating under an NVE ensemble).

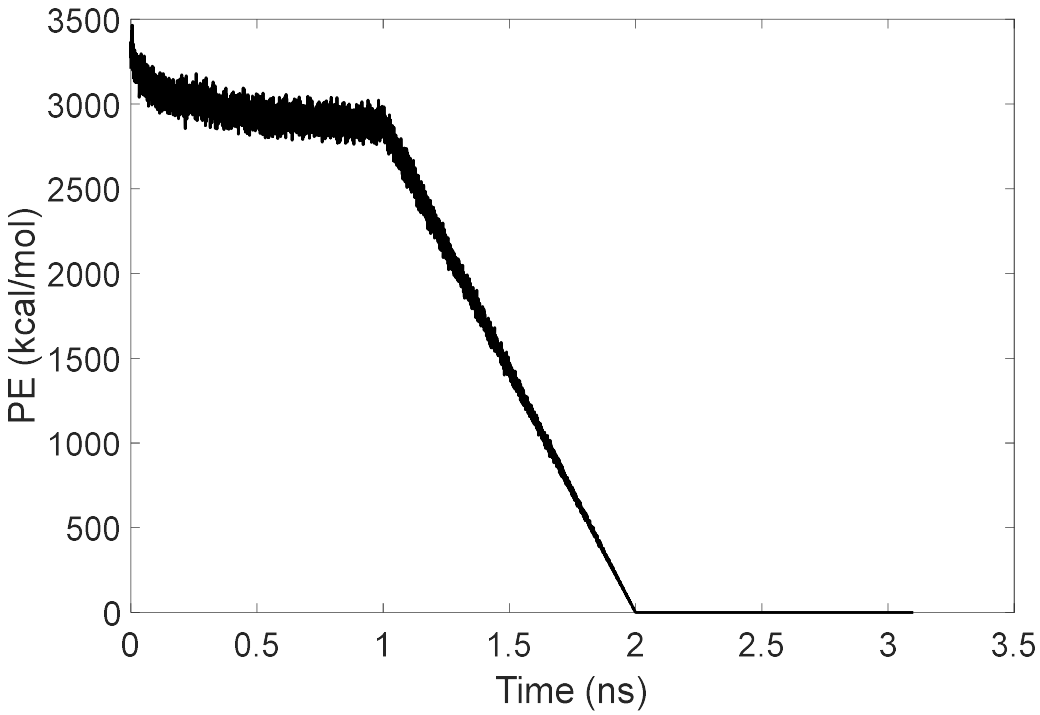

Figure 4. Potential energy vs. time for the PMMA relaxation process. The polymer was held at 300 K for the first ns, after which it was cooled to 0 K and held at that temperature.

Several different relaxation methods in LAMMPS were investigated. However, other methods yielded structures with a higher relative PE and an increased number of IF modes compared to the structure obtained from the relaxation method above. Briefly, two alternative relaxation processes used in failed attempts to further relax the structure were:

1) Increasing the annealing time by holding the structure at 300 K for a time period longer than 1 ns. In this case, the PE did not decrease any further, and after performing and LD calculation, a larger number of IF modes were observed compared to the best-case described above.

2) Increasing the annealing temperature from 300 to 800 K. In this case, the resultant PE of the final relaxed structure was much higher than the best-case, and there were more IF modes present.

It is suspected that this inability to obtain further relaxation is because the Polymer Modeler tool actually does well at creating a structure close to a local minimum energy-state (see *Appendix A. Commands used to Generate Amorphous Polymer Supercells via the Polymer Modeler*). If the polymer is heated at too high a temperature or for too long a time period, it consequently changes its structure, to the point where it actually relaxes to a higher-energy configuration. This finding is consistent with MD simulations run to determine the TC of a-PMMA. In such cases, when held at 300 K, atoms in the polymer began to "wander" after 1 ns (simulations were consequently limited to 900 ps), causing structural changes in the polymer. Before ~1 ns, the average (and maximum) displacement of the atoms is 1-2 Å, commensurate with the expected vibrational amplitude for atoms at room temperature. However, beyond 1 ns, displacements of ~4 Å were often observed.

With a stable structure obtained, the next step is to begin to analyze the thermal properties of the material. While some analysis of the bulk properties (i.e. the material's total TC) can be obtained from simple MD runs, of particular interest are the specific dynamics at play within the material, which is dependent on the vibrational modes of the material. Determining these modes necessitates the use of another method of analysis, namely, LD.

2.1.2 Lattice Dynamics

The second major tool (apart from MD) used to analyze normal modes and thermal properties of the materials is LD, which is a means by which atomic positions and velocities

can be decomposed into a linear superposition of unique vibrational modes. Understanding the physics of how these modes interact to transport heat in a material provides an additional level of insight into the dynamics of thermal transport beyond the results of a simple calculation of the material TC. The specifics of the method are described here.

Consider a collection of N atoms in a stable configuration at 0 K[7]. These atoms can be of one or multiple species and arranged in any configuration, crystalline or amorphous (or some mixture of the two). At low to moderate temperatures, the atoms will vibrate around their equilibrium location. These vibrations may be complex and appear random, but in fact follow strict rules regarding their excitation. The vibrations of the atoms can be collectively decomposed into $3N$ *normal modes*, which in superposition can completely describe the dynamics of the system. That there exist $3N$ such modes is because for a given atom, one can write 3 independent equations of motion (1 each in the x-, y-, and z-directions) for each atom in the system; LD is the means by which one can simultaneously solve all equations of motion. The resulting $3N$ solutions to the equations of motion are the $3N$ normal modes.

First, consider a well relaxed crystalline material with PE Φ. The PE can be written as a Taylor expansion around the equilibrium positions of the atoms as

[7]Actually LD techniques can still be applied in cases where the atoms are not stable and/or are not at 0 K. However, such situations are less common and not pertinent to this dissertation; this work will be restricted to relaxed structures at 0 K. Boundary conditions also need not be periodic, although for all cases disused in this work, they are.

$$\Phi = \Phi_0 + \sum_{i\alpha} \left.\frac{\partial \Phi}{\partial u_{i,\alpha}}\right|_0 u_{i,\alpha} + \frac{1}{2}\sum_{i,j}\sum_{\alpha,\beta} \left.\frac{\partial^2 \Phi}{\partial u_{i,\alpha}\partial u_{j,\beta}}\right|_0 u_{i,\alpha}\, u_{j,\beta} + \frac{1}{3!}\sum_{i,j,k}\sum_{\alpha,\beta,\gamma} \left.\frac{\partial^3 \Phi}{\partial u_{i,\alpha}\partial u_{j,\beta}\partial u_{k,\gamma}}\right|_0 u_{i,\alpha}\, u_{j,\beta} u_{k,\gamma} + \ldots \quad (4)$$

where Φ_0 is the PE at 0 K and $u_{i,\alpha}$ is the atomic coordinate of the i^{th} atom, in the α-direction.

At equilibrium, all first derivatives of energy with respect to position (i.e. forces) are by definition 0:

$$\left.\frac{\partial \Phi}{\partial u_{i,\alpha}}\right|_0 = 0 \quad (5)$$

The second derivatives are termed the second-order force constants:

$$\Upsilon_{ij,\alpha\beta} = \left.\frac{\partial^2 \Phi}{\partial u_{i,\alpha}\partial u_{j,\beta}}\right|_0 \quad (6)$$

Similarly, the third derivatives are third-order force constants:

$$\psi_{ijk,\alpha\beta\gamma} = \left.\frac{\partial^3 \Phi}{\partial u_{i,\alpha}\partial u_{j,\beta}\partial u_{k,\gamma}}\right|_0 \quad (7)$$

And so on. Equation (4) can therefore be rewritten for atoms at equilibrium as

$$\Phi = \frac{1}{2}\sum_{i,j}\sum_{\alpha,\beta} \Upsilon_{\alpha\beta} u_{i,\alpha} u_{j,\beta} + \frac{1}{3!}\sum_{i,j,k}\sum_{\alpha,\beta,\gamma} \psi_{\alpha\beta\gamma} u_{i,\alpha} u_{j,\beta} u_{k,\gamma} + \ldots \quad (8)$$

For small displacements around equilibrium, higher order terms can be neglected, and the total PE is approximated as

$$\Phi = \frac{1}{2}\sum_{i,j}\sum_{\alpha,\beta}\Upsilon_{\alpha\beta}u_{i,\alpha}u_{j,\beta} \tag{9}$$

For N atoms, this equation yields $3N$ linearly independent equations, which can be cast as

$$m_b\ddot{\mathbf{u}}\begin{pmatrix} l \\ b \end{pmatrix} = -\sum_{b'l'}\Upsilon\left(bl;b'l'\right)\cdot\mathbf{u}\begin{pmatrix} l' \\ b' \end{pmatrix} \tag{10}$$

where m_b is the mass of atom b, $\ddot{\mathbf{u}}\begin{pmatrix} l \\ b \end{pmatrix}$ is the acceleration vector of atom b in unit cell l, $\Upsilon\left(bl;b'l'\right)$ is the 3×3 force constant matrix describing the interactions between atoms bl and $b'l'$, $\mathbf{u}\begin{pmatrix} l' \\ b' \end{pmatrix}$ is the displacement of atom $b'l'$ from its equilibrium position, and the summation is over all atoms in the system. First, assume a harmonic, plane-wave solution (which is the solution for a simple crystal) to Eq. (10); one can then sum over all modes with frequencies $\omega\begin{pmatrix} \mathbf{k} \\ \nu \end{pmatrix}$:

$$\mathbf{u}\begin{pmatrix} l \\ b \end{pmatrix} = \frac{1}{\sqrt{m_b N}}\sum_{\mathbf{k}}\mathbf{e}_b\begin{pmatrix} \mathbf{k} \\ \nu \end{pmatrix}\exp\left[i\left(\mathbf{k}\cdot\mathbf{r}_0\begin{pmatrix} l \\ b \end{pmatrix} - \omega\begin{pmatrix} \mathbf{k} \\ \nu \end{pmatrix}t\right)\right] \tag{11}$$

where $\mathbf{r}_0\begin{pmatrix} l \\ b \end{pmatrix}$ is the equilibrium position of the b^{th} atom in the l^{th} unit cell, $\mathbf{e}_b\begin{pmatrix} \mathbf{k} \\ \nu \end{pmatrix}$ is the eigenvector describing the direction of motion for atom b for the mode described by $\mathbf{k}$ on dispersion branch ν, and t is time. (Note that in Eq. (11), i is not an index, but rather $i = \sqrt{-1}$.)

Substituting Eq. (11) into Eq. (10) yields

$$\omega^2\begin{pmatrix}\mathbf{k}\\ \nu\end{pmatrix}\cdot\mathbf{e}\begin{pmatrix}\mathbf{k}\\ \nu\end{pmatrix}=\mathbf{D}(\mathbf{k})\cdot\mathbf{e}\begin{pmatrix}\mathbf{k}\\ \nu\end{pmatrix} \tag{12}$$

Here, $\mathbf{D}(\mathbf{k})$ is the dynamical matrix, which in addition to containing information about the eigenvectors and frequencies of vibrational modes in the material also describes the stiffness of the material. It is given by

$$D_{\alpha,\beta}(bb',\mathbf{k})=\frac{1}{\sqrt{m_b m_{b'}}}\sum_{l'}\Upsilon_{\alpha\beta}(b0,b'l')\cdot\exp\left(i\mathbf{k}\cdot\left[\mathbf{r}_0\begin{pmatrix}l'\\ 0\end{pmatrix}-\mathbf{r}_0\begin{pmatrix}l\\ 0\end{pmatrix}\right]\right) \tag{13}$$

From here, one can further construct the density of states (DOS), calculate temperature-dependent heat capacity, etc. However, it is important to note that no information is provided about the TC of the individual modes, which arises due to the higher order terms that were neglected.

It is important to note here also that according to LD, when symmetry is broken, the solutions to the equations of motion have to change to reflect this breaking of symmetry, which results in a loss of periodicity of some modes (which results diffusons) and/or spatial localization (which results in locons). Another way to conceptualize the rationale for the existence of locons is that when an atom is distinct from all other atoms, it will require specially tailored solutions. If other atoms with similar characteristics are not close by, then these specially tailored solutions that are required to describe these locally unique atoms must themselves be localized. By understanding this effect of symmetry breaking, one can then identify what is likely to lead to a material system with a large fraction of locons.

The means by which LD methods are used to understand disordered materials is also slightly different from that used for crystals. In an amorphous material, one does not define

a unit cell, but rather treats the entire structure as a single supercell, allowing the use of SCLD by applying LD at the Γ point ($\mathbf{k}=0$) of the supercell. Thus, whereas the solutions to Eq. (12) are assumed to be plane-waves within the supercell for a crystalline material, they are not constrained as such for an amorphous material. If one makes this restriction (by applying it only at the Γ point), Eq. (13) reduces to

$$D_{\alpha,\beta}\left(bb',\mathbf{k}=0\right)=\frac{1}{\sqrt{m_b m_{b'}}}\sum_{l'}\Upsilon_{\alpha\beta}\left(b0,b'l'\right) \tag{14}$$

In this way, LD can be generalized to any material, even if it is not a simple, periodic structure. It should also be noted that for an SCLD calculation applied at the Γ point, all eigenvectors resulting from the calculation have real (i.e. not complex/imaginary) values [138].

For a relaxed structure, the dynamical matrix is symmetric and Hermitian, so it should yield real values for the frequency and eigenvectors of each mode. However, there is an interesting observation to make regarding the LD calculations of a-PMMA, namely the presence of IF modes. These modes are not typically found in stable, relaxed structures at 0 K; most references in the literature are to a single such mode with an IF, which corresponds to a transition state [139-147]. In such cases, all other modes in a system are found to have real frequencies (RF's) [139, 140]. One notable – and comparatively common – exception in which more than one IF mode is observed at a time is instantaneous normal mode analysis (INMA) [148]. INMA applies LD to atoms that are not at equilibrium, but rather at positions corresponding to those from a snapshot of a single instant from an MD run at a non-zero temperature. The technique is typically applied to

liquids, which have no “stable” atomic configuration, and IF modes (typically ~5-30% of the total modes [148-154]) show up in such cases.

Although there is scant discussion in the literature of LD calculations of amorphous supercells, some preliminary observations exist that raises the possibility of IF modes being present, even in the ground state. The first observation to make is simply the structure of the polymers themselves – as noted in Chapter 1, this work is limited to discussing thermoplastics and not thermosets. In such materials, the strength of the intramolecular bonds (i.e. covalent bonds within a single polymer chain) are roughly two orders of magnitude larger than intermolecular van der Waals and hydrogen bonding. This large disparity in forces, in combination with the different atomic species, orbital hybridizations, functional groups, etc. leads to a highly-asymmetrical potential energy surface (PES), which generally results in less innate stability within the material. Furthermore, as noted previously, after being held at elevated temperatures for a sufficient period of time, the polymer chains will begin to gradually “walk”, shifting the equilibrium location of their constituent atoms, particularly near the end of the chains. Finally, it is worth highlighting some results of Zhang & Luo [99], who have provided evidence of the effect of conformational changes in crystalline polyethylene chains on the TC. They observed that above 400 K, the volume of the polymer chains increases dramatically, and the TC drops by an order of magnitude along the direction of the chain. The interpretation provided by Zhang & Luo is that in such cases, some chain segments “flip” from an all-trans conformation to one in which there is some mixture of cis and trans units. They hypothesize that when this change happens, the kinks formed by this inconsistency in conformation of

the polymer units serves as an impediment to phonons that would otherwise conduct heat along the chain, resulting in a dramatic decrease in TC along the direction of the chain.

While the polymers studied in this dissertation do not include polyethylene, nor are they crystalline, it is possible that similar effects could occur. If this is indeed the case, one must consider the possibility of IF modes resulting from LD calculations that indicate a structural change in the polymer, such as a cis-to-trans monomer rotation.

Another possibility is that due to the unique nature of polymers, perhaps even at 0 K, their behavior is somewhat analogous to a liquid at 0 K (e.g. liquid helium), and some modes will always be IF modes, regardless of how well-relaxed the structure is. While this hypothesis is beyond the scope of this dissertation, the possibility is intriguing to consider.

All LD calculations in this work have been carried out using the General Utility Lattice Program (GULP) [155]. GULP allows one to determine all relevant information about the normal modes of a periodic supercell, including frequencies and eigenvectors. It also has built-in capabilities to handle both TBC and DREIDING potentials.

While LD can yield a mode with an IF, when plotting vs. frequency, IF modes are typically represented instead with negative values (i.e. a mode with $\omega = 10i$ THz will be depicted as having a frequency $\omega = -10$ THz), since the result of the LD calculation is a negative eigenvalue equal to ω^2. This dissertation will follow this same convention. Furthermore, there will at times be references to "high" and "low" frequency modes; in such cases – specifically in relation to IF modes – this refers to the magnitude of the frequency. Thus, an IF mode with $\omega = 20i$ THz would have a "higher frequency" than a mode with $\omega = 10i$ THz.

2.2 Initial Results

Presented here are some initial results of calculations that have motivated the research discussed in the remaining chapters of this work. Specifically, LD calculations performed for a-Ge and a-PMMA are discussed, with extra attention given to similarities and differences between the two materials.

The DOS of a-Ge and a-PMMA are plotted in Fig. 5 below. Note that IF modes in a-PMMA were indeed observed; consistent with previous literature, these modes are plotted on the negative frequency axis.

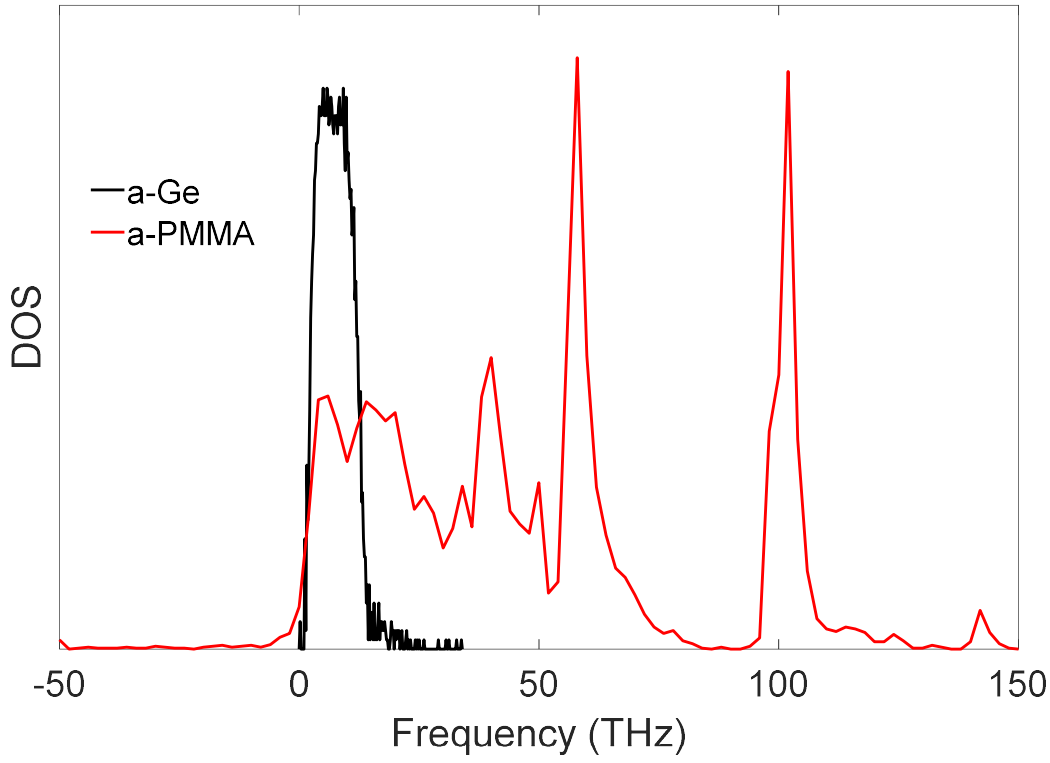

Figure 5. DOS of a-Ge and a-PMMA. Modes with an IF are plotted on the negative x-axis.

The PR of each mode vs. frequency is plotted in Fig. 6.

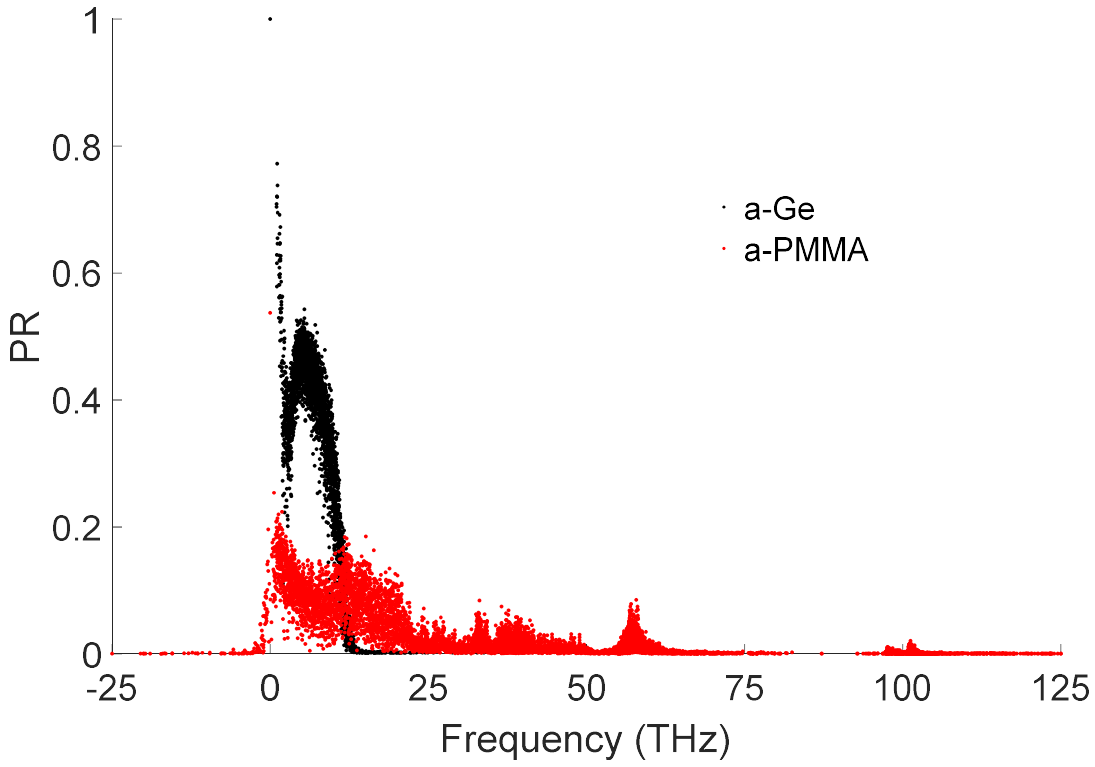

Figure 6. PR vs. frequency for a-Ge and a-PMMA.

The results in Fig. 6 are notable for several reasons. First, examining a-Ge, it is evident that in general, low-frequency modes are delocalized (i.e. their PR is $\gtrsim 0.1$), whereas high-frequency modes exhibit a much higher degree of localization. One notable exception is the presence of partially localized modes with PR $\lesssim 0.3$ at low frequencies (i.e. < 10 THz), a result which is unusual, even for amorphous materials [3]. It has been observed that in some systems, mode localization is an artifact of a small supercell (typically, $\lesssim$ 1,000 atoms) [60]; the anomalously low PR of low-frequency modes observed in a-Ge may be one such case.

Even more striking are the results for a-PMMA, in which 126/9024 (1.40%) of the modes have an IF; interestingly, as discussed in Section *2.1.1.3 Example Relaxation Procedure for Poly(methyl methacrylate),* this structure is relaxed, at least to a meta-stable state (i.e.

atoms do not move at 0 K), so the presence of IF modes is somewhat unexpected in this regard. However, from another perspective, IF modes are perhaps not entirely surprising; as mentioned, one could anticipate such modes to be present and correspond to conformation changes in the polymer. It should be noted, however, that the mere presence of IF modes does not necessitate observing any actual conformation changes.

Apart from the presence of IF modes, the other striking feature of the modes in a-PMMA is the extremely high degree of localization of the modes. The vast majority of the modes are what would typically be considered locons (i.e. PR < 0.1), and virtually every mode has a PR < 0.2. Such a high degree of localization is quite surprising and, does not appear to have been observed in simulations of any other class of bulk material. Localization vs. frequency typically follows the same general trend exhibited by a-Ge (though typically without the partial low-frequency localization observed here). The observance of *any* low-frequency localized modes would be notable. That *every* mode appears at least partially localized is quite unexpected.

Furthermore, when viewing these modes, they appear delocalized: the eigenvectors are often spread across much if not all of the supercell, even for modes with low PR's. Consider for example the modes shown below in Fig. 7.

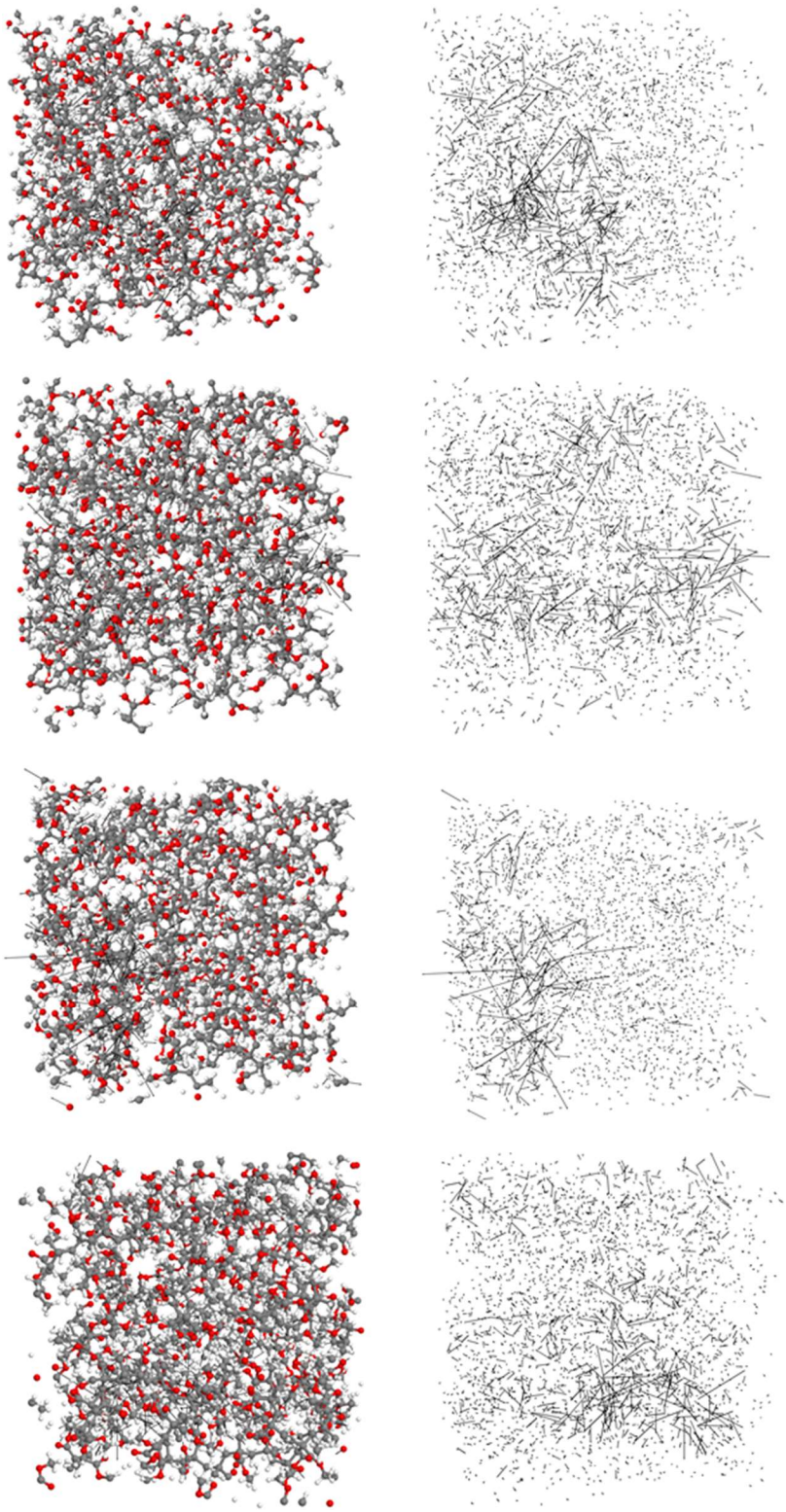

Figure 7. Low-PR modes in a-PMMA. C shown in gray, O in red, and H in white, with the eigenvectors shown in black. Atoms removed in figures on the right for clarity. The PR of each mode from top to bottom is 0.029, 0.033, 0.038, and 0.037.

While some degree of localization is evident, the modes shown here still clearly consist of atoms that are excited across much of the supercell, despite the fact that the PR of each mode is ≤ 0.05 – well below the traditional PR cutoff for locons. This result in and of itself is unusual and not one that has been discussed previously in the literature. No other bulk material has been shown to have such low-PR, low-frequency modes; that these modes actually appear delocalized is even more intriguing and leads to several questions.

2.3 Remaining Questions

The presence of IF modes in a-PMMA, as well as the anomalously low PR of all the modes has led to the definition of several fundamental questions that will define the scope of the remainder of this work. This section will define five over-arching questions and provide an initial hypothesis for each. After further describing the methods used in *Chapter 3. Analysis Techniques and Methods*, the remainder of this dissertation will be devoted to answering the five questions listed here.

One motivation for these questions is whether or not the findings for a-PMMA hold for other amorphous polymers, which will be tested for by answering the questions outlined below not only for a-PMMA, but also for a-PS and a-PVC. While this work expressly does not attempt to generalize the results beyond these materials, it would not be surprising if many of the findings here apply broadly to other thermoplastics. Furthermore, this work is restricted to thermoplastics (see Section *1.4 Thermal Transport in Amorphous Polymers* for a rationale for this limitation), but the same questions can and should be asked of thermosets as well.

2.3.1 Question 1: The Persistence of Mode Localization in Different-Sized Supercells

The first question is a preliminary one, but one that is important to answer before proceeding with any further analysis. As noted previously, mode localization can be an artifact of a small supercell [60], and in such cases, were one to study a larger supercell, the average PR of the modes would be higher. Thus, the first question is simply:

> *Does the low average PR observed in a-PMMA persist across different supercell sizes, and is this also the case for the other amorphous thermoplastics in this study?*

This degree of localization is hypothesized to be an inherent property of amorphous polymers: localization itself is already an inherent property of disordered materials, and there are additional factors that could lead to a further increase in degree of localization. In the case of polymers, due to 1) the strong covalent bonds along polymer chain backbones and the much weaker bonds between chains and 2) the fact that these chains are in an amorphous configuration (i.e., there is significant inhomogeneity in both bond strength and stereochemistry), it is hypothesized that a greater degree of localization will persist, regardless of polymer type or supercell size. In other words, due to the highly asymmetric and inhomogeneous PES, it is expected that due to the highly asymmetric PES, the low PR measured is an inherent property of amorphous polymers (and more specifically, the thermoplastics in this study), and not simply an artifact of supercell size.

2.3.2 *Question 2: The Anomalously Low Participation Ratio of Normal Modes in Amorphous Polymers*

As noted in Question 1, according to PR, it appears the modes in a-PMMA are almost exclusively locons (and presumably in other polymers too). Assuming this localization is not an artifact of supercell size, many questions remain regarding the modes in amorphous polymers:

> *With most modes having a low PR ascribed to locons, are the modes actually localized, or would an alternative descriptor indicate they are delocalized?*

It appears at first glance that the modes in a-PMMA are localized, since their PR's are in fact low, but from viewing the eigenvectors for these vibrations, many of them do not look completely localized. While these modes are energetically localized based on the PR, it is hypothesized that an alternative descriptor of localization based on how the modes are confined spatially or in terms of different polymer chains may elucidate more information about the degree/aspects of how these modes are localized. In particular, an alternate descriptor may indicate the modes are in some way delocalized.

2.3.3 *Question 3: The Contribution of Localized Modes to Thermal Conductivity*

Ultimately, the behavior of normal modes in polymers as they relate to TC is of primary interest. Thus, while the high degree of localization is in and of itself intriguing, even more interesting is understanding the relationship between how localized a mode is and its total contribution to TC:

Do localized modes contribute to TC in the amorphous thermoplastics in this study?

Based on the results of Lv & Henry [6, 12], it seems reasonable to predict that locons will be a significant carrier of thermal energy in amorphous polymers, especially since (according to PR) they are the predominant mode type. However, such a result would still be surprising, as most work to this point has indicated that locons have a small/negligible contribution to TC. Furthermore, it is hypothesized that there will be a positive correlation between a mode's PR and the magnitude of its TC, consistent with Lv & Henry's results.

2.3.4 Question 4: The Nature of Imaginary Frequency Modes

Next, consider IF modes. In particular, though existence of IF modes was anticipated, there remains the question of *what* these modes actually are:

Do IF modes correspond to conformation changes in the studied thermoplastics? If not, is there any evidence of some other structural change between metastable states occurring?

The IF modes are hypothesized to correspond to conformation changes, consistent with Zhang & Luo's [121] identification of such instabilities in polyethylene chains.

2.3.5 Question 5: The Contribution of Imaginary Frequency Modes to Thermal Conductivity

Finally, as with highly localized modes, the question exists whether or not IF modes can in fact contribute to the TC of amorphous polymers. Because these modes may be some

change to the structure of the polymer, perhaps they do not play an active role in transporting heat and it is possible to simply neglect them, i.e.:

> *Do IF modes contribute to TC in the amorphous thermoplastics in this study?*

Since the polymer chains are disordered already, unlike Zhang & Luo's study [121] where the conformation flips have bene shown to have a dramatic effect on TC, in the case of an amorphous polymer, IF modes are predicted to be conformation changes that do not affect TC. Therefore, the impact of IF modes is at most small, and possibly negligible. It is possible however that these modes have more significant contributions to TC – commensurate with the RF modes in the polymer.

These questions will be answered in the next few chapters of this dissertation. However, first further detail is provided of some of the methods used to set up the simulations and calculations of the TC of normal modes. Following that description, this dissertation will delve into what the methods show about vibrational modes in amorphous polymers, and specific focus will be given to answering the aforementioned questions and testing the corresponding hypotheses.

CHAPTER 3. ANALYSIS TECHNIQUES AND METHODS

This chapter begins with a description of how MD simulations – simulations which evaluate the motion of atoms over time – are initialized. There is a particular focus on the interatomic potential used to describe the PES in the material and on the atomic structure of the material. The accuracy of both these variables is critical to obtaining meaningful results from MD.

This chapter will then delve into the details underpinning the means used to determine the TC contributions of individual vibrational modes, namely the Green-Kubo Modal Analysis (GKMA) method [6, 12, 13, 156-158]. GKMA utilizes a LD modal decomposition of individual atomic velocities to ascribe some fraction of the total heat flux in a material to each mode or group of modes; this method has been developed and validated elsewhere [6, 12, 13, 156, 157] and is central to the entirety of this dissertation.

3.1 Methods to Initialize a Molecular Dynamics Simulation

As noted in Chapter 2, there are two critical components to a MD simulation: an accurate EIP and an accurate atomic structure. The methods used to generate both of these components are discussed here.

3.1.1 Creating Phonon-Optimized Empirical Interatomic Potentials

There are many instances where generating a material's structure and EIP is simple and straightforward. In the case of structure, one can easily generate an accurate crystal structure of any size given the basis set and size of the simulation domain. In the case of an EIP, one could use an existing potential such as Lennard-Jones [100] or Tersoff [101],

or use DFT to determine the interatomic forces at every timestep. However, there exist many situations in which the structure, EIP, or both are not readily available and must instead be generated from scratch. Of particular relevance to this work are situations in which the structure is not well-defined, such as amorphous materials, or the EIP does a poor job of predicting accurate thermal properties (e.g. TC). In such cases, one must generate the structure and/or potential from some combination of first-principles and experimental results. What follows is a description of how both EIP's and amorphous structures were generated for simulations of a-Ge.

As the name suggests, EIP's are empirical; as such, their functional form does not come from first principles but rather is fitted to the PES of a material. The goal of any EIP should be an accurate description of interatomic energies and forces, such that the MD simulation in which the potential is used accurately reproduces real-world properties, such as lattice constant and lattice energy [123], elastic modulus [123], TC [159], or molecular conformation [125]. In practice however, it can be challenging to reproduce mechanical, thermal, and chemical (among other) properties simultaneously, and potentials are often optimized to accurately reproduce a specific subset of properties, such as the Tersoff potential accurately reproducing elastic properties of silicon while sacrificing accuracy in describing its surface energy [123].

One approach to optimizing potentials is to choose a particular functional form and fit the parameters of the function to a set of training data. This is the approach used in this work to generate potentials to describe a-Ge.

The method used herein is termed the Phonon Optimized Potentials (POPS) method [135]. POPS is both a methodology and general philosophy with tenets for how one can approach

the problem of developing an EIP specifically intended for describing phonons (and more broadly, normal modes in general). POPS fits parameters to a training set using a genetic algorithm (GA), which iteratively refines parameters in a potential until either the error between the values produced by the objective function and the training data drops below some threshold or the algorithm reaches a maximum number of iterations. While the specifics of this process are not the focus of this dissertation, more information about GA's can be found in Coley's *An introduction to genetic algorithms for scientists and engineers* [102].

An important component of a GA is the training data to which the parameters in the function are fit; the potentials described here have been generated by fitting to results from DFT. While DFT allows for highly accurate solutions to the Schrödinger equation, the method is typically limited to at most a few hundred atoms, as computational costs scale with the third power of the number of electrons/atoms; MD simulations utilizing EIP's on the other hand scale linearly with number of atoms. The general method employed here is to use DFT to simulate many thousands of small "nanoclusters" of the material in question (in this case, 64-100 atom clusters of a-Ge), outputting atom position, total system energy, interatomic forces, and stresses. These values are then used to train the EIP, whose parameters are optimized iteratively via the GA, until the function can accurately reproduce the DFT results. Once the EIP has been fitted, and it is no longer necessary to perform DFT calculations to obtain accurate results, the EIP can be employed in computationally tractable MD simulations with several orders of magnitude more atoms than DFT. While much more can be said about the use of GAs to generate fitted EIPs, the reader is referred to Rohskopf et al. [103] for a detailed explanation of the procedure invoked here.

3.1.2 Generating Amorphous Structures

Of equal importance to an EIP is the structure being simulated. Generating a crystalline structure (i.e. creating a list of atomic positions for atoms in a crystal) is straightforward. However, selecting atomic coordinates for an amorphous structure is considerably more challenging, as by definition, there is no long-range order in amorphous structures. One successful approach employed to generate such structures is a melt-quench procedure[104-107], whereby an MD simulation is carried out in which a crystalline material is melted and quickly quenched, freezing the atoms in a random, amorphous configuration.

Other methods have also been developed to generate amorphous structures, but they are not without their own drawbacks. For example, many methods rely on using an existing interatomic potential to modify an existing crystal structure [108, 109]. More sophisticated methods such as Reverse Monte-Carlo have also been proposed [110-112], however the method is inherently more sophisticated and much more difficult to implement than the method described here. This newly-developed method, which was also used to create small clusters of a-Ge for the aforementioned DFT calculations, is the focus of this section.

There are several means by which one may describe the structure of an amorphous material. One such descriptor is the radial distribution function (RDF), $g(r)$, which measures the average number of neighboring atoms as a function of distance, r, from a central atom. This quantity is normalized by the average density of the material, such that

$$g(r) = \frac{\text{local density}}{\text{bulk density}} = \frac{dn}{4\pi r^2 dr}\frac{1}{\rho} \tag{15}$$

where n is the number of atoms and ρ is the bulk density. The RDF measures the average number of atoms in a thin shell of width dr at a distance r from any central atom and therefore describes the local density (normalized by the bulk density) in the neighborhood of a central atom as a function of distance from that atom. A fictitious example RDF can be found in Fig. 8a below. Note that for small values of r, $g(r) = 0$, implying atoms have some minimum spacing between them; at large values, $\lim_{r \to \infty} g = 1$, implying the average density far from a central atom is simply the bulk density of the material, which must be true for an isotropic material. In between these limits, various nearest neighbor peaks can be observed; typically, the first nearest neighbor peak has the largest maximum value for the RDF.

As mentioned previously, it is often desirable to create an amorphous structure that satisfies a particular RDF, as the RDF is essentially a measure of the short-order range of atoms in the material. Though determining the RDF of a structure given atomic position is straightforward, the reverse problem of generating an amorphous structure based on an RDF is a considerably more challenging task. It is worth noting that unlike crystals, in an amorphous structure, the location of the atoms is by no means unique, and there exist myriad structures with the same RDF. Because the amorphous structure is therefore not deterministic, a probabilistic approach is taken to generate an amorphous structure from an RDF, i.e. atoms are placed with some degree of randomness, but probabilities are weighted in such a manner that the resulting structure satisfies the target RDF. The method is described in the following paragraphs, and a two-dimensional version of the procedure is illustrated in Fig. 8.

1. First, a domain is initialized with a probability field such that there is an equal likelihood of placing an atom at any location within the domain (Fig. 8b). Thus, the probability of placing an atom at some location, $\mathrm{P}(x,y,z)$ is equal to the probability of placing an atom at any other location, i.e. $\mathrm{P}(x,y,z)=\mathrm{P}(x',y',z')$. In the algorithm, this method is implemented by discretizing the entire domain that is to be filled, assigning a non-normalized probability value of $\mathrm{P}_{\mathrm{raw}}(x,y,z)=1$ at every point, then normalizing each probability by the sum of raw probabilities at every point, i.e. $\mathrm{P}(x,y,z)=\dfrac{\mathrm{P}_{\mathrm{raw}}(x,y,z)}{\sum_x\sum_y\sum_z \mathrm{P}_{\mathrm{raw}}(x,y,z)}$.
2. The first atom (atom 1) is placed at a random location (because $\mathrm{P}(x,y,z)=\mathrm{P}(x',y',z')$).
3. The probability of placing a subsequent atom at a distance r from atom 1 is permanently modified by multiplying the existing probability field by $g(r)$ (Fig. 8c, 8d). In other words, in the neighborhood of the newly located atom, $\mathrm{P}_{\mathrm{raw,new}}(x,y,z)=\mathrm{P}_{\mathrm{raw,old}}(x,y,z)\,g(r)$, where r is the distance from the newly-placed atom to the location for which $\mathrm{P}_{\mathrm{raw}}$ is being modified. Thus, the chance of placing an atom immediately next to an already-placed atom (i.e. within the minimum interatomic spacing) will be zero (because $g(r)=0$ for small r), while the probability of placing an atom far from the recently-placed atom remains the same (i.e. the probability is multiplied by $\lim_{r\to\infty} g(r)=1$). The raw probabilities are re-normalized after each atom placement.

4. When placing a second atom, the modification of the probability field around atom 1 remains intact, even as the probability of placing an atom near atom 2 is modified (Fig. 8e).
5. Atoms continue to be added to the domain (Figs. 8f & 8g) until the desired density (i.e. the bulk density) is achieved (Fig. 8h).

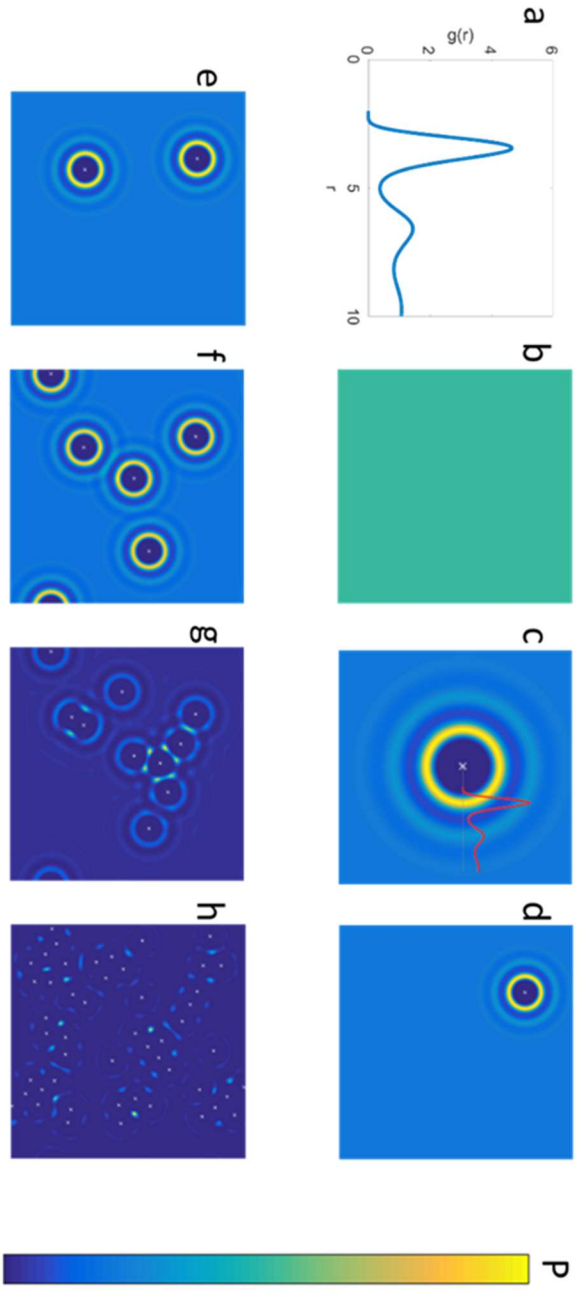

Figure 8. Illustration of atom-placement method. Atom locations depicted with a small white marker, and the normalized probability is shown in color – dark blue represents a probability of 0, while the maximum probability for any given step is shown in bright yellow. From the top left: (a) Target RDF used to generate the structure (b) The domain is initialized with a uniform probability field (c) Zoomed in illustration depicting the effect of placing an atom on the nearby probability field (target RDF shown in red) (d) Probability field after placing a single atom (e) after placing 2 atoms (f) after placing 5 atoms (g) after placing 10 atoms (h) after placing 50 atoms.

When two atoms are placed near each other, their effect on the probability of placing additional atoms in regions where they both alter the probability field interferes multiplicatively, i.e. $\mathrm{P}_{\mathrm{raw,new}}\left(x,y,z\right)=\mathrm{P}_{\mathrm{raw,old}}\left(x,y,z\right)g\left(r_{\mathrm{atom1}}\right)g\left(r_{\mathrm{atom2}}\right)$. As an example: if an atom with a maximum RDF $g\left(r\right)=3$ at the nearest neighbor peak were to be placed in the domain, the probability of placing a subsequent atom within the nearest neighbor ring of the original atom is 3x higher than the probability of placing an atom in an empty region of the domain far from the original atom. (In Fig 9c., this would correspond with a 3x likelihood of placing an atom at a given location within the bright yellow ring as compared to placing it at some location in the light blue space far from atom 1.) If a subsequent atom is then placed close to the first one, such that the nearest neighbor rings overlap, the probability of locating a third atom at a location where the nearest neighbor rings of the first two atoms overlap would thus be 9x the probability of locating an atom in empty space. The effects of this interference are most apparently in Fig. 8g.

Note that due to the increased likelihood of placing an atom in a high-probability location (e.g. in the nearest neighbor ring), the relative probability of locating an atom far from other atoms (i.e. in the "empty" part of the domain) decreases. Thus, although the chance of placing an atom in empty space in, e.g. Fig. 8f has not been altered directly, it has indirectly been reduced, as the chance of instead placing atoms close to already-placed atoms has increased. In other words, for a location far from the most recently-placed atom, $\mathrm{P}_{\mathrm{raw}}\left(x,y,z\right)$ remains unaltered, but the normalization factor will change.

Although perhaps not obvious or expected *prima facie*, agreement between the target RDF and the calculated RDF of the generated structure is quite good in both the two- and three-

dimensional cases. Fig. 9 shows the result of running the above algorithm in 2-D, while Fig. **10** shows an experimentally measured a-Ge target RDF[113] and resulting RDF after using the algorithm to generate the atomic positions.

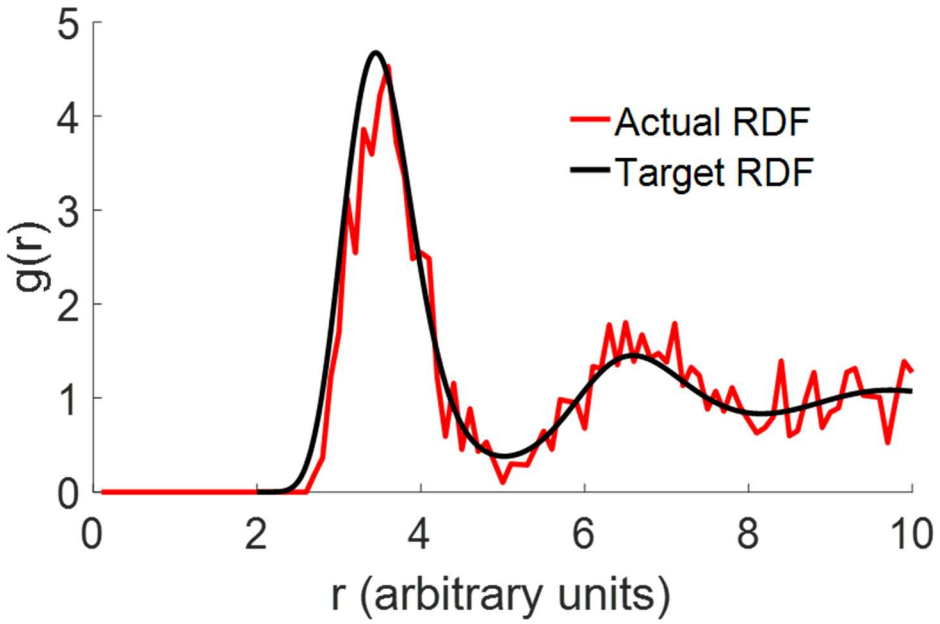

Figure 9. Comparison between a simple target RDF, and RDF of structure generated in 2-D using the procedure outlined above.

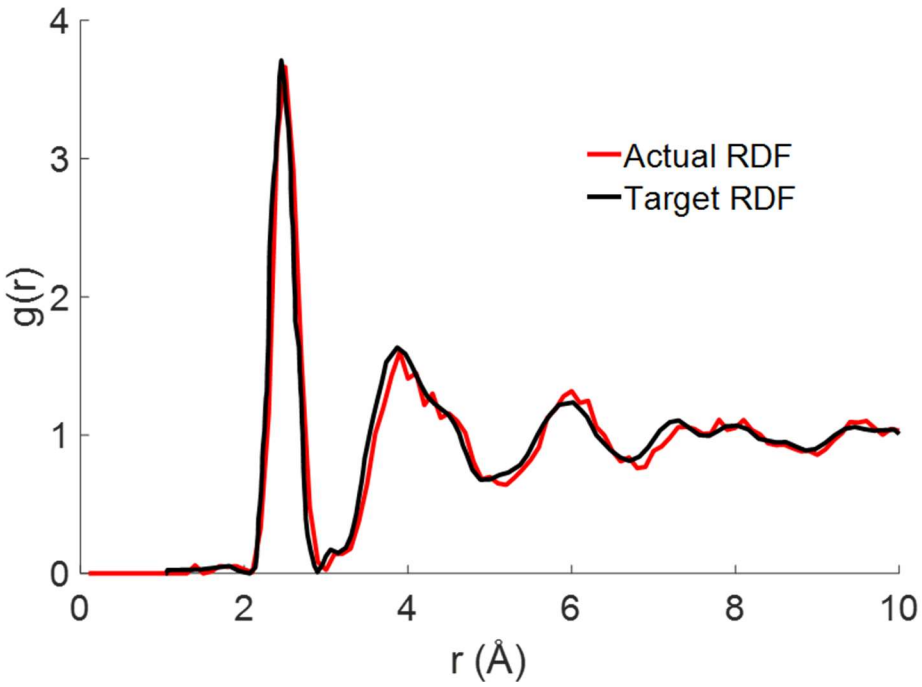

Figure 10. Comparison between experimentally measured (target) RDF of a-Ge, and the RDF of a structure generated using the procedure outlined above. Experimental results taken from [160].

This method has currently been developed only for use with single-component (i.e. monatomic) materials. Presumably, one could generalize this method to multi-component materials, however one would need to account for the multiple RDF's that exist not only between materials of the same atom type, but also between atoms of different types. This capability has not yet been developed however, so the aforementioned Polymer Modeler was used to generate the structure for the amorphous polymers studied in this work [98] (see *Appendix A. Commands used to Generate Amorphous Polymer Supercells via the Polymer Modeler*).

3.1.3 Results of Generating Phonon-Optimized Empirical Interatomic Potentials for Amorphous Germanium

After running the POPS algorithm and creating 1,000 atom a-Ge supercells with an appropriate RDF, for each potential, a melt-quench process was applied to the structure using MD[8]. The temperature of the system was first set to 5,000 K and held there for 1 ns in an NVT ensemble, after which the system was quenched to 300 K over 10 ps. (Ideally, the extreme rate of cooling causes the atoms to freeze in an amorphous, rather than crystalline state; many potentials still resulted in the atoms aligning in a crystalline configuration, and were consequently not used for subsequent calculations.) After cooling, the structure was held at 300 K using an NVT ensemble. The system was then allowed to run under and NVE ensemble for 500 ps; during this time, the PE of the system remained constant, indicating a lack of any structural changes. Finally, the system was relaxed to 0 K using a minimization process similar to that applied to a-PMMA (see Section *2.1.1.3 Example Relaxation Procedure for Poly(methyl methacrylate)*). Potentials of various forms were studied, including hybrid Morse-Born-Coulomb [161-163], the Spectral Neighbor Analysis Potential [114], and deep neural networks. While none of these potentials resulted in structurally stable a-Ge, a hybrid Tersoff-Born-Coulomb (TBC) [123, 162, 163] potential form did yield stable a-Ge. In total, three sets of parameters with the same functional form (but different parameter values, which varied significantly) were obtained, which were termed TBC-1, TBC-2, and TBC-3. See *Appendix C. Parameters for the Tersoff-Buckingham-Coulomb Potentials* for values of the parameters. In all cases, when

[8]Because of the melt-quench procedure, it was actually not necessary to start with the correct RDF, so long as the resulting RDF from the melt-quench procedure is accurate. Regardless, the DFT calculations the GA uses to create an EIP in the first place *do* rely on accurate amorphous structures.

an LD calculation was applied to the relaxed superlattices, the systems were found to have all RF modes.

While this work is focused on studies of the TBC-1 potential, some limited results for TBC-2 and TBC-3 potentials are shown, in particular the results of a melt-quench process for a-Ge supercells. The resultant RDF for each potential can be found in Fig. 11 below.

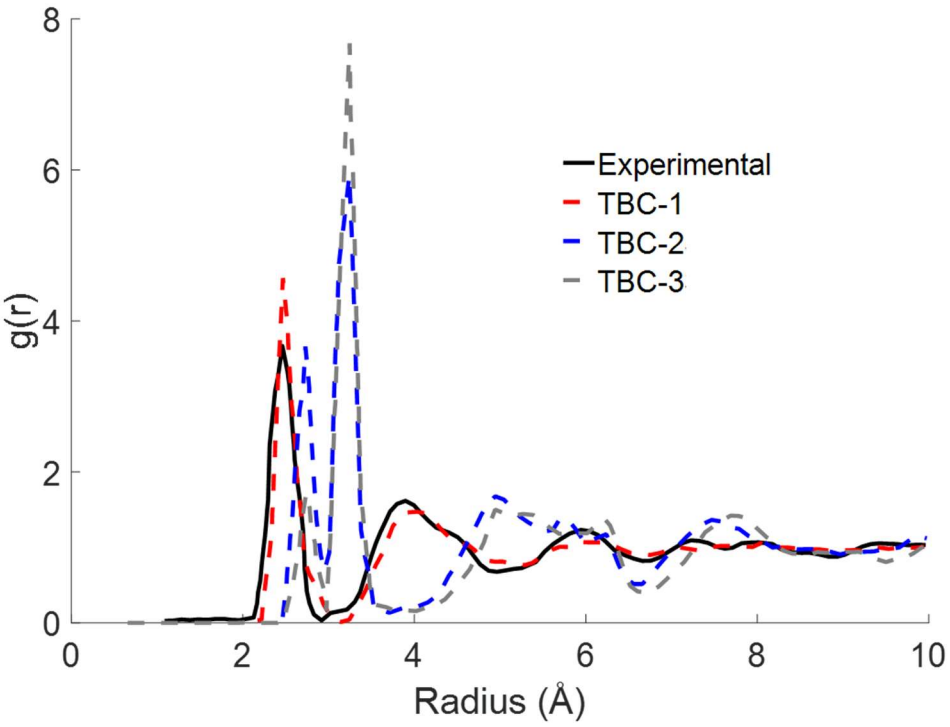

Figure 11. RDF of a-Ge supercells modeled using the TBC-1, TBC-2, and TBC-3 potentials after a melt-quench procedure. Experimental results taken from [160].

After going through a melt-quench procedure, it is clear that the TBC-2 and TBC-3 potentials caused the a-Ge to relax to a substantially different structure than that measured experimentally. TBC-1 however accurately reproduces the experimentally measured structure of a-Ge, thus it is of particular interest.

While an ability to generate potentials and structures that at the very least reproduce an accurate RDF is useful, a description of how to calculate thermal properties, and in particular, TC, is needed. Some well-established methods do exist to calculate the total TC of a material using either equilibrium MD, specifically Green-Kubo (GK) analysis (discussed further in the next section) or non-equilibrium MD whereby one applies a temperature gradient and determines TC from Fourier's law. However, such calculations neglect quantum effects and provide only information about the total TC, failing to generate insight into the specific mechanisms/modes that effect TC in the material and necessitating more powerful methods. One such method, which is used in this dissertation, is the recently-developed GKMA [6, 12, 13, 156-158]. GKMA combines LD techniques with GK analysis to calculate the contribution of individual vibrational modes to a material's total TC.

3.2 The Green-Kubo Method

This section begins with a description of the GK method, then delves into the details of GKMA and what makes it such a powerful tool for understanding TC in disordered materials.

3.2.1 Green-Kubo Analysis

The GK method is a perturbation method based on the linearized Liouville equation [164, 165]. For a system comprised of N particles with known positions and momenta, one can determine the thermal conductivity of a system via

$$\mathbf{k}_{\alpha\beta}\left(T,\omega\right)=\frac{V}{k_{\mathrm{B}}T^{2}}\int_{0}^{\infty}\left\langle \mathbf{Q}_{\alpha}\left(0\right)\cdot\mathbf{Q}_{\beta}\left(t\right)\right\rangle \cdot\exp\left(-i\omega\cdot t\right)dt \tag{16}$$

where $\mathbf{k}_{\alpha\beta}\left(T,\omega\right)$ is a tensor that gives TC in the $\alpha\beta$ direction for a given temperature at a specific thermal perturbation frequency, ω, V is the volume of the system, k_{B} is Boltzmann's constant, T is the system temperature, and t is time. The $\left\langle \ \right\rangle$ operator denotes the time autocorrelation of the two heat flux values inside the brackets. A detailed derivation of this equation can be found elsewhere [15, 16, 164, 165].

When considering the timescales over which atoms oscillate (i.e. the THz regime), the frequency is several orders of magnitude larger than the frequency at which temperature perturbations typically occur (anywhere from MHz down to <1 Hz), thus of primary interest is the zero-frequency limit for steady state heat conduction, allowing Eq. (17) to be rewritten as

$$\mathbf{k}_{\alpha\beta}\left(T\right)=\frac{V}{k_{\mathrm{B}}T^{2}}\int_{0}^{\infty}\left\langle \mathbf{Q}_{\alpha}\left(0\right)\cdot\mathbf{Q}_{\beta}\left(\tau\right)\right\rangle d\tau \tag{17}$$

While Eq. (18) is certainly of some use, it cannot be applied in this form to MD simulations. V and T are simple to extract from a simulation, but the heat current, $\mathbf{Q}$, cannot be calculated directly. One can, however, follow the method proposed by Hardy [166] and derive the heat current as a function of quantities that are easily determined from MD:

$$\mathbf{Q}\left(t\right)=\frac{1}{V}\sum_{i}\left[E_{i}\dot{\mathbf{u}}_{i}+\sum_{j}\left(-\nabla_{\mathbf{r}_{i}}\Phi_{j}\cdot\dot{\mathbf{u}}_{i}\right)\mathbf{r}_{ij}\right] \tag{18}$$

where E_i is the total (i.e., potential plus kinetic) energy of atom i, $\dot{\mathbf{u}}_i$ is the velocity of atom i, Φ_j denotes PE of atom j, and $\mathbf{r}_{ij}$ is distance between atom i and j. Substituting

this equation back into Eq. (18), allows one to calculate $\mathbf{k}$ entirely from quantities easily obtained via MD.

The two terms in brackets in Eq. (19) correspond to the convective and conductive terms, respectively. The convective term dominates in liquids and gases [167], while the conductive term is dominant in solids [168].

It is worth pointing out how different the GK method is from the PGM. First, the PGM is a method based on scattering events, whereby a phonon's trajectory is altered by another particle or structural feature (e.g. a defect or a different atom type) in the material, and TC is inversely proportional to the frequency of these scattering events. Conversely, the GK method is based on the autocorrelation of the heat flux at different points in time, where TC is proportional to the strength of the autocorrelation.

A result of this difference is that the GK method therefore does not require the existence of propagating phonons with a well-defined wave vector and can be applied without any sort of corrective approximations or fitting parameters to disordered materials, in which some vibrational modes are not propagating or even delocalized. That a wave-vector is not necessary means that accounting for diffusons and locons is easily managed, and the effect of these modes on TC is implicitly included in the calculation. The ability of GK analysis to describe disordered materials without any modifications to the theory is arguably the strongest advantage to using it over the PGM. For the same reason it can be applied to modes without a wave vector, the GK method can also be used to calculate the TC not only of solid materials (a limitation that applies to the PGM), but also to liquids and gases.

The GK method also allows one to include all degrees of anharmonicity – i.e. 3-phonon, 4-phonon, up to $3N$-phonon interactions – implicitly. Accounting for all orders of anharmonicity is simple and has a minimal effect on computational complexity or expense: one need only to use an anharmonic (i.e. not a simple quadratic) functional form for the EIP. (Of course, describing anharmonic effects *accurately* depends on the accuracy of the potential.) The PGM on the other hand must explicitly account for 2-, 3-, 4-, etc. phonon interactions. While 2- and 3-phonon interactions are certainly the most common type of phonon interaction, the total number of interactions for which to account increases exponentially with phonon number, making it infeasible to account for more than ~4-phonon interactions. For this reason, it is preferable to use the GK method, as GK automatically includes all interactions without having to treat them explicitly.

There is however one glaring drawback to GK analysis that limits its usefulness for studying heat transfer mechanisms via MD, namely, whereas the PGM can attribute TC to a mode or collection of modes, GK analysis will provide only bulk values of TC. Using a combination of GK analysis and LD, however, can allow one to determine the contribution of any given subset of modes to the total TC of the system. This method, GKMA, is a powerful tool to determine mode-level contributions without any of the approximations required by the PGM. Thus, GKMA is uniquely situated to provide an unprecedented degree of information when analyzing vibrational modes' effect on TC in disordered materials.

3.2.2 Green-Kubo Modal Analysis

Recalling the discussion of modal decomposition from Section *2.1.2 Lattice Dynamics*, the position or velocity of any given atom at any given instant can be written as a linear sum of modal excitations. First, normal mode coordinates of position, $X_n(t)$, and velocity, $\dot{X}_n(t)$, for mode n are calculated via

$$X_n(t) = \sum_i \sqrt{m_i}\mathbf{e}_{i,n}^{\ *} \cdot \mathbf{u}_i(t) \tag{19a}$$

$$\dot{X}_n(t) = \sum_i \sqrt{m_i}\mathbf{e}_{i,n}^{\ *} \cdot \dot{\mathbf{u}}_i(t) \tag{19b}$$

where * denotes the complex conjugate. However, as discussed in Section *2.1.2 Lattice Dynamics*, for a SCLD calculation at the Γ point, all eigenvectors have real values, so they are their own complex conjugate. Eqs. (20) can be inverted to yield

$$\mathbf{u}_i(t) = \sum_n \mathbf{u}_{i,n}(t) = \frac{1}{\sqrt{m_i}} \sum_n \mathbf{e}_{i,n} \cdot X_n(t) \tag{20a}$$

$$\dot{\mathbf{u}}_i(t) = \sum_n \dot{\mathbf{u}}_{i,n}(t) = \frac{1}{\sqrt{m_i}} \sum_n \mathbf{e}_{i,n} \cdot \dot{X}_n(t) \tag{20b}$$

These equations allow one to determine the modal velocity of an atom at any instant in time. The modal velocities (and modal displacements) of an atom will always sum to the atom's total velocity (or total displacement). One can apply the modal decomposition of velocities obtained from Eq. (21b) to the velocity term in Eq. (19) yielding the modal heat flux:

$$\mathbf{Q}_n(t)=\frac{1}{V}\sum_i\left[E_i\left(\frac{1}{m_i^{1/2}}\mathbf{e}_{i,n}\dot{X}_n(t)\right)+\sum_j\left(-\nabla_{\mathbf{r}_i}\Phi_j\cdot\left(\frac{1}{m_i^{1/2}}\mathbf{e}_{i,n}\dot{X}_n(t)\right)\right)\mathbf{r}_{ij}\right] \tag{21}$$

These modal heat fluxes sum to the total heat flux in the system:

$$\begin{aligned}\mathbf{Q}&=\sum_n^{3N}\mathbf{Q}_n(t)=\sum_n^{3N}\frac{1}{V}\sum_i\left[E_i\dot{\mathbf{u}}_{i,n}(t)+\sum_j\left(-\nabla_{\mathbf{r}_i}\Phi_j\cdot\dot{\mathbf{u}}_{i,n}(t)\right)\mathbf{r}_{ij}\right]\\&=\sum_n^{3N}\frac{1}{V}\sum_i\left[E_i\left(\frac{1}{\sqrt{m_i}}\mathbf{e}_{i,n}\dot{X}_n(t)\right)+\sum_j\left(-\nabla_{\mathbf{r}_i}\Phi_j\cdot\left(\frac{1}{\sqrt{m_i}}\mathbf{e}_{i,n}\dot{X}_n(t)\right)\right)\mathbf{r}_{ij}\right]\end{aligned} \tag{22}$$

The values of $\mathbf{Q}_n(t)$ are the heat fluxes attributed to each mode, n, and $\mathbf{Q}(t)=\sum_n\mathbf{Q}_n(t)$. Substituting Eq. (22) into Eq. (18), one can obtain the modal form of Eq. (18):

$$k_n=\frac{V}{k_{\mathrm{B}}T^2}\int\left\langle\mathbf{Q}_n(t+t')\cdot\mathbf{Q}_n(t)\right\rangle dt' \tag{23}$$

This equation is a powerful tool which, for the first time, allows one to easily ascribe a TC to each individual mode in any material. Further, one can determine the cross-correlation between any two modes in the system via

$$k_{nn'}=\frac{V}{k_{\mathrm{B}}T^2}\int\left\langle\sum_n\mathbf{Q}_n(t+t')\cdot\sum_{n'}\mathbf{Q}_{n'}(t)\right\rangle dt'=\frac{V}{k_{\mathrm{B}}T^2}\sum_{n,n'}\int\left\langle\mathbf{Q}_n(t+t')\cdot\mathbf{Q}_{n'}(t)\right\rangle dt' \tag{24}$$

Eq. (25) gives the correlation between mode n and n', which is distinctly different from determining 2-phonon interactions as in the PGM. Here, the quantity calculated is the time cross-correlation of the amplitude of two modes. This correlation can persist over hundreds of picoseconds [169], and a larger value (i.e. stronger correlation) results in an increased TC. Conversely, when calculating 2-phonon interactions within the framework of the PGM, one is determining how often two wave packets of phonons cause one another to

scatter. These interactions are assumed to persist on a timescale orders of magnitude shorter than the lifetime of the phonon [15, 16] and do not correspond to the mode-mode cross correlations in GKMA.

Eqs., (22) and (25) allows one to characterize the contribution of any vibrational mode to TC, either directly via Eq. (22) or indirectly from its effect on other vibrational modes via Eq. (25). Furthermore, the quantities in these equations can be determined from MD simulations, assuming an LD calculation has been performed previously to determine the normal modes.

The LAMMPS source code has also been modified to enable potential-agnostic GKMA calculations. The details of this modification are given in *Appendix D. Modifications Made to the Large-Scale Atomic/Molecular Massively Parallel Simulator to Enable Potential-Agnostic Green-Kubo Modal Analysis*, while the source code for these modifications can be found in the subsequent appendix, *Appendix E. compute gkma Source Code*.

Because GKMA allows one to ascribe a TC to each mode, and because one can determine the mode's frequency, a quantum correction (QC) can be applied to the TC contribution from the mode, i.e. one can account for the fact that vibrational modes follow a Bose-Einstein distribution and at low temperature may not be fully excited, according to

$$C_q(\omega,T)=\frac{k_{\mathrm{B}}x^2}{V}\frac{e^x}{\left(e^x-1\right)^2}\ ;x=\frac{h\omega}{k_{\mathrm{B}}T} \tag{25}$$

where $C_q\left(\omega,T\right)$ is the QC heat capacity.

This work will largely be neglecting QC because, while the correction is necessary to understand the actual TC of the system, what is more pertinent here is how different modes and classes of modes interact, some of which span a wide range of frequencies that may otherwise be suppressed due to QC. Consider for instance the spike in the DOS of a-PMMA at 100 THz, observable in Fig. 5. These modes would have a negligible effect on TC if QC is applied, but the modes are also interesting based on their large number and the degree of delocalization they exhibit compared to other modes in a-PMMA. These modes would have until now been considered locons and assumed not to contribute to TC, so it will be interesting to see if any of these high-frequency modes have a significant TC, at least assuming one ignores QC.

CHAPTER 4. LOCALIZATION AND THERMAL CONDUCTIVITY OF NORMAL MODES IN AMORPHOUS POLY(METHYL METHACRYLATE)

This chapter will focus on the major findings for the three amorphous polymers studied: a-PMMA, a-PS, and a-PVC. For the sake of brevity, the results will focus particularly on a-PMMA as representative of the overall findings, and the results for a-PS and a-PVC are provided when there are significant differences in the findings for a-PMMA.

The focus of this chapter is twofold. The first focus is on addressing Questions 1 & 2 by describing the degree of localization according to PR and proposing alternative methods one could use to understand mode localization in disordered materials. From there, the focus will shift to answering Question 3, in particular by delving into the contribution of individual vibrational modes to TC, with emphasis on the relationship between the degree of mode localization and its total TC contribution.

4.1 Question 1: The Persistence of Mode Localization in Different-Sized Supercells

Question: *Does the low average PR observed in a-PMMA persist across different supercell sizes, and is this also the case for the other amorphous thermoplastics in this study?*

Hypothesis: *Localization is an inherent property of amorphous polymers: localization itself is already an inherent property of disordered materials, and there are additional factors that could lead to a further increase in the degree of localization. In the case of*

polymers, due to 1) the strong covalent bonds along polymer chain backbones and the much weaker bonds between chains and 2) the fact that these chains are in an amorphous configuration (i.e., there is significant inhomogeneity in both bond strength and stereochemistry), it is likely that a greater degree of localization will persist, regardless of polymer type or supercell size. Thus, it is hypothesized that due to the highly asymmetric PES, the low PR measured is an inherent property of amorphous polymers (and more specifically, the thermoplastics in this study), and not simply an artifact of supercell size.

If the extreme localization observed were either an artifact of a small supercell or unique to a-PMMA, many of the other questions explored in this dissertation become far less relevant to amorphous polymers in general. However, if this localization is found to hold across different polymers and supercell sizes, one can begin to note trends in the behavior of the normal modes in thermoplastics without the need to qualify findings for a particular polymer/supercell size.

To test this hypothesis, LD calculations have been performed on supercells of different sizes for a-PMMA, a-PS, and a-PVC. These supercells were created using the Polymer Modeler and relaxed using the procedure outlined in Section *2.1.1.3 Example Relaxation Procedure for Poly(methyl methacrylate)*. The results are shown below in Figs. 12-14.

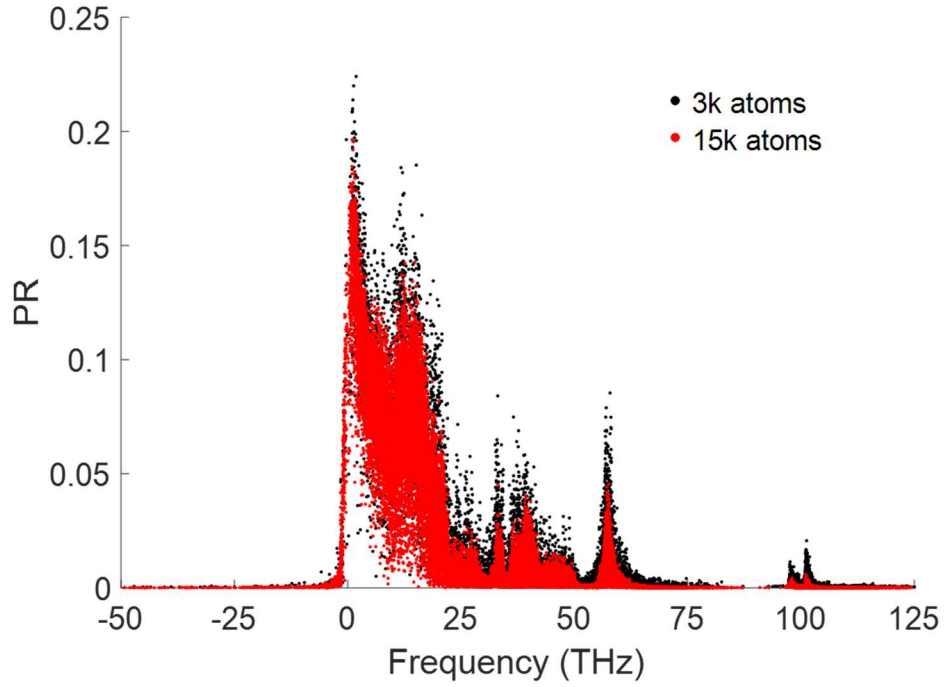

Figure 12. PR as a function of frequency for a-PMMA supercells with 3,008 and 15,020 atoms.

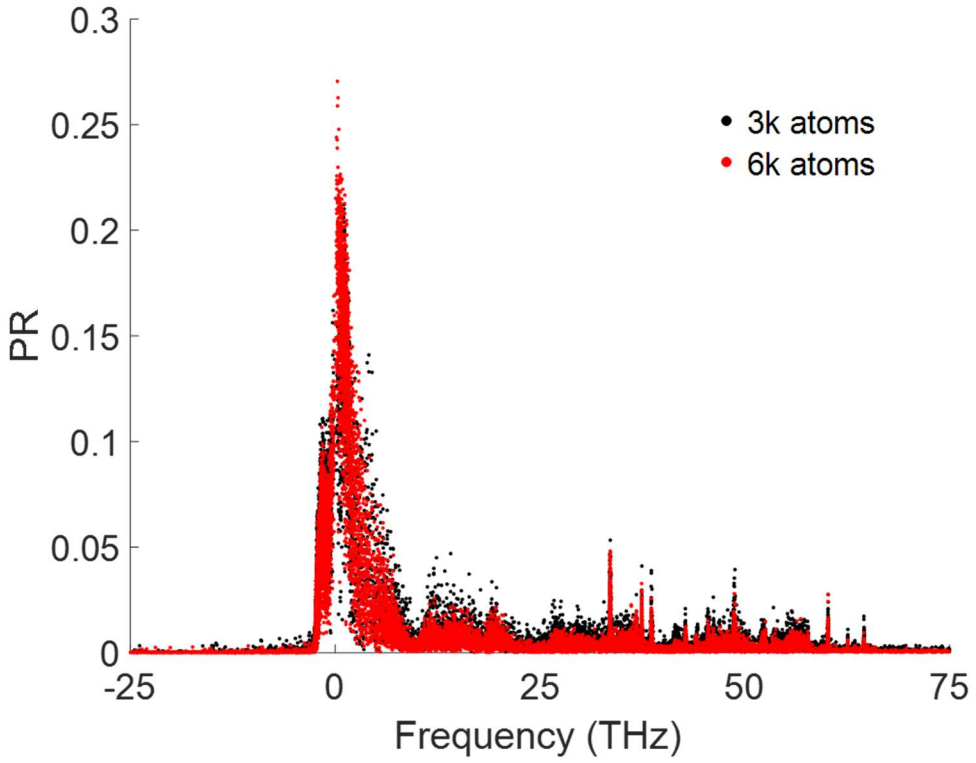

Figure 13. PR as a function of frequency for a-PS supercells with 3,208 and 6,416 atoms.

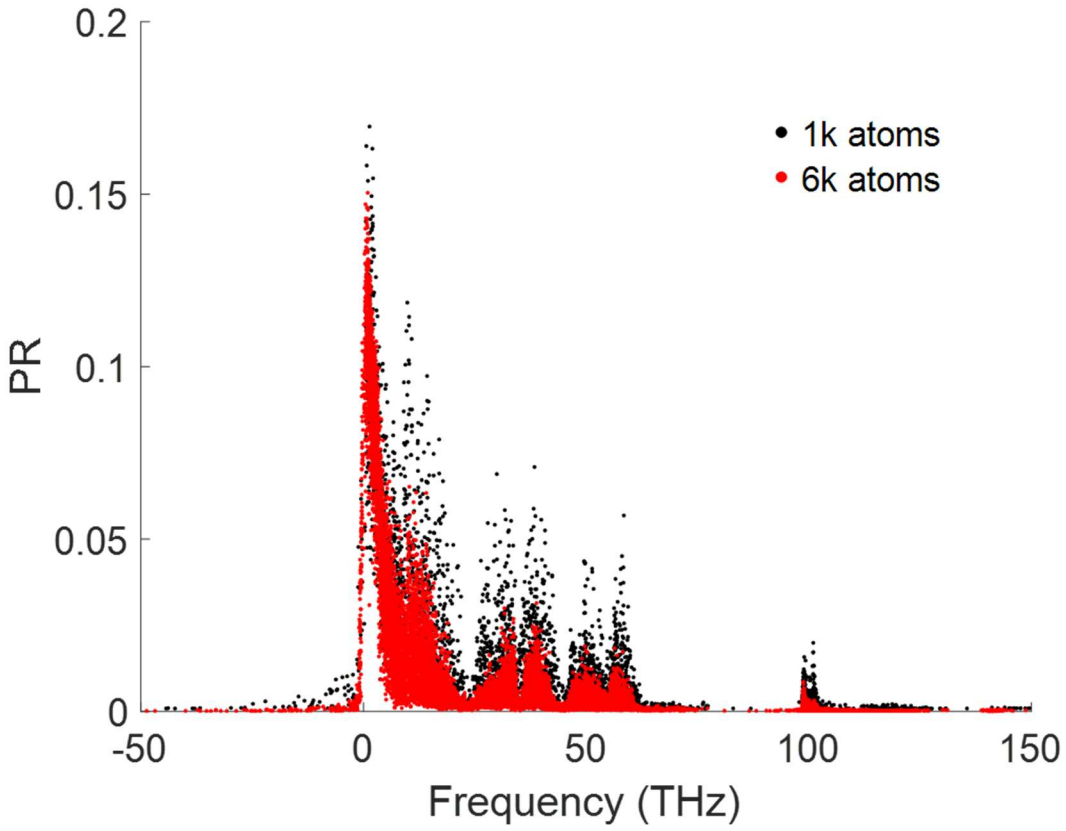

Figure 14. PR as a function of frequency for a-PVC supercells with 1,208 and 6,020 atoms.

The first result worth noting is that the degree of localization in the modes of a-PS and a-PVC is consistent with those observed in a-PMMA: most modes have a PR < 0.2. This finding is significant, since if the results were unique to a-PMMA, the system would be interesting to study as an anomaly, but the findings would not be broadly applicable/generalizable to other polymers. It should be noted again that a-PMMA, a-PS, and a-PVC have significantly different structures, i.e., the monomers are comprised of 15, 16, and 6 atoms respectively, PS is the only polymer with an aromatic ring, the polymers contain different functional groups, etc. Thus, if the results are consistent across the polymers, it seems reasonable to postulate that they may be relevant for many other thermoplastics as well.

As can be seen from Figs. 12-14, the relationship between PR and frequency remains unchanged for different numbers of atoms in the supercell, even in the most extreme case (a-PMMA with a 5x disparity in atom number); apart from the density of points, the two datasets are virtually indistinguishable. In fact, the one observable difference is that the modes in supercells with more atoms are actually slightly *more* localized; if any discrepancy between supercells of different sizes were expected, it would be the opposite [60]. Due to the high computational cost of running GKMA, particularly with a potential as complex as the DREIDING potential, detailed calculations (such as GKMA) were performed on the smaller-sized systems. While there may be some neglect of long wavelength propagons in doing so, the difference is expected to be negligible (based on accumulations computed later in this thesis).

The degree of mode localization observed is rather surprising, particularly at low frequencies: it is reasonable to expect that at some point, low-frequency acoustic wave propagons appear as sound waves with a much higher PR. Presumably, propagons will be observed in these materials, but only if one studies much larger supercells ($\gtrsim 10^4$-10^6 atoms); however, relaxing such a large supercell and performing LD/GKMA calculations is beyond the scope of this work, due to its projected computational cost.

For this reason, the work described herein neglects propagons when examining thermal transport in amorphous thermoplastics. There is the possibility for other interesting thermal transport phenomena due to propagons if one performs studies at length scales of, e.g. 1-10 μm, rather than ~30 nm. However, the possibility of other interesting phenomena at larger scales due to propagons should not detract from the findings for diffusons and locons presented in this dissertation.

As noted previously, addressing Question 1 is straightforward, and the question is largely a preliminary one that is necessary to address before delving into the nature of the normal modes in the polymer systems. But it is critical to have resolved this question, as the remainder of this chapter is predicated on the fact that the modes not only in a-PMMA but also in a-PS and a-PVC exhibit an unusually high degree of localization. However, simply noting the degree of localization does not provide insight into the behavior and interaction of the modes themselves. Furthermore, as noted in *Chapter 2. Initial Observations*, many modes with PR < 0.1 nonetheless appear rather delocalized, such as those shown in Fig. 7, which has been reprinted below. The next section will explore some alternative methods of describing this localization and its relationship to modal TC in amorphous polymers.

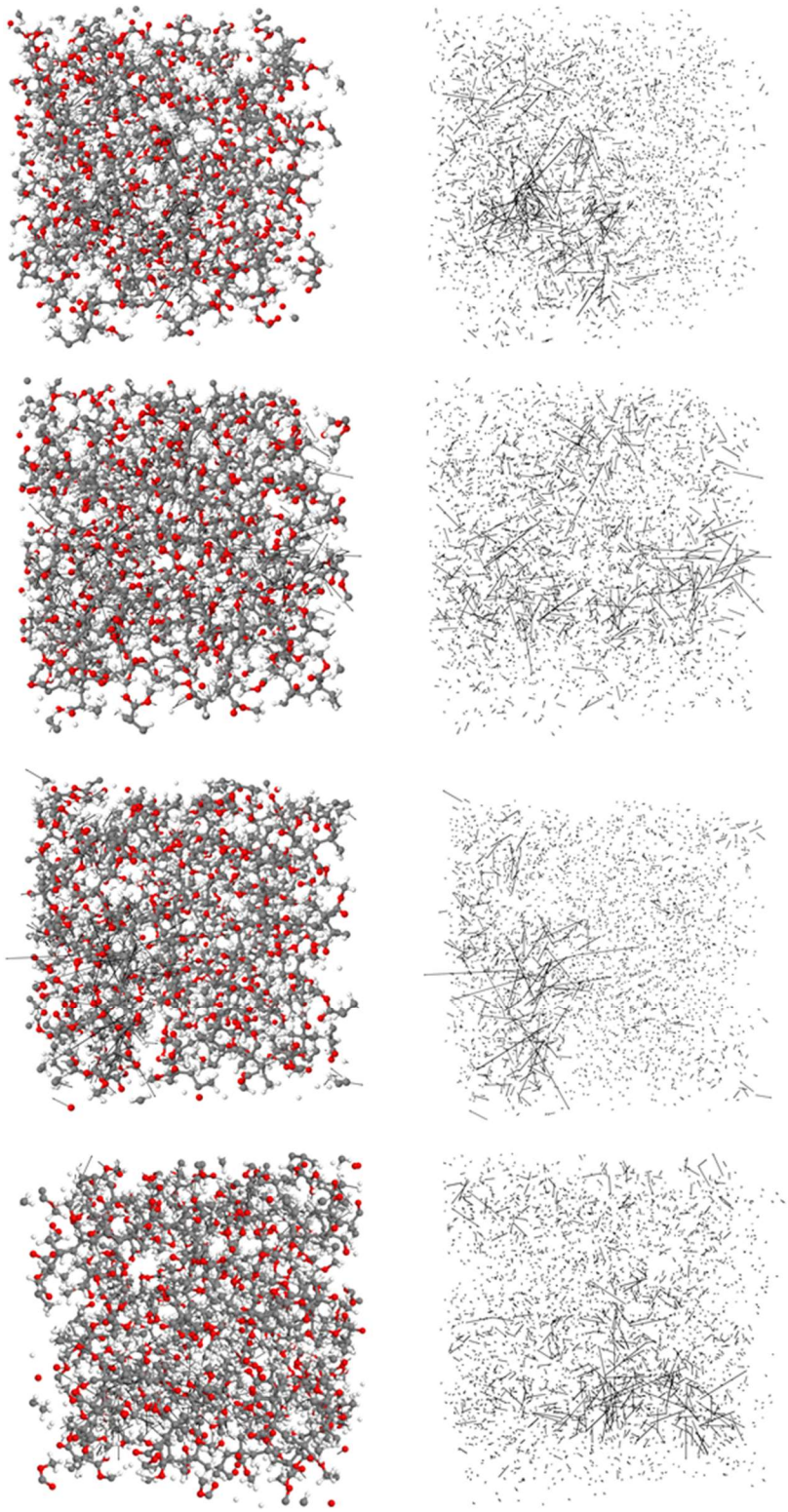

Figure 7. Low-PR modes in a-PMMA. C shown in gray, O in red, and H in white, with the eigenvectors shown in black. Atoms removed in figures on the right for clarity. The PR of each mode from top to bottom is 0.029, 0.033, 0.038, and 0.037.

4.2 Question 2: The Anomalously Low Participation Ratio of Normal Modes in Amorphous Polymers

Question: *With most modes having a low PR ascribed to locons, are the modes actually localized, or would an alternative descriptor indicate they are delocalized?*

Hypothesis: *While these modes are localized based on the PR, it is hypothesized that an alternative descriptor of localization based on how the modes are confined spatially or in terms of different polymer chains will elucidate more information about the degree/aspects of how these modes are localized. In particular, an alternate descriptor may indicate the modes are in some way delocalized.*

As pointed out in the previous section, the high degree of localization observed (according to PR) is not unique to a-PMMA but is also observed in a-PS and a-PVC, thus, it is expected that the findings detailed here may apply broadly to many thermoplastics. It is worth first revisiting the concept of PR, however, to discuss what the descriptor does and does not say about a mode. Referring back to Eq. (3), PR is a normalized summation of the square of the eigenvectors of a mode over every atom in the supercell. The only information necessary for this summation is the number of atoms and the eigenvectors. PR ranges from $1/N$ to 1. Values close to $1/N$ describe a mode localized to one or a few atoms, whereas a value close to 1 indicates a mode for which the vibrations are spread evenly across all atoms in the system. These values can be understood most easily for a monatomic system:

revisiting the formula for PR, $PR_n = \frac{\left(\sum_i^N \mathbf{e}_{i,n}^2\right)^2}{N\sum_i^N \mathbf{e}_{i,n}^4}$, the metric is a function of each atom's eigenvector squared. Because an eigenvector corresponds directly to an atomic displacement from equilibrium, and because interatomic potentials are approximately harmonic at small displacements, the energy of an atom in a vibration is directly proportional to the magnitude squared of the eigenvector describing its motion. Thus, for a monatomic material with no isotopes, the PR is the square of the sum of the energy of each individual atom in a vibrational mode. However, the energy of an atom is also proportional to its mass, a fact for which the PR does not account. Thus, in the case of a material comprised of atoms of highly disparate masses (H vs. C, O, and/or Cl in this case), the PR may perhaps be low simply due to the difference in mass of different elements.

PR does not provide information about how a vibrational mode is spatially distributed. For example, some vibrational modes exist for which most of the energy is confined to a few atoms in a small region of space, but there exists a "tail" of atoms with much lower but still non-zero eigenvectors[9]; examples of such modes can be seen in Fig. 7. These modes have a PR ≤ 0.05, indicating the modes are localized (i.e. the PR is well below 0.1).

Although the modes' energies are localized to a few atoms, one could argue there may still exist means by which the mode can transfer energy to other regions of the supercell via the atoms in the tail of the distribution. In such cases, while the PR is comparably quite low,

[9]Technically, many atoms' eigenvectors are "non-zero" but their value is so small as to be insignificant (e.g. $< 10^{-10}$). For the purposes of this text, such values are treated as 0, as they have no bearing on the dynamics of the system.

the mode could still be considered delocalized and perhaps behave similarly to modes with larger PR's.

Amorphous polymers in particular are an interesting case to study *vis-à-vis* mode localization, even beyond spatially concentrated (but not entirely localized) modes with a tail of eigenvectors. Because amorphous polymers are comprised of multiple separate chains, one could argue that the most important aspect of a vibrational mode is not how it is distributed in space, but rather, how it is distributed amongst the different chains in the supercell. The argument here is similar to that for a spatially delocalized mode: due to the weak interaction (due to intermolecular bonding) between atoms in separate polymer chains but the relatively strong interaction of atoms (due to covalent bonding) within a chain, vibrational energy can propagate along a single polymer chain much more easily than it is transferred between chains. Vibrational energy may therefore end up confined to a particular polymer chain with little opportunity to be transferred to another polymer chain.

This section will discuss two newly-developed methods for describing the localization of vibrational modes. The first method is a descriptor of modal spatial localization, namely the *Modal Spatial Extent* (MSE), which accounts for not only the magnitude of atoms' eigenvectors, but also their spatial proximity to other eigenvectors. The second method is a means for measuring how spread a mode is among different polymer chains: the descriptor modifies the method for PR calculation, summing over single polymer chains, rather than the entire supercell. These new descriptors have been found to provide useful information about vibrational modes that is not provided by a simple PR calculation; in some cases, the metrics provide surprising insight into the dynamics of the polymer

systems that may ultimately help guide the design of new materials with extreme thermal properties.

4.2.1 The Mode Spatial Extent

As has been shown in Fig. 7, many vibrational modes with low PR's appear to be at least somewhat spatially delocalized. It seems reasonable to assume that while these modes would traditionally be classified as locons, perhaps their behaviour is more akin to diffusons. To determine whether such similarities exist necessitates first creating a means by which one can quantify the degree of spatial localization of the modes.

4.2.1.1 Method for Calculating the Mode Spatial Extent

When considering how a mode is spatially distributed, it is helpful to understand how energy is spread across a supercell. Consider the vibrational modes from Fig. 7. To visualize how the energy is distributed spatially, one can divide a supercell into thin rectangular "slices" of atoms and sum the square of the eigenvectors the atoms of in a given slice to give a single value. This value for each slice can then be plotted as a function of location in the direction perpendicular to the slices. The result of this summation for each of the modes in each of the x-, y-, and z-directions in Fig. 7 can be seen clearly on the left half of Fig. 15.

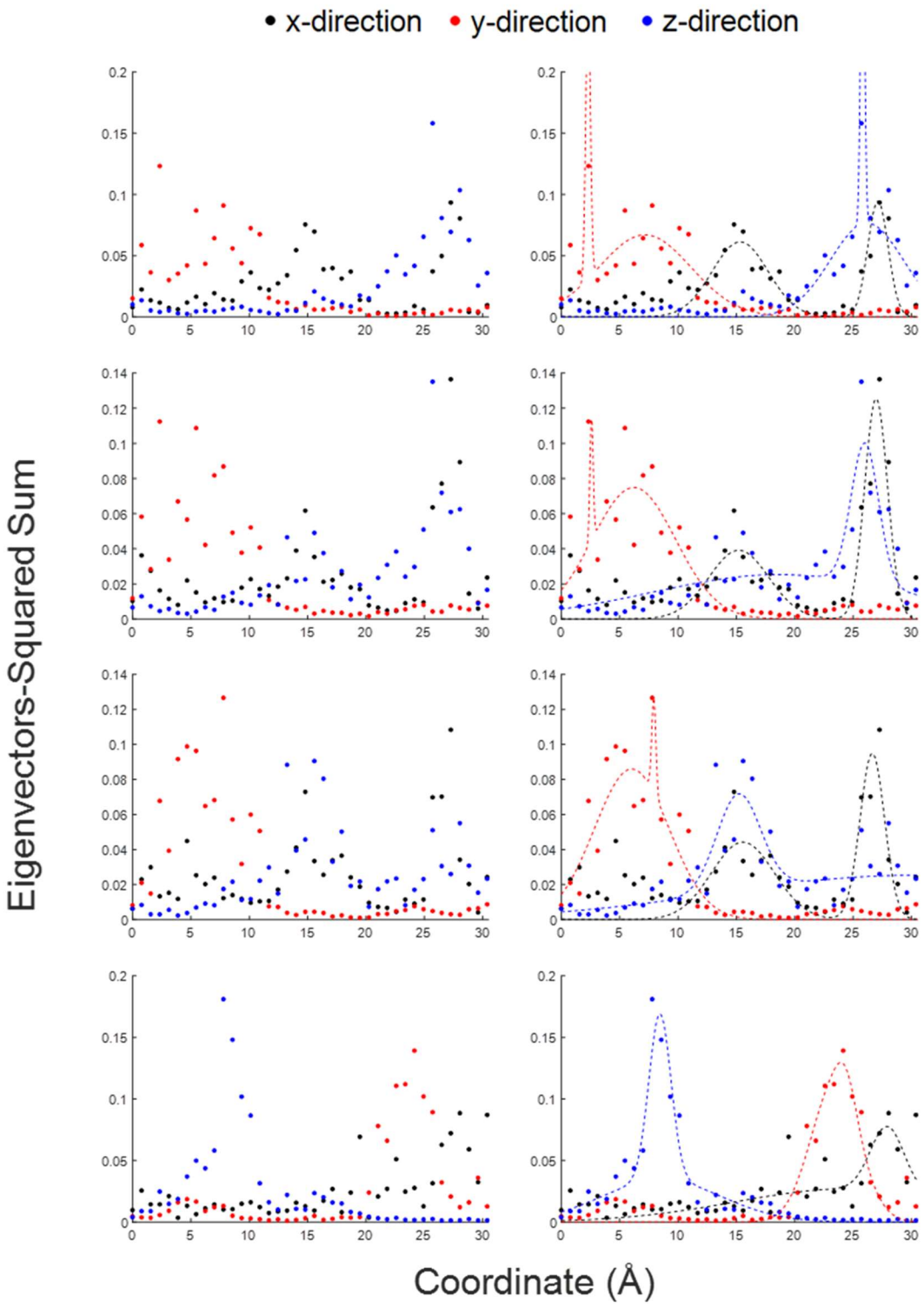

Figure 15. Sum of eigenvectors (left) in each of 40 thin "slices" in the x- (black), y- (red), and z- (blue) directions, plotted vs the coordinate in the respective direction. Each plot corresponds to the respective mode shown in Fig. 7. The right half of the figure shows the data on the left fit with a two-term Gaussian.

The goal of this section is to find a descriptor of how these points are distributed spatially. If one considers the plots on the left of Fig. 15, the distribution of eigenvector sums resembles that of Gaussians. While a single Gaussian can describe the general shape of these curves, fitting a two-term Gaussian ($f(x) = a_1 e^{-\left(\frac{x-b_1}{c_1}\right)^2} + a_2 e^{-\left(\frac{x-b_2}{c_2}\right)^2}$) allows the function to more accurately capture the behavior of the eigenvector-sums, [10] since many modes either have two peaks or have a long tail offset far away from a major peak.

One result of this fitting procedure are the variances of the Gaussian peaks (i.e. their widths). A wide peak indicates a long "tail" of eigenvectors, which would indicate a mode is delocalized, while a narrow peak would correspond to only a few atoms whose eigenvectors are much larger than their neighbors, indicating a localized mode. The resultant variances of the Gaussian peaks in each of the three spatial directions are then averaged. It is this resulting average of variances that is defined as the Mode Spatial Extent (MSE), which is a new means by which mode localization can be described. This process is further detailed in *Appendix F. Description of the Procedure for Calculating the Mode Spatial Extent*, which gives an example calculation for a vibrational mode in a-Ge and further discusses the choice of a two-term Gaussian.

The MSE has units of distance and is typically expressed in Å; it can be thought of as the effective "size" of a vibrational mode, similar to the MFP of a phonon. In cases where the MSE is on the order of the atomic spacing or lower (~1 Å), the mode can be considered highly spatially localized, while in cases in which the MSE is much greater than the

[10] See *Appendix F. Description of the Procedure for Calculating the Mode Spatial Extent* for further rationale of using a two-term Gaussian vs. other functional forms.

interatomic spacing (~10 Å), the mode may have the majority of its energy localized on a few atoms (if it has a low PR), but it is possible that many other atoms still participate, and thus its displacement field is still somewhat delocalized. In this study, any mode with an MSE of $\gtrsim$ 10 Å will has a size on the order of the dimensions of the supercell; thus, the mode can be considered spatially delocalized. While this cutoff is not exact (just as the cutoff between, e.g. infrared and microwaves is not exact), 10 Å seems to be a reasonable value to distinguish between partially and fully spatially delocalized modes. Regardless, the most important cutoff to consider is 1 Å, as this cutoff is what allows one to determine which modes are spatially localized, and which extend through at least some significant portion of the supercell. Modes with MSE values in between (~1-10 Å) can be considered to have partially delocalized displacement fields.

The next section will show some results of MSE calculations and why the MSE can serve as a useful compliment to PR. The modes that will be discussed have low PR's but nevertheless according to the MSE are at least partially delocalized. Also included are situations in which using the MSE in addition to PR proves useful, particularly when attempting to understand the relationship between mode localization and TC (a topic which will be discussed in further detail later in the chapter).

4.2.1.2 Using the Mode Spatial Extent for Describing Mode Localization

Now that the MSE has been described, it is necessary to determine when it is useful. The first and most obvious application – which has been noted several times and which was the impetus for creating the MSE in the first place – is to determine whether a vibrational mode with a low PR has a tail of small but non-zero eigenvectors. This section will show

vibrational modes in a-Ge and a-PMMA with small values of PR and large MSE's to assess the efficacy of the MSE at describing such modes.

First, consider a-Ge, which is perhaps less interesting than a-PMMA, as it is monatomic and has a relatively uniform structure for an amorphous material. However, there exist modes with low PR's and high MSE's which appear delocalized. Fig. 16 shows two such low-PR modes with MSE > 10 Å.

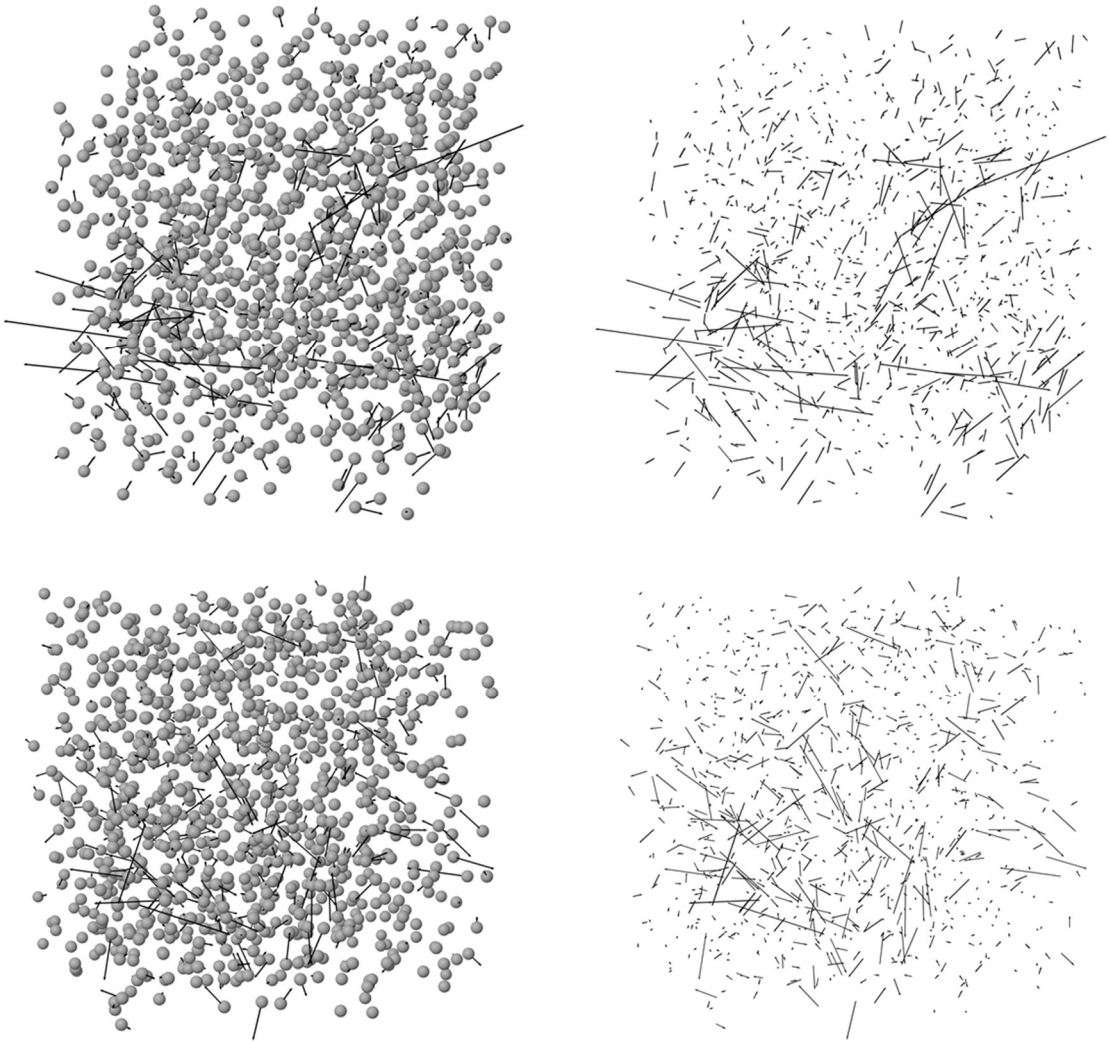

Figure 16. Low-PR, high-MSE modes in a-Ge. The top mode has PR = 0.076, MSE = 30 Å, while the bottom mode has PR = 0.050, MSE = 92 Å. Atoms removed in figures on the right for clarity.

While only two modes are included here, there are numerous other modes with PR < 0.1 and MSE > 10 Å. Of the 3,000 modes in the a-Ge supercell studied, 46 total modes fit these criteria.

The situation is similar for a-PMMA; in this system, of the 9024 total vibrational modes, 1,519 (16.8%) have PR < 0.1 and MSE > 10 Å. Four examples of such modes have been included in Fig. 17.

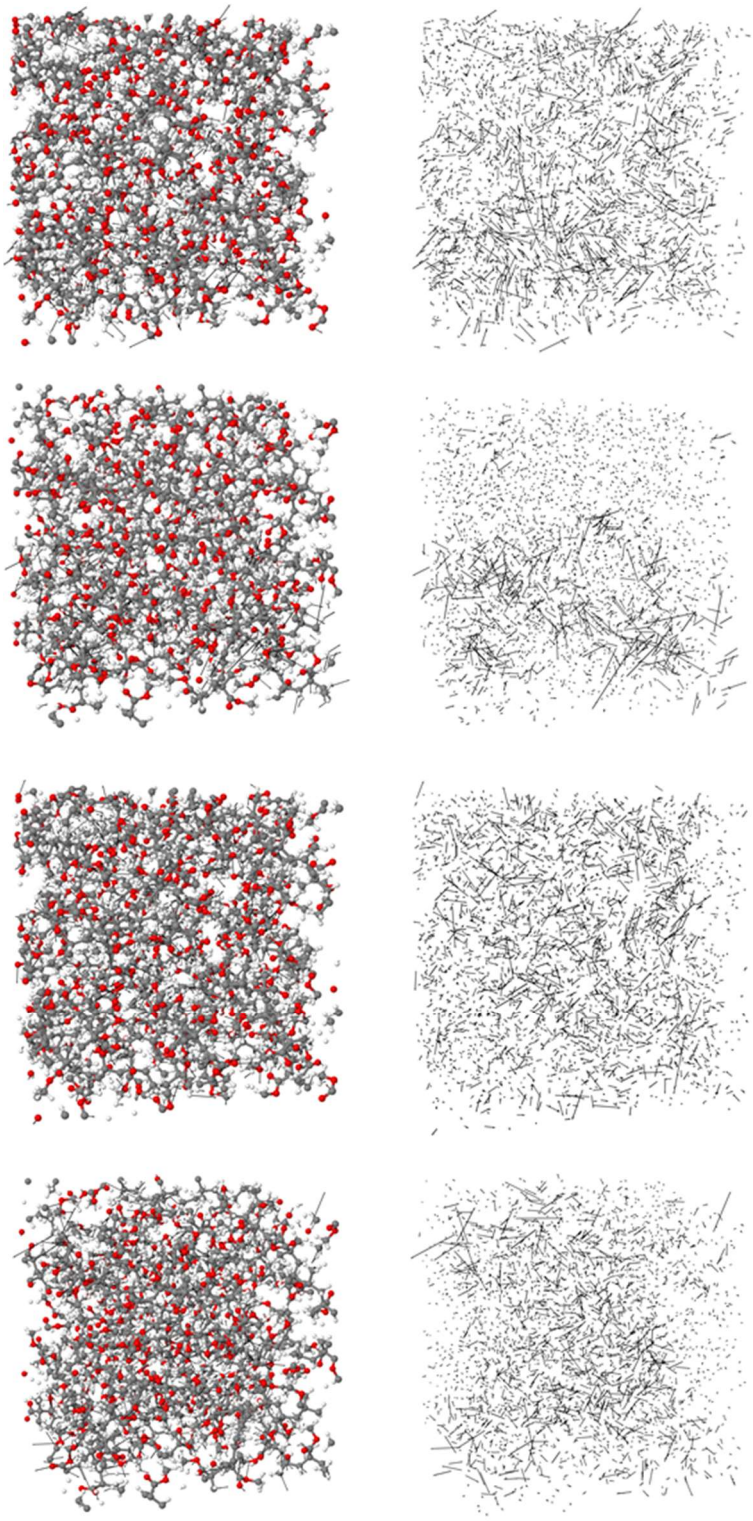

Figure 17. Low-PR, high-MSE modes in a-PMMA. The values of PR and MSE for the modes from top to bottom are 0.036 & 116 Å, 0.027 & 422 Å, 0.05 & 392 Å, and 0.036 & 331 Å. Atoms removed in figures on the right for clarity.

From visual inspection of the eigenvectors in Figs. 16 and 17, one can see that the modes do exhibit some degree of delocalization. Thus, if nothing else, the MSE can tell one whether or not a mode will *look* delocalized. This result in and of itself is perhaps not particularly useful, but there is more to say about the MSE. First, consider a-Ge. Fig. 18 shows the PR and MSE as a function of frequency.

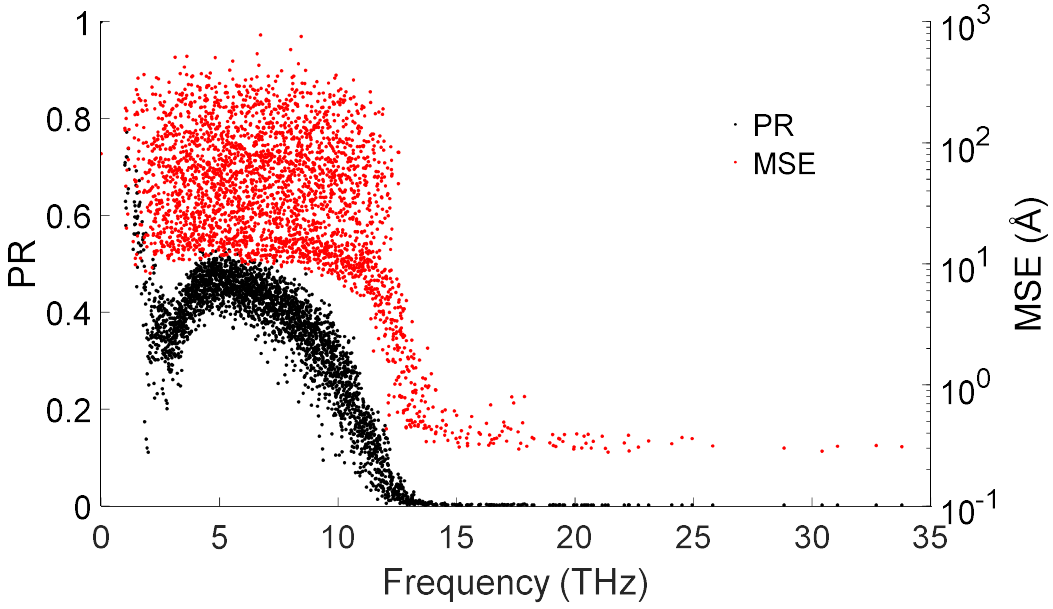

Figure 18. PR and MSE of each mode in the a-Ge supercell studied as a function of frequency.

Perhaps the most standout difference between the two metrics plot in Fig. 18 is the subset of a few modes with frequencies ~2 THz with a low PR but a large MSE. Whereas the PR indicates that the modes in this frequency range are locons, the MSE indicates they span the supercell (i.e. the MSE of all low-frequency modes is $\gtrsim$ 10 Å). Both observations are valid: for the modes in question, a few atoms have eigenvectors much larger than the remainder of the atoms in the supercell leading to a low PR, however, the remaining atoms still participate in the mode, resulting in a larger MSE and a spatially delocalized mode.

One such mode is included in Fig. 19; this mode is also used for an example calculation of MSE in *Appendix F. Description of the Procedure for Calculating the Mode Spatial Extent*.

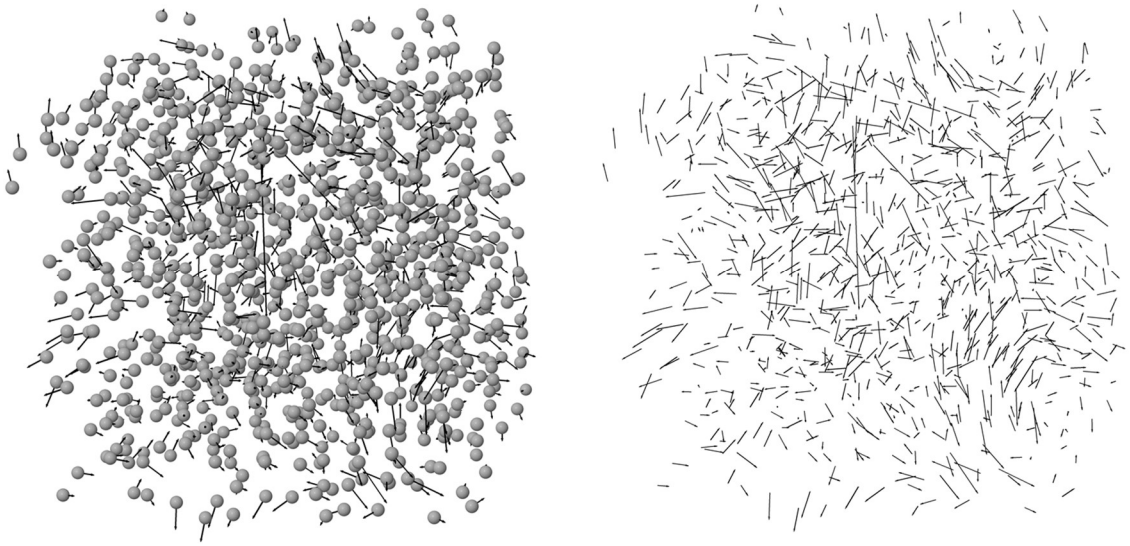

Figure 19. A vibrational mode in a-Ge with PR = 0.11 & MSE = 48 Å. Note the single large vertical eigenvector in the top middle of the figure and the comparatively small eigenvectors of the other atoms. Atoms removed in figures on the right for clarity.

If one examines the eigenvectors of this mode, it is apparent that many of the atoms' eigenvectors have a magnitude similar to that of atoms in other vibrational modes (the scaling of eigenvectors is the same as that in Fig. 16. However, there is a single atom with a much larger eigenvector (the vertical arrow visible in the middle of the supercell), which causes the PR of the mode to be lower than it would be otherwise. From other calculations not included in this dissertation, this low PR seems to be an artifact of a small supercell size, as discussed in *Section 2.2 Initial Results*. It is interesting that the MSE is less susceptible to artificially indicating localization as compared to PR, which can have stronger dependence on the supercell size. For example, in Fig. 18, all of the low-frequency modes in a-Ge are delocalized according to MSE, but several are localized according to PR.

Ignoring for the moment the handful of low-frequency, low-PR modes in a-Ge, both the PR and MSE exhibit a transition around 12 THz between delocalized and localized modes, indicating a degree of consistency between the two methods; though the MSE has been designed specifically to describe aspects of localization not necessarily captured by PR, it is nonetheless expected that many, if not most modes described as localized via one descriptor will also be localized according to the other.

It should also be pointed out that, as mentioned previously, once the MSE of a mode in a system exceeds ~10 Å, a larger MSE does not generally indicate a more delocalized mode[11]. Thus, the fact that the MSE of most modes with ω < 12 THz spans 2 orders of magnitude is actually insignificant and does not appear to provide additional insight into the behavior of the modes. This is because the 1-10 Å regime is the most significant.

Many of the same observations can be made for a-PMMA. Fig. 20 shows the PR and MSE of the modes in a-PMMA as a function of frequency.

[11]It has not been determined whether this finding remains true for a much larger supercell with dimensions of, say 200 Å x 200 Å x 200 Å, but the finding does hold across all situations studied in this dissertation. See Appendix F for further discussion.

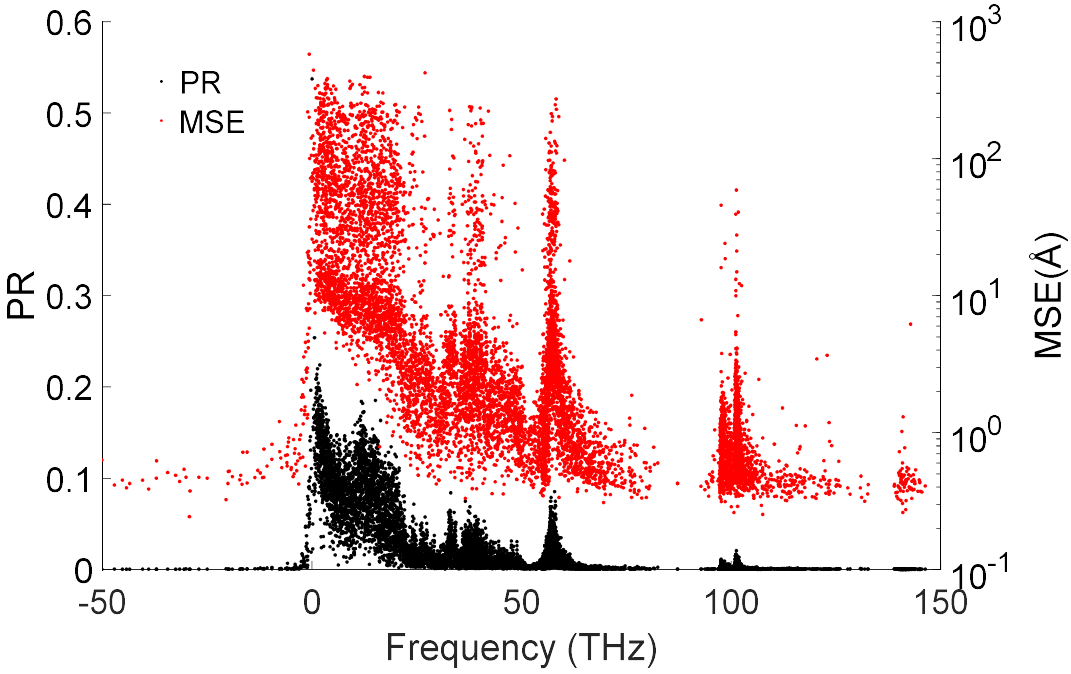

Figure 20. PR and MSE of each mode in the a-PMMA supercell studied as a function of frequency.

Here, modes with $\omega > 25$ THz are of particular interest. According to the MSE, many of these modes are spatially delocalized, despite a (rather) low PR. Visually inspecting some of these modes – the modes shown in Fig. 17 are examples – it is apparent that these modes do in fact exhibit some degree of delocalization. This result is rather surprising – much more so than the discovery of a few low-frequency, low-PR modes in a-Ge. In the case of a-PMMA, the PR indicates that while almost *all* the modes are locons (90% have a PR < 0.1), the MSE calculations indicate 25% of the modes are spatially delocalized (MSE > 10 Å) and a further 47% of the modes are partially-delocalized (1 Å < MSE < 10 Å). The disparity between these two results is remarkable, particularly in comparison to the results for a-Ge. The results for a-PS and a-PVC are similar: for a-PS, 95% of modes have a PR < 0.1, but 11% have an MSE greater than 10 Å, and 41% have an MSE between 1 and 10 Å;

for a-PVC, 97.2% of modes have a PR < 0.1, despite 14% having an MSE greater than 10 Å, and 58% have an MSE between 1 and 10 Å.

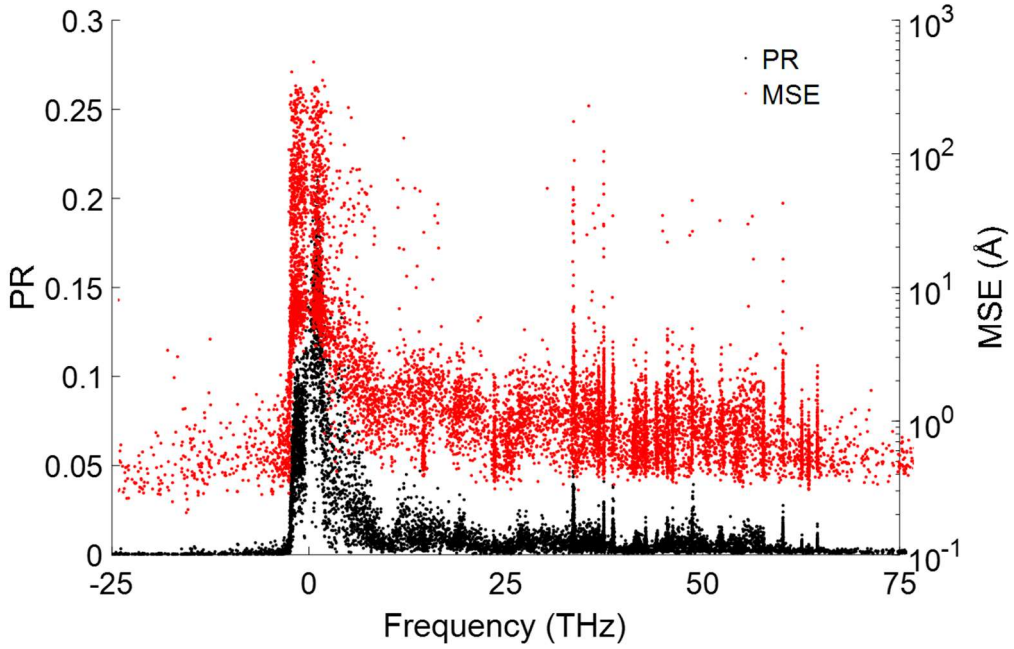

Figure 21. PR and MSE of each mode in the a-PS supercell studied as a function of frequency.

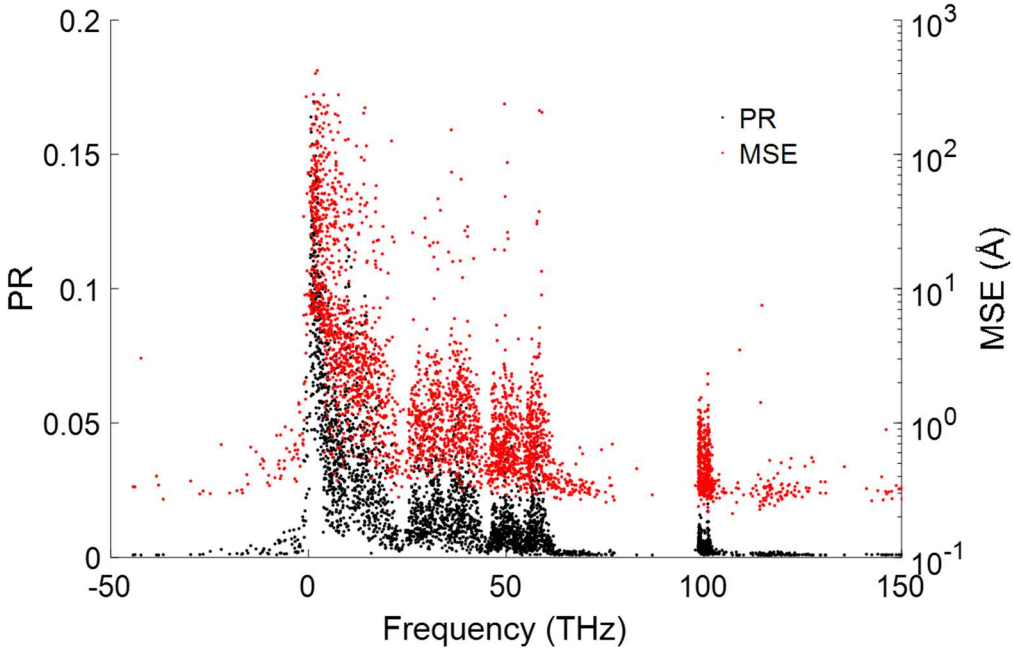

Figure 22. PR and MSE of each mode in the a-PVC supercell studied as a function of frequency.

As with prior trends, the fact that this discrepancy between PR and MSE holds across such different amorphous thermoplastics is a good indication that that it is useful to supplement calculations of PR with MSE to better understand the degree of spatial confinement of modes in amorphous polymers. It does not seem unreasonable to postulate that similar results might also exist for thermosets, although this hypothesis has not yet been tested. Regardless, this discrepancy between descriptors is an indication that perhaps "locons" (specifically, modes with PR < 0.1) may be able to interact with other modes more than previously thought, thereby – contrary to the findings of many previous studies [53-56] – playing an important role in thermal transport. These findings are discussed in *Section 4.3 Question 3: The Relationship Between Mode Localization and Thermal Conductivity in Amorphous Thermoplastics*, regarding how modes with different degrees of localization contribute to thermal transport. However, first another recently-developed descriptor of mode localization will be introduced, namely, a calculation of the PR of a single polymer chain, (rather than the entire supercell).

4.2.2 The Participation Ratio of a Polymer Chain

As noted previously in this chapter, while one can examine the spatial confinement of a vibrational mode via the MSE, the unique structure of polymers may potentially lead to a different means of modal confinement, and it is particularly interesting to consider whether there is localization/confinement to a single polymer chain. The argument for why/how this confinement may occur is as follows: due to the extreme disparity between intermolecular and intramolecular bonds (i.e. hydrogen/van der Waals vs. covalent bonds – which are ~10^2 x stronger), atoms are connected much more strongly to other atoms along

a single polymer chain than to atoms in other chains[12]. Thus, a vibration can propagate more easily along a polymer chain, due to the stronger bond strength between atoms along the chain. This preference for propagation along a single chain could in turn lead to localization within a chain, rather than a particular region of space. However, it appears that no one has ever performed a study, computational or experimental, to examine if modes do in fact localize to single polymer chains. The procedure for calculating the PR has therefore been modified to allow one to determine the degree to which modes are localized to a single polymer chain; this procedure is described in the next section. As with the MSE, the procedure for calculating this new descriptor is first discussed, after which some interesting results are shown.

4.2.2.1 Method for Calculating the Polymer Chain Participation Ratio

First, consider again the formula for calculating PR:

$$PR_n = \frac{\left(\sum_i^N \mathbf{e}_{i,n}^2\right)^2}{N\sum_i^N \mathbf{e}_{i,n}^4} \tag{3}$$

In the equation above, N is the total number of atoms in the *supercell*. The only modification made to determine the polymer chain PR (PCPR) is to restrict the sum in the numerator to only those atoms in a single polymer chain, i.e. for a polymer with M atoms in a polymer chain, the PCPR sum would be

[12]Factors such as cross-linking and branching will change how modes are spread across polymer chains. However, accounting for these factors is beyond the scope of this work, as this work is restricting itself to linear polymer chains with no cross-linking.

$$PCPR_n = \frac{\left(\sum_i^M \mathbf{e}_{i,n}^2\right)^2}{N\sum_i^N \mathbf{e}_{i,n}^4} \tag{26}$$

There will be a total of N/M PCPR values for each mode (each corresponding to a single polymer chain). This method has been derived and applied for systems for which there are an equal number of atoms on each chain. If one wished to normalize PCPR for systems with a different number of atoms on each chain, one could presumably normalize the PCPR differently, namely by

$$PCPR*_n = \frac{\left(\sum_i^M \mathbf{e}_{i,n}^2\right)^2}{M\sum_i^N \mathbf{e}_{i,n}^4} \tag{27}$$

If, however, the number of atoms on each polymer chain are the same, these two PCPR's will just differ by a factor of M/N, and there is no particular reason to use one value over the other. This work will use the PCPR defined in Eq. (26).

Comparing the value of each PCPR can provide insight into the localization of modes in polymers. The next section highlights some of these findings.

4.2.2.2 Using the Polymer Chain Participation Ratio for Describing Mode Localization

When assigning $PCPR_1$, $PCPR_2$, etc., for each individual mode, PCPR's are sorted by decreasing value independent of the PCPR values for other modes. The $PCPR_1$ will always be the largest PCPR *for a given mode*, and the $PCPR_{N/M}$ will be the smallest. Thus, the $PCPR_1$ for one mode may correspond to a different polymer chain than the $PCPR_1$ for a

different mode, thus if one wishes to compare all modes on a single polymer chain, one will compare a mix of $PCPR_1$'s, $PCPR_2$'s, etc. In fact, assuming a large enough supercell with a polydispersity of 1 for all polymer chains (and that the polymer is indeed amorphous), an even distribution of $PCPR_1$'s (and $PCPR_2$'s, and so on) among the chains in the supercell is expected. This is indeed the case for the polymer systems studied: in the case of each polymer (each of which has four equal-length polymer chains), approximately 25% of the modes have a $PCPR_1$ that corresponds to a particular polymer chain. (A different 25% of modes have a $PCPR_1$ corresponding to a second chain, and so on.) Furthermore, for the 25% of modes with a $PCPR_1$ on one particular chain, for any given mode, there is a 33% chance the $PCPR_2$ will correspond to any one of the remaining three chains, and so on. Thus, the PCPR of any given mode is effectively independent of the PCPR for any other mode.

Whereas the values for PR can range from $1/N$ to 1, values of the PCPR will range from 0 to M^2/N^2. In the case where a mode is confined entirely to a single chain, the $PCPR_1$ will be equal to the PR of the mode, and all other PCPR's will be 0. In the case that a mode is evenly spread across all polymer chains, the maximum PCPR of each chain is M^2/N^2 : assuming each chain has an equal number of atoms, and given that the PR must be ≤ 1, the value of $\sum_i^M \mathbf{e}_{i,n}^2$ in Eq. (26) must be $\leq M/N$. Thus, the value of $\left(\sum_i^M \mathbf{e}_{i,n}^2\right)^2$ must be $\leq M^2/N^2$. Furthermore, following a similar argument, the PR of a mode is equal to the 2-norm (the square root of the sum of squares) of the PCPR's of that mode.

To illustrate how the PCPR can be used, consider first an illustration of how it works. Fig. 23 below shows the eigenvectors of a mode with ω = 101 THz. This mode has PCPR values that range from 5.6 x 10^{-4} to 6.4 x 10^{-4}.

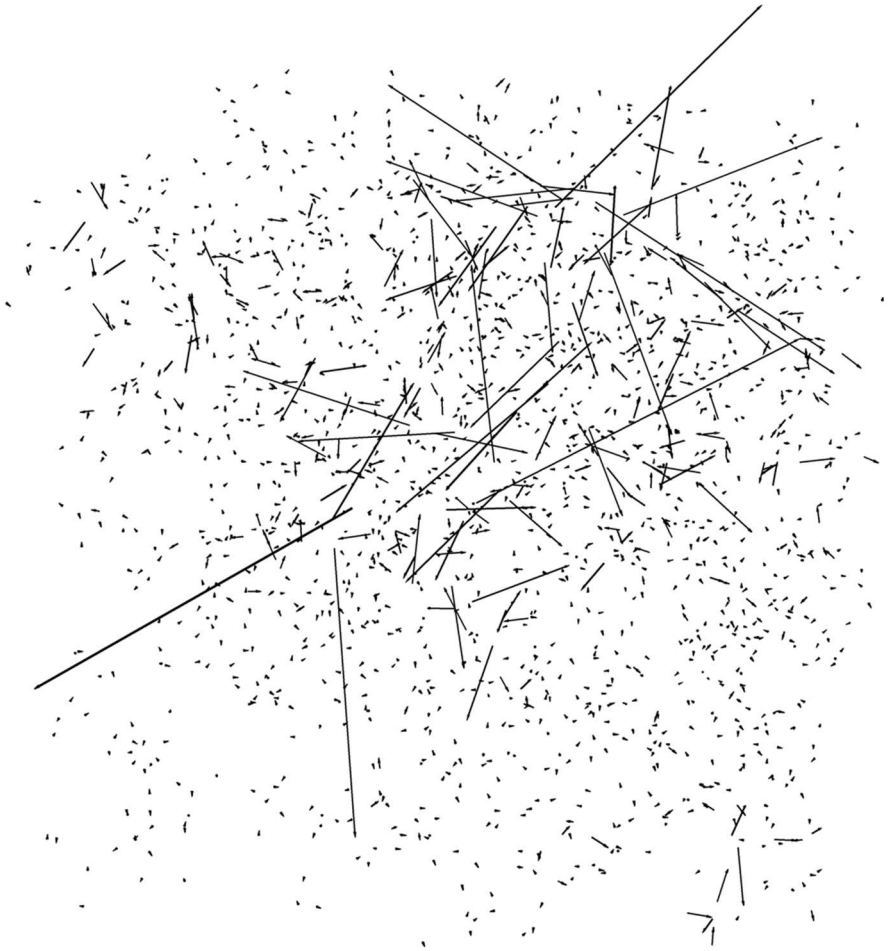

Figure 23. Eigenvectors of a normal mode in a-PMMA with ω = 101 THz, PR = 0.01, and MSE = 3.3 Å.

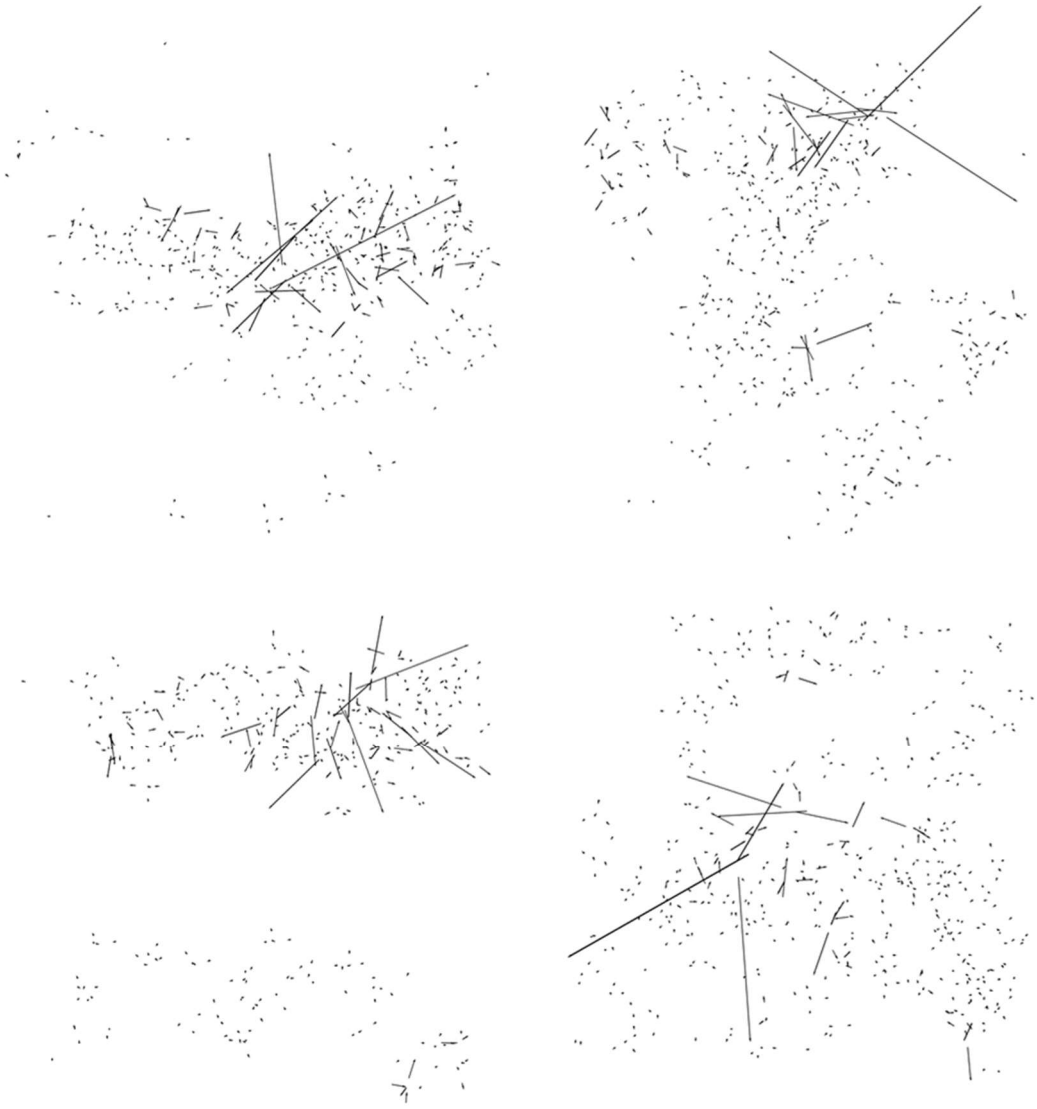

Figure 24. The same mode as in Fig. 23, but with the eigenvectors only shown for a single polymer chain in each case: $PCPR_1 = 6.4 \times 10^{-4}$ (top left), $PCPR_2 = 6.3 \times 10^{-4}$ (top right), $PCPR_3 = 6.0 \times 10^{-4}$ (bot left), and $PCPR_4 = 5.6 \times 10^{-4}$ (bot right). The difference between $PCPR_1$ and $PCPR_4$ is only 13%.

While there is some amount of spatial localization apparent in this and other similar modes, it is still remarkable how spatially diffuse the mode is, considering its high frequency and low PR (0.01). For the mode shown, the eigenvectors of each of the four polymer chains are plotted separately in Fig. 24. Note that on each polymer chain, at least some of the eigenvectors of the atoms are large: were the mode localized to a single chain, the

eigenvectors in three of the four images would appear as just dots (i.e. their length would be ~0).

To understand the PCPR more broadly, consider the PCPR's of each mode in a-PMMA as a function of frequency, plotted in Fig. 25 below.

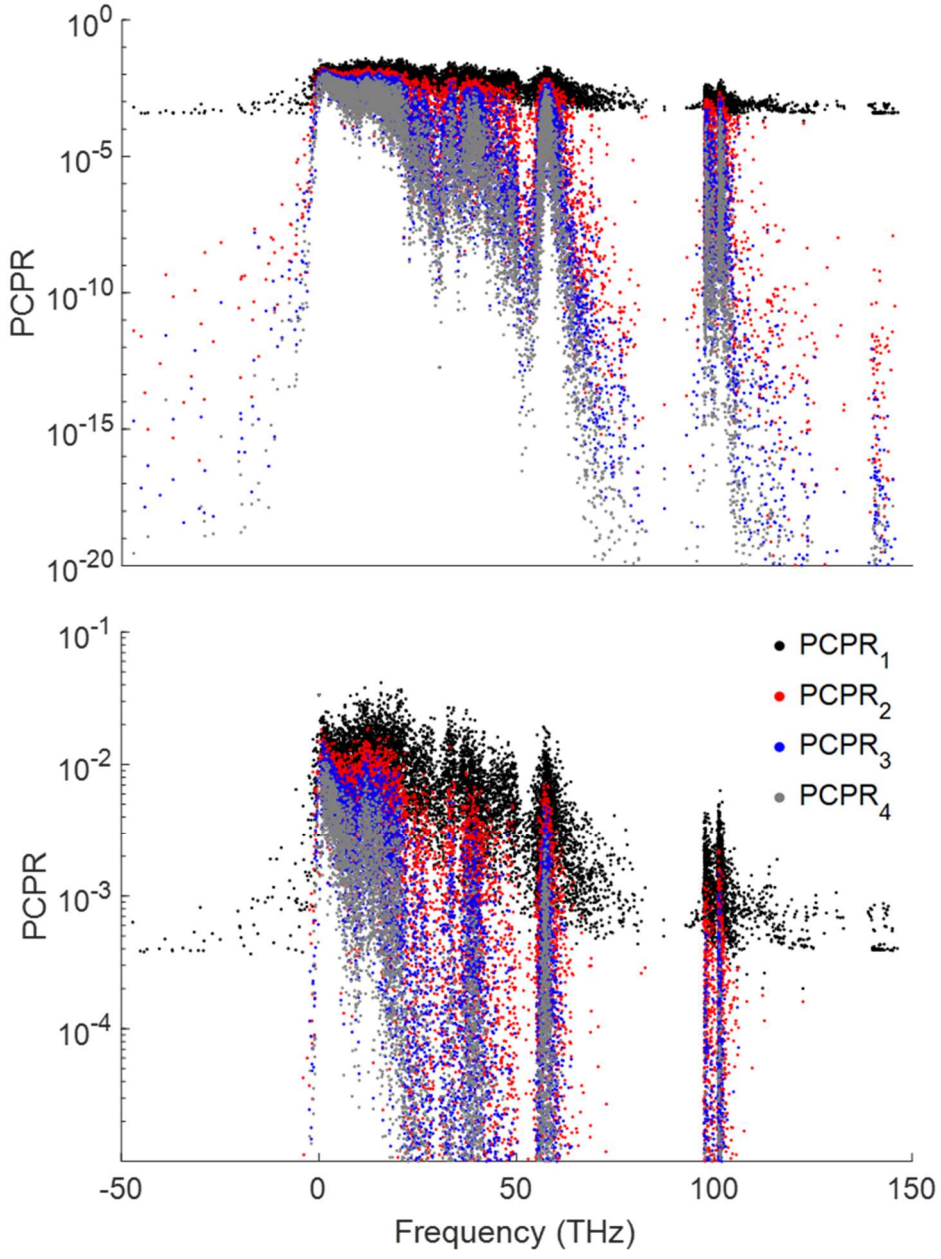

Figure 25. PCPR values for each mode in a-PMMA as a function of frequency. The bottom figure is a zoomed-in version of the top figure.

As discussed in the previous section, the largest PCPR ($PCPR_1$) must be between $1/N$ and M^2/N^2; this confinement is apparent in Fig. 25. On the other hand, all other PCPR's can range from 0 to M^2/N^2, so compared to other PCPR's, the $PCPR_1$ is restricted to a small range of values.

It is the $PCPR_2$ that will indicate whether a mode is confined to a single polymer chain or if it is spread across multiple chains: if the $PCPR_2$ is on the order of the $PCPR_1$ (i.e. $\gtrsim 1/N$), the total magnitude of vibration of atoms on at least two chains (obtained by summing the square of the magnitude of the eigenvectors on a given chain) will be roughly equal on at least two polymer chains. On the other hand, if the $PCPR_2$ is much lower (i.e. more than 1-2 orders of magnitude) than the $PCPR_1$, the atoms with a significant degree of excitation for that mode exist primarily on one chain, and thus the mode is localized to that single chain. Similarly, the third highest PCPR ($PCPR_3$, and so on) can give one an indication of *how* spread among different polymer chains a mode is. If the $PCPR_{N/M}$ (the lowest PCPR for a mode) is close to the value of the $PCPR_1$, then the mode is spread evenly among all the polymer chains in the supercell.

Considering Fig. 25, it is apparent that most IF modes and many high-frequency RF modes are localized to a single chain (i.e. their $PCPR_2$'s are extremely low). Interestingly, there appear to be frequency bands of modes (around 50 THz for instance), in which the modes are almost entirely localized mostly to a single chain, whereas other bands contain modes exhibiting a wide range of degree of localization. In fact, one unexpected result here is the number of large $PCPR_2$, $PCPR_3$, and $PCPR_4$ values at high frequencies. Consider, for instance, modes with frequency ~100 THz (which is the frequency band that includes the

mode shown in Figs. 23 & 24). Even though, based on other amorphous materials that have been studied in the past, it would be expected that these modes are highly localized vibrations (probably involving only a few H atoms), the modes are spread across not just two, but *all four* polymer chains (as evidenced by large $PCPR_4$ values)[13].

Returning to Fig. 25, while there is unsurprisingly a notable difference between the trends of $PCPR_1$ and $PCPR_2$, there is not as significant a difference between the general trend in $PCPR_2$, $PCPR_3$, and $PCPR_4$ for most modes. Consider, for instance, the RF modes with ω < 10 THz (IF modes will be discussed in *Chapter 5. Imaginary Frequency Modes in Amorphous Polymers*). Of the 1143 modes that fall in this frequency window, with the exception of a single $PCPR_4$, all PCPR's for all modes are > 10^{-5}, and virtually every $PCPR_4$ is within two orders of magnitude of the $PCPR_1$. Thus, each low-frequency mode is spread among all four polymer chains and in this sense can be considered "delocalized"[14].

Another interesting observation from Fig. 25 is that modes are generally either spread across all polymer chains in a supercell (as they are at low frequencies) or confined to a single polymer chain. In other words, localization with respect to polymer chains appears to mostly be all-or-nothing, as there are very few modes in a-PMMA that experience significant vibrations on exactly two or three polymer chains. There are very few modes with "large" (i.e. $\gtrsim 10^{-5}$) $PCPR_2$'s that have extremely small (say, < 10^{-10}) $PCPR_3$'s – of

---

[13]For the mode shown in Figs. 23 & 24, although the mode is evenly divided among four different polymer chains according to PR, it is not because every atom is excited equally, as in the case of low-frequency delocalized modes, but rather because a few atoms are excited on each polymer chain. This result indicates that while modes may not be entirely localized, they are also not completely delocalized, which is consistent with the mode's MSE (3.3 Å).

[14]In fact, based on PCPR, noticeable chain localization does not occur until ~20 THz, and significant localization does not occur until ~60 THz.

the 9024 modes in a-PMMA, only 62 such modes fit these criteria. It was expected that perhaps there are solutions to the equations of motion that would describe a localized interaction between exactly two polymer chains while largely ignoring other atoms in the system; in such cases, one would expect a large $PCPR_2$ and a small $PCPR_3$, however the existence of such modes seem to be minimal. Thus, with very few exceptions, if a mode spans more than one polymer chain, it spans all polymer chains, at least for the systems studied here.

The exceptions to this finding exist as a handful of modes with high $PCPR_2$'s and rather low $PCPR_3$'s (evident at ~80 THz and ~120 THz in Fig. 25 for instance). These modes are notable because they occur in frequency ranges where modes are otherwise confined to a single polymer chain. Furthermore, in general, the DOS is rather low in these frequency ranges, so for a particular low $PCPR_2$ mode (which again, is the case for most modes in these frequency bands), there exist very few other modes with which the given mode can couple. These high $PCPR_2$ modes will be discussed further in *Section 4.3.2 The Relationship Between Thermal Conductivity and Mode Localization in Amorphous Polymers*.

Returning to Question 2, the majority of modes in amorphous polymers can be considered localized, in that the PR is <0.1, the MSE is < 1 Å (i.e. the "size" of the mode is small), and the $PCPR_2$ of the given mode is multiple orders of magnitude lower than its $PCPR_1$. In such cases, the mode can be considered localized regardless of the measure of localization. There are some instances where categorizing the mode as localized will depend on the method of classification used. As will be shown in the next section, it is often these modes

which exhibit interesting trends in TC compared to modes for which all measures of localization are in agreement.

4.3 Question 3: The Relationship Between Mode Localization and Thermal Conductivity in Amorphous Thermoplastics

Question: *Do localized modes contribute to TC in the amorphous thermoplastics in this study?*

Hypothesis: *Locons will be a significant carrier of thermal energy in amorphous polymers, especially since, as has been observed, they are the predominant mode type. However, it is hypothesized that a larger PR will correspond to larger TC contributions.*

As has been noted previously, the prevailing sentiment is that locons are negligible contributors to heat flow [2, 3, 12, 52-56]. These modes are thought to be too spatially confined to interact with other modes at similar frequencies, so the energy in a locon remains largely "trapped". It has also been pointed out however that recent work utilizing GKMA [6] has provided evidence that in a-SiO_2, locons are actually significant contributors to TC. It is worth noting here that a-SiO_2 is comprised of multiple atomic species in a disordered structure; thus, while the material is still quite different from a polymer, it does share some characteristics with polymers that indicates similar results may be observed when studying polymers.

This work will predominantly focus on the relationship between mode localization and TC in polymers, as these results are by far the most compelling. However, presented first is a quick study of a-Ge, which can serve as a point of comparison.

4.3.1 The Relationship Between Thermal Conductivity and Mode Localization in Amorphous Germanium

The TC of each mode is shown below in Fig. 26 as a function of frequency, Fig. 27 as a function of PR, and Fig. 28 as a function of MSE. Modes that will be discussed in more detail in this section are highlighted in red. The TC accumulation as a function of frequency is also plotted in Fig. 29.

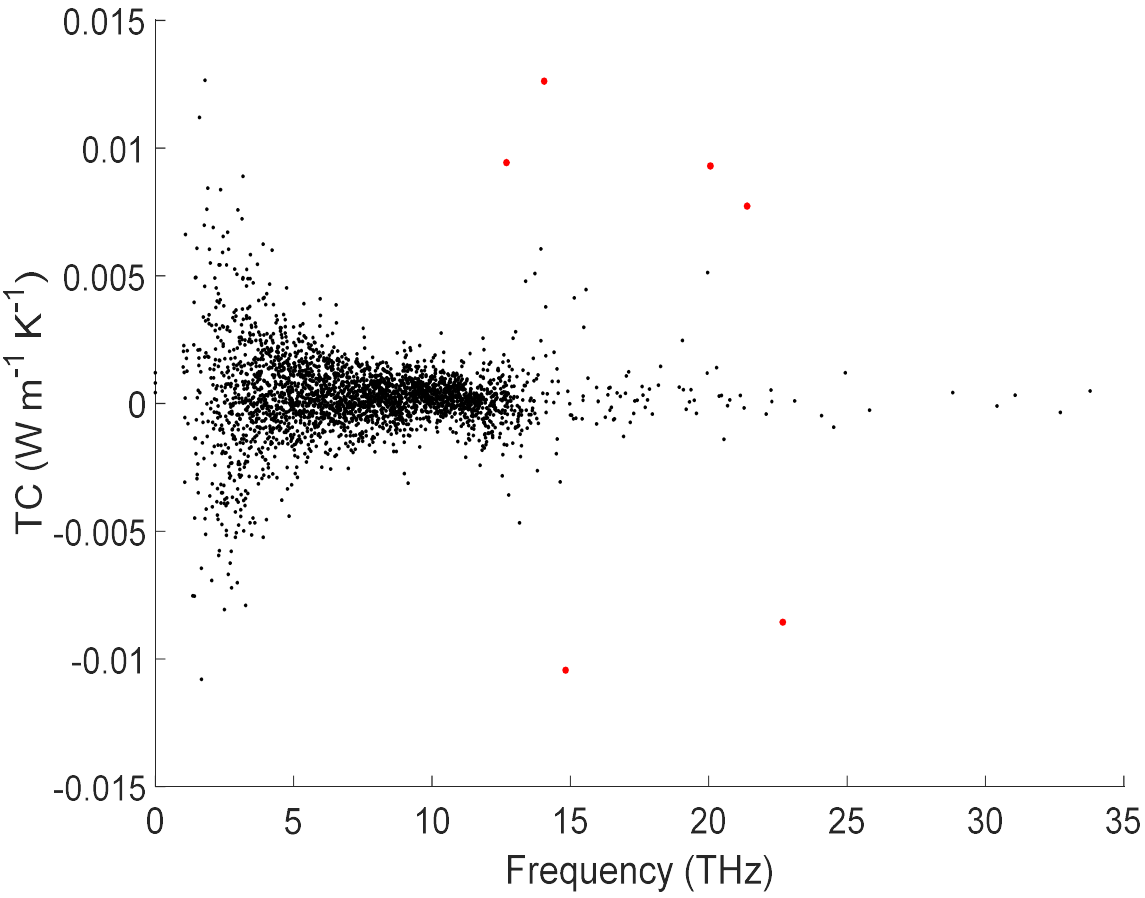

Figure 26. Modal TC vs. frequency for a-Ge. The modes shown in larger red dots are high-frequency modes with a large TC. They are also shown in red in Figs. 27 and 28.

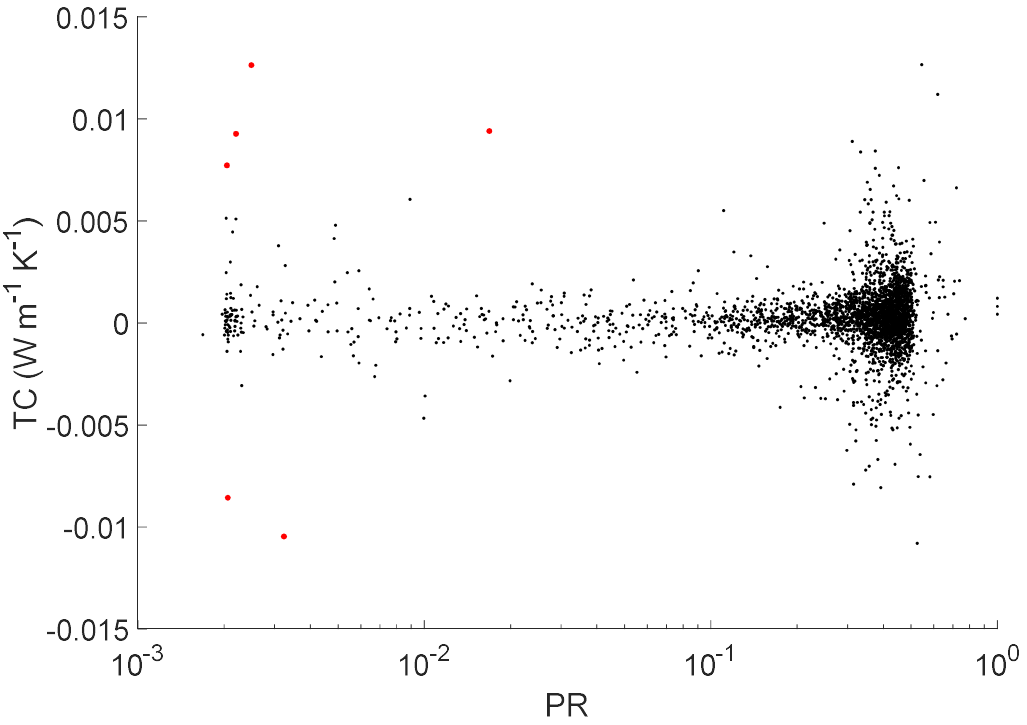

Figure 27. Modal TC vs. PR for a-Ge. The modes shown in larger red dots are the same as those in red in Figs. 26 and 28.

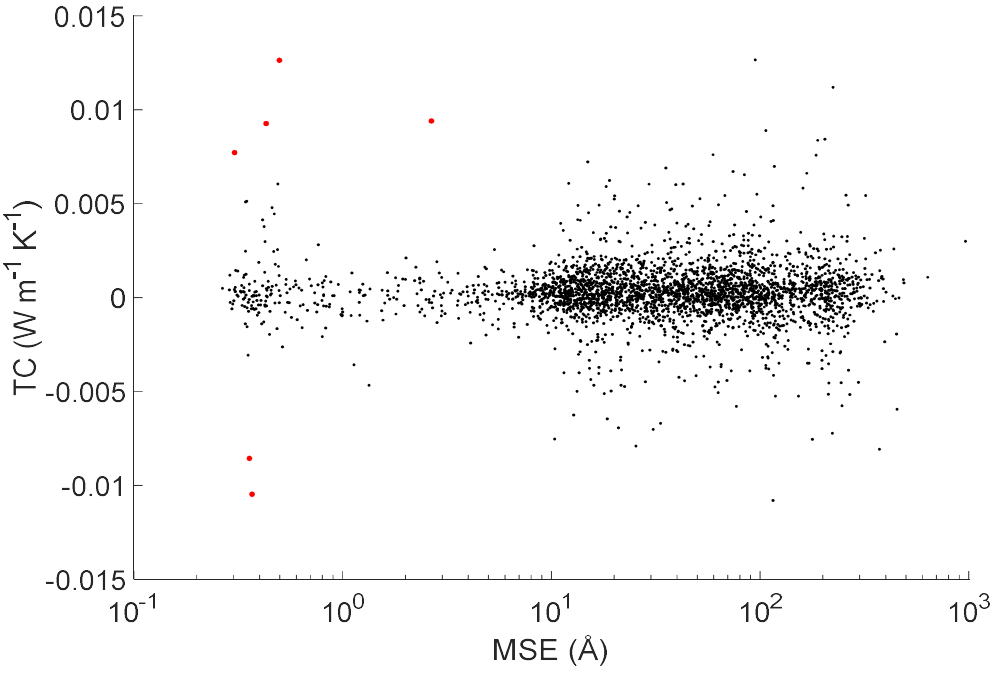

Figure 28. Modal TC vs. MSE for a-Ge. The modes shown in larger red dots are the same as those in red in Figs. 26 and 27.

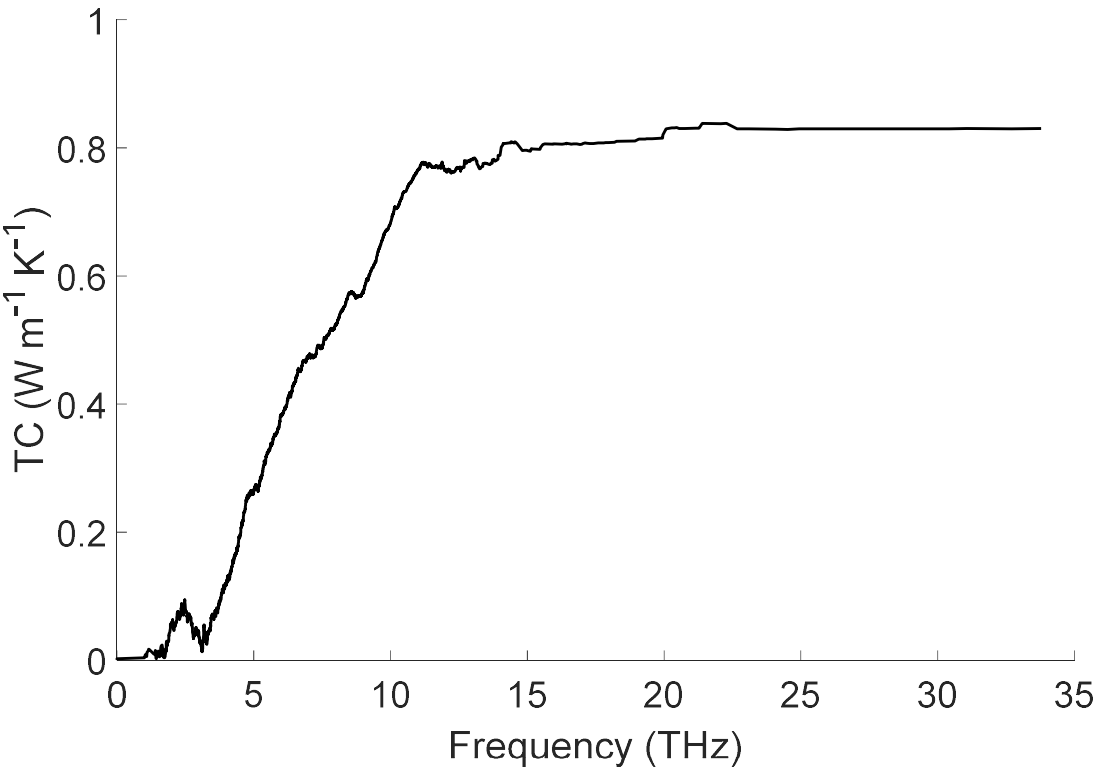

Figure 29. TC accumulation as a function of frequency for a-Ge.

The results obtained for a-Ge are – broadly – in line with previous observations: the TC of low-frequency, delocalized modes tend to be much larger in magnitude than that of high-frequency localized modes[15]. It is apparent, however, that there are exceptions to this finding, namely the modes highlighted in red. After examining these modes further, there does not appear to be anything particularly unusual about the character of these modes when compared to other modes with similar frequencies. Qualitatively, they appear quite similar to other modes with a similar frequency and degree of localization. One notable

[15]This work will be focusing on the magnitude of modal TC, rather than whether it is positive or negative. This is because in general, the trends observed are independent of whether the TC of a mode is positive or negative, but not of its absolute magnitude.

(but perhaps unsurprising) result regarding the anomalous modes becomes apparent when plotting the cross-correlation[16] of all the modes in a-Ge, shown in Fig. 30.

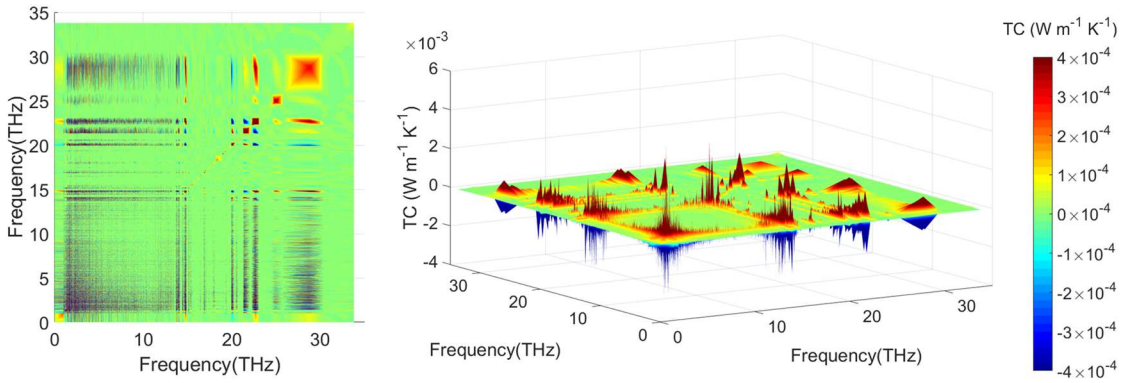

Figure 30. Cross correlation of all modes in a-Ge, shown from two different perspectives. The range of the colorbar is limited intentionally to emphasize features of the correlation map.

Two separate bands near 15 and 20 THz respectively can be observed in the figure, which correspond to the modes highlighted in Figs. 26-28. It is quite apparent that the modes highlighted are interacting with modes at all frequencies much more than other comparable modes. This higher degree of interaction leads to a higher magnitude of TC for these high-frequency modes, however, the majority of the TC is still due to a large number of modes in a relatively small frequency range (~2-5 THz).

The anomalously high TC locons aside, the behavior of a-Ge is for the most part in-line with previous findings and most of the results are to be expected: as noted, the low-frequency delocalized modes are expected to contribute the most to TC, which for the most part is indeed the case. In the next section, these results be compared to those for amorphous polymers, and several significant differences will be highlighted.

[16]Cross-correlation between modes is discussed in Section *3.2.2 Green-Kubo Modal Analysis*. It is a measure of the collective contribution of two different modes to the system's TC.

4.3.2 The Relationship Between Thermal Conductivity and Mode Localization in Amorphous Polymers

Fig. 31 gives the modal TC of a-PMMA[17] as a function of frequency, and Fig. 32 gives the accumulation of TC with respect to frequency.

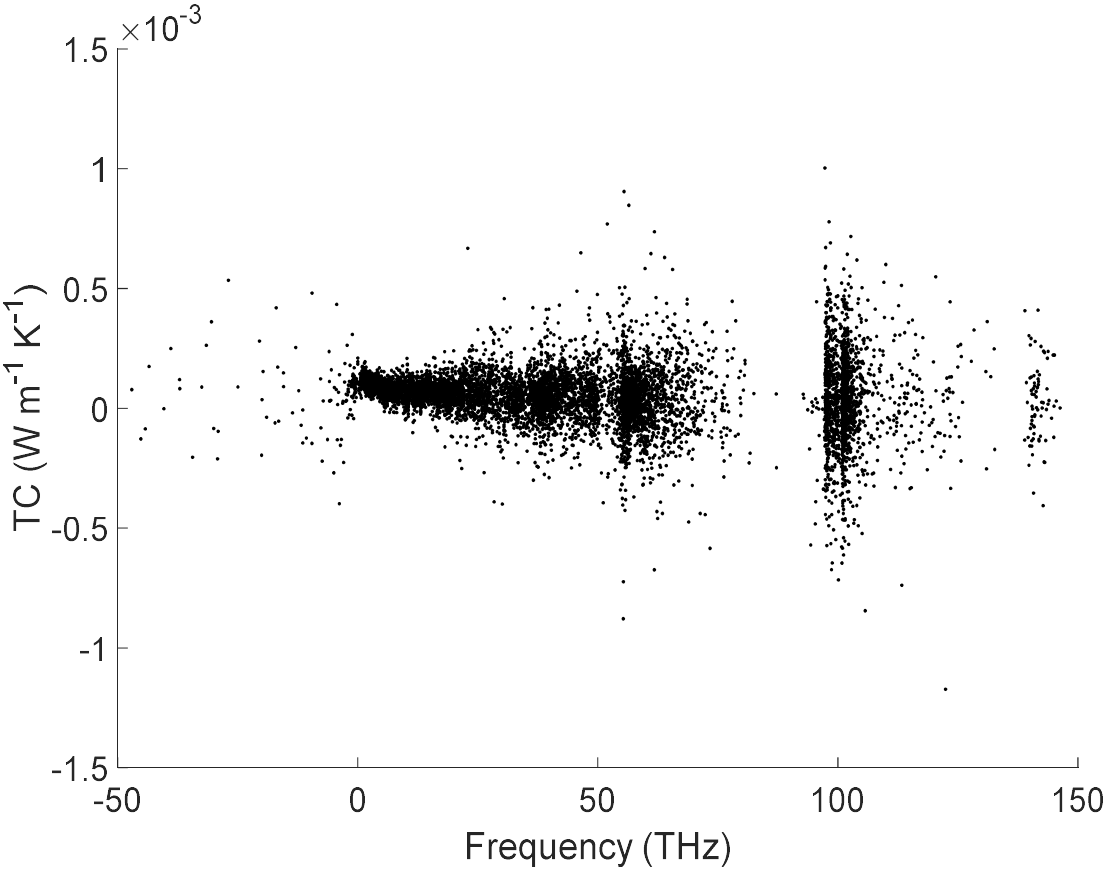

Figure 31. Modal TC vs. frequency for a-PMMA.

[17]As with the rest of this chapter, findings will focus on a-PMMA for the sake of brevity and clarity, but important or unusual results for a-PS and a-PVC will be discussed when appropriate.

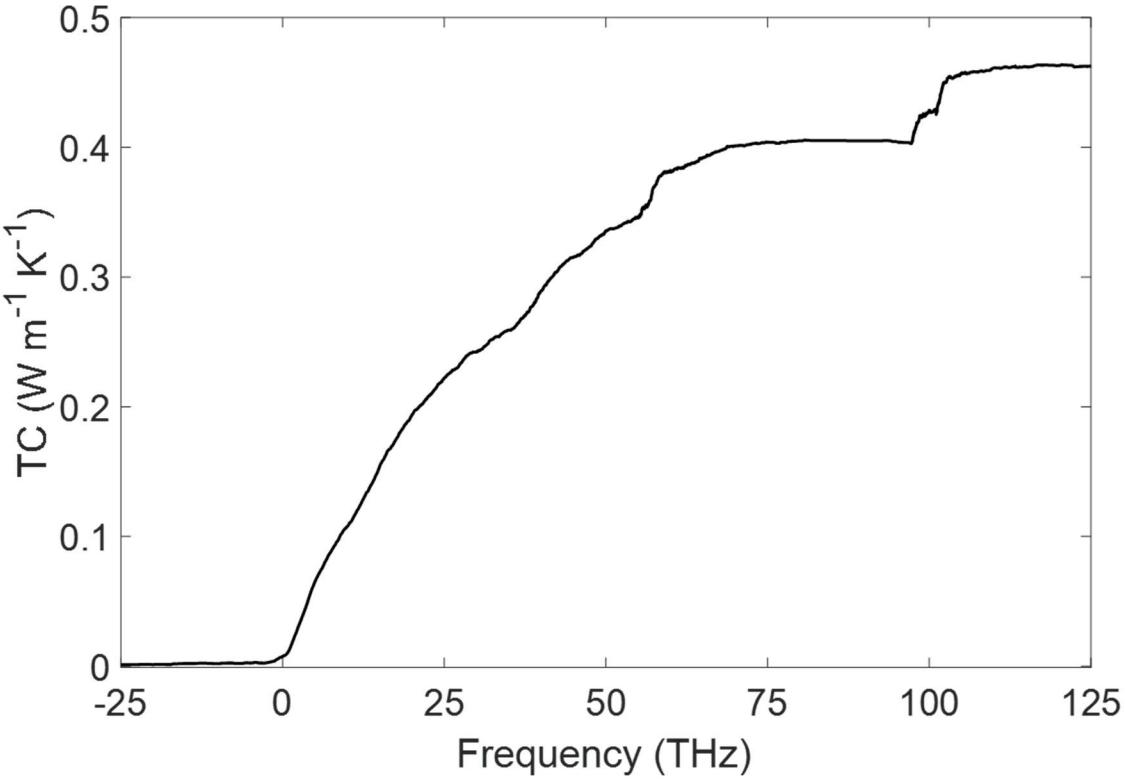

Figure 32. TC accumulation as a function of frequency for a-PMMA.

What is immediately striking about these figures is the disparity between the TC contribution of low-frequency modes and higher-frequency modes, particularly those > 50 THz. (Though certainly of interest, the contribution IF modes will not be discussed until *Chapter 5. Imaginary Frequency Modes in Amorphous Polymers*). Unlike the case for a-Ge, the lowest average magnitude TC modes are those with the *lowest* frequency. This trend is even more apparent when comparing TC to degree of localization, whether PR[18] or MSE:

[18] Comparisons can also be made based on PCPR. However, because there is not a single PCPR for a mode, this comparison is more involved and will be discussed later in this section.

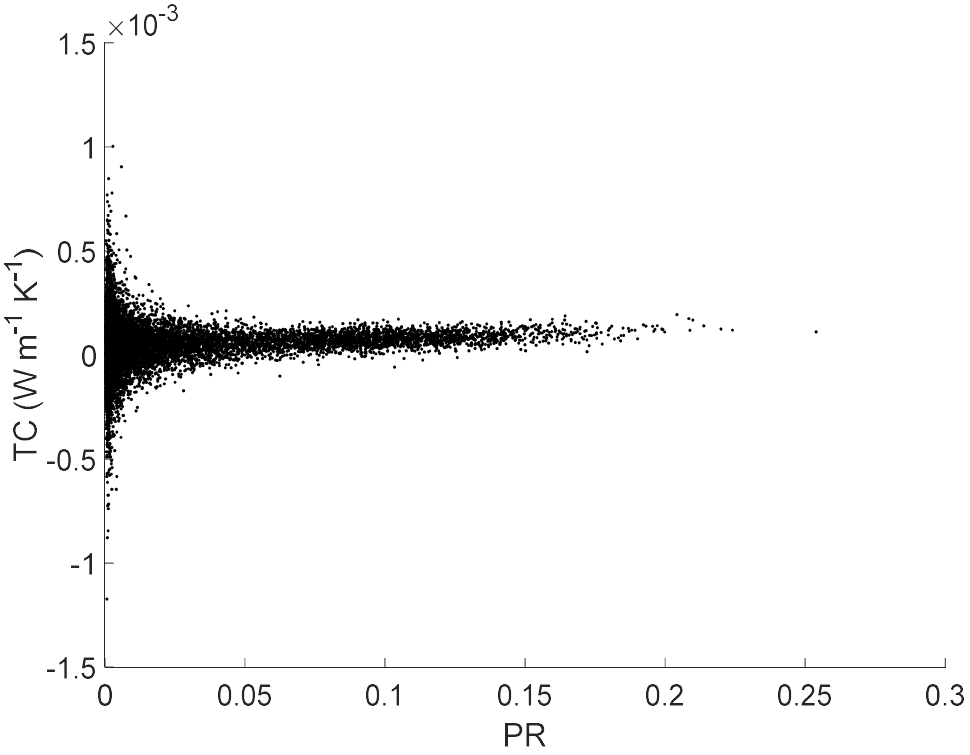

Figure 33. Modal TC vs. PR for a-PMMA.

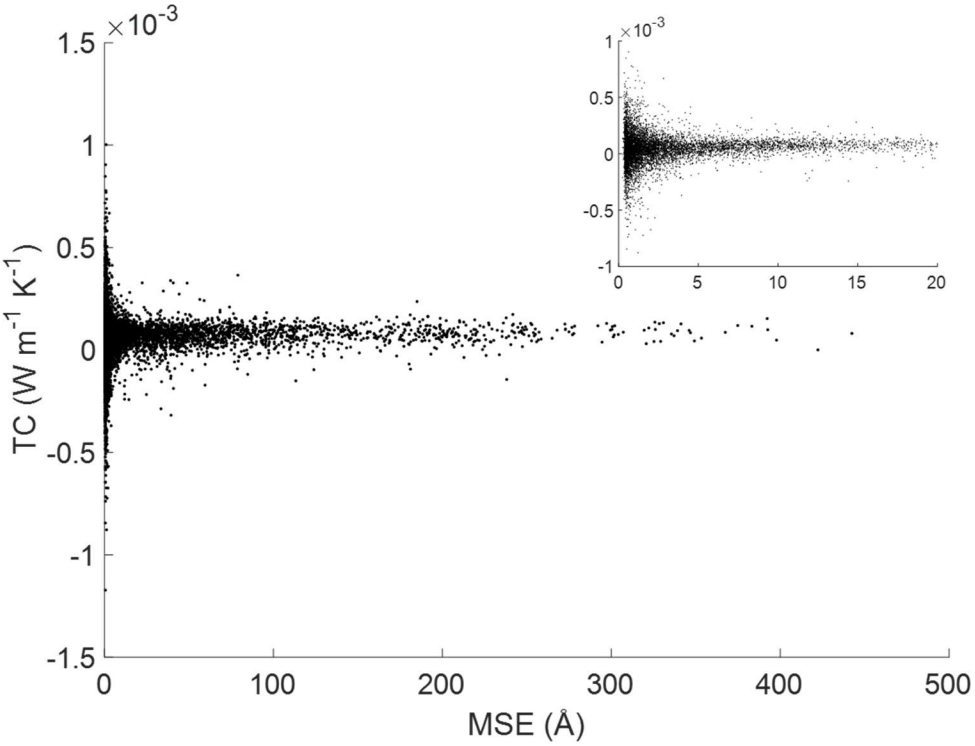

Figure 34. Modal TC vs. MSE for a-PMMA.

The trend here is shocking, but persistent across all three polymers studied: the more localized the mode, the higher the TC magnitude is likely to be. In all other materials studied to this point [2, 3, 6, 12, 52-56], a consistent trend was observed of delocalized vibrational modes comprising the majority of total TC: even in the case of Lv & Henry, [6], locons were found to contribute only 10% of the total TC of the system. The findings presented here for polymers are a radical departure from this paradigm, with locons in the materials studied accounting for well over half the total TC of the materials. In fact, while a low PR or low MSE alone is a good predictor of the magnitude of the modal TC, when accounting for both quantities, the trend becomes even stronger.

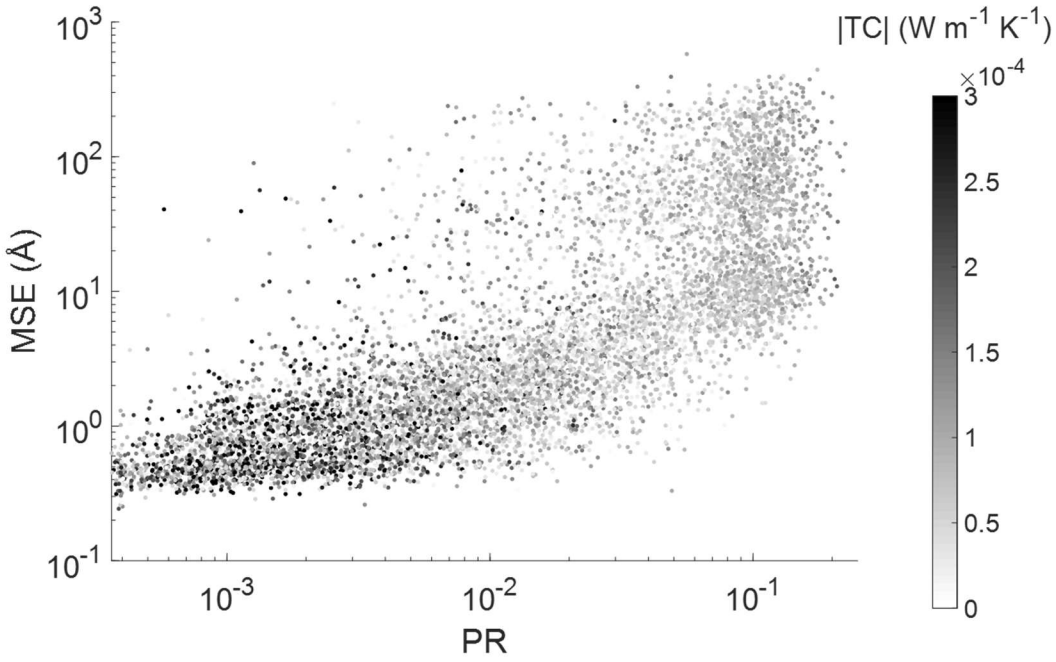

Figure 35. Magnitude of modal TC (shown using grayscale) as a function of PR and MSE for a-PMMA. Note the range of the colorbar only extends to 3 x 10^{-4} W m^{-1} K^{-1}, though the largest modal TC is ~1.2 x 10^{-3} W m^{-1} K^{-1}

It can be seen in Figs. 33-35 that the modes with the largest magnitude of TC are those with a PR < 0.01, an MSE of < 3 Å, or especially those which satisfy both criteria. The data is broken down in Table 1. This table gives the average magnitude of TC *per mode* (which is 9.88 x 10^{-5} W m^{-1} K^{-1} for all modes in the system) and breaks down this TC contribution based on degree of mode localization.

Table 1. Number of modes and average of the absolute value of the TC of each mode for a-PMMA, sorted by different measures of localization.

Localization Delineation	Number of Modes (N)	$\sum^{N}\lvert k\rvert \Big/ N$ (W m^{-1} K^{-1})
all modes	9024	9.88 x 10^{-5}
PR < 0.01	4208	12.8 x 10^{-5}
PR > 0.01	4816	7.25 x 10^{-5}
MSE < 3 Å	4992	11.7 x 10^{-5}
MSE > 3 Å	4032	7.62 x 10^{-5}
PR < 0.01 & MSE < 3 Å	3799	13.2 x 10^{-5}
PR > 0.01 or MSE > 3 Å	5225	7.48 x 10^{-5}

While a PR < 0.01 or an MSE < 3 Å is a good predictor of a high TC magnitude, modes that fit both criteria have even higher TC's than those that fit only a single criterion. This finding is interesting because it means that by applying different measures of localization, one can more strongly predict the magnitude of TC for a given vibrational mode. That is, using both measures of localization is the best way to predict modes with the largest magnitude TC. The relationship between modal TC and localization is puzzling, and while a full explanation will not be posited in this dissertation, there do exist some results that provide hints at what may be special about these highly-localized, high TC modes.

To explain what is special about these modes, first, consider again the relationship between modal TC and PCPR. As noted, the value of particular interest in such cases is the $PCPR_2$, i.e. the second largest PCPR for a given mode. For some modes, all the PCPR (and particularly, the $PCPR_4$) values are large (which does not mean the actual PR of the mode is large). This is the case with low frequency RF modes and some bands of high frequency modes in a-PMMA (see Fig. 25, reproduced below), in which the mode is spread across all four polymer chains. However, there exist a few modes with large ($> 10^{-5}$) $PCPR_2$'s and low ($< 10^{-10}$) $PCPR_3$'s (consider, e.g. around 50 THz). These modes are interesting because they all exist in frequency ranges where most modes are confined to a single chain, and *no* modes are spread across three or more chains. Thus, on an individual polymer chain basis, the modes with large $PCPR_2$'s in these frequency bands (of which there are a total of 62 out of 9024) are the only modes that are at all delocalized onto a second chain. Interestingly, the average magnitude of these 62 modes' TC is 18.4×10^{-5} W m^{-1} K^{-1}. This value is 60% *higher* than the average magnitude of TC for modes with both a low PR and MSE but for which no PCPR criteria are applied, and it is nearly *twice* the magnitude of the average mode in a-PMMA. Thus, it appears there is something unique/interesting about these modes.

To discern why these modes with high $PCPR_2$'s and low $PCPR_3$'s are so important, consider the cross-correlation of the modal TC in a-PMMA.

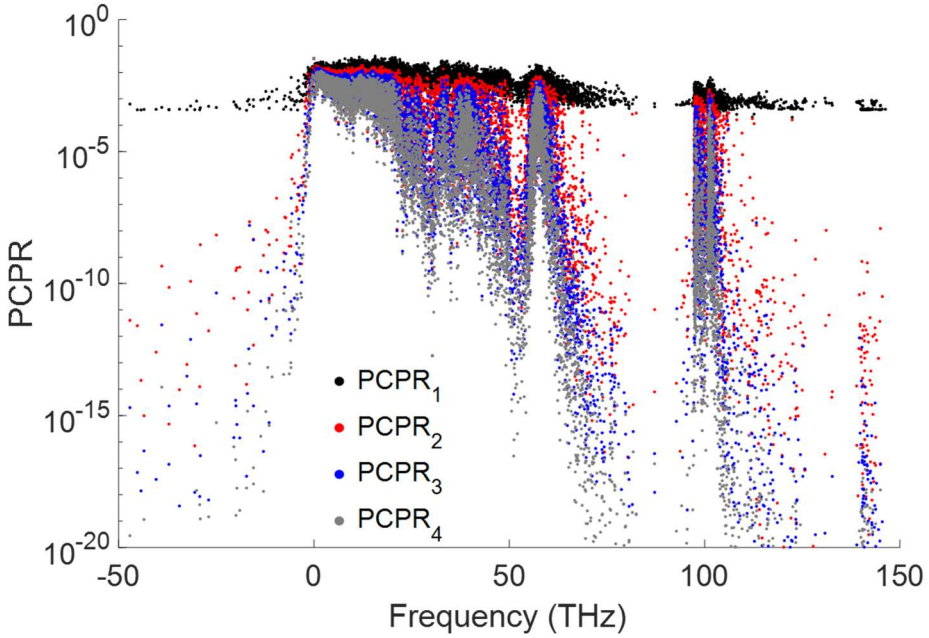

Figure 25. PCPR values for each mode in a-PMMA as a function of frequency.

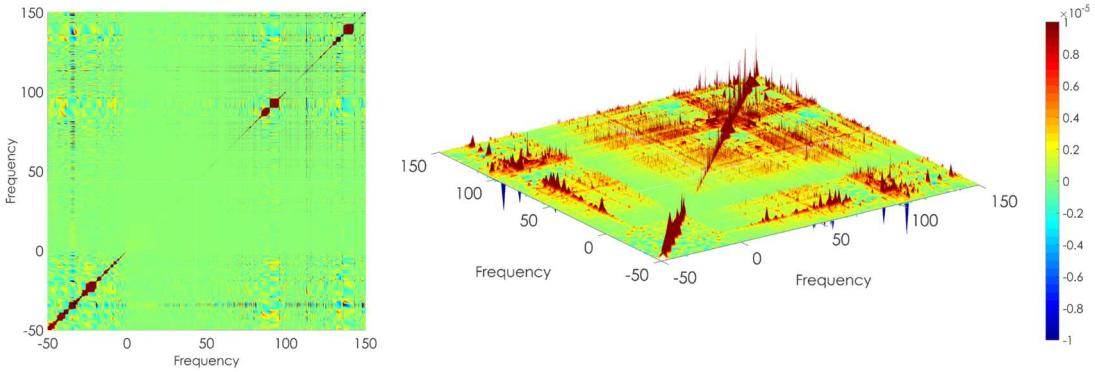

Figure 36. Cross correlation of all modes in a-PMMA, shown from two different perspectives. The range of the colorbar is limited intentionally to emphasize features of the correlation map.

Examining Fig. 25 first, note the modes in the frequency ranges 65-95 THz and >105 THz. There are few modes in this frequency range, and the modes that do exist are mostly localized to a single polymer chain. Virtually every mode has a $PCPR_3 < 10^{-8}$, indicating that the modes exist on *at most* two polymer chains. However, as pointed out in Section *4.2.2.2 Using the Polymer Chain Participation Ratio for Describing Mode Localization*, among this already sparse collection of modes, only a handful have a $PCPR_2 > 10^{-5}$. Thus,

nearly all modes in this frequency range are confined to a single polymer chain, and a few are spread across exactly two chains.

Considering these high $PCPR_2$, low $PCPR_3$ modes (in the frequency bands 65-95 THz and > 105 THz), these modes have a large cross-correlation with other modes, particularly those at similar frequencies. For modes in these frequency ranges, those with $PCPR_2 > 10^{-5}$ only comprise 39/4512 (0.86%) of all other modes in these frequency windows. Furthermore, the average TC of any mode pair in which one mode has $PCPR_2 > 10^{-5}$ is 2.72×10^{-8} W m^{-1} K^{-1}, while the average cross-correlation TC for a mode is 1.83×10^{-8} W m^{-1} K^{-1}. Thus, the modes highlighted here with large $PCPR_2$'s also contribute disproportionately to TC.

The situation is similar for a-PS. First, consider modal TC as a function of MSE. Here, all modes with a $PCPR_2 > 10^{-5}$ and $PCPR_3 < 10^{-14}$ are highlighted in red. (Note this is a more stringent cutoff than used for a-PMMA, but the rationale is the same.)

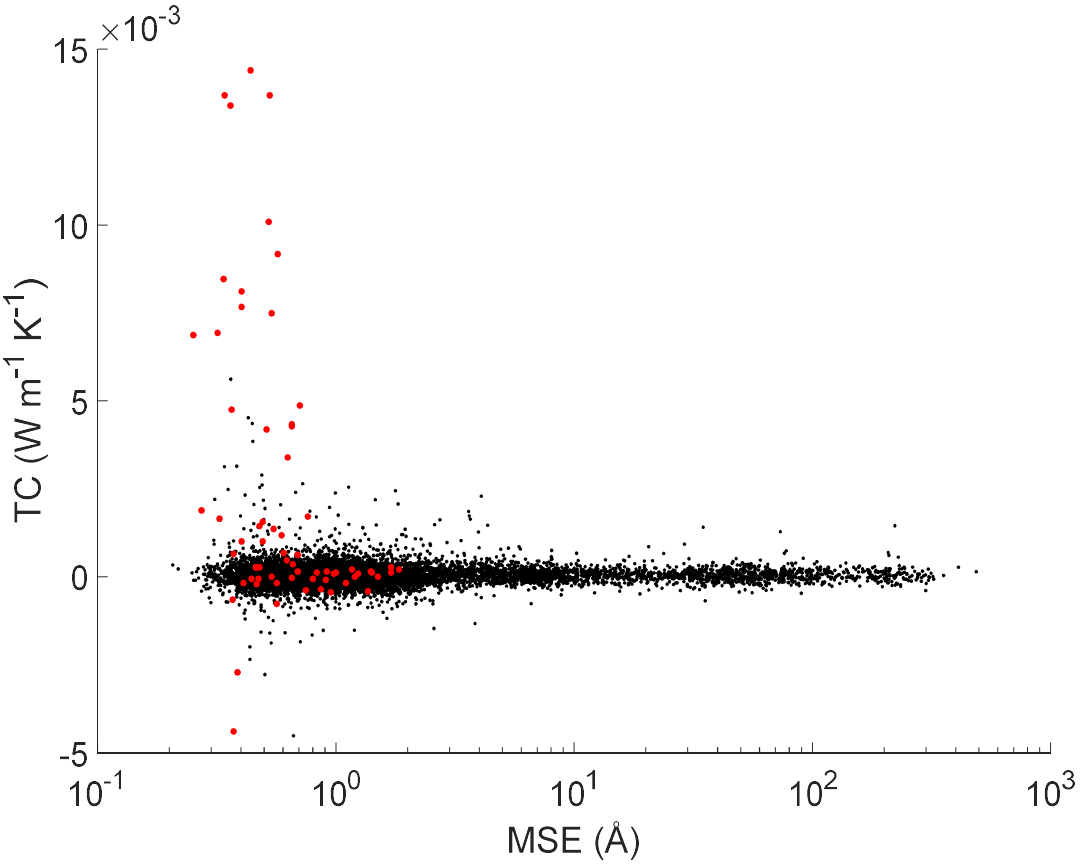

Figure 37. Modal TC vs. MSE for a-PS. Modes with a $PCPR_2 > 10^{-5}$ and $PCPR_3 < 10^{-14}$ shown in red.

Here, the results are striking, and even more so when one compares the average magnitude of TC for the modes shown in red: whereas the average TC magnitude of a mode in a-PS is 20.9 x 10^{-5} W m^{-1} K^{-1}, the average TC magnitude of the 67 modes shown in red in Fig. 37 is a full order of magnitude higher at 26.2 x 10^{-4} W m^{-1} K^{-1}. Now consider the PCPR vs. frequency for these modes, as well as their cross-correlation.

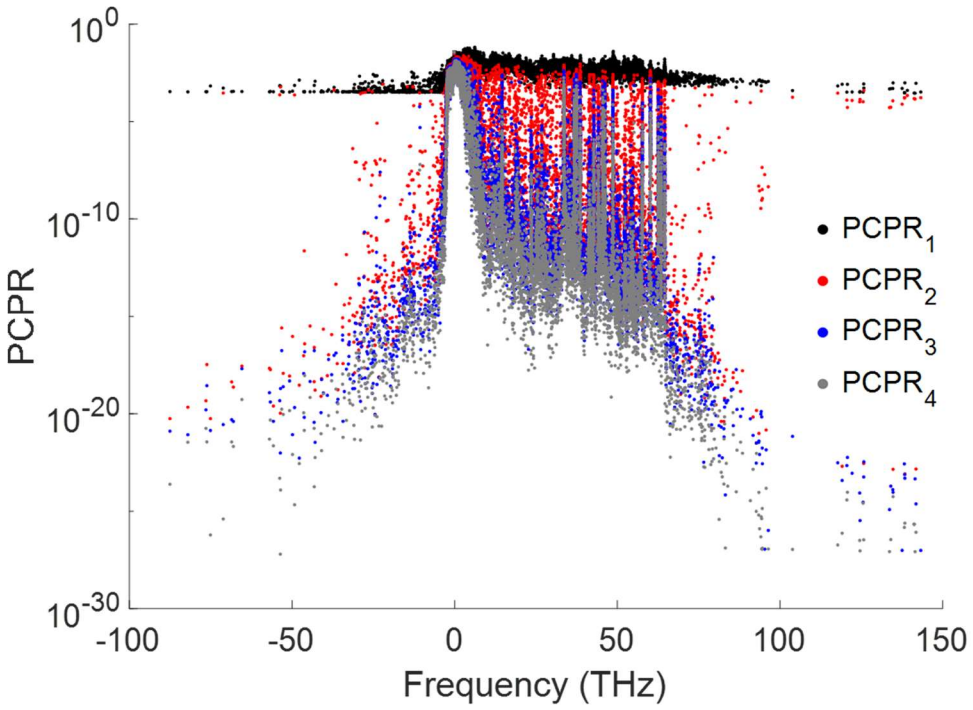

Figure 38. PCPR values for each mode in a-PS as a function of frequency.

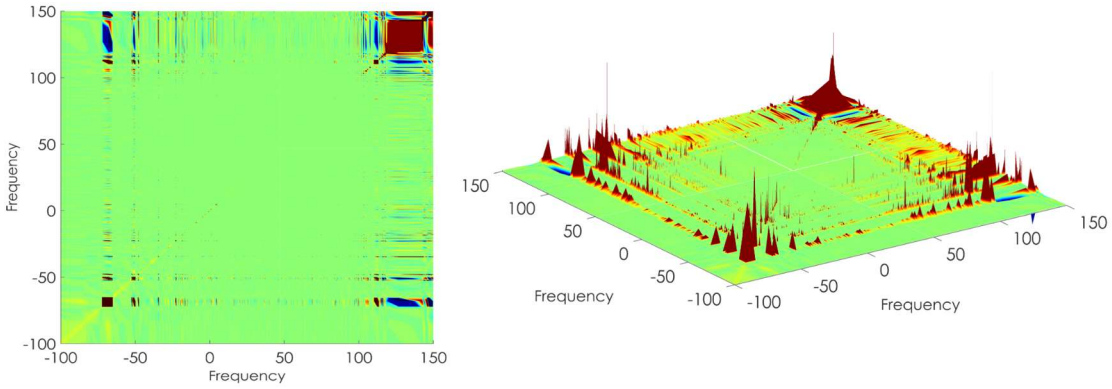

Figure 39. Cross correlation of all modes in a-PS, shown from two different perspectives. The range of the colorbar is limited intentionally to emphasize features of the correlation map.

Once again, as evident in Fig. 38, there are frequency windows in which no modes have a significant $PCPR_3$, but a few have a large $PCPR_2$, e.g. $\omega > 65$ THz. As with a-PMMA, it is exactly these modes that exhibit a high cross-correlation with other modes observable in Fig. 39.

For comparison, using only one of the two PCPR's as a mode selection criterion does not yield nearly as strong a disparity: for the a-PS supercell studied, the average TC magnitude of all modes with $PCPR_3 < 10^{-14}$ is 49.2 x 10^{-5} W m^{-1} K^{-1}, while the average TC magnitude of all modes with $PCPR_2 > 10^{-5}$ is 21.4 x 10^{-5} W m^{-1} K^{-1}.

These findings suggest that in certain frequency ranges, modes present on two separate polymer chains play an interesting role in conducting heat in the polymer. It seems reasonable to postulate that these modes act as a conduit by which heat moves between polymer chains. For modes that exist in frequency ranges for which nearly all modes are primarily confined to a single chain (e.g. in the 65-95 THz range for a-PMMA) the few modes that do span multiple chains may become the only means by which thermal energy can be easily transported between chains. The alternative is for the modes to couple with modes with a significantly different frequency that span multiple polymer chains. This correlation between modes with different frequencies does happen, as evidenced by the high degree of off-diagonal correlation apparent in Fig. 36. However, the path of least resistance is via modes that can easily couple to one another, which is generally modes with similar frequencies; modes with dissimilar frequencies require a larger degree of anharmonicity to interact significantly [170].

These findings appear to be new, and they differ from the behavior of modal TC of other disordered materials. As noted several times, the disparity in intra- and inter-molecular bond strength in polymers is roughly two orders of magnitude, so heat is expected to propagate more easily along a polymer chain than between polymer chains. However, due to the amorphous structure of the polymers and how entangled the polymers chains are, it makes sense that many of the modes involve atoms from multiple polymer chains. What

was not expected, however, is the large frequency bands in which modes are confined to a single polymer chain; it is within these bands where modes that span multiple polymer chains are particularly important.

Although the results here are quite insightful, realistically, more than fully explaining the TC of commercially available polymers, the results are most useful for guiding the next round of inquiry into polymer TC. Some remaining questions are presented below that, if addressed, could lead to some guiding principles for the design of polymers with enhanced thermal properties; also included are some suggestions of what those guiding principles might look like. It should be emphasized that while these suggestions are based on conclusions drawn from the current results, there is much additional inquiry to be done before one can make any truly well-founded assertions about the means by which polymer TC can be altered.

For example, one could ask how and why certain vibrational modes enhance TC between different polymer chains. It has been shown here that modes that exist among multiple polymer chains can have significantly larger TC's in polymer systems – at least in a fictitious system in which high-frequency modes can be excited at room temperature. A natural question to ask is then "why don't modes at lower temperatures show the same high magnitude of TC?" It has been shown that improving the degree to which a mode persists across multiple polymer chains can lead to an increased TC. Such an improvement could possibly be obtained by e.g. mechanical means: it is well-known that mechanical stretching of a polymer leads to an increase in TC [117, 171, 172], and the results presented here support the theory that this improvement is due to the alignment of polymer fibers, which creates a more periodic structure, leading to modal delocalization across multiple polymer

chains. Alternately, if one could find a way to further *decrease* delocalization, perhaps one could achieve TC's even lower than those that currently exist.

Considering Question 3, the answer is surprisingly that not only do localized modes contribute to TC, but they actually have a *larger* TC magnitude than do delocalized modes, regardless of whether one uses PR or MSE to measure localization. Interestingly these high-TC localized modes do show some degree of delocalization if one considers PCPR: the highest TC modes with a PR < 0.1 and MSE < 1 Å are those with a $PCPR_2$ that is within 3 orders of magnitude of the $PCPR_1$.

4.4 Summary of Findings

4.4.1 Questions Answered in this Chapter

Question 1: *Does the low average PR observed in a-PMMA persist across different supercell sizes, and is this also the case for the other amorphous thermoplastics in this study?*

Answer: The low PR observed in PMMA is similar across all polymers studied and for different size supercells.

Question 2: *With most modes having a low PR ascribed to locons, are the modes actually localized, or would an alternative descriptor indicate they are delocalized?*

Answer: While low-PR modes may be localized to a few atoms, for *locons with a high MSE*, there is a significant "tail" of excited atoms that extends through the supercell; for *locons with a high PCPR2*, atoms on multiple polymer chains experience a significant

degree of excitation. Thus, while still these modes are localized according to PR, the atom excitation is still spread throughout the supercell in ways that could impact the TC.

Question 3: *Do localized modes contribute to TC in the amorphous thermoplastics in this study?*

Answer: Locons contribute to TC on a per-mode basis as much or more than other classes of modes, and a negative correlation between PR and TC is observed, contrary to what was expected. This trend persists regardless of the means by which localization is measured.

4.4.2 Discussion

This chapter has provided several new insights into the TC of amorphous thermoplastics. It has been shown that the polymer supercells studied are large enough to capture the spectrum of thermal vibrations in the materials, apart from long-wavelength acoustic propagons, which are expected to show up at much larger length scales. While studying these modes at such a large length scale is computationally infeasible, there is much that can be said about the diffusons and locons observed in the systems studied herein.

The first finding to highlight is one noted in Chapter 2 – the vibrational modes observed in amorphous polymers are surprisingly localized. The maximum PR of any mode observed in the polymers studied is 0.25,[19] which is much lower than any other system in the literature. This result is quite surprising, but persistent across all three thermoplastics studied.

[19]Again, excluding the three translational modes that arise from any LD calculation.

This chapter also presents two newly-developed alternative means by which to quantify a mode's localization, either spatially or with respect to individual polymer chains – namely the MSE and PCPR, respectively. The MSE, which is measured in Å, gives the effective size of a mode. If the MSE is significantly greater than the interatomic spacing (~1 Å), the mode can be considered spatially delocalized, whereas a mode with an MSE below this value is spatially localized. Surprisingly, the amorphous polymer modes with the largest magnitude TC in the system are those with a low PR *and* low MSE. This finding is entirely counter to results for essentially every other class of material that has been studied in a similar manner – generally in disordered materials, the modes with the largest TC are low-frequency, highly delocalized propagating modes.

The PCPR is calculated in the same manner as the PR, but the sum is carried out over a single polymer chain, rather than the entire supercell. Considering all PCPR values for a given mode provides an indication of how much that mode is confined to a single polymer chain vs. spread amongst multiple chains. Of particular interest is the $PCPR_2$, which is the second largest PCPR value for a particular mode. If this value is significant (i.e. $\gtrsim 10^{-5}$), the mode can be considered to be delocalized with respect to polymer chains. Further values of PCPR (i.e. $PCPR_3$, $PCPR_4$, etc.) are generally less important for understanding the thermal properties of the mode, except in some cases where there exists a large disparity between $PCPR_2$ and $PCPR_3$. In frequency ranges in which most modes have low PCPR values (other than $PCPR_1$), the few modes with a large $PCPR_2$ have anomalously large TC magnitudes, up to an order of magnitude larger than other modes in the system.

The most significant finding in this chapter is that, contrary to what has been found for all other classes of materials, in the amorphous thermoplastics studied here, localized modes

are the largest contributor to TC. This finding is true whether one considers localization based on atom number (measured by PR), or by the effective "size" of the mode (as measured by MSE). Furthermore, modes localized according to both metrics have even larger TC's than modes that are localized according to only a single metric. When considering these localized modes, the ones exhibiting the largest TC are those in which atoms on at least 2 polymer chains are excited (i.e. have a non-zero eigenvector magnitude). Because these are rare, they are hypothesized to couple to other modes with similar frequencies that allow heat to move between polymer chains.

The next steps are to further verify the findings presented here before attempting to exploit some of the more interesting phenomena that have been observed. There exist several avenues of further exploration, and while they are not addressed in this work due to time/resource constraints, these questions will hopefully be explored in detail in the future, as the ultimate payoff from both a scientific and commercial perspective could be enormous.

CHAPTER 5. IMAGINARY FREQUENCY MODES IN AMORPHOUS POLYMERS

One avenue of inquiry that until now has been left undiscussed is the behavior of IF modes in amorphous polymers. These modes are in many ways similar to the RF modes observed, but there are some distinct differences that warrant further inquiry. The initial hypothesis posited here regarding these modes was that they represent structural changes in the polymers, such as conformation flipping.

This chapter will answer Questions 4 and 5 (which were first presented in Chapter 2), focusing first on understanding the nature of IF modes before delving into their contribution to TC. IF modes have been observed in all three amorphous polymer systems studied, and while the percentage of total modes that have an IF varies greatly among the systems studied, in all cases studied, they comprise significantly less than half of all modes in the system. Thus, while they are perhaps not the most important class of modes to consider, the question remains of whether or not they contribute to TC. While several interesting results/features of IF modes will be pointed out, this work will refrain from making strong claims about the modes, as there remain questions on the exact nature/origin of the modes. As in *Chapter 4. Localization and Thermal Conductivity of Normal Modes in Amorphous* , a-PMMA will be used as an example, but once again significantly different results for a-PS or a-PVC will be noted.

5.1 Question 4: The Nature of Imaginary Frequency Modes

Question: *Do IF modes correspond to conformation changes in the studied thermoplastics? If not, is there any evidence of some other structural change between metastable states occurring?*

Hypothesis: *IF modes correspond to conformation changes, consistent with Zhang & Luo's [121] identification of such instabilities in polyethylene chains.*

Perhaps the first and most obvious means of testing this hypothesis is to visualize the motion of atoms in the polymer systems. Consider first some examples of high-frequency[20] IF modes shown in Fig. 40. These vibrations are simple 2-atom vibrations, with an H atom oscillating antiparallel to the C atom to which it is connected (or in the case of a-PVC, a neighboring H atom).

[20]As a reminder, in the context of IF modes, "high" refers to the *magnitude* of the frequency.

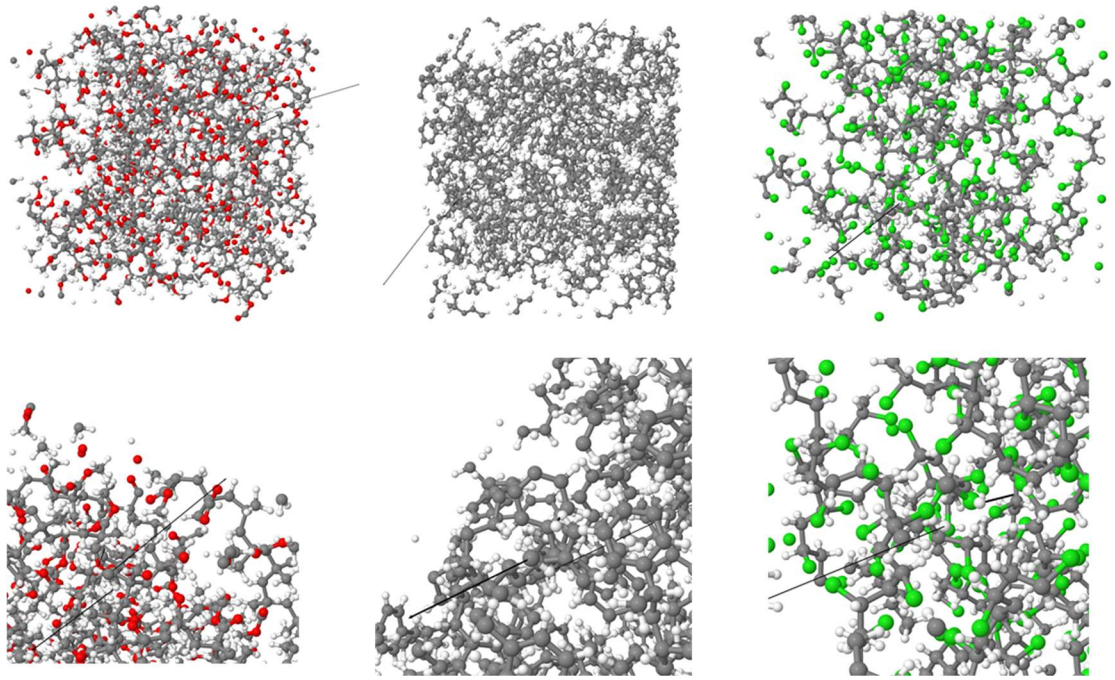

Figure 40. IF modes in a-PMMA (left), a-PS (middle), and a-PVC (right). C shown in gray, O in red, H in white, and Cl in green, with the eigenvectors shown in black. The images on the bottom are a magnified view of the modes.

It is hard to see how such vibrations would correspond to a conformation change of the polymer. The vibrations are quite simple, and an H and C atom moving in such a manner would not lead to any sort of change in the polymer structure. Furthermore, there exist low-frequency, spatially-delocalized IF vibrations that are so widespread throughout the polymer supercells that it seems unlikely that they could correspond to any sort of structural change. Consider Fig. 41: the vibrations involve nearly every atom in the polymer, and it is hard to envision a structural change involving every atom in the system changing its equilibrium position.

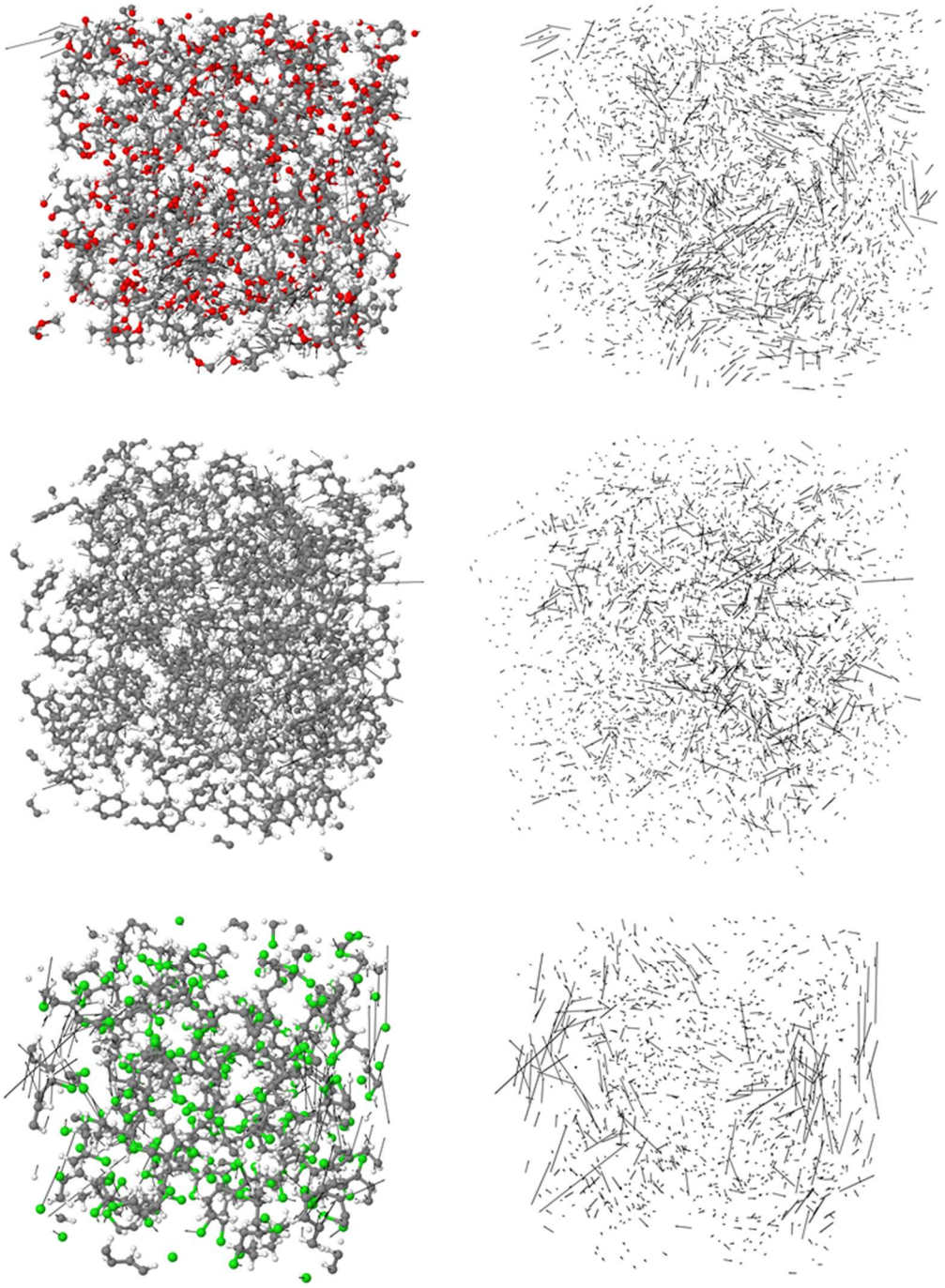

Figure 41. Example of low-frequency, spatially-delocalized IF modes in a-PMMA (top), a-PS (middle), and a-PVC (bottom). Atoms removed in figures on the right for clarity.

It seems reasonable to conclude that the IF modes observed in these systems do *not* correspond to any structural changes in the polymer, but rather appear qualitatively indistinguishable from highly-localized RF modes.

One of the few distinct differences observed between IF and RF modes is the high degree of localization that happens at low frequencies. Consider Fig. 20, which is reprinted below. While a few low-frequency modes are spatially delocalized, the PR and MSE drop to near-minimal values at frequencies larger than ~2 THz: the MSE's of the modes are at most 1 Å, and the PR's of the modes drop to values on the order of $1/N$.

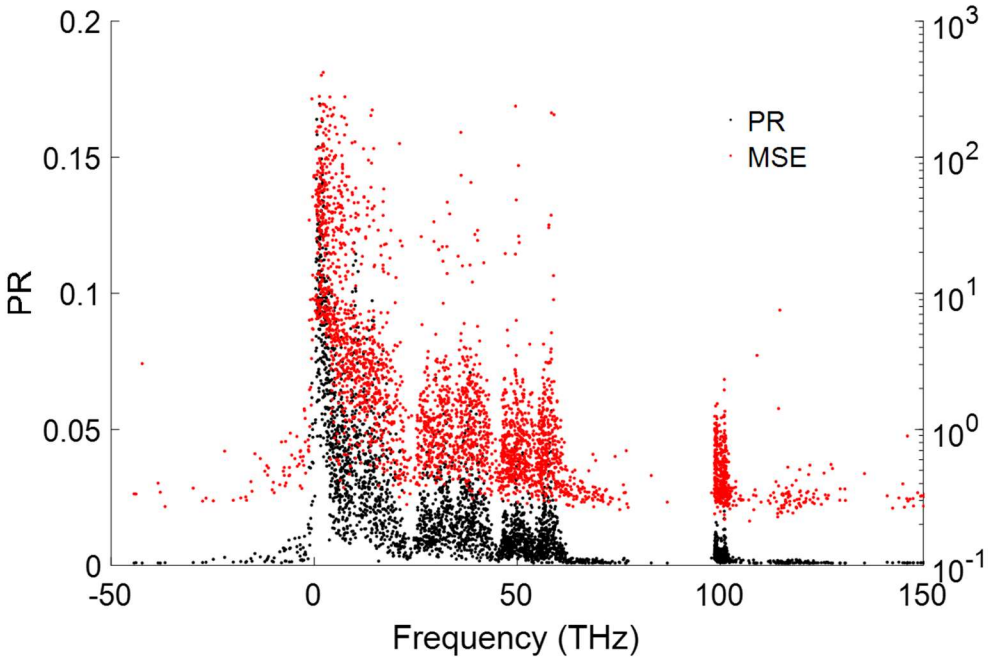

Figure 20. PR and MSE of each mode in the a-PMMA supercell studied as a function of frequency.

Fig. 42 below shows some examples of low-frequency localized IF modes in a-PMMA. Note that such highly-localized RF modes are not observed at similarly low (real) frequencies.

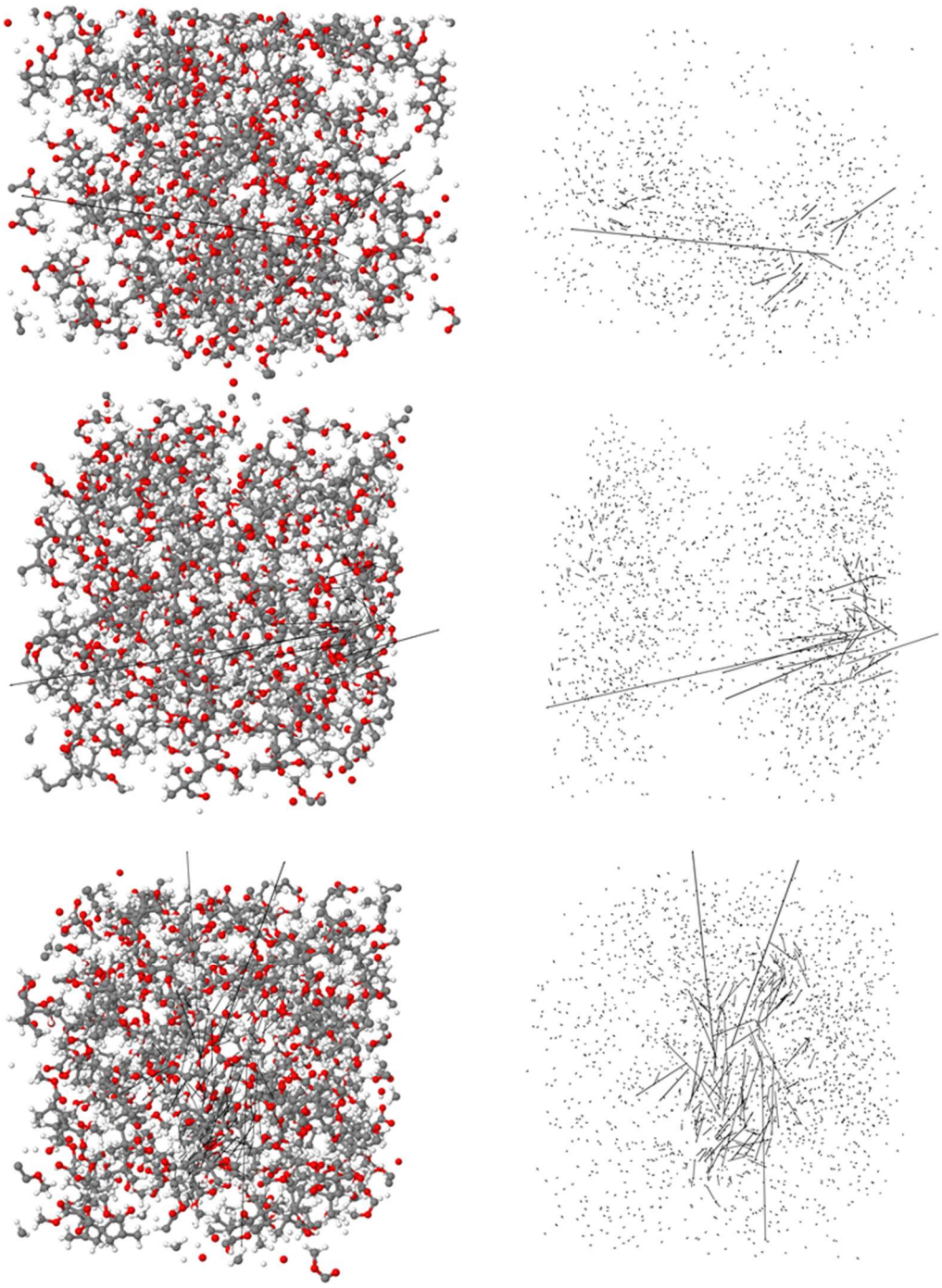

Figure 42. Low-frequency localized IF modes in a-PMMA. All modes shown have a frequency with a magnitude < 5 THz, a PR < 0.005, and an MSE < 1 Å. Atoms removed in figures on the right for clarity.

Finally, note one particular class of IF modes observed in a-PMMA and shown in Fig. 43.

All of these modes consist of three H atoms from a single methyl group rotating around the

central C atom, with the magnitude of the eigenvectors of all other atoms in the system close to 0. These modes are IF modes, and interestingly, they occur over a wide range of frequency magnitudes: 13.0 to 20.5 THz. While it is difficult to say exactly why these modes yield IF's, it is interesting to note that the rotation of a methyl group does not correspond to any flipping of the polymer. Thus, for these particular modes at least, no evidence exists in support of the hypothesis that IF correspond to conformational flipping.

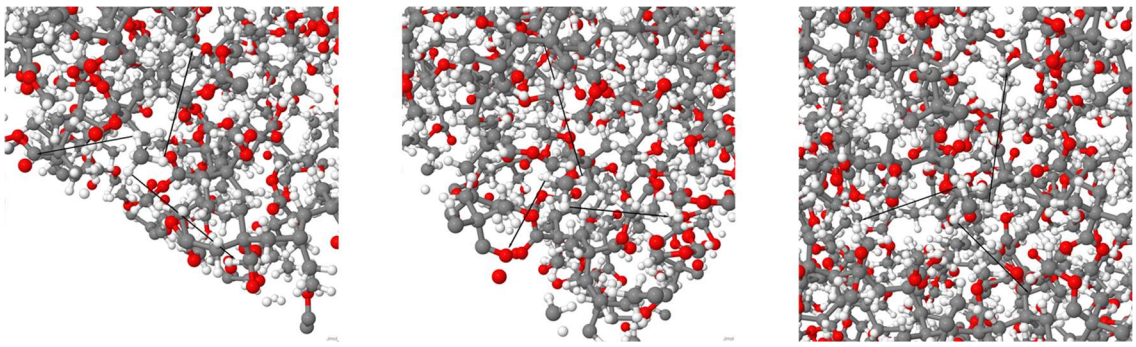

Figure 43. Vibrational modes involving the rotation of a methyl group in a-PMMA. For clarity, the eigenvector magnitude has been scaled down by 5x in this image compared to other images in this document (unless explicitly noted).

While examining individual IF modes does not show any evidence of a structural change in the amorphous thermoplastics studied here, there is further evidence that no structural changes occur. Fig. 44 shows the temperature of a-PMMA as a function of time. Similar temperature results were observed for both a-PS and a-PVC.

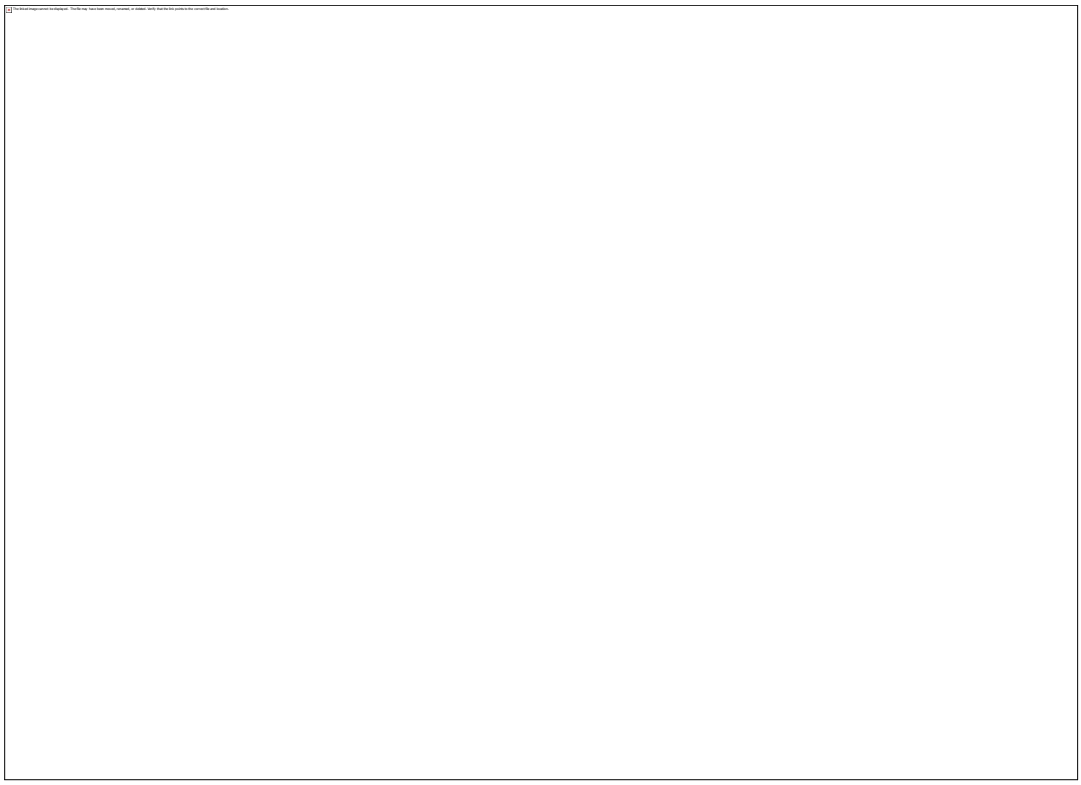

Figure 44. Temperature vs. time for both a-Ge and a-PMMA. The fluctuations observed in a-PMMA are similar to those of a-Ge. Furthermore, there are no step changes evident in the temperature of either simulation, indicating a lack of structural change.

While there are fluctuations in the temperature, these fluctuations are expected – compare the temperature fluctuations with those observed in a-Ge, for which no structural change occurs. The fluctuations are actually smaller in the case of a-PMMA (which is expected, as a-PMMA has 3x as many atoms, so the average fluctuations should be lower). What is *not* observed in the temperature of a-PMMA is any step change in the system temperature, which is what is observed in the case of a structural change. When a structural change happens in a material, the material moves to a lower (or higher) energy state; the PE is then converted into kinetic energy, which increases (or decreases) the temperature of the system. The lack of temperature change in a-PMMA is a conclusive means of showing that there

is no “flipping” of polymer chains or any other structural change; the lack of visual evidence of a structural change only serves to reinforce this conclusion.

Although IF modes do not appear to correspond to any sort of conformational change in the systems studied, it is still of interest to quantify whether IF modes contribute to TC. Some reasons why these modes may or may not have an appreciable TC have been noted in Chapter 2, but much of the rationale provided there was predicated on the assumption that the modes involved a structural change in the polymer. Thus, some uncertainty remains of exactly what to expect regarding the TC of IF modes, given that the initial assumption about the nature IF modes are was incorrect.

5.2 Question 5: The Contribution of Imaginary Frequency Modes to Thermal Conductivity

Question: *Do IF modes contribute to TC in the amorphous thermoplastics in this study?*

Hypothesis: *In the case of an amorphous polymer, IF modes are conformation changes that do not affect TC. Therefore, the impact of IF modes is at most small, and possibly negligible. It is possible however that these modes have more significant contributions to TC – commensurate with the RF modes in the polymer.*

Though some questions remain regarding exactly what causes an IF mode, GKMA methods can still be applied to these modes to see what contributions they have to TC. Figs. 45-49 shows the TC of each mode in a-PMMA as a function of the mode’s frequency with accompanying accumulation plots.

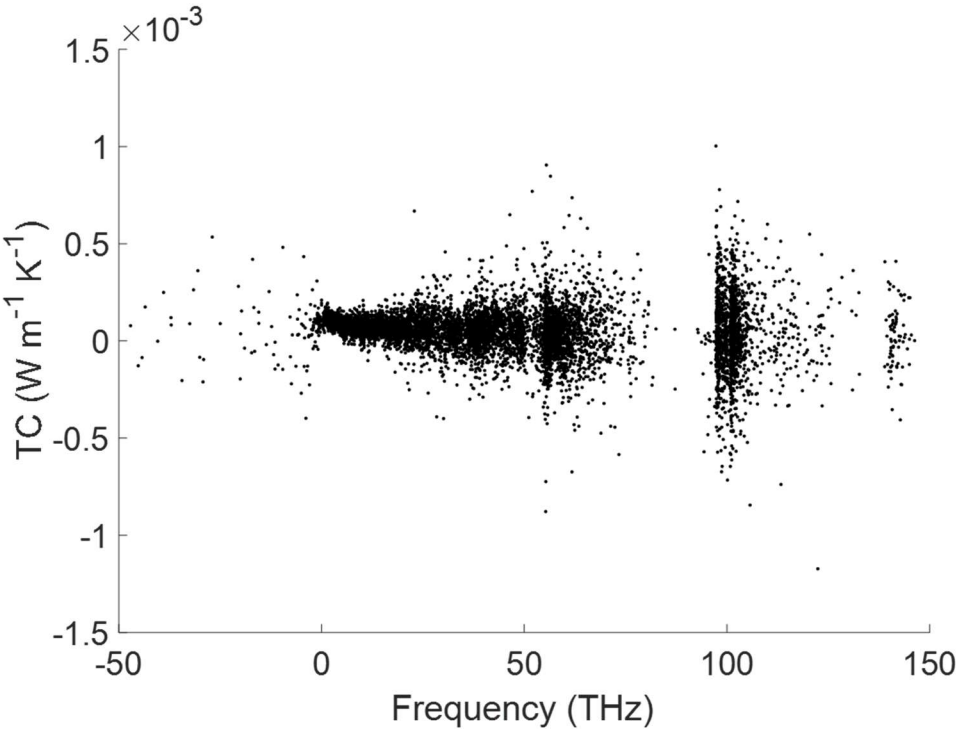

Figure 45. TC of each mode in a-PMMA as a function of frequency.

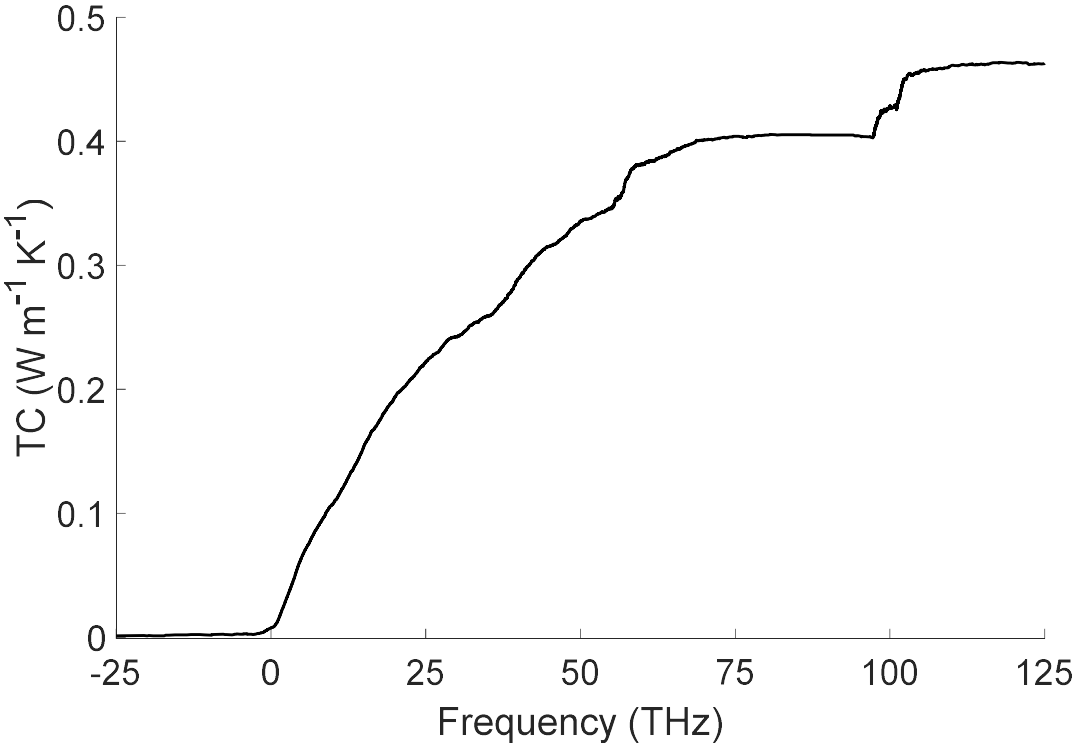

Figure 46. TC accumulation of modes in a-PMMA as a function of frequency.

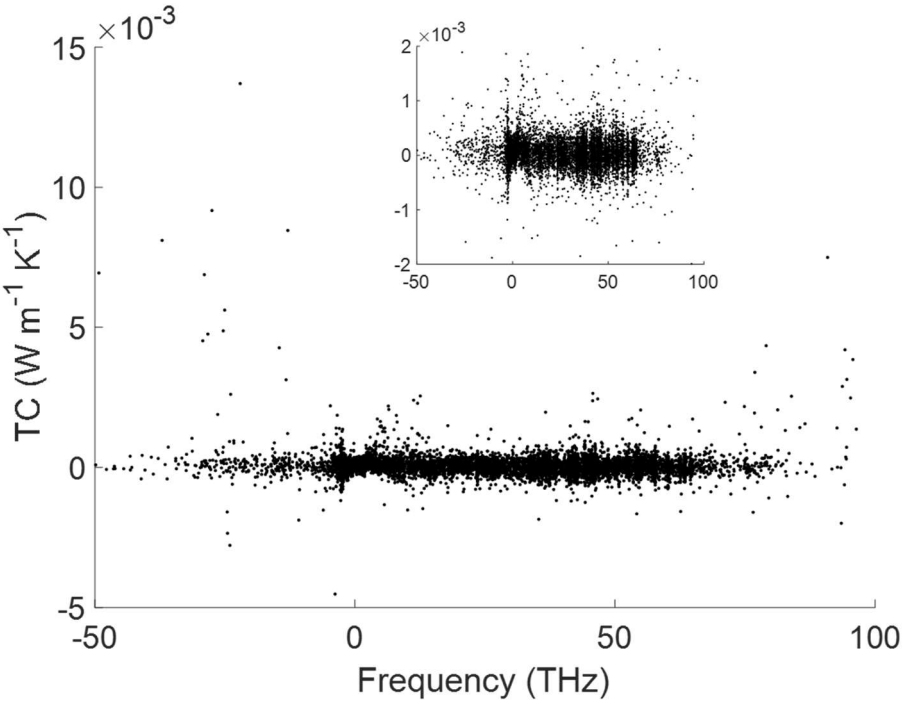

Figure 47. TC of each mode in a-PS as a function of frequency. Inset shows modes with a reduced y-axis to emphasize how TC varies with frequency.

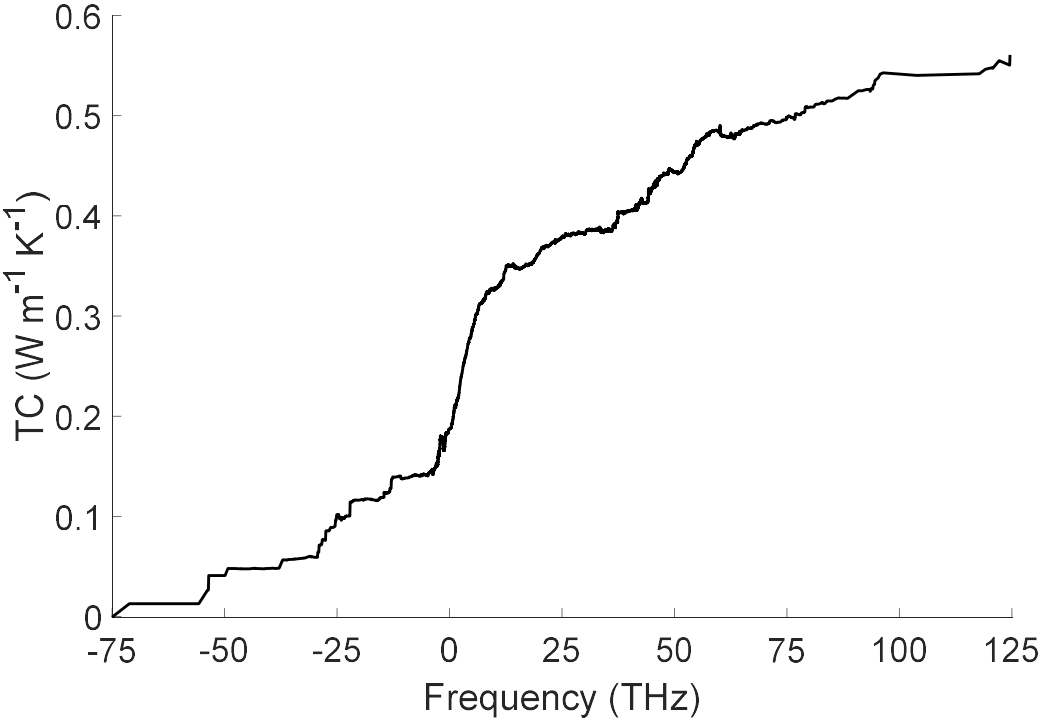

Figure 48. TC accumulation of modes in a-PS as a function of frequency.

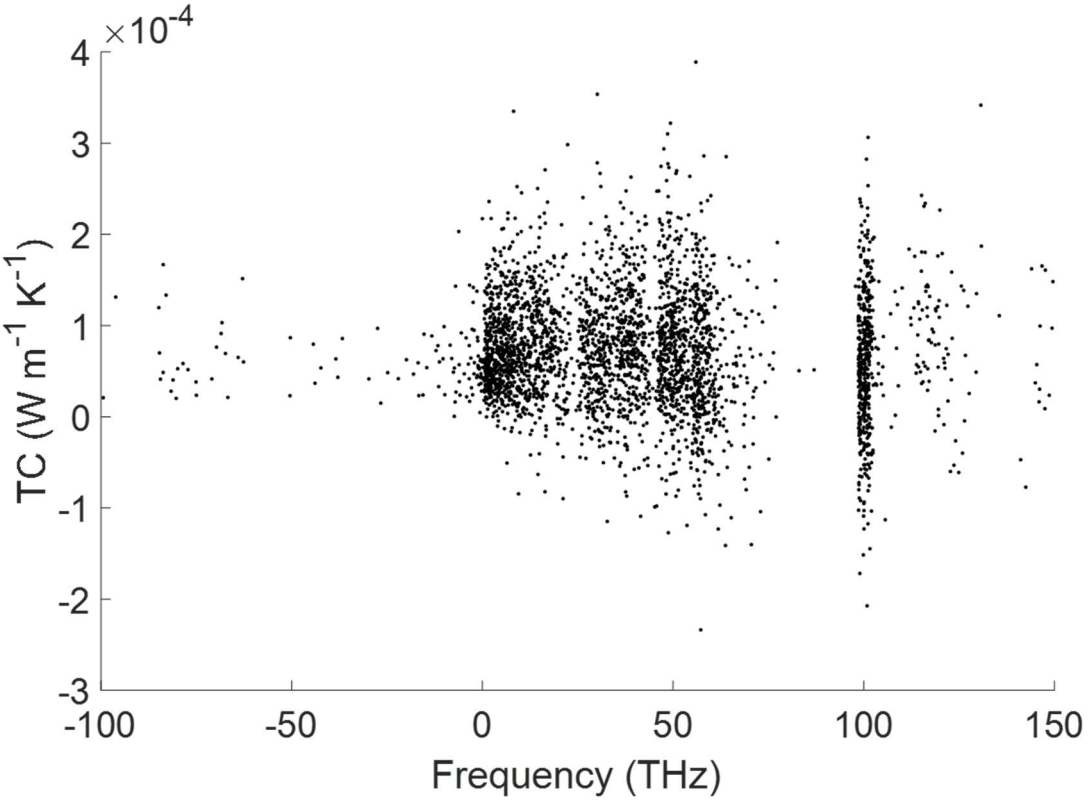

Figure 49. TC of each mode in a-PVC as a function of frequency.

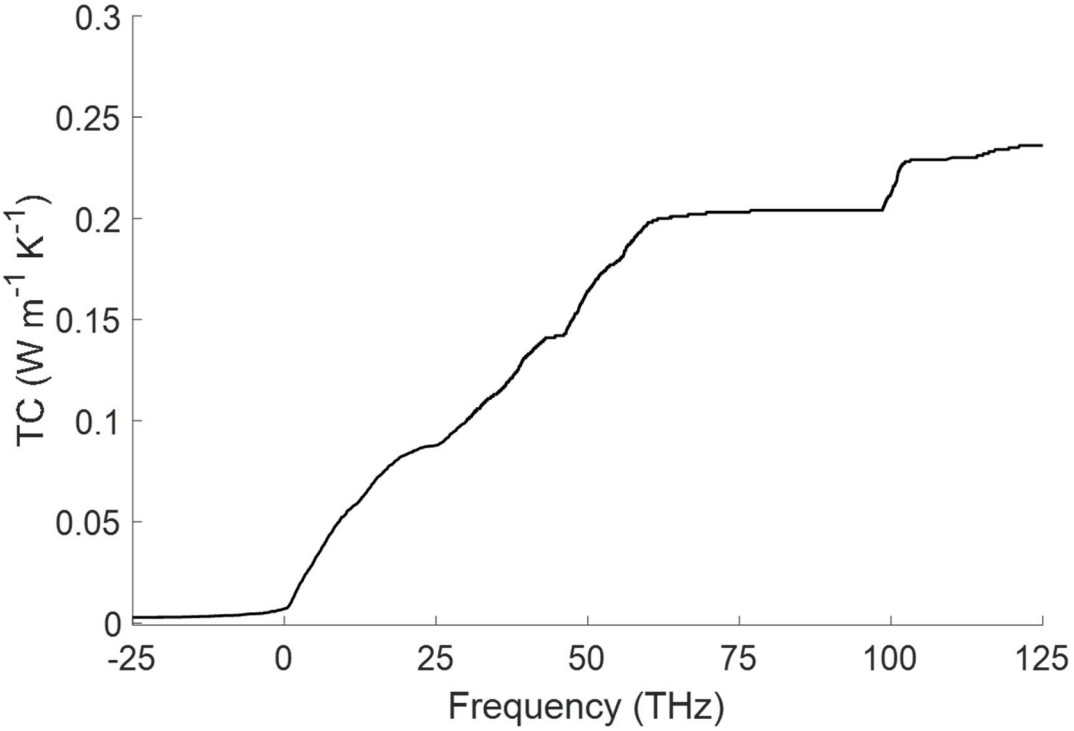

Figure 50. TC accumulation of modes in a-PVC as a function of frequency.

Accumulations as a function of PR and MSE can be found in *Appendix G. Additional Thermal Conductivity Data for Amorphous Poly(methyl methacrylate), Amorphous Polystyrene, and Amorphous Polyvinyl Chloride*.

In the case of every polymer, the TC of the IF modes are comparable to the TC of RF modes. In the case of a-PS, 17% of the modes are IF modes, thus it seems reasonable that they account for a significant portion of the (non-QC) TC.

Limiting the discussion for the moment to a-PS and revisiting the hypothesis for this question, these results were not anticipated. The hypothesis is in part due to some initial uncertainty as to the nature of IF modes – it was thought that the modes might correspond to structural changes in the polymer, and because the polymer is amorphous, that these structural changes might not have a significant impact on TC, particularly given that many of the modes are highly localized. However, the findings presented here are completely counter to these expectations. Not only do the IF modes contribute significantly, they in fact contribute disproportionately to the polymer's TC, accounting for 33% of the total TC of the system; their contribution on average is therefore ~2x that of an average RF mode, given then comprise 17% of the total modes.

Upon delving further into the reason for the anomalously large TC of some of the IF modes in a-PS, the findings mirror those for RF modes: the modes with large TC's are exactly those modes with large $PCPR_2$ values in frequency ranges where most modes have low $PCPR_2$'s and all modes have low $PCPR_3$'s. Fig. 51 replots the data from Fig. 47, but highlighted in red are the 20 IF modes with the largest $PCPR_2$ values and a frequency

magnitude > 5 THz (to exclude the low-frequency delocalized IF modes, which also have large $PCPR_2$'s).

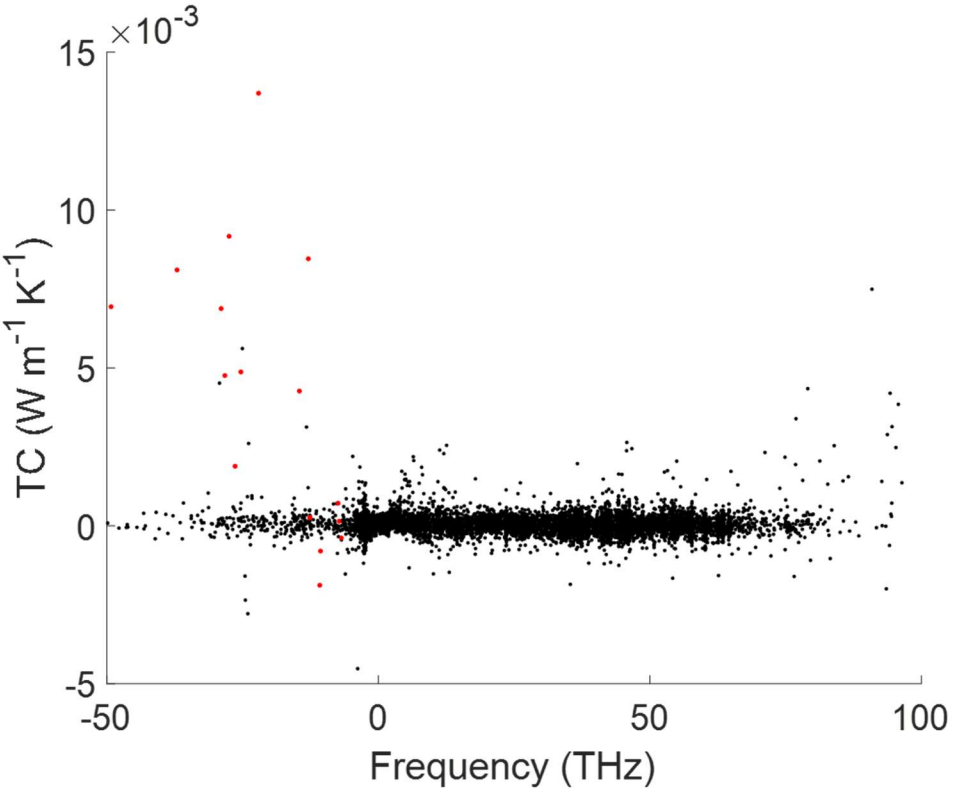

Figure 51. TC of each mode in a-PS as a function of frequency. Modes with a frequency < -5 THz and large $PCPR_2$ values are plotted in red.

This work has already discussed at length the rationale for why modes with high $PCPR_2$ modes can have disproportionately large TC's, but it is interesting to note the same behavior observed for RF modes is observed for IF modes as well.

It is also worth pointing out here that not only is the total contribution from IF modes different between a-PS and the other two polymers, but even the general profile of TC in each is quite different. The magnitude of the largest TC modes in a-PS is an order of magnitude larger than that of the modes in a-PMMA or a-PVC. Furthermore, as can be

seen in Fig. 51, the highest TC modes are actually IF modes! In the cases of a-PMMA and a-PVC, the modes with the largest magnitude are RF modes.

There are several other interesting findings to note, but for which no immediate explanation is available. For example, the relationship between TC and frequency is similar for a-PMMA and a-PVC, but distinctly different form a-PS. Another interesting observation is that – consistent with the localization of the modes – TC magnitude increases much more quickly with increasing (magnitude of) frequency for IF modes than for RF modes, particularly in the cases of a-PMMA and a-PVC. In particular, if one examines the frequency range -10 to 10 THz in Fig. 45 or 49, the TC magnitude of the IF modes almost instantly reaches 5 x 10^{-4} W m^{-1} K^{-1} and 2 x 10^{-4} W m^{-1} K^{-1}, whereas the TC of RF modes do not reach similar values until ~25 THz and ~10 THz, respectively. This discrepancy in TC magnitude mirrors the extreme localization, which occurs even at ~-1 THz. In other words, the correlation between TC and spatial localization (i.e. the highest magnitude TC modes are the most highly localized) is consistent between IF and RF modes; IF modes just reach higher degrees of localization/higher magnitudes of TC at much lower frequencies.

It is worth noting that while there are differences in exactly how much IF modes contribute to TC in the three thermoplastics studied here, in every case, the IF modes do contribute to TC. On a per-mode basis, the contribution from the IF modes is on-par with, if not greater than, the per-mode contribution from RF modes. Thus, the TC contribution from IF modes cannot be ignored and should be considered when characterizing the thermal behavior of polymers.

5.3 Summary of Findings

5.3.1 Questions Answered in this Chapter

Question 4: *Do IF modes correspond to conformation changes in the studied thermoplastics? If not, is there any evidence of some other structural change between metastable states occurring?*

Answer: There is no evidence that IF modes are conformation changes or that they behave differently than RF modes.

Question 5: *Do IF modes contribute to TC in the amorphous thermoplastics in this study?*

Answer: IF modes have a per-mode contribution to TC commensurate with RF modes exhibiting a similar degree of localization. Therefore, they cannot be neglected.

5.3.2 Discussion

This chapter has shown that IF modes behave similarly to RF modes in nearly every aspect, other than the frequency at which localization happens. The modes do not appear correspond to any type of structural change, but rather qualitatively resemble RF modes. However, it has not been proven exhaustively that every single IF mode in the polymer systems studied does *not* correspond to a structural change, and it is conceivable that some still could.

The TC contribution from IF modes is not only commensurate with RF modes, but (particularly in the case of a-PS modes), the total TC is due disproportionately to IF modes. These results are not what was initially expected, but given the other findings presented

here, perhaps they ought to be. Ultimately, the most important point here may not be any particular observation regarding IF or RF modes, but rather that regardless of the mode type, what is important is the mode's $PCPR_2$ (at least for modes in certain frequency ranges).

Comparing the TC of the three polymers studied in this dissertation, there are many similarities between how different classes of modes contribute to TC in the materials. In particular, a-PMMA and a-PVC share many similarities when comparing TC accumulation functions: both show a small (but measurable) positive contribution to TC from IF modes, while most of the contribution to TC comes from $\lesssim$ 60 THz RF modes. In each case however, the materials show a noticeable increase in TC (~10% of the total TC) at ~100 THz where there is a spike in the DOS. In the case of PS, the majority of TC is still due to modes with frequencies in the range of 0-60 THz, however, IF comprise approximately 25% of the total TC of the material. This much larger contribution from IF modes in a-PS is not entirely surprising: IF modes comprise 17% of modes in a-PS, while they comprise < 5% of modes in a-PMMA and a-PVC. Thus, once on accepts that IF modes can contribute to TC in amorphous thermoplastics, it is reasonable to expect that a material with a higher percentage of IF modes would have a larger contribution to TC from them. Furthermore, while a small increase in TC can again be observed around 100 THz, the increase is much smaller than in a-PMMA or a-PVC, which is consistent with the smaller number of modes (and correspondingly lower spike in DOS) at 100 THz in a-PS.

There are many avenues of further study that could be pursued. In particular, there is potential for further study into the nature of IF modes. It is still not fully understood what gives rise to these modes, or why they are localized at such low frequencies. While it seems

quite possible that perhaps the modes have something to do with the given polymer being in a metastable, rather than a fully relaxed state, no conclusive evidence exists to prove this assertion. Understanding why IF modes occur, whether a different relaxation scheme can reduce/eliminate them, and whether such modes ever do correspond to structural changes are all open questions that still need to be resolved.

It has also been shown that in the cases of both RF and IF modes, those with high $PCPR_2$ values can have a disproportionate effect on the TC of the material. As pointed out in *Chapter 4. Localization and Thermal Conductivity of Normal Modes in Amorphous* , understanding how to suppress such modes may allow one to better control the thermal properties of the polymer.

CHAPTER 6. CONCLUSIONS

This dissertation has primarily investigated normal modes of vibration in amorphous thermoplastic polymers, namely a-PMMA, a-PS, and a-PVC. The studies have focused on two aspects of these modes, namely their high degree of localization, and the existence of modes with an imaginary frequency.

The major findings in this dissertation center around the existence of highly-localized modes in amorphous thermoplastics and their anomalously large contributions to TC in those materials. Not only were the materials studied herein found to have an unusually high number of extremely-low (< 0.1) PR modes, but these modes were found to be the largest contributors to TC in the polymers. Furthermore, IF modes were found to contribute to the TC of the polymers studied, a result which was somewhat unintuitive. In general, these results are a drastic departure from findings in any other class of materials studied to date, and answering the questions proposed for this dissertation has revealed new and unexpected results about how heat can propagate in amorphous thermoplastics.

6.1 Questions Answered in this Dissertation

Question 1: *Does the low average PR observed in a-PMMA persist across different supercell sizes, and is this also the case for the other amorphous thermoplastics in this study?*

Answer: The low PR observed in PMMA is similar across all polymers studied and for different size supercells.

Question 2: *With most modes having a low PR ascribed to locons, are the modes actually localized, or would an alternative descriptor indicate they are delocalized?*

Answer: While low-PR modes may be localized to a few atoms, for *locons with a high MSE*, there is a significant "tail" of excited atoms that extends through the supercell; for *locons with a high PCPR2*, atoms on multiple polymer chains experience a significant degree of excitation. Thus, while still these modes are localized according to PR, the atom excitation is still spread throughout the supercell in ways that could impact the TC.

Question 3: *Do localized modes contribute to TC in the amorphous thermoplastics in this study?*

Answer: Locons contribute to TC on a per-mode basis as much or more than other classes of modes, and a negative correlation between PR and TC is observed, contrary to what was expected. This trend persists regardless of the means by which localization is measured.

Question 4: *Do IF modes correspond to conformation changes in the studied thermoplastics? If not, is there any evidence of some other structural change between metastable states occurring?*

Answer: There is no evidence that IF modes are conformation changes or that they behave differently than RF modes.

Question 5: *Do IF modes contribute to TC in the amorphous thermoplastics in this study?*

Answer: IF modes have a per-mode contribution to TC commensurate with RF modes exhibiting a similar degree of localization. Therefore, they cannot be neglected.

6.2 Summary of Findings

Chapter 2. Initial Observations provides some critical technical details necessary for understanding the most important results presented in later chapters. The chapter next outlines some preliminary findings that spurred the investigation detailed in the proceeding sections. These findings are centered around the existence of IF modes and the surprisingly low PR of the modes in a-PMMA. The chapter concludes by identifying five primary questions raised by these initial findings and suggest a hypothesis for each.

Chapter 3. Analysis Techniques and Methods provides further technical details on some less critical aspects of this work, including EIP's and amorphous structures were generated for a-Ge and details of GKMA.

Chapter 4. Localization and Thermal Conductivity of Normal Modes in Amorphous is an in-depth treatment of spatially localized vibrational modes in amorphous polymers. The chapter describe two new methods for describing mode localization, namely the MSE and PCPR, both of which have been found to be useful quantities. MSE provides a measure of the spatial localization of a mode, while PCPR values can inform one as to how distributed a mode is among multiple polymer chains. Upon investigating the relationship between PR, MSE, and modal TC, it is found that the more highly-localized a mode, the more likely the magnitude of its TC is large. Further, the $PCPR_2$ can correlate strongly with the magnitude of modal TC, so long as the mode is in a frequency range in which most modes are confined to a single polymer chain. Although still unproved, it is postulated that this result is because such modes act as a means whereby otherwise confined thermal energy

can be transferred between chains. Some means by which these findings could possibly be exploited are suggested to further improve the thermal properties of amorphous polymers.

Chapter 5. Imaginary Frequency Modes in Amorphous Polymers applies many of the same methods utilized in *Chapter 4* to IF modes. These modes are found not to correspond to conformational changes in the polymers as expected, but rather appear qualitatively identical to RF modes. The one significant difference that is observed is how localized the modes become (and consequently, how quickly the magnitude of TC increases) at low frequency magnitudes. This work raises many questions regarding IF modes, including questions relating to the nature of the modes and whether or not one should always expect to observe them in polymer systems.

6.3 Future Work

These finding motivate further avenues of exploration of TC in amorphous polymers. Among the questions raised by the findings presented here, some significant ones include:

1) Understanding how effects vary in the same thermoplastics with different structures. For instance, do all the same trends persist in much larger supercells? This works has provided evidence that transferring heat between polymer chains can be a significant bottleneck to increasing TC. It seems reasonable then to assume that, at least up to some critical length, increasing the molecular weight may allow heat to propagate further into a material before reaching a bottleneck (i.e. before the heat must be transferred to another polymer chain). Is this ever the case? Which other properties of polymer chemistry (e.g. tacticity, polydispersity, branching, the presence of

hydrogen bonds, etc.) tend to be correlated with large or small TC, and what does this correlation look like?

2) Understanding the persistence of the trends observed in other polymers. Are the same trends observed in larger-sized other thermoplastics? Thermosets? Semi-amorphous, semi-crystalline polymers? Discovering exceptions to the findings presented here may provide a deeper level of insight that what is currently available. For instance, if modes in thermosets with large $PCPR_2$'s do not exhibit unusually high TC, perhaps a means of reducing the strength of inter-chain bonding would not reduce the TC of the material, whereas it might for thermoplastics.

3) Inquiry into how to tune the TC of polymers. For example, is there any way to take advantage of the TC contribution from large $PCPR_2$ modes? What other means are available to affect the bulk TC of the polymer? How do processes such as drawing affect the modes of amorphous polymers, and how do those changes in mode character then affect the TC of the material?

The anomalous high-frequency, high-TC modes observed here have TC's roughly one order of magnitude larger than comparable lower-frequency modes. If one could envision a system in which all such modes in the polymer had a similar magnitude of TC due to an increased inter-chain presence, the resultant bulk TC would consequently also be an order of magnitude larger – on the order of ~1 W m^{-1} K^{-1}. While this TC is still low compared to most other materials, the ability to create polymers with such a TC could open up several possibilities for polymers from which they are currently limited due to their low TC.

An even more exciting prospect is to further *reduce* the TC of polymers. Polymers already possess some of the lowest TC's of any material at room temperature and represent one of the best inexpensive options for providing thermal insulation using a bulk material. If one could reduce TC by an order of magnitude, the resultant materials would have TC's on the order of 0.01 W m^{-1} K^{-1} or lower, on par with the lowest TC's ever observed in bulk materials at room temperature [120].

Perhaps a first means by which one might attempt to reduce TC is to design a material with more vibrational modes confined to a single polymer chain. If one could, for example, decrease the PCPR's (apart from the $PCPR_1$ of course) of low-frequency modes, would the resultant TC of that mode be decreased as well? Perhaps one could develop a means by which the strength of a polymer's intermolecular bonds can be reduced, more effectively trapping heat within individual polymer chains. How exactly one might effect this confinement is unclear, but as one suggestion, perhaps one could introduce certain interstitial species (polymer or otherwise – the nature of these interstitials is a question for further inquiry), which could have an effect on bulk TC similar to adding impurities to a pure crystal or creating nanostructured interfaces. In the parlance of the PGM, the interstitials would be additional scattering sites in the material. It seems that a more correct perspective is that of correlation, in which case one could argue the presence of interstitials may serve to reduce the ability of polymer chains' vibrations to remain correlated with one another. Regardless of the paradigm, the introduction of interstitials would ideally serve to confine more modes to a single polymer chain, resulting in a reduced TC.

Care must be taken when introducing interstitials to an amorphous polymer; one could argue that any material that is miscible with an amorphous polymer could *increase* the

degree of coherence between polymer chains. Polymers in particular are usually immiscible with other materials and only blend with a small number of materials. It seems reasonable to expect that in such a case, adding another material to the polymer would only serve to increase the degree of coherence between polymer chains; however, it is not guaranteed that this would be the case. One could, for example, make a similar argument for random alloys (e.g. Si-Ge). However, in such cases, the addition of an alloying element will serve to decrease the TC of the material [15, 16]. Thus, the question of the effect on TC of adding a second material to an amorphous polymer is one worth studying in further detail.

While still quite challenging, even a more modest reduction of TC by a factor of two would have huge commercial implications. Consider for example PS, which is an inexpensive means of providing thermal insulation for homes and appliances, food and drink, etc., in the form of Styrofoam. To improve the insulating efficiency of PS by a factor of two would consequently mean a 2x reduction in the amount of material needed to provide a given level of insulation. Considering the US produces 3 million tons of Styrofoam per year [115] and it is not considered economic to recycle [173]1-13, reducing the amount needed by 1.5 million tons (or even an amount approaching to this figure) would have both significant commercial and environmental impacts; the global impact would be greater still. Similarly, if the TC of PMMA could be reduced by a factor of 2x, it would perhaps be economical to manufacture windows for buildings from the material in some cases, reducing energy costs for conditioning the space. Reducing the TC of PVC – often used in plumbing – could reduce the amount of insulation necessary and/or reduce risks of pipes freezing and bursting.

Finally, while there have been some interesting observations made about IF modes, there is still much not understood about them, including even their origin. Furthermore, the reason for the high degree of localization at low-frequencies is unclear, and perhaps explaining the reason for this trend will shed light on the nature of these modes.

The findings of this dissertation are quite intriguing, and there is great potential to build upon them to make significant improvements to commercially available polymers. While it is not certain where exactly these findings will lead, the potential uses of the findings are certainly exciting. Polymers are ubiquitous, and even marginal improvements can have a substantial impact on both the global economy and environment. This work may raise more questions than answers, but hopefully the questions raised here will guide the development of the next generation of smart materials.

APPENDIX A. COMMANDS USED TO GENERATE AMORPHOUS POLYMER SUPERCELLS VIA THE POLYMER MODELER

This appendix details all commands used to create the polymer supercells discussed in this dissertation, namely a-PMMA, a-PS, and a-PVC. These supercells were all created via the Polymer Modeler [174] (<https://nanohub.org/tools/polymod>), a freely-available online research tool. Unless otherwise stated, default options/commands are used at each step.

A.1 Commands for Generating Amorphous Poly(methyl methacrylate) Supercells

The a-PMMA studied in this work is created using the "PMMA (atactic)" option. The number of monomers per chain is set to 50, and the number of polymer chains is 4. Under the "simulation cell" options, the `System volume` option was set to "Specify cell dimensions", with a cell dimension of 30.4. LAMMPS was not run on the supercell using the Polymer Modeler tool, so in the next step of the modeler ("Simulation"), `Simulation choice` is set to "LAMMPS input files only".

A.1 Commands for Generating Amorphous Poly(methyl methacrylate) Supercells

The a-PMMA studied in this work is created using the "PMMA (atactic)" option. The number of monomers per chain is set to 50, and the number of polymer chains is 4. Under the "simulation cell" options, the `System volume` option was set to "Specify cell dimensions", with a cell dimension of 30.4. LAMMPS was not run on the supercell using the Polymer Modeler tool, so in the next step of the modeler ("Simulation"), `Simulation`

`choice` is set to “LAMMPS input files only”. The supercell structure was then ready to be created in the third step, “Simulate”.

A.2 Commands for Generating Amorphous Polystyrene Supercells

The a-PMMA studied in this work is created using the “Polystyrene (atactic)” option. The number of monomers per chain is set to 50, and the number of polymer chains is 4. Under the “simulation cell” options, the `System volume` option was set to “Specify cell dimensions”, with a cell dimension of 32.5817. LAMMPS was not run on the supercell using the Polymer Modeler tool, so in the next step of the modeler (“Simulation”), `Simulation choice` is set to “LAMMPS input files only”. The supercell structure was then ready to be created in the third step, “Simulate”.

A.3 Commands for Generating Amorphous Polyvinyl Chloride Supercells

The a-PS studied in this work is created using the “PVC” option. The number of monomers per chain is set to 50, and the number of polymer chains is 4. Under the “simulation cell” options, the `System volume` option was set to “Specify cell dimensions”, with a cell dimension of 24.684. LAMMPS was not run on the supercell using the Polymer Modeler tool, so in the next step of the modeler (“Simulation”), `Simulation choice` is set to “LAMMPS input files only”. The supercell structure was then ready to be created in the third step, “Simulate”.

APPENDIX B. DESCRIPTION OF RELAXATION PROCESS FOR AMORPHOUS STRUCTURES CREATED IN THE LARGE-SCALE ATOMIC/MOLECULAR MASSIVELY PARALLEL SIMULATOR

Below are the commands used to relax each supercell described in this dissertation.

B.1 Commands for the Relaxation Method for Amorphous Germanium

```
variable dt equal 0.0005 #0.5 fs timestep

 echo screen

# boundary and atoms--------------------------------------------------------------------------

 comm_modify          vel yes

 boundary       p p p
 units          metal
 atom_style     charge

 read_data      lattice.xyz

#potential-----------------------------------------------------------------------

# Pair style commands for TBC-1
  pair_style hybrid/overlay tersoff buck 12 coul/dsf 0.25 12
  set type 1 charge
  pair_coeff * * coul/dsf
  pair_coeff 1 1 buck
  pair_coeff * * tersoff ge_tbc_1.tersoff Ge

  thermo_style   custom step temp press etotal pe vol fmax fnorm nbuild ndanger
  thermo 10000

# initial velocities---------------------------------------------------------------

 velocity         all create 1 424242 rot yes mom yes
 dump             mydump all xyz 10000 pos.xyz
 #dump_modify    mydump format "%E %E %E" sort id
```

```
# Relaxing the Imported structure in the desired temperature----------

 timestep ${dt}1-13

 min_style quickmin
 minimize 0 1e-8 50000 10000000

 fix PotEng all ave/time 1000 1 1000 c_thermo_pe file PE.txt

 fix 1 all npt temp 300 300 0.01 iso 0 0 1000
 run 500000
 unfix 1

 min_style quickmin
 minimize 0 1e-8 50000 10000000

 fix 1 all npt temp 300 300 0.01 iso 0 0 1000
 run 500000
 unfix 1

 min_style quickmin
 minimize 0 1e-8 50000 10000000

 fix 1 all npt temp 300 300 0.01 iso 0 0 1000
 run 500000
 unfix 1

 min_style quickmin
 minimize 0 1e-8 50000 10000000

 fix 1 all npt temp 300 300 0.01 iso 0 0 1000
 run 500000
 unfix 1

 unfix PotEng
 fix TEMPS all ave/time 1000 1 1000 c_thermo_temp file TEMPS.txt

 fix 1 all nve
 run 1000000

 unfix TEMPS

 fix 2 all temp/rescale 1000 300 900 0.01 1.0
 run 200000
 unfix 2
```

```
fix 2 all temp/rescale 1000 900 900 0.01 1.0
run 2000000
unfix 2

run 200000
fix 2 all temp/rescale 1000 900 300 0.01 1.0
run 200000
unfix 2

fix 2 all temp/rescale 1000 300 300 0.01 1.0
run 2000000
unfix 2
run 1000000
unfix 1

minimize 0 1e-8 100000 10000000
dump lastpos all xyz 1 lastpos.xyz
fix 1 all nve
run 1
```

B.2 Commands for the Relaxation Method for Amorphous Poly(methyl methacrylate) and Amorphous Polyvinyl Chloride

```
variable dt equal 1 #0.1 fs timestep

# General parameters
echo    both
read_restart data.dreiding  #this file contains all information about the atoms/bonds in the polymer

thermo_style        custom step etotal ke temp pe ebond eangle edihed eimp evdwl ecoul elong press pxx pyy pzz pxy pxz pyz lx ly lz vol density
thermo          100
thermo_modify     flush yes

# MD parameters
neigh_modify  every 1 delay 5
pair_style       buck/coul/long  12.0 12.0
kspace_style      pppm 1e-4
pair_coeff       1          1          3407.78599213 0.258035858504 31.3691508534   # H_  H_
pair_coeff       1          2          17353.2373206  0.267542023409  135.235974836     # H_  C_3
pair_coeff       1          3          17353.2373206  0.267542023409  135.235974836     # H_  C_2
```

```
pair_coeff      1       4       13693.8677062  0.255243315497  91.7827422702    # H_
O_2
pair_coeff      1       5       13693.8677062  0.255243315497  91.7827422702    # H_
O_3
pair_coeff      2       2       88366.7126395  0.277775402594  583.017658827    # C_3
C_3
pair_coeff      2       3       88366.7126395  0.277775402594  583.017658827    # C_3
C_2
pair_coeff      2       4       69732.3531147  0.264541129506  395.685834216    # C_3
O_2
pair_coeff      2       5       69732.3531147  0.264541129506  395.685834216    # C_3
O_3
pair_coeff      3       3       88366.7126395  0.277775402594  583.017658827    # C_2
C_2
pair_coeff      3       4       69732.3531147  0.264541129506  395.685834216    # C_2
O_2
pair_coeff      3       5       69732.3531147  0.264541129506  395.685834216    # C_2
O_3
pair_coeff      4       4       55027.5202694  0.252510568864  268.546375961    # O_2
O_2
pair_coeff      4       5       55027.5202694  0.252510568864  268.546375961    # O_2
O_3
pair_coeff      5       5       55027.5202694  0.252510568864  268.546375961    # O_3
O_3
run_style       respa 3 2 2 bond 1 pair 2 kspace 3

dump            mydump all xyz 10000 pos.xyz
dump_modify     mydump flush yes

timestep ${dt}

fix NVE1 all nve

fix LANG1 all langevin 200 0 1 12345
run 1000000
unfix LANG1

fix LANG2 all langevin 0 0 1 12345
run 1000000
unfix LANG2

fix LANG3 all langevin 0 0 10 12345
run 1000000
unfix LANG3

write_restart restart_0K.lammps
```

```
run 1000000

write_restart restart_mv.lammps
```

B.3 Commands for the Relaxation Method for Amorphous Polystyrene

```
variable T1 equal 500 #500K anneal temp
variable dt equal 1 #1 fs timestep

# General parameters
echo    both
read_restart data.dreiding  #this file contains all information about the atoms/bonds in the
polymer

# MD parameters
neigh_modify  every 1 delay 5
pair_style       buck/coul/long  12.0 12.0
kspace_style     pppm 1e-4
pair_coeff       1         1         3407.78599213 0.258035858504 31.3691508534   # H_  H_
pair_coeff       1         2         17353.2373206  0.267542023409  135.235974836     #  H_
C_3
pair_coeff       1         3         17353.2373206  0.267542023409  135.235974836     #  H_
C_R
pair_coeff       2         2         88366.7126395  0.277775402594  583.017658827     #  C_3
C_3
pair_coeff       2         3         88366.7126395  0.277775402594  583.017658827     #  C_3
C_R
pair_coeff       3         3         88366.7126395  0.277775402594  583.017658827     # C_R
C_R
run_style        respa 3 2 2 bond 1 pair 2 kspace 3

restart 10000 restart1.lammps restart2.lammps

dump                mydump all xyz 10000 pos.xyz
dump_modify         mydump flush yes

timestep ${dt}

velocity all create $(2*v_T1) 104892 rot yes mom yes

fix NVE1 all nve

fix LANG1 all langevin ${T1} ${T1} 10 12345
run 1000000
unfix LANG1
```

```
fix LANG2 all langevin ${T1} 0 10 12345
run 1000000
unfix LANG2

fix LANG3 all langevin 0 0 10 12345
run 1000000
unfix LANG3

write_restart restart_0K.lammps

run 100000

write_restart restart_mv.lammps
```

APPENDIX C. PARAMETERS FOR THE TERSOFF-BUCKINGHAM-COULOMB POTENTIALS

C.1 TBC-1

```
pair_style hybrid/overlay tersoff buck 12 coul/dsf 0.25 12
set type 1 charge  0.326000
pair_coeff * * coul/dsf
pair_coeff 1 1 buck 37.688000 0.604000 30.369000
pair_coeff * * tersoff ge_tbc_1.tersoff Ge

#   m, lnmma, lambda3, c, d, costheta0, n, beta, lambda2, B, R, D, lambda1, A
Ge Ge Ge 3 1 1.034300 80.527700 5.045000 -0.500900 9.905200 0.168400 0.781200
40.348800 3.1  0.25 3.676800 5400.516300
```

C.2 TBC-2

```
pair_style hybrid/overlay tersoff buck 12 coul/dsf 0.25 12
set type 1 charge  0.079000
pair_coeff * * coul/dsf
pair_coeff 1 1 buck 34.370000 0.480000 468.750000
pair_coeff * * tersoff ge_tbc_1.tersoff Ge

#   m, lnmma, lambda3, c, d, costheta0, n, beta, lambda2, B, R, D, lambda1, A
Ge Ge Ge 3 1 2.593000 19.231000 58.123000 -0.513000 16.050000 2.668000 1.267000
6.780000 3.1 0.25 3.160000 4816.660000
```

C.3 TBC-3

```
pair_style hybrid/overlay tersoff buck 12 coul/dsf 0.25 12
set type 1 charge  -0.422000
pair_coeff * * coul/dsf
pair_coeff 1 1 buck 743.390000 0.290000 628.910000
pair_coeff * * tersoff ge_tbc_1.tersoff Ge

#   m, lnmma, lambda3, c, d, costheta0, n, beta, lambda2, B, R, D, lambda1, A
Ge Ge Ge 3 1 0.049000 78.191000 2.501000 -0.152000 8.440000 6.714000 9.968000
398.260000 3.1 0.25 3.235000 6399.230000
```

APPENDIX D. MODIFICATIONS MADE TO THE LARGE-SCALE ATOMIC/MOLECULAR MASSIVELY PARALLEL SIMULATOR TO ENABLE POTENTIAL-AGNOSTIC GREEN-KUBO MODAL ANALYSIS

This appendix discusses modifications made to the LAMMPS software package that allow for the implementation of GKMA. While previous modifications had been made that allowed GKMA in some situations, those modifications only enabled its usage in specific EIP's. The modifications described herein are the first to allow a user to simulate a material in a way that is potential-agnostic, greatly expanding the number of material classes that can be studied with GKMA in LAMMPS. The discussion here will reference the actual code, included in the subsequent appendix.

The compute *gkma* command has been written to perform GKMA calculations in LAMMPS. This compute command is based on a modified version of LAMMPS's compute *heat/flux* command. Whereas compute *heat/flux* allows one to determine the total heat flux in the x, y, and z directions in a material, compute *gkma* has been written such that it calculates modal contributions to heat flux ($\mathbf{Q}_n$ in Eq. 10). A description of compute *gkma* and an example implementation follow.

N.B. all modifications made to LAMMPS's compute *heat/flux* command are bracketed with comments "GKMA-beg-#" and "GKMA-end-#", where # is a number used to refer to one of three specific blocks of edited code in this text.

The first modification to compute heat/flux (block 1 in compute *gkma*) simply allocates some additional variables, or in a few cases, changing a variable type during allocation. The first substantive change to the code (block 2) reads information about the system eigenvectors, which are stored in the variables *eigx*, *eigy*, and *eigz*. The code is designed to read information from the eignvector.eig file produced by the General Utility Lattice Program (GULP). This file should be located in the same directory as other LAMMPS input files. If the user has obtained eigenvector information from another program, the eigenvector file should be modified to follow GULP's eignvector.eig format exactly, including blank lines, etc. Alternately, the user can modify compute *gkma* to read an eigenvector file that has been formatted differently. Regardless, the user should ensure they have allocated enough memory to store all information from the eigenvector file, which can be a significant memory requirement for larger systems, due to the N^2 scaling of eigenvector information.

The other significant change implemented in compute *gkma* can be found in block 3. There are first several minor alterations made to the code to initialize additional variables, after which the code calculates modal contributions to heat flux. First, Eq. 6 is used to determine modal velocities, *xdotx*, *xdoty*, and *xdotz*. The proceeding for loop then calculates modal heat fluxes, by first implementing Eq. 8 to decompose atomic velocities into modal atomic velocities, *vx*, *vy*, and *vz*, then calculating the contribution of those modal velocities to heat flux, *jcx*, *jcy*, *jcz*, *jvx*, *jvy*, and *jvz* via Eq. 10. These six heat flux quantities are the modally decomposed versions of the identically-named quantities found in compute *heat/flux*. The quantities *vsum* and *actv* are for debugging purposes and can be safely ignored. Finally, in

the last few lines of block 3, the data is reduced (necessary in the event of a multi-processor job) and printed.

The compute *gkma* code has been written so that users can bin modal information about a system. That is, rather than obtaining information about every individual mode's heat flux, the user can use compute *gkma* to obtain the heat flux due to one or several bins of modes. Binning is important for large systems, which require large amounts of memory to store modal heat fluxes and long job walltimes to continually write modal heat flux information. Thus far, the binning process is limited to modes that are adjacent in the eignvector.eig file. Thus, unless the eigenvector file is modified, binning will always occur for modes with similar frequencies.

To perform a compute *gkma* calculation, the user should follow all procedures for running a compute *heat/flux* calculation, i.e. initialize *ke/atom*, *pe/atom*, and *stress/atom* computes and use them as arguments for the compute *gkma* command. As mentioned previously, the user should also ensure a file named "eignvector.eig" is located in the same directory as other LAMMPS input files. The command compute *gkma* in the LAMMPS input is formatted identically to that of compute *heat/flux*, except that the user should also supply information about binning at the end of the command. This information should be formatted as three integers, identified in the compute *gkma* code as *firstmode*, *lastmode*, and *binsize*. These quantities are self-explanatory: *firstmode* gives the first mode (based on the order of the modes in eignvector.eig) for which the user wishes to perform calculations, while *lastmode* gives the last mode for which the user is performing calculations; *binsize* is simply the number of modes to include in a single bin.

Assuming a 1,000-atom system (and thus, 3,000 total vibrational modes), some examples of how this command might be implemented are:

```
compute      modalflux all gkma myKE myPE myStress 1 3000 1
```

This command will provide information about every single mode in the system. It will not actually perform any binning, as the bin size is 1.

```
compute       modalflux all gkma myKE myPE myStress 1 3000
     3000
```

This command's output will be identical to "compute flux all heat/flux myKE myPE myStress". It computes modal heat fluxes for all modes but bins contributions into a bin of 3,000 modes (i.e. every mode in the system). This single output is therefore the sum of all modal contributions and will exactly recover the bulk (i.e. not modal) heat fluxes.

```
compute      modalflux all gkma myKE myPE myStress 1 1000 100
```

Assuming no modification of the eignvector.eig file, this command will compute the modal heat fluxes of the 1,000 modes with the lowest frequencies (as modes are sorted by frequency in the eignvector.eig file output by GULP). There will be 10 heat fluxes output at each timestep. The first value is the sum of contributions from the 100 lowest-frequency modes, etc.

The user should take care that the bin size exactly divides the total number of bins being examined, i.e. mod(*lastbin-firstbin*+1, *binsize*) = 0. While the code will still run if this

condition is not met, the output in such a case has not been examined, and the heat flux values for at least one bin will likely be incorrect.

For the computes listed above (i.e. a *gkma* compute named “modalflux”), the values from the *gkma* compute can be output via the command

```
fix my_ave1 all ave/time Nevery Nrepeat Nfreq c_modalflux[*]
     file modal_output.txt mode vector
```

where the output file is named “modal_output.txt”. (The user can pick any name for both the compute itself and the output file.) The quantities *Nevery Nrepeat Nfreq* are explained in the LAMMPS documentation of fix *ave/time*.

APPENDIX E. COMPUTE GKMA SOURCE CODE

This chapter contains the source code for the two files that need to be added to the src/ directory to enable GKMA calculations as described in the previous appendix. To enable the compute, these two files should be added to the src/ directory, one should update style_compute.h to include compute_gkma.h, and the code can subsequently be compiled as usual.

E.1 Source Code for compute_gkma.cpp

```
/* ----------------------------------------------------------------------
-   LAMMPS - Large-scale Atomic/Molecular Massively Parallel Simulator
   http://lammps.sandia.gov, Sandia National Laboratories
   Steve Plimpton, sjplimp@sandia.gov

   Copyright (2003) Sandia Corporation.  Under the terms of Contract
   DE-AC04-94AL85000 with Sandia Corporation, the U.S. Government retains
   certain rights in this software.  This software is distributed under
   the GNU General Public License.

   See the README file in the top-level LAMMPS directory.
-------------------------------------------------------------------------
-- */

/* ----------------------------------------------------------------------
-
   Contributing authors: German Samolyuk (ORNL) and
                         Mario Pinto (Computational Research Lab, Pune,
India)
-------------------------------------------------------------------------
-- */

#include <math.h>
#include <string.h>
#include "compute_gkma.h"
#include "atom.h"
#include "update.h"
#include "modify.h"
#include "force.h"
#include "group.h"
#include "error.h"
#include "memory.h" //GKMA
#include <iostream> //GKMA
#include <fstream> //GKMA
#include <string> //GKMA
```

```
using namespace LAMMPS_NS;

#define INVOKED_PERATOM 8

/* ----------------------------------------------------------------------
- */

ComputeGKMA::ComputeGKMA(LAMMPS *lmp, int narg, char **arg) :
  Compute(lmp, narg, arg),
  id_ke(NULL), id_pe(NULL), id_stress(NULL)
{
  if (narg != 9) error->all(FLERR,"Illegal compute GKMA command");

  //GKMA-beg-1
  bigint natoms = atom->natoms;
  array_flag = 1;
  firstmode = force->inumeric(FLERR,arg[6]);
  lastmode = force->inumeric(FLERR,arg[7]);
  binsize = force->inumeric(FLERR,arg[8]);
  nummodes = lastmode-firstmode+1;
  numbins = floor(nummodes/binsize);
  size_array_rows = numbins;
  size_array_cols = 6;
  extarray = 1;
  //GKMA-end-1

  // store ke/atom, pe/atom, stress/atom IDs used by heat flux computation
  // insure they are valid for these computations

  int n = strlen(arg[3]) + 1;
  id_ke = new char[n];
  strcpy(id_ke,arg[3]);

  n = strlen(arg[4]) + 1;
  id_pe = new char[n];
  strcpy(id_pe,arg[4]);

  n = strlen(arg[5]) + 1;
  id_stress = new char[n];
  strcpy(id_stress,arg[5]);

  int ike = modify->find_compute(id_ke);
  int ipe = modify->find_compute(id_pe);
  int istress = modify->find_compute(id_stress);
  if (ike < 0 || ipe < 0 || istress < 0)
    error->all(FLERR,"Could not find compute gkma compute ID");
  if (strcmp(modify->compute[ike]->style,"ke/atom") != 0)
    error->all(FLERR,"Compute gkma compute ID does not compute ke/atom");
  if (modify->compute[ipe]->peatomflag == 0)
    error->all(FLERR,"Compute   gkmka   compute   ID   does   not   compute
pe/atom");
  if (modify->compute[istress]->pressatomflag == 0)
    error->all(FLERR,
               "Compute gkma compute ID does not compute stress/atom");

  memory->create(array,3*natoms,6,"gkma:array");
```

```
  //GKMA-beg-2
  std::ifstream eigfile;
  eigfile.open("eignvector.eig");

  std::string val;
  double doubleval;
  memory->create(eigx,nummodes*natoms,"gkma:eigx");
  memory->create(eigy,nummodes*natoms,"gkma:eigy");
  memory->create(eigz,nummodes*natoms,"gkma:eigz");

  for (int i=0; i<=natoms+3 ; i++){
    getline(eigfile,val);
  }
  for (int i=0; i<firstmode-1; i++){
    for (int j=0; j<natoms+2; j++) getline(eigfile,val);
  }
  for (int i=0; i<nummodes; i++){
    getline(eigfile,val);
    getline(eigfile,val);
    for (int j=0; j<natoms; j++){
      eigfile >> doubleval;
      eigx[i*natoms+j]=doubleval; //values are grouped by eigenvector,
not by atom
      eigfile >> doubleval;
      eigy[i*natoms+j]=doubleval;
      eigfile >> doubleval;
      eigz[i*natoms+j]=doubleval;
    }
    getline(eigfile,val);
  }
  eigfile.close();
  //GKMA-end-2
}

/* ----------------------------------------------------------------------
- */

ComputeGKMA::~ComputeGKMA()
{
  delete [] id_ke;
  delete [] id_pe;
  delete [] id_stress;
  delete [] array;  //GKMA
}

/* ----------------------------------------------------------------------
- */

void ComputeGKMA::init()
{
  // error checks

  int ike = modify->find_compute(id_ke);
  int ipe = modify->find_compute(id_pe);
  int istress = modify->find_compute(id_stress);
  if (ike < 0 || ipe < 0 || istress < 0)
```

```
    error->all(FLERR,"Could not find compute gkma compute ID");

  c_ke = modify->compute[ike];
  c_pe = modify->compute[ipe];
  c_stress = modify->compute[istress];
}

/* ----------------------------------------------------------------------
- */

void ComputeGKMA::compute_array()
{
  invoked_array = update->ntimestep;

  // invoke 3 computes if they haven't been already

  if (!(c_ke->invoked_flag & INVOKED_PERATOM)) {
    c_ke->compute_peratom();
    c_ke->invoked_flag |= INVOKED_PERATOM;
  }
  if (!(c_pe->invoked_flag & INVOKED_PERATOM)) {
    c_pe->compute_peratom();
    c_pe->invoked_flag |= INVOKED_PERATOM;
  }
  if (!(c_stress->invoked_flag & INVOKED_PERATOM)) {
    c_stress->compute_peratom();
    c_stress->invoked_flag |= INVOKED_PERATOM;
  }

  // heat flux vector = jc[3] + jv[3]
  // jc[3] = convective portion of heat flux = sum_i (ke_i + pe_i) v_i[3]
  // jv[3] = virial portion of heat flux = sum_i (stress_tensor_i .
v_i[3])
  // normalization by volume is not included

  double *ke = c_ke->vector_atom;
  double *pe = c_pe->vector_atom;
  double **stress = c_stress->array_atom;

  double **v = atom->v;
  int *mask = atom->mask;
  int nlocal = atom->nlocal;
  //GKMA-beg-3
  bigint natoms = atom->natoms;
  double **f = atom->f;
  int *type = atom->type;
  double *mass = atom->mass;
  tagint *tag = atom->tag;

  double jcx[nummodes];
  double jcy[nummodes];
  double jcz[nummodes];
  double jvx[nummodes];
  double jvy[nummodes];
  double jvz[nummodes];
  for (int i=0; i < nummodes; i++) {
    jcx[i]=jcy[i]=jcz[i]=jvx[i]=jvy[i]=jvz[i]=0;
```

```
  }
  double eng;
  double xdotx[nummodes];
  double xdoty[nummodes];
  double xdotz[nummodes];
  double vx;
  double vy;
  double vz;

  double vsum[nlocal], actv[nlocal];

  for (int i = 0; i < nummodes; i++) {
    xdotx[i]=xdoty[i]=xdotz[i]=0;
    for (int j = 0; j < nlocal; j++) {
      if (mask[j] & groupbit) {
        xdotx[i] += sqrt(mass[type[j]])*eigx[i*natoms+tag[j]-1]*v[j][0];
        xdoty[i] += sqrt(mass[type[j]])*eigy[i*natoms+tag[j]-1]*v[j][1];
        xdotz[i] += sqrt(mass[type[j]])*eigz[i*natoms+tag[j]-1]*v[j][2];
      }
    }
  }
  for (int i = 0; i < nlocal; i++) {
    if (mask[i] & groupbit) {
      eng = pe[i] + ke[i];
      vsum[i] = actv[i] = 0;
      for (int j = 0; j < nummodes; j++) {
        vx=1/sqrt(mass[type[i]])*eigx[j*natoms+tag[i]-1]*xdotx[j];
        vy=1/sqrt(mass[type[i]])*eigy[j*natoms+tag[i]-1]*xdoty[j];
        vz=1/sqrt(mass[type[i]])*eigz[j*natoms+tag[i]-1]*xdotz[j];
        jcx[j] += eng*vx;
        jcy[j] += eng*vy;
        jcz[j] += eng*vz;
        jvx[j] -= stress[i][0]*vx + stress[i][3]*vy +
          stress[i][4]*vz;
        jvy[j] -= stress[i][3]*vx + stress[i][1]*vy +
          stress[i][5]*vz;
        jvz[j] -= stress[i][4]*vx + stress[i][5]*vy +
          stress[i][2]*vz;
        vsum[i] += vx;
        actv[i] = v[i][0];
      }
    }
  }

  // convert jv from stress*volume to energy units via nktv2p factor

  double data[numbins][6];
  for (int i = 0; i < numbins; i++) {

data[i][0]=data[i][1]=data[i][2]=data[i][3]=data[i][4]=data[i][5]=0;
  }
  double nktv2p = force->nktv2p;
  for (int i = 0; i < numbins; i++) {
    for (int j = 0; j < binsize; j++) {
      data[i][0]+=jcx[j+i*binsize]+jvx[j+i*binsize]/nktv2p;
      data[i][1]+=jcy[j+i*binsize]+jvy[j+i*binsize]/nktv2p;
      data[i][2]+=jcz[j+i*binsize]+jvz[j+i*binsize]/nktv2p;
```

```
      data[i][3]+=jcx[j+i*binsize];
      data[i][4]+=jcy[j+i*binsize];
      data[i][5]+=jcz[j+i*binsize];
    }
  }

  // sum across all procs
  // 1st 3 terms are total heat flux
  // 2nd 3 terms are just conductive portion
  MPI_Allreduce(data[0],array[0],6*numbins,MPI_DOUBLE,MPI_SUM,world);
  //GKMA-end-3
}
```

E.2 Source Code for compute_gkma.h

```
/* -*- c++ -*- ----------------------------------------------------------
-
   LAMMPS - Large-scale Atomic/Molecular Massively Parallel Simulator
   http://lammps.sandia.gov, Sandia National Laboratories
   Steve Plimpton, sjplimp@sandia.gov

   Copyright (2003) Sandia Corporation.  Under the terms of Contract
   DE-AC04-94AL85000 with Sandia Corporation, the U.S. Government retains
   certain rights in this software.  This software is distributed under
   the GNU General Public License.

   See the README file in the top-level LAMMPS directory.
-------------------------------------------------------------------------
-- */

#ifdef COMPUTE_CLASS

ComputeStyle(gkma,ComputeGKMA)

#else

#ifndef LMP_COMPUTE_GKMA_H
#define LMP_COMPUTE_GKMA_H

#include "compute.h"

namespace LAMMPS_NS {

class ComputeGKMA : public Compute {
 public:
  ComputeGKMA(class LAMMPS *, int, char **);
  ~ComputeGKMA();
  void init();
  void compute_array();

 private:
  char *id_ke,*id_pe,*id_stress;
  double *eigx, *eigy, *eigz; //AND-GKMA
  class Compute *c_ke,*c_pe,*c_stress;
  int firstmode, lastmode, binsize, nummodes, numbins;
```

```
};

}

#endif
#endif

/* ERROR/WARNING messages:

E: Illegal ... command

Self-explanatory.  Check the input script syntax and compare to the
documentation for the command.  You can use -echo screen as a
command-line option when running LAMMPS to see the offending line.

E: Could not find compute gkma compute ID

Self-explanatory.

E: Compute gkma compute ID does not compute ke/atom

Self-explanatory.

E: Compute gkma compute ID does not compute pe/atom

Self-explanatory.

E: Compute gkma compute ID does not compute stress/atom

Self-explanatory.


*/
```

APPENDIX F. DESCRIPTION OF THE PROCEDURE FOR CALCULATING THE MODE SPATIAL EXTENT

This chapter contains an example calculation of the MSE applied to a vibrational mode in a-Ge. The chapter also contains some further discussion about the use of a two-term Gaussian as the functional form to which the data is fit.

F.1 Description of the Mode Spatial Extent Calculation

The mode selected for this example is one of the low-frequency vibrational modes in a-Ge that has an unusually low PR. This mode is illustrated below in Fig. 19, with frequency ω = 2.0 THz and PR = 0.11. Traditionally, such a mode would be considered a diffuson based on its (low) frequency, but its PR indicates the mode is a locon. From simple visual inspection, one can see there is a significant degree of delocalization of the eigenvectors: while there is a single atom with a particularly large amplitude (the vertical eigenvector in the top-middle of the figure), the other atoms in the system are still significantly excited. The MSE for this mode will be determined first, after which it will be shown that the metric can accurately capture the tail of eigenvectors and indicate that the mode is spatially delocalized.

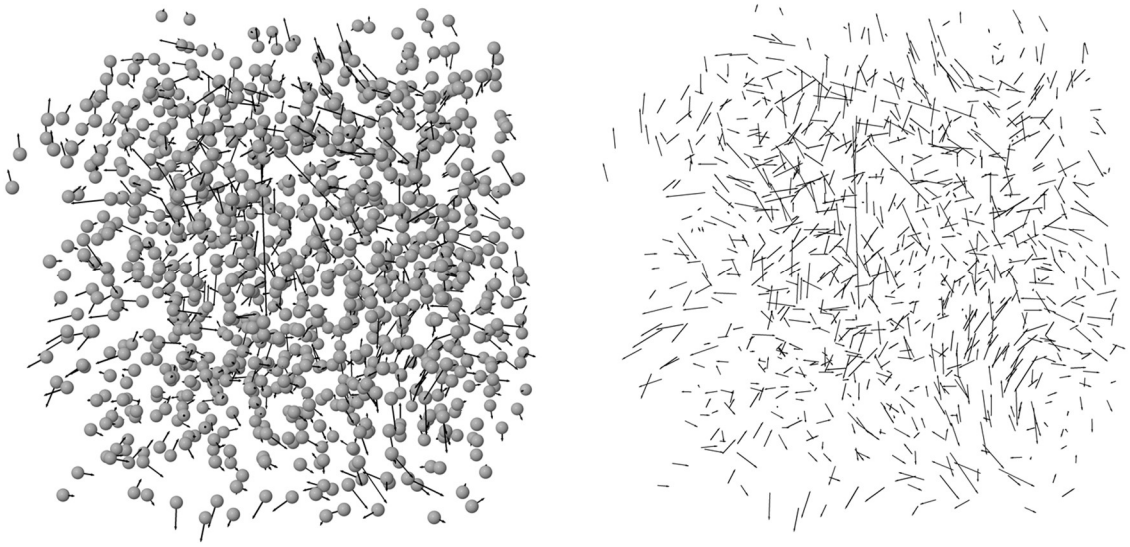

Figure 19. A vibrational mode in a-Ge with PR = 0.11 & MSE = 48 Å. Note the single large vertical eigenvector in the top middle of the figure and the comparatively small eigenvectors of the other atoms. Atoms removed in figures on the right for clarity.

To start, first divide the supercell into thin slices in each of the x-, y-, and z-directions. This example will focus only on the slides perpendicular to the x-direction, but note that the process is repeated in the other two directions. Here, 40 slices are used for the calculation, but this method has been found to be highly insensitive to the number of slices used, so long as they are fairly thin ($\lesssim$ 2 Å), but thick enough to each contain a substantial number of atoms ($\gtrsim$ 30 atoms). Sensitivity to the number of bins is discussed further at the end of this section. Given that the dimensions of the supercell are 30 Å on each side, each slice is 0.75 Å x 30 Å x 30 Å. In every slice, sum the squares of all the eigenvectors to produce a single value per slice, resulting in a total of 40 values that are a function of position in the x-direction. Fig. 52 below shows the result of this process.

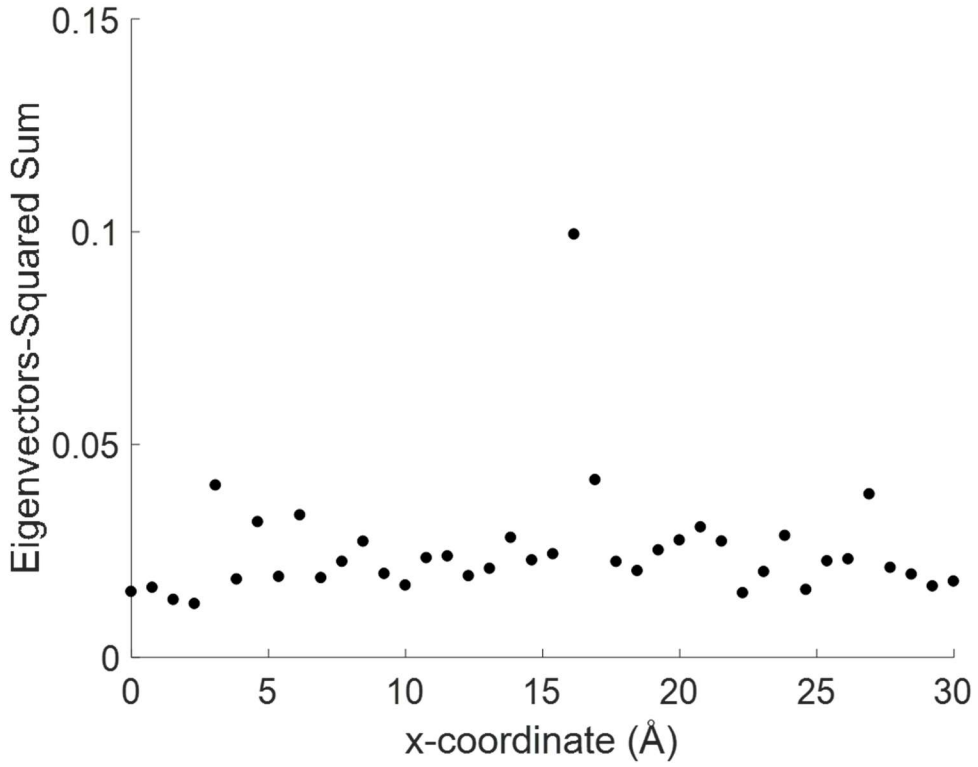

Figure 52. Result of summing the square of eigenvectors in each slice of a-Ge, as a function of distance in the *x*-direction.

Next, fit the data to a two-term Gaussian with the form[21]

$$f(x) = a_1 e^{-\left(\frac{x-b_1}{c_1}\right)^2} + a_2 e^{-\left(\frac{x-b_2}{c_2}\right)^2} \tag{28}$$

The functional form is centered around the largest single value and periodic images of the data are include on either side, but the total data to which the curve is fit is only the length of the supercell. Thus for instance, if for a 30 Å supercell, the largest datapoint were located at x = 5 Å, the curve would be fit to data ranging from x = -10 Å to x = 20 Å.

The parameters of interest for the purposes of determining the MSE are c_1 and c_2, which give the half-width of the Gaussian peaks; these values effectively allow one to assign a

[21] Justification for this functional form can be found in the next section.

"size" to the modes. Even though there may be a single point with a value much greater than the other values – as is the case in Fig. 52 – the intent is to capture the tail of small, but non-zero eigenvectors, necessitating a two-term rather than a one-term Gaussian. Why the two-term form is necessary is illustrated using the simple example in Fig. 53 below:

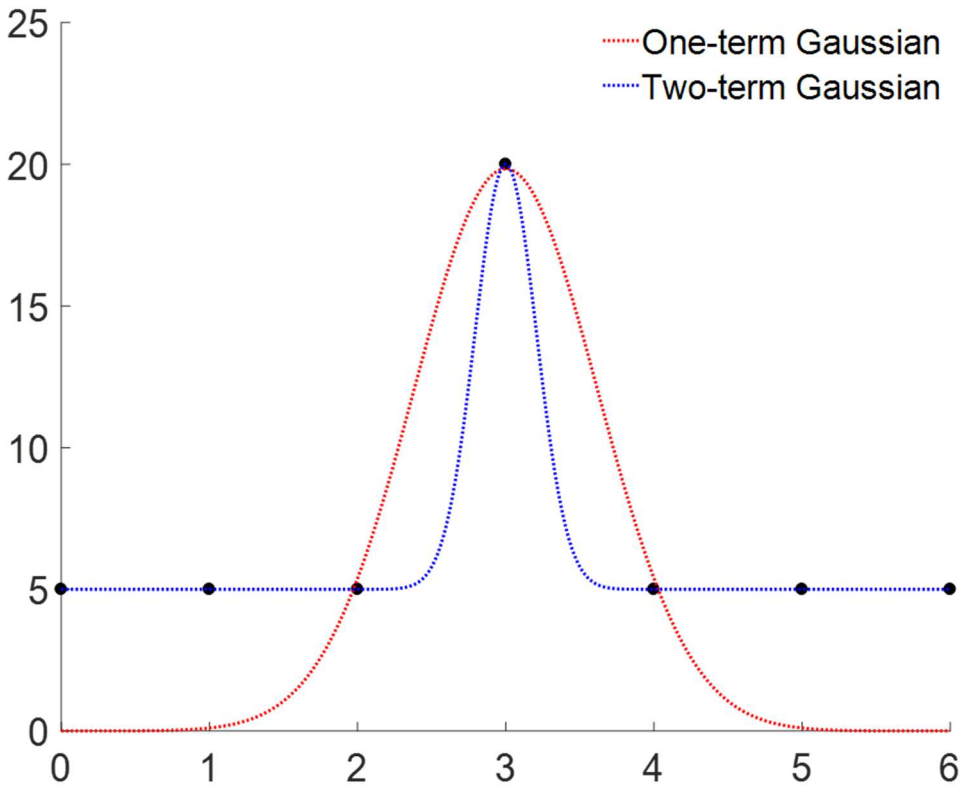

Figure 53. Illustration of the difference between using one-term and two-term Gaussian functional forms. The two curves are fit to the black datapoints.

For the two-term Gaussian, the values of the peak half-widths are $c_1 = 0.292$ and $c_2 = 1.64$ x 10^4, whereas for the one-term Gaussian, a single value of $c = 0.876$ is obtained. (The units of the x-axis are arbitrary for this example.) The one-term form is therefore able to provide information about the approximate width of the peak (i.e. the spacing between the datapoint at $x = 3$ and the surrounding datapoints), but it does not tell one anything about the value of the other datapoints. On the other hand, the two-term Gaussian captures the

width of the peak (the c_1 value), while also capturing the non-zero aspects of the other datapoints (the c_2 value). For comparison, if all the data in Fig. 53 other than the middle datapoint were set equal to 0 instead of 5, the resultant half-width values would be c_1 = 0.443 and c_2 = 0.576; that both c values are low in this case indicates the "mode" represented in this example is localized.

Returning to Fig. 52, when the data is fit using the two-term Gaussian functional form, the following is obtained:

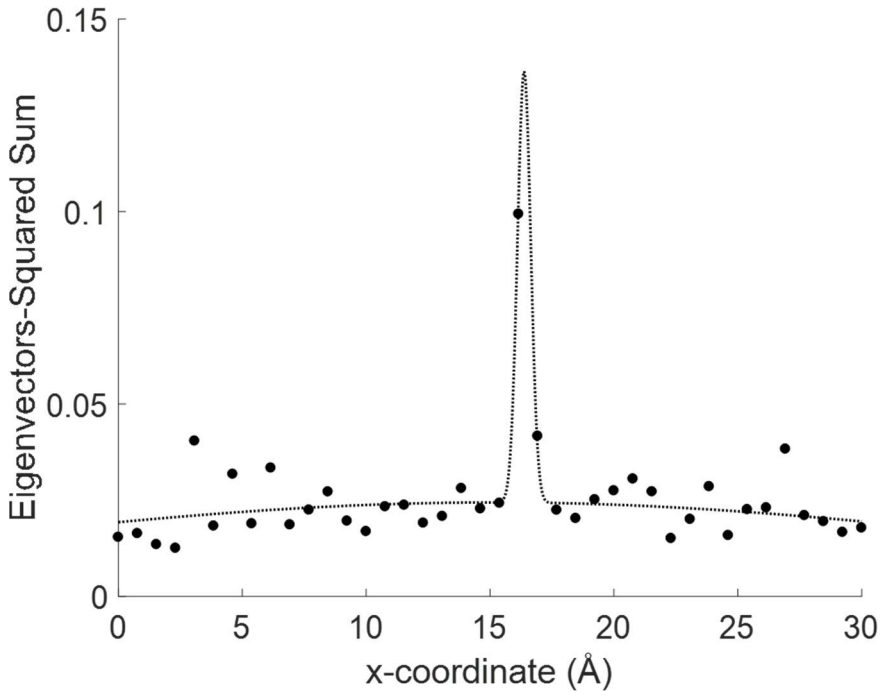

Figure 54. Results of fitting a two-term Gaussian function to the data shown in Fig. 52.

The parameters obtained from the fit shown in Fig. 54 are listed below in Table 2.

Table 2. Result and parameters of fitting a two-term Gaussian to the data shown in Fig. 46.

Parameter	Value
a_1	0.112
a_2	0.0244
b_1	16.4 Å
b_2	15.2 Å
c_1	0.379 Å
c_2	31.2 Å

Note that, similar to the results of the fit from Fig. 53, for the results listed in Table 2, the value of c_1 captures the width of the narrow peak at x = 15.75 Å, and the value of c_2 captures the non-zero values of the data in the remainder of the supercell.

Next, repeat this process in the y- and z- directions and average all six c values to calculate the MSE. For the mode shown here, the result is the following.

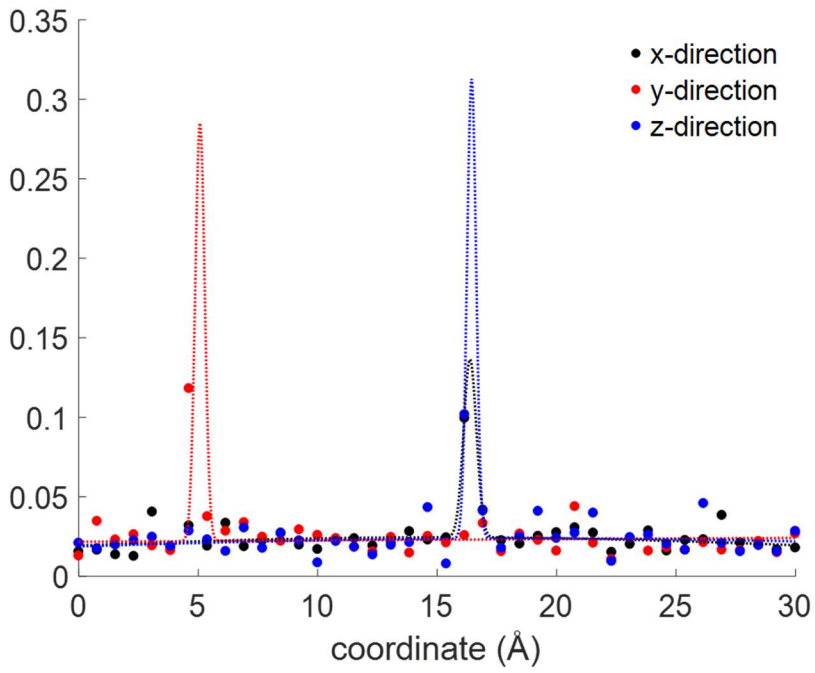

Figure 55. Result of fitting a two-term Gaussian curve to the data in each of the x-, y-, and z-directions.

The c values in the y- and z-directions are $c_1 = 0.281$ Å, $c_2 = 216$ Å and $c_1 = 0.268$ Å, $c_2 = 38.7$ Å, respectively. The average of all six c values, (which is defined as the MSE), is 48 Å, indicating the mode is delocalized, despite a PR of only 0.11. Note that although the fitting procedure does a poor job of capturing the correct maximum peak height (evident for both the y- and z-directions), this method is insensitive to this error, and a correct peak height is not important here.

F.2 Rationale for a Two-term Gaussian Functional Form

The method for calculating MSE uses a two-term Gaussian as the functional form to which the data is fit. While this form is not necessarily the only form that could be used, it has been found to be an appropriate descriptor, and the best option of all forms considered for

this dissertation. This section will describe in further detail the rationale for using a two-term Gaussian over a different functional form.

The procedure for calculating MSE has been tested for functional forms other than a two-term Gaussian, including a one-term Gaussian (i.e. a normal distribution), a quadratic polynomial, and a horizontal line, with a delta function at the largest single value; interestingly, the efficacy of the method is largely insensitive to the functional form selected. However, the two-term Gaussian provides the best fit to the data and appears to be the most consistent at capturing the tail of non-zero eigenvectors.

The average R^2 value of fit for different functional forms has been calculated for each mode in the a-PMMA supercell studied. Table 3 provides the average R^2 for both one- and two-term Gaussian forms, as well as two other functional forms: a parabola and horizontal line with a delta function at the largest value.

Table 3. Comparison of R^2 values for different functional forms used to determine MSE.

Functional Form	R^2
One-term Gaussian	0.56
Two-term Gaussian	0.75
Parabolic	0.19
Horizontal line + delta function	0.06

Here it can be seen that the two-term Gaussian functional form exhibits by far the best fit for the data considered here. Some examples have been included below in which the two-term Gaussian can be seen to be a superior fit to the one-term form. These modes are the same ones shown in Fig. 15, which is also reproduced here.

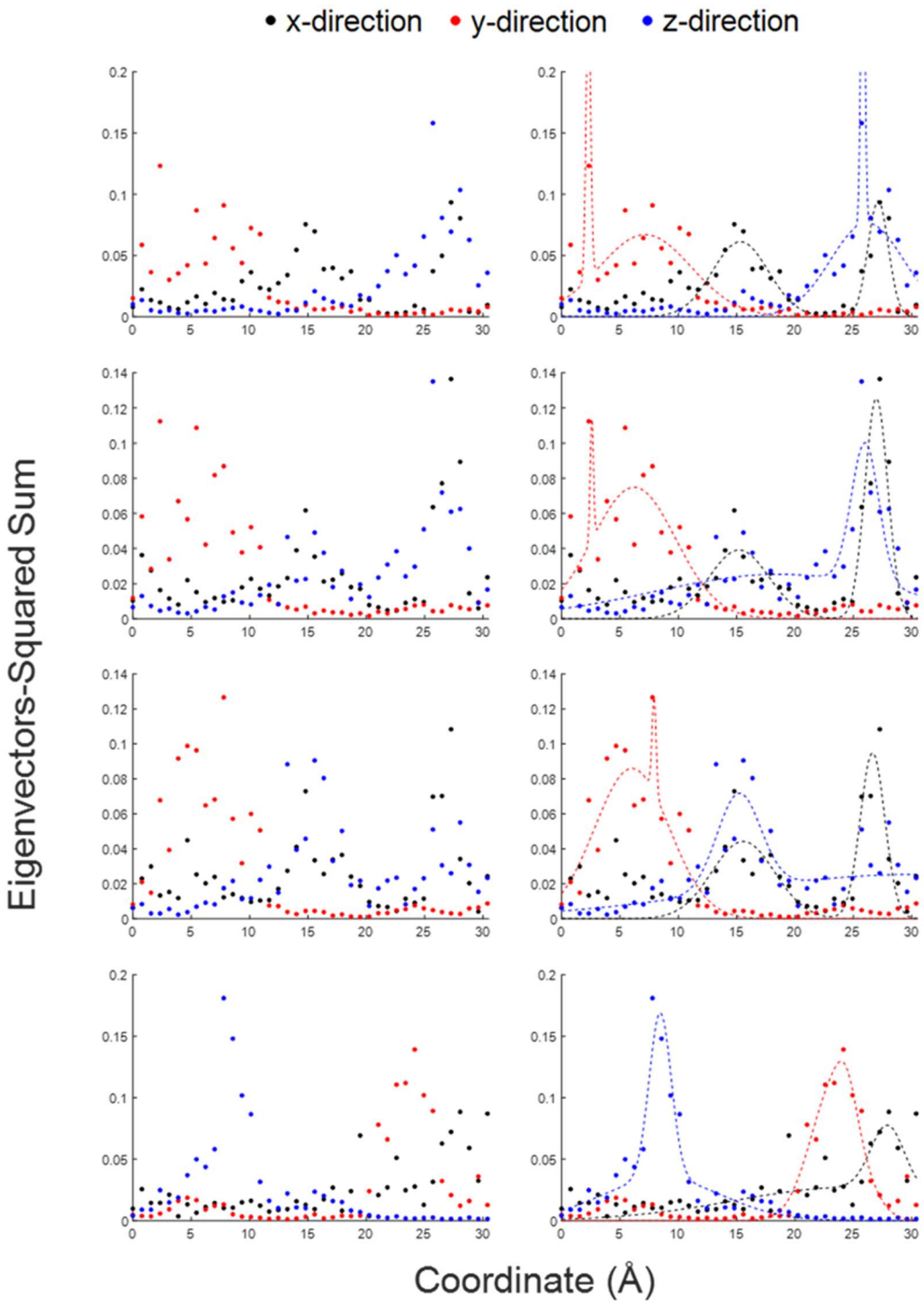

Figure 15. Sum of eigenvectors (left) in each of 40 thin "slices" in the x- (black), y- (red), and z- (blue) directions, plotted vs the coordinate in the respective direction. Each plot corresponds to the respective mode shown in Fig. 7. The right half of the figure shows the data on the left fit with a two-term Gaussian.

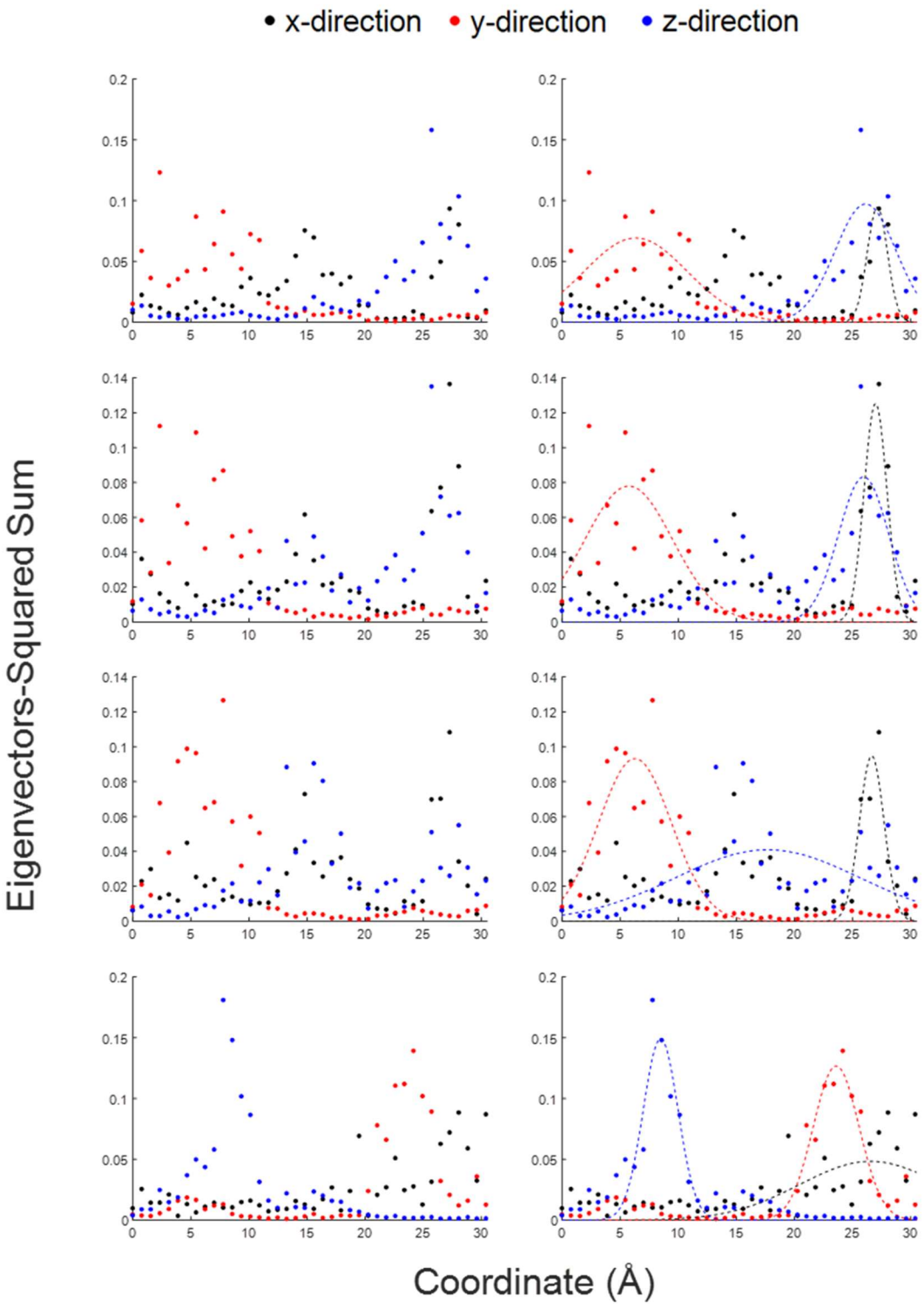

Figure 56. Sum of eigenvectors (left) in each of 40 thin "slices" in the x- (black), y- (red), and z- (blue) directions, plotted vs the coordinate in the respective direction. Each plot corresponds to the respective mode shown in Fig. 7. The right half of the figure shows the data on the left fit with a one-term Gaussian.

The fit is evidently better in Fig. 15, which should be unsurprising, considering a two-term Gaussian provides additional degrees of freedom. However, it is apparent that the two-term functional form also better accounts for modes for which the distribution of eigenvector sums is not a simple Gaussian – consider the data in the x-direction for the first mode shown. There are two distinct Gaussian-shaped peaks for this mode, making the two-term Gaussian function a much better fit than the one-term option.

Interestingly, as noted however, the functional form is not particularly important if one considers how localization varies with frequency. Actually, it is surprising how consistently the MSE can describe localization in spite of the functional form, as is evident in Fig. 57.

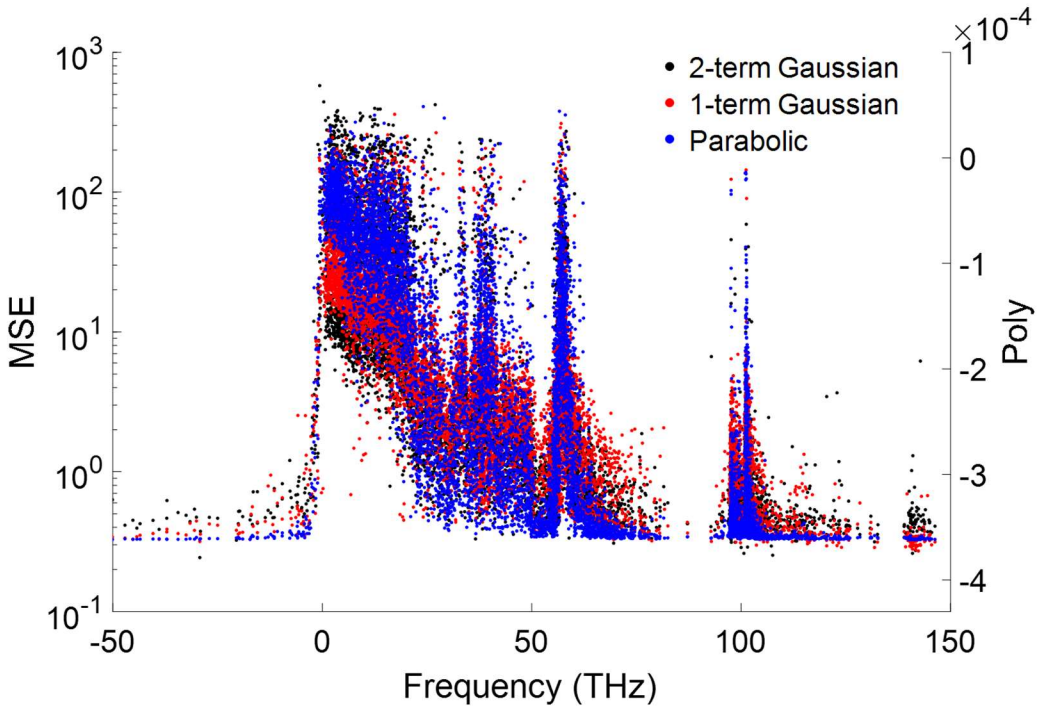

Figure 57. The result of using different functional forms for the MSE fitting, including a two-term Gaussian, one-term Gaussian, and parabolic functions.

The data shows the result of calculating the MSE using a two-term and a one-term Gaussian (black and red, respectively), as well as the result of fitting the data to a parabola, and using the ”width” (i.e. the coefficient of the x^2 term) as the measure of localization; the data is scaled arbitrarily to match with the results of a Gaussian fitting, but the consistency between the forms is still quite apparent.

The MSE was also calculated for the large (15,020 atom) a-PMMA supercell. The results of this calculation vs. frequency are shown in Fig. 58 below, along with the MSE of the 3,008 atom a-PMMA supercell.

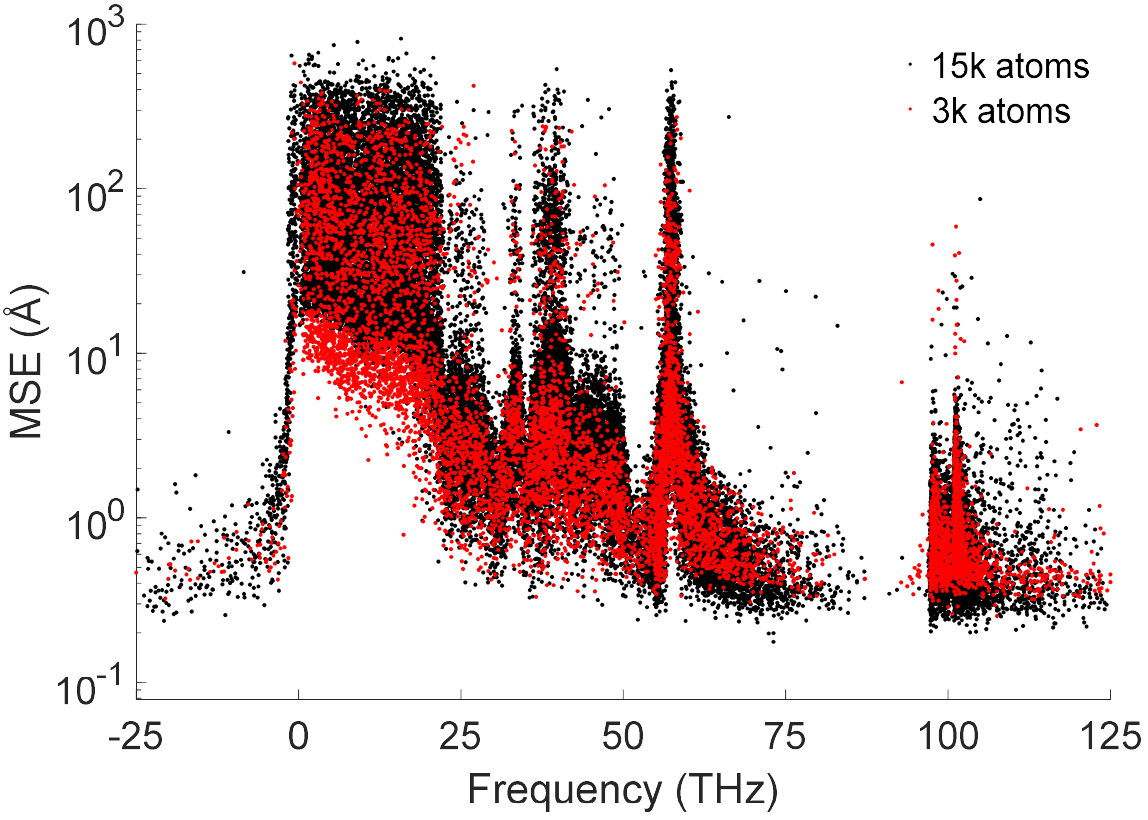

Figure 58. MSE vs. frequency for a-PMMA supercells with 15,020 and 3,008 atoms.

Looking at Fig. 58, it is evident that the MSE is consistent across different supercell sizes. On average, the MSE of many modes in the 0-50 THz range is slightly lower for the smaller

supercell, which is unsurprising considering the smaller dimensions of the 3k atom supercell; given that the dimensions of the smaller supercell are only about 60% of those of the larger supercell, it stands to reason that the MSE (which is effectively a measure of the size of the mode) would also on average be smaller as well. Regardless, the overall findings based on MSE are the same for both supercells: modes with IF's tend to be highly localized (i.e. their MSE is $\lesssim$ 1 Å), modes with frequencies between 0 and 25 THz are delocalized and span the entire supercell (MSE $\gtrsim$ 10 Å), modes with frequencies between 25 and 50 THz show some degree of localization (1 Å < MSE < 10 Å), and most modes with frequencies > 50 THz are localized (MSE < 1 Å), with "spikes" of delocalized modes evident at specific frequency bands.

The MSE has also be found to yield results that are largely independent of bin size. Fig. 59 shows the MSE of each mode in a-PMMA, calculated using both 40 and 60 bins. The MSE is consistent when using a different number of bins.

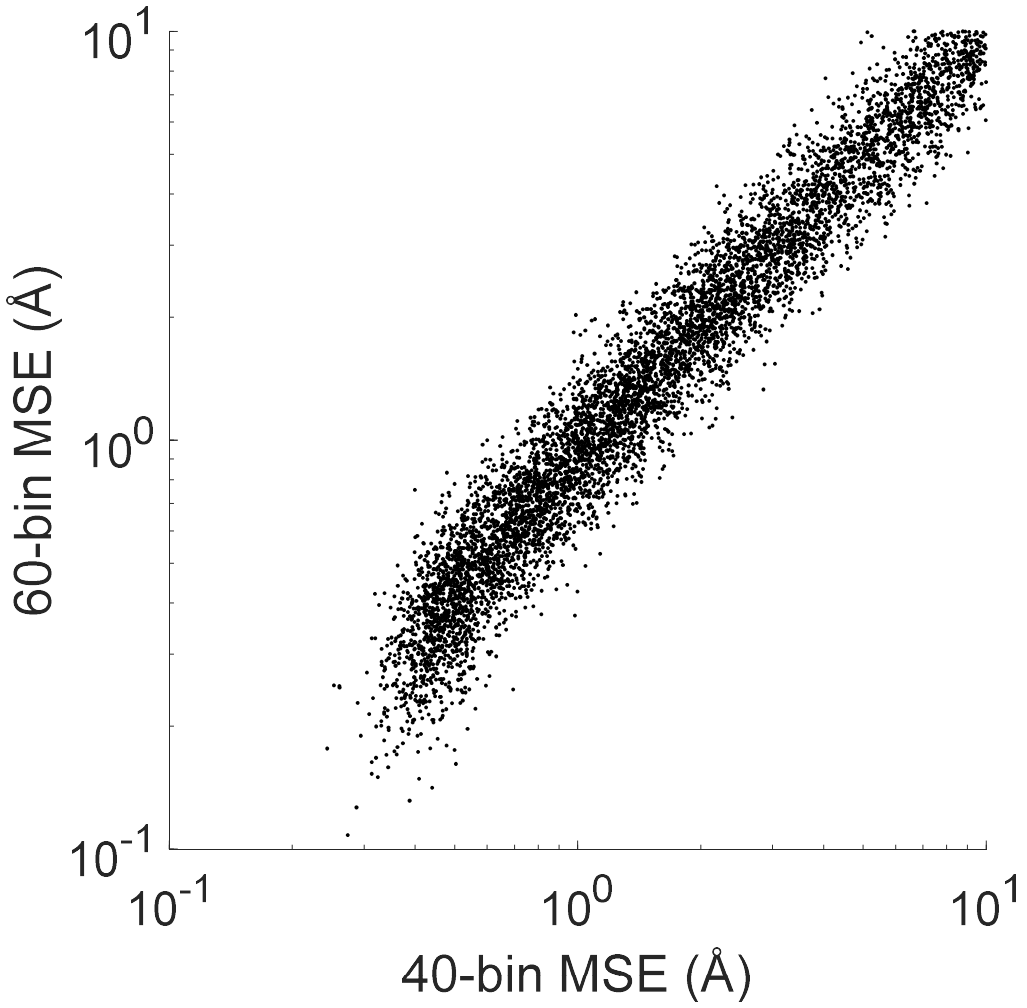

Figure 59. Comparison of MSE of each mode in a-PMMA, calculated using 40 bins and using 60 bins.

It can be seen that while changing the binning does have some effect on the MSE, the method is still generally quite consistent. Of the modes shown in Fig. 59, the largest difference in MSE is a factor of 2. This difference occurs when the MSE is well below 1 Å, which is where some discrepancy between the MSE for different bin sizes is evident. The reason for this discrepancy is due to the "resolution" of the procedure for calculating MSE: when using a larger number of bins, the minimum distance between each point being fit decreases, which in turn decrease the minimum width of a Gaussian peak. If one considers an extreme case in which a mode exists entirely on a single atom, the MSE would

scale with the width of a single bin. Thus, by using more bins (and consequently, a smaller bin width), for highly localized modes, the MSE is found to be slightly smaller. However, this effect is only observed at sizes < 1 Å, in which case the mode can in be considered localized, regardless of bin size.

For comparison, the MSE calculated using a horizontal line and delta function is extremely sensitive to bin size. This is because the two-term Gaussian MSE is a measure of the peak widths and is therefore insensitive to the actual value of the sum, unlike for instance a horizontal line with a delta function. If the width of a slice were to increase by a factor of two, the sum of eigenvectors in a given slice would roughly double. For the two-term Gaussian functional form, it is evident that the value from fitting remains largely unchanged. However, because the horizontal line and delta function is effectively a measure of the average sum of each slice, changing the magnitude of that sum will have a significant impact on the value calculated, as shown below in Fig. 60.

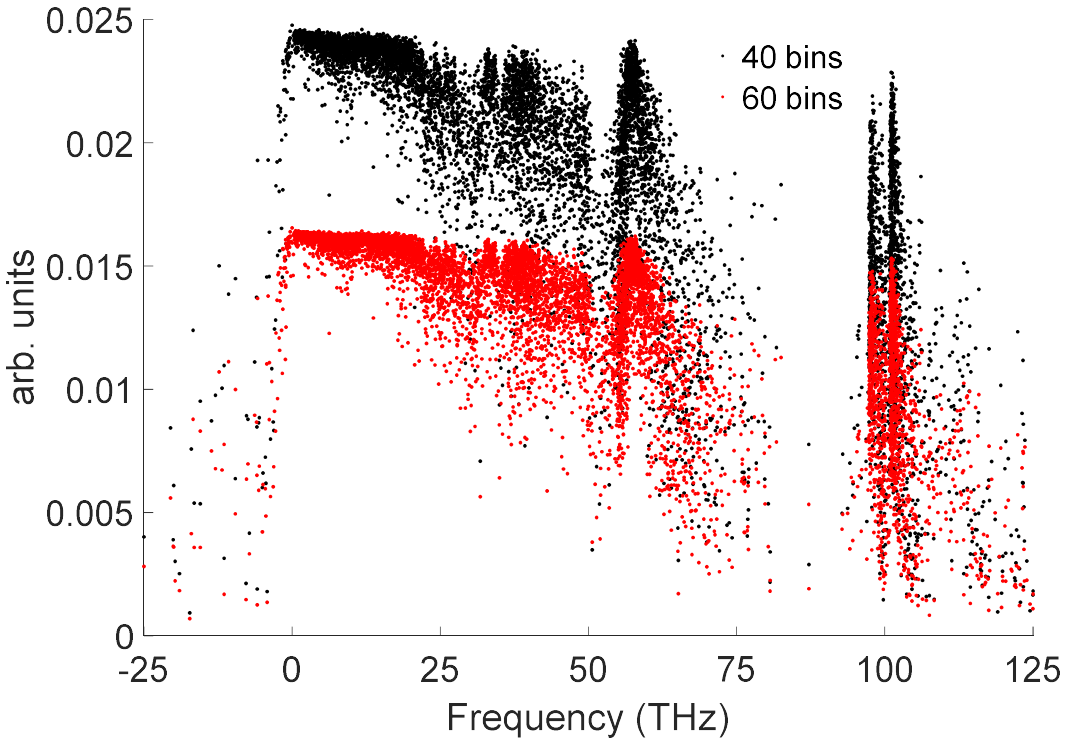

Figure 60. Comparison of the MSE calculated using a horizontal line plus a delta function for different bin sizes. The y-axis is the value of the intercept when the horizontal line is fit to the data.

Here, it is evident that changing the bin size has a strong effect on the calculated MSE. The value of the MSE for a mode calculated in this manner is approximately inversely proportional to the number of bins. Thus, for a given mode the MSE calculated for a horizontal line and delta function using 40 bins is approximately 50% larger than for a mode calculated using 60 (i.e. 50% more) bins. As shown in Fig. 59, his dependence on bin size does not exist for a two-term Gaussian MSE. Thus, this is functional form used for all MSE calculations unless explicitly stated otherwise.

APPENDIX G. ADDITIONAL THERMAL CONDUCTIVITY DATA FOR AMORPHOUS POLY(METHYL METHACRYLATE), AMORPHOUS POLYSTYRENE, AND AMORPHOUS POLYVINYL CHLORIDE

This chapter presents the modal TC of each of the three polymers studied in this dissertation, both on a per-mode basis, and as an accumulation function. The data included here compliments that shown in the text.

G.1. Modal Thermal Conductivity Data as a Function of Participation Ratio and Mode Spatial Extent

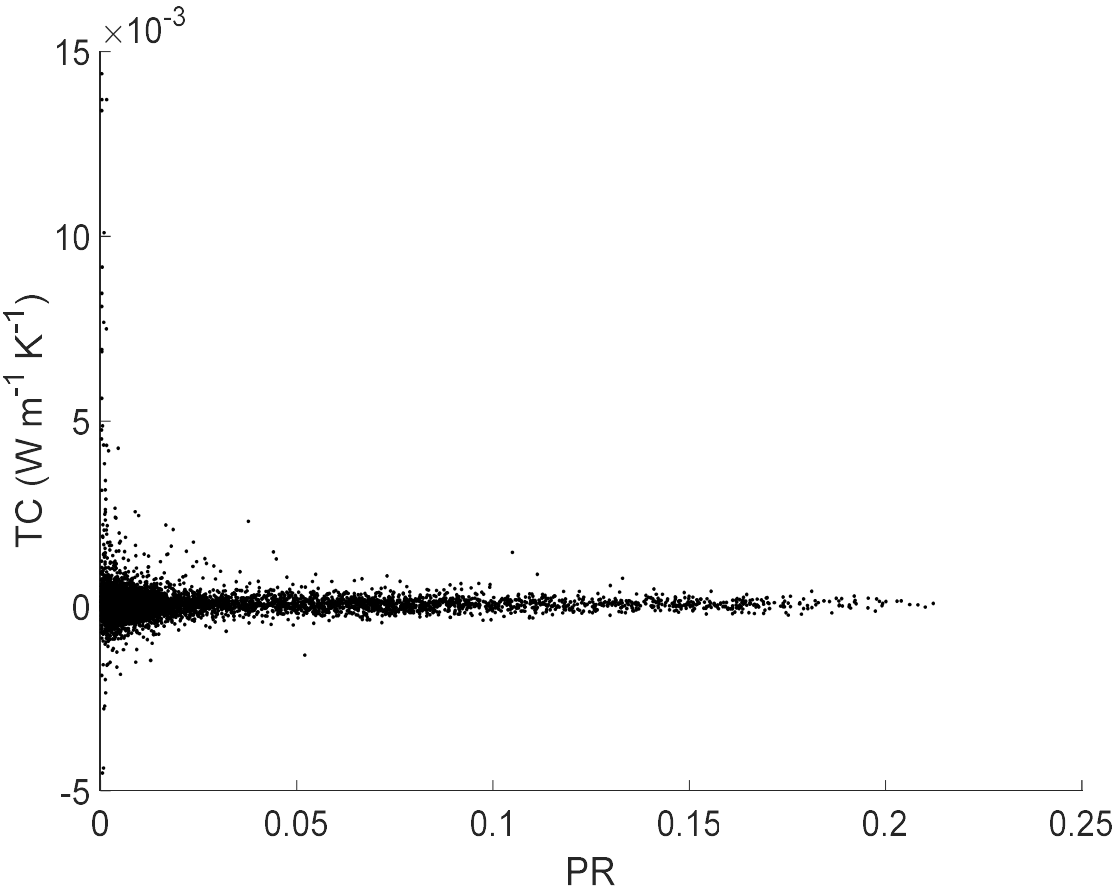

Figure 61. Modal TC of a-PS as a function of PR.

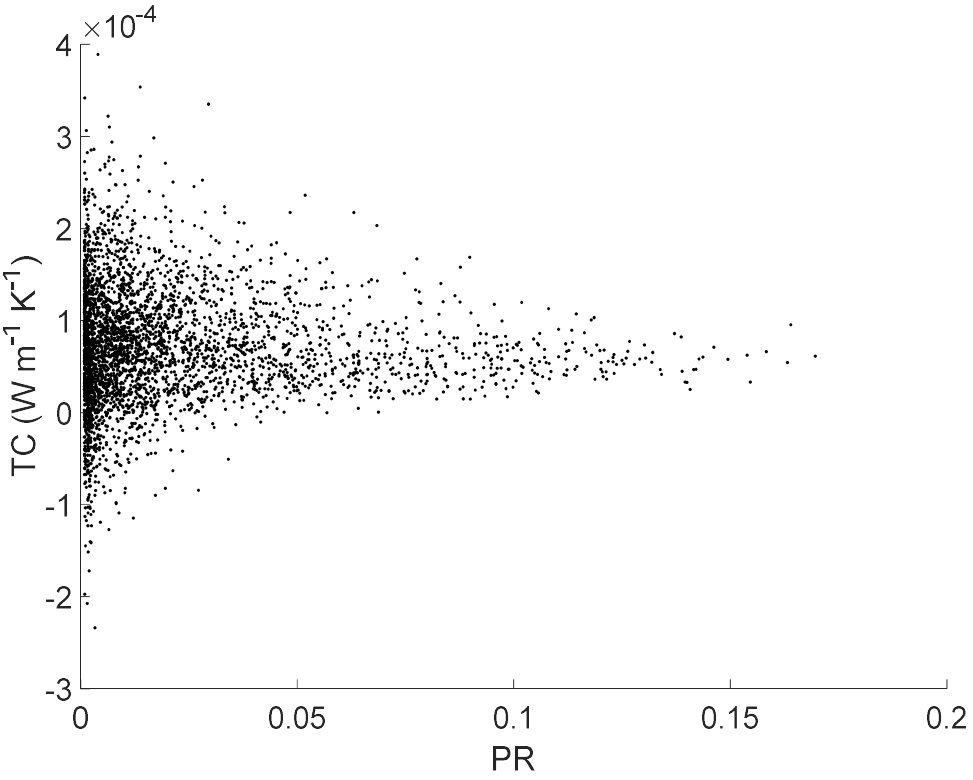

Figure 62. Modal TC of a-PVC as a function of PR.

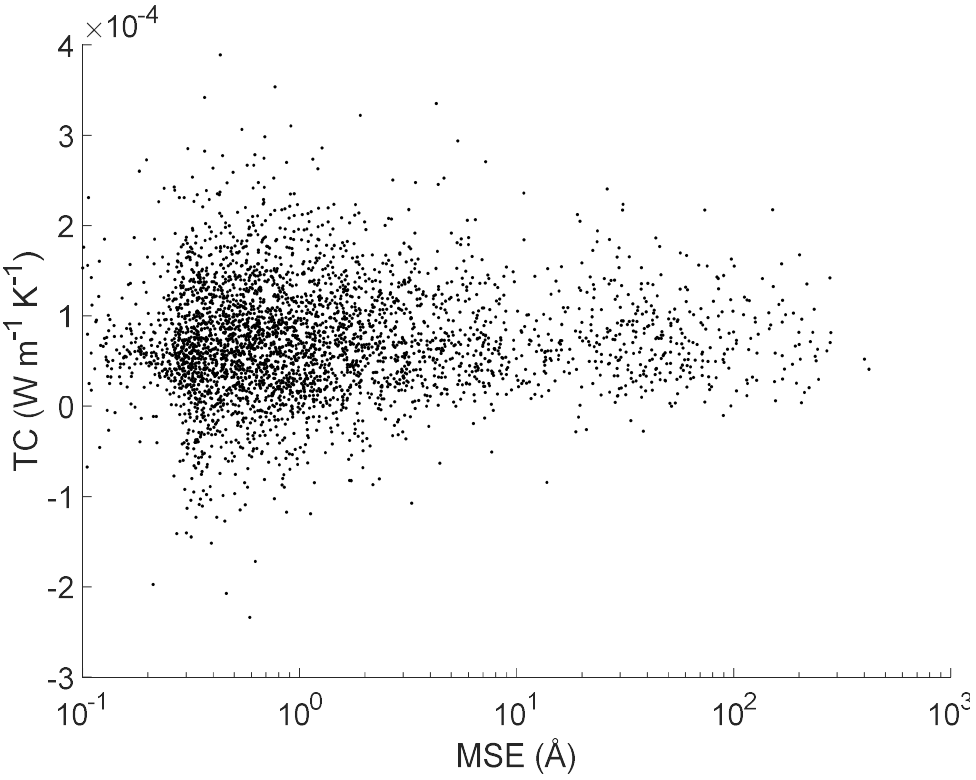

Figure 63. Modal TC of a-PVC as a function of MSE.

G.2. Modal Thermal Conductivity Accumulations as a Function of Participation Ratio and Mode Spatial Extent

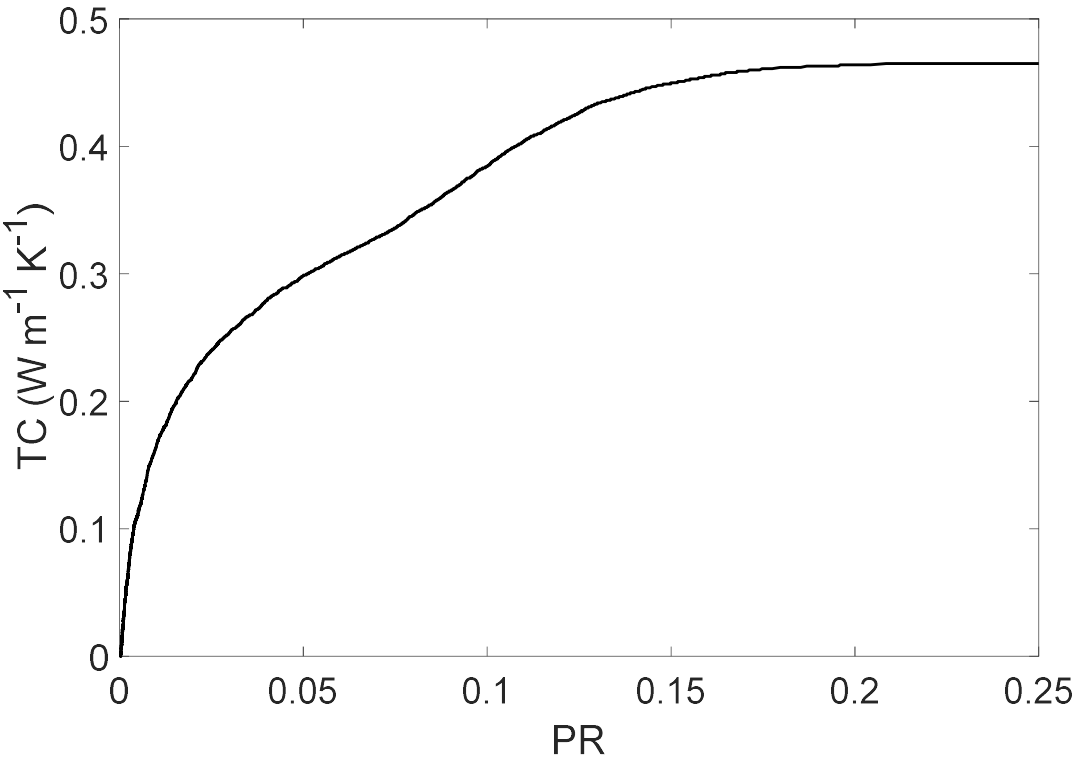

Figure 64. TC accumulation of a-PMMA as a function of PR.

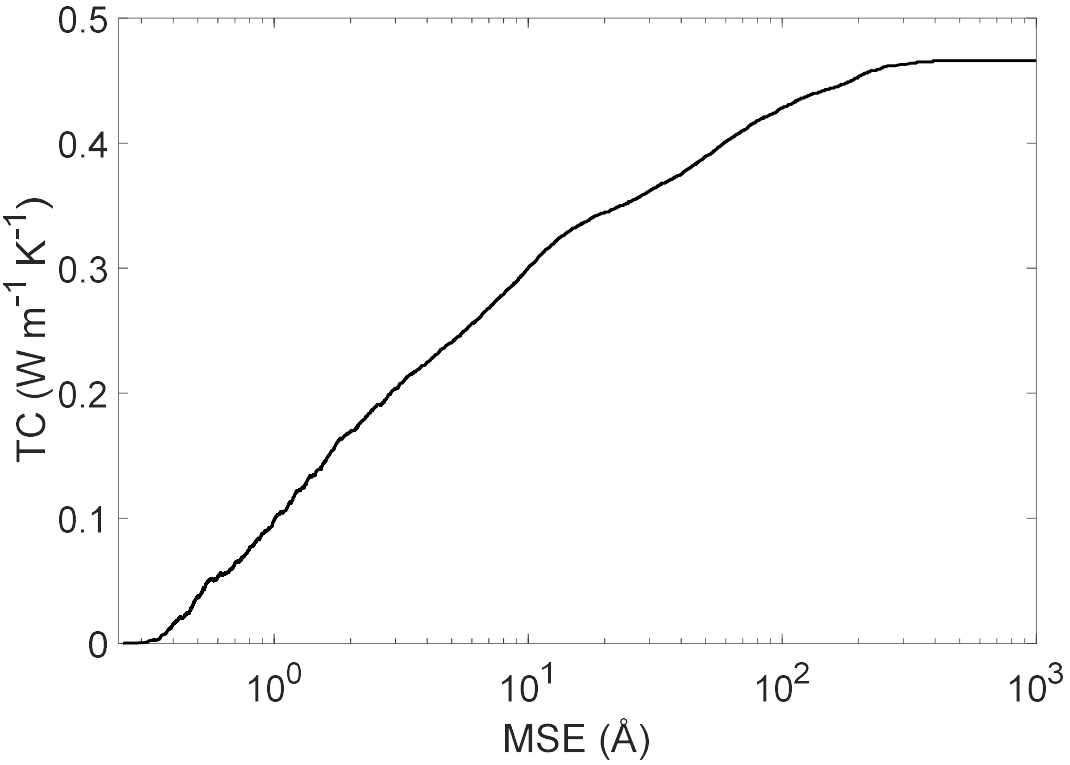

Figure 65. TC accumulation of a-PMMA as a function of MSE.

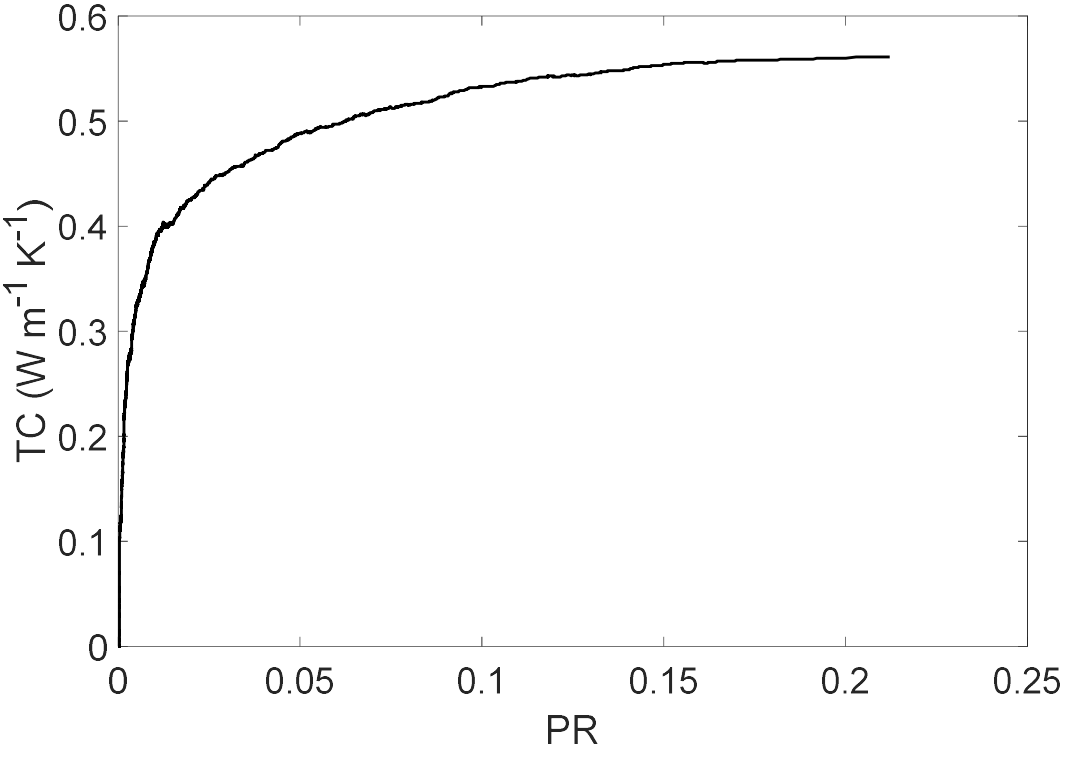

Figure 66. TC accumulation of a-PS as a function of PR.

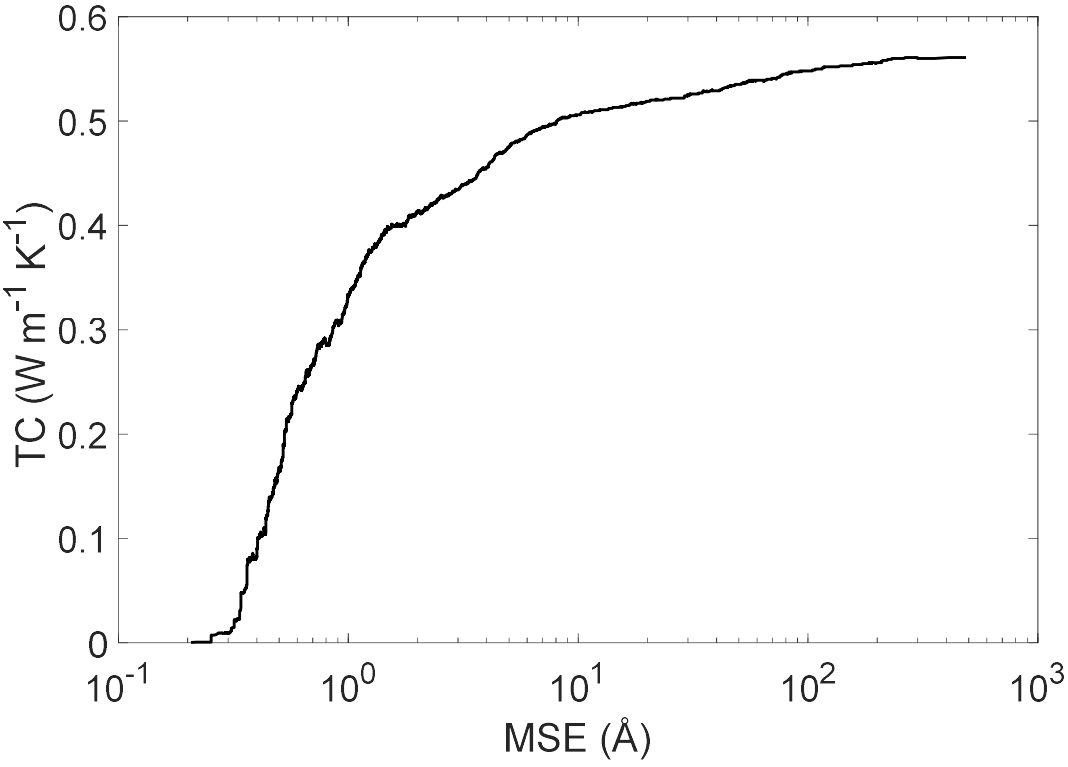

Figure 67. TC accumulation of a-PS as a function of MSE.

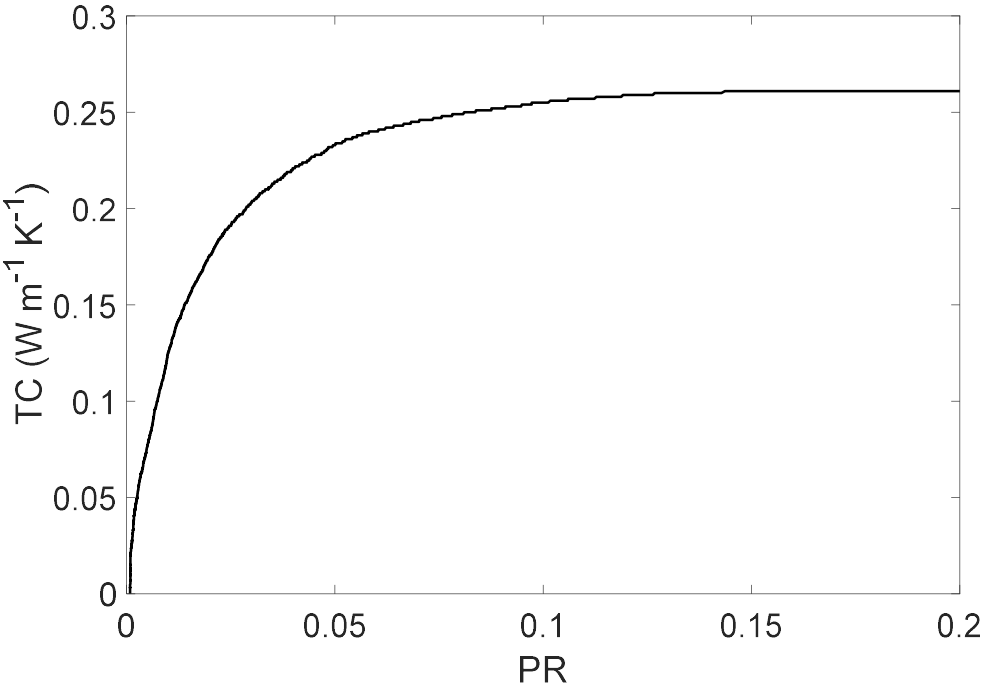

Figure 68. TC accumulation of a-PVC as a function of PR.

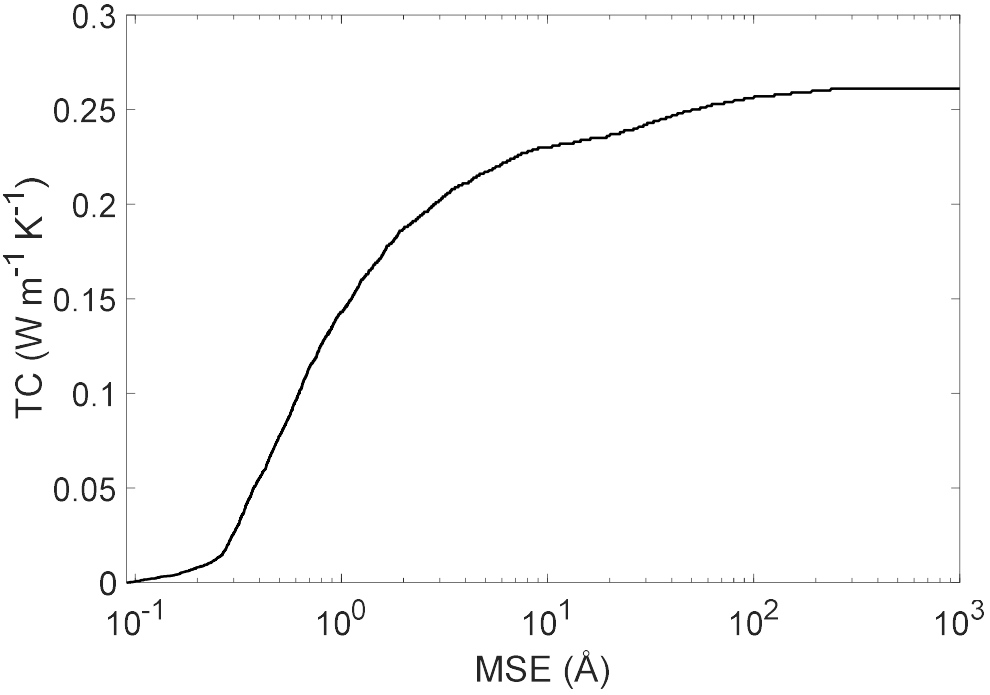

Figure 69. TC accumulation of a-PVC as a function of MSE.

REFERENCES

1. Klemens, P., *The scattering of low-frequency lattice waves by static imperfections.* Proceedings of the Physical Society. Section A, 1955. **68**(12): p. 1113.

2. Allen, P.B. and J.L. Feldman, *Thermal conductivity of disordered harmonic solids.* Physical Review B, 1993. **48**(17): p. 12581.

3. Allen, P.B., et al., *Diffusons, locons and propagons: Character of atomie yibrations in amorphous Si.* Philosophical Magazine B, 1999. **79**(11-12): p. 1715-1731.

4. McGaughey, A.J.H. and M. Kaviany, *Phonon Transport in Molecular Dynamics Simulations: Formulation and Thermal Conductivity Prediction*, in *Advances in Heat Transfer*, G.A. Greene, et al., Editors. 2006, Elsevier. p. 169-255.

5. Baldi, G., et al., *Thermal conductivity and terahertz vibrational dynamics of vitreous silica.* Physical Review B, 2008. **77**(21): p. 214309.

6. Lv, W. and A. Henry, *Non-negligible Contributions to Thermal Conductivity From Localized Modes in Amorphous Silicon Dioxide.* Scientific Reports, 2016. **6**: p. 35720.

7. Agne, M.T., R. Hanus, and G.J. Snyder, *Minimum thermal conductivity in the context of diffuson-mediated thermal transport.* Energy & Environmental Science, 2018. **11**(3): p. 609-616.

8. Jugdersuren, B., et al., *Thermal conductivity of amorphous and nanocrystalline silicon films prepared by hot-wire chemical-vapor deposition.* Physical Review B, 2017. **96**(1): p. 014206.

9. Moon, J., B. Latour, and A.J. Minnich, *Propagating elastic vibrations dominate thermal conduction in amorphous silicon.* Physical Review B, 2018. **97**(2): p. 024201.

10. Allen, P.B., et al., *Thermal conductivity of insulating Bi 2 Sr 2 YCu 2 O 8 and superconducting Bi 2 Sr 2 CaCu 2 O 8: Failure of the phonon-gas picture.* Physical Review B, 1994. **49**(13): p. 9073.

11. Sun, T. and P.B. Allen, *Lattice thermal conductivity: Computations and theory of the high-temperature breakdown of the phonon-gas model.* Physical Review B, 2010. **82**(22): p. 224305.

12. Lv, W. and A. Henry, *Examining the validity of the phonon gas model in amorphous materials.* Scientific reports, 2016. **6**: p. 37675.

13. Seyf, H.R., et al., *Rethinking phonons: The issue of disorder.* npj Computational Materials, 2017. **3**(1): p. 49.

14. Peierls, R., *On the kinetic theory of thermal conduction in crystals*, in *Selected Scientific Papers Of Sir Rudolf Peierls: (With Commentary)*. 1997, World Scientific. p. 15-48.

15. Chen, G., *Nanoscale Energy Transport and Conversion: A Parallel Treatment of Electrons, Molecules, Phonons, and Photons*. 2005: Oxford University Press.

16. Zhang, Z.M., *Nano/microscale heat transfer*. 2007: McGraw-Hill New York.

17. Einstein, A., *On the motion of small particles suspended in liquids at rest required by the molecular-kinetic theory of heat.* Annalen der physik, 1905. **17**: p. 549-560.

18. Einstein, A., *Die plancksche theorie der strahlung und die theorie der spezifischen waerme.* Annalen der Physik, 1907. **327**(1): p. 180-190.

19. Debye, P., *Zur theorie der spezifischen wärmen.* Annalen der Physik, 1912. **344**(14): p. 789-839.

20. Seyf, H., *Revisiting the Theory of Alloy Thermal Conductivity*. 2019, Georgia Institute of Technology.

21. Gordiz, K. and A. Henry, *Phonon transport at interfaces: Determining the correct modes of vibration.* Journal of Applied Physics, 2016. **119**(1): p. 015101.

22. Ziman, J.M., *Electrons and Phonons*. 2001, New York: Oxford University Press.

23. Lindsay, L., *First principles peierls-boltzmann phonon thermal transport: a topical review.* Nanoscale and Microscale Thermophysical Engineering, 2016. **20**(2): p. 67-84.

24. Srivastava, G.P., *The physics of phonons*. 1990: CRC press.

25. Broido, D.A., et al., *Intrinsic lattice thermal conductivity of semiconductors from first principles.* Applied Physics Letters, 2007. **91**(23): p. 231922.

26. Tian, Z., et al., *Phonon conduction in PbSe, PbTe, and PbTe 1− x Se x from first-principles calculations.* Physical Review B, 2012. **85**(18): p. 184303.

27. McGaughey, A.J. and M. Kaviany, *Quantitative validation of the Boltzmann transport equation phonon thermal conductivity model under the single-mode relaxation time approximation.* Physical Review B, 2004. **69**(9): p. 094303.

28. Cahill, D.G. and R.O. Pohl, *Thermal properties of a tetrahedrally bonded amorphous solid: CdGeAs 2.* Physical Review B, 1988. **37**(15): p. 8773.

29. Cahill, D.G. and R.O. Pohl, *Thermal conductivity of amorphous solids above the plateau.* Physical review B, 1987. **35**(8): p. 4067.

30. Shamsa, M., et al., *Thermal conductivity of diamond-like carbon films.* Applied Physics Letters, 2006. **89**(16): p. 161921.

31. Liu, X., et al., *High thermal conductivity of a hydrogenated amorphous silicon film.* Physical review letters, 2009. **102**(3): p. 035901.

32. Dames, C. and G. Chen, *Theoretical phonon thermal conductivity of Si/Ge superlattice nanowires.* Journal of Applied Physics, 2004. **95**(2): p. 682-693.

33. Seol, J.H., et al., *Two-dimensional phonon transport in supported graphene.* Science, 2010. **328**(5975): p. 213-216.

34. Garg, J., et al., *Role of disorder and anharmonicity in the thermal conductivity of silicon-germanium alloys: A first-principles study.* Physical review letters, 2011. **106**(4): p. 045901.

35. Garg, J. and G. Chen, *Minimum thermal conductivity in superlattices: A first-principles formalism.* Physical Review B, 2013. **87**(14): p. 140302.

36. Tian, Z., S. Lee, and G. Chen, *Heat Transfer in Thermoelectric Materials and Devices.* Journal of Heat Transfer, 2013. **135**(6): p. 061605-061605.

37. Abeles, B., *Lattice Thermal Conductivity of Disordered Semiconductor Alloys at High Temperatures.* Physical Review, 1963. **131**(5): p. 1906-1911.

38. Esfarjani, K., J. Garg, and G. Chen, *Modeling Heat Conduction From First Principles.* Annu. Rev. Heat Transf, 2014. **17**: p. 9–47.

39. Feng, T. and X. Ruan, *Prediction of Spectral Phonon Mean Free Path and Thermal Conductivity with Applications to Thermoelectrics and Thermal Management: A Review.* Journal of Nanomaterials, 2014. **2014**: p. 206370.

40. Lindsay, L., D.A. Broido, and T.L. Reinecke, *Ab initio thermal transport in compound semiconductors.* Physical Review B, 2013. **87**(16): p. 165201.

41. Tadano, T. and S. Tsuneyuki, *Self-consistent phonon calculations of lattice dynamical properties in cubic SrTiO3 with first-principles anharmonic force constants.* Physical Review B, 2015. **92**(5): p. 054301.

42. Tadano, T., Y. Gohda, and S. Tsuneyuki, *Anharmonic force constants extracted from first-principles molecular dynamics: applications to heat transfer simulations.* Journal of Physics: Condensed Matter, 2014. **26**(22): p. 225402.

43. Wang, X. and B. Huang, *Computational study of in-plane phonon transport in Si thin films.* Sci Rep, 2014. **4**: p. 6399.

44. Shiomi, J., K. Esfarjani, and G. Chen, *Thermal conductivity of half-Heusler compounds from first-principles calculations.* Physical Review B, 2011. **84**(10): p. 104302.

45. Cahill, D.G., et al., *Nanoscale thermal transport. II. 2003–2012.* Applied Physics Reviews, 2014. **1**(1): p. 011305.

46. Seyf, H.R., et al. *Revisiting the theory of disordered alloy thermal conductivity*. in *APS March Meeting Abstracts*. 2017.

47. Henry, A.S. and G. Chen, *Spectral phonon transport properties of silicon based on molecular dynamics simulations and lattice dynamics.* Journal of Computational and Theoretical Nanoscience, 2008. **5**(2): p. 141-152.

48. Minnich, A.J., et al., *Thermal conductivity spectroscopy technique to measure phonon mean free paths.* Physical review letters, 2011. **107**(9): p. 095901.

49. Weber, L. and E. Gmelin, *Transport properties of silicon.* Applied Physics A, 1991. **53**(2): p. 136-140.

50. Regner, K.T., et al., *Broadband phonon mean free path contributions to thermal conductivity measured using frequency domain thermoreflectance.* Nature communications, 2013. **4**: p. 1640.

51. Allen, P.B., et al., *Diffusons, locons and propagons: Character of atomic vibrations in amorphous Si.* Philosophical Magazine B, 1999. **79**(11-12): p. 1715-1731.

52. Ni, H., X. Li, and H. Gao, *Elastic modulus of amorphous SiO 2 nanowires.* Applied Physics Letters, 2006. **88**(4): p. 043108.

53. Alam, M., et al., *Influence of strain on thermal conductivity of silicon nitride thin films.* Journal of Micromechanics and Microengineering, 2012. **22**(4): p. 045001.

54. Alam, A., R.K. Chouhan, and A. Mookerjee, *Thermal conductivity and diffusion-mediated localization in Fe 1− x Cr x alloys from first principles.* Physical Review B, 2011. **84**(22): p. 224309.

55. Yu, X. and D.M. Leitner, *Thermal conductivity computed for vitreous silica and methyl-doped silica above the plateau.* Physical Review B, 2006. **74**(18): p. 184305.

56. Leitner, D.M., *Vibrational energy transfer and heat conduction in a one-dimensional glass.* Physical Review B, 2001. **64**(9): p. 094201.

57. Oligschleger, C. and J. Schön, *Simulation of thermal conductivity and heat transport in solids.* Physical Review B, 1999. **59**(6): p. 4125.

58. Courtens, E., et al., *The vibrational modes of glasses.* Solid state communications, 2001. **117**(3): p. 187-200.

59. Parshin, D. and C. Laermans, *Interaction of quasilocal harmonic modes and boson peak in glasses.* Physical Review B, 2001. **63**(13): p. 132203.

60. Crupi, C., et al., *Low-temperature specific heat in caesium borate glasses.* Philosophical Magazine, 2007. **87**(3-5): p. 741-747.

61. Schirmacher, W., *Thermal conductivity of glassy materials and the "boson peak.* EPL (Europhysics Letters), 2006. **73**(6): p. 892.

62. Zhou, Z., et al., *On the existence of Einstein oscillators and thermal conductivity in bulk metallic glass.* Applied physics letters, 2006. **89**(3): p. 031924.

63. Schirmacher, W., G. Ruocco, and T. Scopigno, *Acoustic attenuation in glasses and its relation with the boson peak.* Physical review letters, 2007. **98**(2): p. 025501.

64. d'Angelo, G., et al., *Boson peak in alkaline borate glasses: Raman spectroscopy, neutron scattering, and specific-heat measurements.* Physical Review B, 2009. **79**(1): p. 014206.

65. Shenogin, S., et al., *Predicting the thermal conductivity of inorganic and polymeric glasses: The role of anharmonicity.* Journal of Applied Physics, 2009. **105**(3): p. 034906.

66. Krivchikov, A., et al., *Effects of internal molecular degrees of freedom on the thermal conductivity of some glasses and disordered crystals.* Physical Review B, 2012. **85**(1): p. 014206.

67. Schober, H., U. Buchenau, and V. Gurevich, *Pressure dependence of the boson peak in glasses: Correlated and uncorrelated perturbations.* Physical Review B, 2014. **89**(1): p. 014204.

68. Feldman, J.L., P.B. Allen, and S.R. Bickham, *Numerical study of low-frequency vibrations in amorphous silicon.* Physical Review B, 1999. **59**(5): p. 3551.

69. Fabian, J., et al., *Numerical study of anharmonic vibrational decay in amorphous and paracrystalline silicon.* Physical Review B, 2003. **67**(22): p. 224302.

70. Zink, B., R. Pietri, and F. Hellman, *Thermal conductivity and specific heat of thin-film amorphous silicon.* Physical review letters, 2006. **96**(5): p. 055902.

71. Liu, X., et al., *High thermal conductivity of a hydrogenated amorphous silicon film.* Physical review letters, 2009. **102**(3): p. 035901.

72. He, Y., D. Donadio, and G. Galli, *Heat transport in amorphous silicon: Interplay between morphology and disorder.* Applied Physics Letters, 2011. **98**(14): p. 144101.

73. Liu, X., et al., *Anomalously High Thermal Conductivity of Amorphous Silicon Films Prepared by Hot-wire Chemical Vapor Deposition.* Chinese Journal of Physics, 2011. **49**(1): p. 359-368.

74. He, Y., et al., *Lattice thermal conductivity of semiconducting bulk materials: atomistic simulations.* Physical Chemistry Chemical Physics, 2012. **14**(47): p. 16209-16222.

75. Zhan, T., et al., *Phonons with long mean free paths in a-Si and a-Ge.* Applied Physics Letters, 2014. **104**(7): p. 071911.

76. Braun, J.L., et al., *Size effects on the thermal conductivity of amorphous silicon thin films.* Physical Review B, 2016. **93**(14): p. 140201.

77. Kwon, S., et al., *Unusually High and Anisotropic Thermal Conductivity in Amorphous Silicon Nanostructures.* ACS nano, 2017. **11**(3): p. 2470-2476.

78. Moon, J. and A.J. Minnich, *Sub-amorphous thermal conductivity in amorphous heterogeneous nanocomposites.* Rsc Advances, 2016. **6**(107): p. 105154-105160.

79. Seyf, H.R. and A. Henry, *A method for distinguishing between propagons, diffusions, and locons.* Journal of Applied Physics, 2016. **120**(2): p. 025101.

80. Yang, H.-S., et al., *Anomalously high thermal conductivity of amorphous Si deposited by hot-wire chemical vapor deposition.* Physical Review B, 2010. **81**(10): p. 104203.

81. Wang, Y., F. Yang, and P. Xiao, *Glass-like thermal conductivities in (La1-x1Yx1) 2 (Zr1-x2Yx2) 2O7-x2 (x= x 1+ x 2, 0⩽ x⩽ 1.0) solid solutions.* Acta materialia, 2012. **60**(20): p. 7024-7033.

82. Giri, A., et al., *On the minimum limit to thermal conductivity of multi-atom component crystalline solid solutions based on impurity mass scattering.* Scripta Materialia, 2017. **138**: p. 134-138.

83. Andersson, O. and A. Inaba, *Thermal conductivity of crystalline and amorphous ices and its implications on amorphization and glassy water.* Physical Chemistry Chemical Physics, 2005. **7**(7): p. 1441-1449.

84. Konstantinov, V., et al., *Isochoric thermal conductivity of solid carbon oxide: the role of phonons and 'diffusive'modes.* Journal of Physics: Condensed Matter, 2006. **18**(43): p. 9901.

85. Chiritescu, C., et al., *Ultralow thermal conductivity in disordered, layered WSe2 crystals.* Science, 2007. **315**(5810): p. 351-353.

86. Korolyuk, O., et al., *Heat transfer in solid methyl alcohol.* Low Temperature Physics, 2009. **35**(4): p. 290-293.

87. Giri, A., et al., *Kapitza resistance and the thermal conductivity of amorphous superlattices.* Journal of Applied Physics, 2015. **118**(16): p. 165303.

88. Tlili, A., et al., *Thermal transport properties in amorphous/nanocrystalline metallic composites: A microscopic insight.* Acta Materialia, 2017. **136**: p. 425-435.

89. Sosso, G.C., et al., *Thermal transport in phase-change materials from atomistic simulations.* Physical Review B, 2012. **86**(10): p. 104301.

90. Wang, Y., Z. Song, and Z. Xu, *Mechanistic transition of heat conduction in two-dimensional solids: A study of silica bilayers.* Physical Review B, 2015. **92**(24): p. 245427.

91. Zhu, T. and E. Ertekin, *Phonons, localization, and thermal conductivity of diamond nanothreads and amorphous graphene.* Nano letters, 2016. **16**(8): p. 4763-4772.

92. Barker Jr, A. and A.J. Sievers, *Optical studies of the vibrational properties of disordered solids.* Reviews of Modern Physics, 1975. **47**(S2): p. S1.

93. Chang, I. and S. Mitra, *Long wavelength optical phonons in mixed crystals.* Advances in Physics, 1971. **20**(85): p. 359-404.

94. Chen, Y.-S., W. Shockley, and G. Pearson, *Lattice Vibration Spectra of Ga As x P 1− x Single Crystals.* Physical Review, 1966. **151**(2): p. 648.

95. Verleur, H. and A. Barker Jr, *Infrared Lattice Vibrations in Ga As y P 1− y Alloys.* Physical Review, 1966. **149**(2): p. 715.

96. Beltukov, Y., V. Kozub, and D. Parshin. *Vibrations in amorphous solids beyond the Ioffe-Regel criterion*. in *Journal of Physics: Conference Series*. 2013. IOP Publishing.

97. Gospodarev, I., et al., *Ioffe-Regel crossover and boson peaks in disordered solid solutions and similar peculiarities in heterogeneous crystal structures.* Fizika Nizkikh Temperatur, 2008. **34**(8): p. 829-841.

98. Shintani, H. and H. Tanaka, *Universal link between the boson peak and transverse phonons in glass.* Nature materials, 2008. **7**(11): p. 870.

99. Feher, A., et al., *The Features of Low Frequency Atomic Vibrations and Propagation of Acoustic Waves in Heterogeneous Systems*, in *Waves in Fluids and Solids*. 2011, InTech.

100. McGaughey, A. and J.M. Larkin, *Predicting phonon properties from equilibrium molecular dynamics simulations.* Ann. Rev. Heat Transfer, 2014. **17**: p. 49-87.

101. Larkin, J.M. and A.J. McGaughey, *Thermal conductivity accumulation in amorphous silica and amorphous silicon.* Physical Review B, 2014. **89**(14): p. 144303.

102. Larkin, J.M. and A.J. McGaughey, *Predicting alloy vibrational mode properties using lattice dynamics calculations, molecular dynamics simulations, and the virtual crystal approximation.* Journal of Applied Physics, 2013. **114**(2): p. 023507.

103. Baldi, G., et al., *Emergence of Crystal-like Atomic Dynamics in Glasses at the Nanometer Scale.* Physical Review Letters, 2013. **110**(18): p. 185503.

104. Baldi, G., et al., *Sound Attenuation at Terahertz Frequencies and the Boson Peak of Vitreous Silica.* Physical Review Letters, 2010. **104**(19): p. 195501.

105. Baldi, G., et al., *Thermal conductivity and terahertz vibrational dynamics of vitreous silica.* Physical Review B, 2008. **77**(21): p. 214309.

106. Ruzicka, B., et al., *Evidence of anomalous dispersion of the generalized sound velocity in glasses.* Physical Review B, 2004. **69**(10): p. 100201.

107. Feldman, J., *Calculations of the generalized dynamic structure factor for amorphous silicon.* Journal of non-crystalline solids, 2002. **307**: p. 128-134.

108. Horbach, J., W. Kob, and K. Binder, *High frequency sound and the boson peak in amorphous silica.* The European Physical Journal B-Condensed Matter and Complex Systems, 2001. **19**(4): p. 531-543.

109. Taraskin, S. and S. Elliott, *Determination of the Ioffe-Regel limit for vibrational excitations in disordered materials.* Philosophical Magazine B, 1999. **79**(11-12): p. 1747-1754.

110. Bell, R. and P. Dean, *Atomic vibrations in vitreous silica.* Discussions of the Faraday society, 1970. **50**: p. 55-61.

111. Murphy, N., R. Wortis, and W. Atkinson, *Generalized inverse participation ratio as a possible measure of localization for interacting systems.* Physical Review B, 2011. **83**(18): p. 184206.

112. Seyf, H.R., et al., *The Importance of Phonons with Negative Phase Quotient in Disordered Solids.* Scientific reports, 2018. **8**(1): p. 2627.

113. Mott, N., *Electrons in disordered structures.* Advances in Physics, 1967. **16**(61): p. 49-144.

114. Cohen, M.H., H. Fritzsche, and S. Ovshinsky, *Simple band model for amorphous semiconducting alloys.* Physical Review Letters, 1969. **22**(20): p. 1065.

115. DeAngelis, F., et al., *Thermal Transport in Disordered Materials.* Nanoscale and Microscale Thermophysical Engineering, 2019. **23**(2): p. 81-116.

116. Gordiz, K. and A. Henry, *Phonon transport at crystalline Si/Ge interfaces: the role of interfacial modes of vibration.* Scientific reports, 2016. **6**: p. 23139.

117. Choy, C., *Thermal conductivity of polymers.* Polymer, 1977. **18**(10): p. 984-1004.

118. Kommandur, S. and S.K. Yee, *An empirical model to predict temperature-dependent thermal conductivity of amorphous polymers.* Journal of Polymer Science Part B: Polymer Physics, 2017. **55**(15): p. 1160-1170.

119. Henry, A., *Thermal transport in polymers.* Annu. Rev. Heat Transfer, 2013. **17**: p. 485-520.

120. Duda, J.C., et al., *Exceptionally low thermal conductivities of films of the fullerene derivative PCBM.* Physical review letters, 2013. **110**(1): p. 015902.

121. Zhang, T. and T. Luo, *Morphology-influenced thermal conductivity of polyethylene single chains and crystalline fibers.* Journal of Applied Physics, 2012. **112**(9): p. 094304.

122. Plimpton, S., *Fast parallel algorithms for short-range molecular dynamics.* Journal of computational physics, 1995. **117**(1): p. 1-19.

123. Tersoff, J., *Empirical interatomic potential for silicon with improved elastic properties.* Physical Review B, 1988. **38**(14): p. 9902.

124. Car, R. and M. Parrinello, *Phys Rev Lett 55: 2471*. 1985.

125. Mayo, S.L., B.D. Olafson, and W.A. Goddard, *DREIDING: a generic force field for molecular simulations.* Journal of Physical chemistry, 1990. **94**(26): p. 8897-8909.

126. Floriano, W.B., et al., *HierVLS hierarchical docking protocol for virtual ligand screening of large-molecule databases.* Journal of medicinal chemistry, 2004. **47**(1): p. 56-71.

127. Kekenes-Huskey, P.M., et al., *Fidelity of phenylalanyl-tRNA synthetase in binding the natural amino acids.* The Journal of Physical Chemistry B, 2003. **107**(41): p. 11549-11557.

128. Wang, P., et al., *Virtual screening for binding of phenylalanine analogues to phenylalanyl-tRNA synthetase.* Journal of the American Chemical Society, 2002. **124**(48): p. 14442-14449.

129. Brameld, K.A. and W.A. Goddard, *Ab initio quantum mechanical study of the structures and energies for the pseudorotation of 5 '-dehydroxy analogues of 2 '-deoxyribose and ribose sugars.* Journal of the American Chemical Society, 1999. **121**(5): p. 985-993.

130. Datta, D., et al., *Interaction of E. coli outer-membrane protein A with sugars on the receptors of the brain microvascular endothelial cells.* Proteins: Structure, Function, and Bioinformatics, 2003. **50**(2): p. 213-221.

131. Datta, D., et al., *Mechanism for antibody catalysis of the oxidation of water by singlet dioxygen.* Proceedings of the National Academy of Sciences, 2002. **99**(5): p. 2636-2641.

132. Tersoff, J., *Modeling solid-state chemistry: Interatomic potentials for multicomponent systems.* Physical review B, 1989. **39**(8): p. 5566.

133. Buckingham, R. and J. Corner, *Tables of second virial and low-pressure Joule-Thomson coefficients for intermolecular potentials with exponential repulsion.* Proceedings of the Royal Society of London. Series A. Mathematical and Physical Sciences, 1947. **189**(1016): p. 118-129.

134. Fennell, C.J. and J.D. Gezelter, *Is the Ewald summation still necessary? Pairwise alternatives to the accepted standard for long-range electrostatics.* The Journal of chemical physics, 2006. **124**(23): p. 234104.

135. Rohskopf, A., et al., *Empirical interatomic potentials optimized for phonon properties.* NPJ Computational Materials, 2017. **3**(1): p. 27.

136. Kluge, M.D., J.R. Ray, and A. Rahman, *Amorphous-silicon formation by rapid quenching: A molecular-dynamics study.* Physical Review B, 1987. **36**(8): p. 4234.

137. Bitzek, E., et al., *Structural relaxation made simple.* Physical review letters, 2006. **97**(17): p. 170201.

138. Dove, M.T., *Introduction to Lattice Dynamics*. 1993: Cambridge University Press.

139. Truong, T.N. and D.G. Truhlar, *Ab initio transition state theory calculations of the reaction rate for OH+ CH4→ H2O+ CH3.* The Journal of Chemical Physics, 1990. **93**(3): p. 1761-1769.

140. Vineyard, G.H., *Frequency factors and isotope effects in solid state rate processes.* Journal of Physics and Chemistry of Solids, 1957. **3**(1-2): p. 121-127.

141. Bruice, T.C. and F.C. Lightstone, *Ground state and transition state contributions to the rates of intramolecular and enzymatic reactions.* Accounts of chemical research, 1999. **32**(2): p. 127-136.

142. Gillan, M., *Quantum-classical crossover of the transition rate in the damped double well.* Journal of Physics C: Solid State Physics, 1987. **20**(24): p. 3621.

143. Gezelter, J.D., E. Rabani, and B. Berne, *Can imaginary instantaneous normal mode frequencies predict barriers to self-diffusion?* The Journal of chemical physics, 1997. **107**(12): p. 4618-4627.

144. Gonzalez-Lafont, A., T.N. Truong, and D.G. Truhlar, *Interpolated variational transition-state theory: Practical methods for estimating variational transition-state properties and tunneling contributions to chemical reaction rates from electronic structure calculations.* The Journal of chemical physics, 1991. **95**(12): p. 8875-8894.

145. Fan, L. and T. Ziegler, *Nonlocal density functional theory as a practical tool in calculations on transition states and activation energies. Applications to elementary reaction steps in organic chemistry.* Journal of the American Chemical Society, 1992. **114**(27): p. 10890-10897.

146. Miller, W.H., *Semiclassical limit of quantum mechanical transition state theory for nonseparable systems.* The Journal of chemical physics, 1975. **62**(5): p. 1899-1906.

147. Pollak, E., *Theory of activated rate processes: A new derivation of Kramers' expression.* The Journal of chemical physics, 1986. **85**(2): p. 865-867.

148. Buchner, M., B.M. Ladanyi, and R.M. Stratt, *The short-time dynamics of molecular liquids. Instantaneous-normal-mode theory.* The Journal of chemical physics, 1992. **97**(11): p. 8522-8535.

149. Cho, M., et al., *Instantaneous normal mode analysis of liquid water.* The Journal of chemical physics, 1994. **100**(9): p. 6672-6683.

150. Adams, J.E. and R.M. Stratt, *Instantaneous normal mode analysis as a probe of cluster dynamics.* The Journal of Chemical Physics, 1990. **93**(2): p. 1332-1346.

151. La Nave, E., et al., *Instantaneous normal mode analysis of supercooled water.* Physical review letters, 2000. **84**(20): p. 4605.

152. Seeley, G. and T. Keyes, *Normal-mode analysis of liquid-state dynamics.* The Journal of Chemical Physics, 1989. **91**(9): p. 5581-5586.

153. Wan, Y. and R.M. Stratt, *Liquid theory for the instantaneous normal modes of a liquid.* The Journal of chemical physics, 1994. **100**(7): p. 5123-5138.

154. Wu, T.M. and R.F. Loring, *Phonons in liquids: A random walk approach.* The Journal of chemical physics, 1992. **97**(11): p. 8568-8575.

155. Gale, J.D. and A.L. Rohl, *The general utility lattice program (GULP).* Molecular Simulation, 2003. **29**(5): p. 291-341.

156. Lv, W. and A. Henry, *Direct calculation of modal contributions to thermal conductivity via Green–Kubo modal analysis.* New Journal of Physics, 2016. **18**(1): p. 013028.

157. Lv, W. and A. Henry, *Phonon transport in amorphous carbon using Green–Kubo modal analysis.* Applied Physics Letters, 2016. **108**(18): p. 181905.

158. Seyf, H.R., et al., *Using Green-Kubo modal analysis (GKMA) and interface conductance modal analysis (ICMA) to study phonon transport with molecular dynamics.* Journal of Applied Physics, 2019. **125**(8): p. 081101.

159. Rohskopf, A., et al., *Phonon optimized potentials.* arXiv preprint arXiv:1610.02353, 2016.

160. Alvarez, F., et al., *Radial distribution functions of ab initio generated amorphous covalent networks.* Physical Review B, 2002. **65**(11): p. 113108.

161. Girifalco, L.A. and V.G. Weizer, *Application of the Morse potential function to cubic metals.* Physical Review, 1959. **114**(3): p. 687.

162. Tosi, M.P., *Cohesion of ionic solids in the Born model*, in *Solid state physics*. 1964, Elsevier. p. 1-120.

163. Wolf, D., et al., *Exact method for the simulation of Coulombic systems by spherically truncated, pairwise r− 1 summation.* The Journal of chemical physics, 1999. **110**(17): p. 8254-8282.

164. Kubo, R., *Statistical-mechanical theory of irreversible processes. I. General theory and simple applications to magnetic and conduction problems.* Journal of the Physical Society of Japan, 1957. **12**(6): p. 570-586.

165. Kubo, R., M. Yokota, and S. Nakajima, *Statistical-mechanical theory of irreversible processes. II. Response to thermal disturbance.* Journal of the Physical Society of Japan, 1957. **12**(11): p. 1203-1211.

166. Hardy, R.J., *Energy-flux operator for a lattice.* Physical Review, 1963. **132**(1): p. 168.

167. Teng, K.-L., et al., *Enhanced thermal conductivity of nanofluids diagnosis by molecular dynamics simulations.* Journal of nanoscience and nanotechnology, 2008. **8**(7): p. 3710-3718.

168. McGaughey, A.J. and M. Kaviany, *Phonon transport in molecular dynamics simulations: Formulation and thermal conductivity prediction.* Advances in Heat Transfer, 2006. **39**: p. 169-255.

169. Lv, W., et al., *Understanding Divergent Thermal Conductivity in Single Polythiophene Chains Using Green–Kubo Modal Analysis and Sonification.* The Journal of Physical Chemistry A, 2017. **121**(30): p. 5586-5596.

170. Molina, A., P. Smereka, and P.M. Zimmerman, *Exploring the relationship between vibrational mode locality and coupling using constrained optimization.* The Journal of chemical physics, 2016. **144**(12): p. 124111.

171. Shen, S., et al., *Polyethylene nanofibres with very high thermal conductivities.* Nature nanotechnology, 2010. **5**(4): p. 251.

172. Singh, V., et al., *High thermal conductivity of chain-oriented amorphous polythiophene.* Nature nanotechnology, 2014. **9**(5): p. 384-390.

173. *Evergreen Partnering Group, Inc. v. Pactiv Corp*, in *F. 3d*. 2013, Court of Appeals, 1st Circuit. p. 33.

174. Haley, B.P., et al., *Polymer modeler.* 2010.